ADHESION AND THE SURFACE ENERGY COMPONENTS OF NATURAL MINERALS AND AGGREGATES

A Thesis

by

CLINT MATTHEW MILLER

Submitted to the Office of Graduate Studies of
Texas A&M University
in partial fulfillment of the requirements for the degree of

MASTER OF SCIENCE

August 2010

Major Subject: Geology

ADHESION AND THE SURFACE ENERGY COMPONENTS OF NATURAL MINERALS AND AGGREGATES

A Thesis

by

CLINT MATTHEW MILLER

Submitted to the Office of Graduate Studies of
Texas A&M University
in partial fulfillment of the requirements for the degree of

MASTER OF SCIENCE

Approved by:

Chair of Committee,	Bruce Herbert
Committee Members,	Dallas Little
	Terry L. Wade
	Hongbin Zhan
Head of Department,	Andreas Kronenberg

August 2010

Major Subject: Geology

ABSTRACT

Adhesion and the Surface Energy Components of Natural Minerals and Aggregates.

(August 2010)

Clint Matthew Miller, B.S., Texas A&M University

Chair of Advisory Committee: Dr. Bruce Herbert

A range of geochemical reactions are controlled by the interfacial characteristics of rocks and minerals. Many engineered and natural systems are affected by geochemical reactions that occur at interfaces. Asphalt-aggregate adhesion in road construction is influenced by the interfacial characteristics of the aggregate. Likewise, the remediation of nonaqueous-phase liquid contaminants, such as trichloroethylene or methyl *tert*-butyl ether, is controlled by the interactions between mineral surfaces and the organic liquid. Many natural systems are also influenced by reactions at interfaces. The migration of petroleum in sedimentary basins is influenced by the wettability of the surfaces of the basin pore space. Adhesion of organisms, such as bacteria or lichens, to rock surfaces is controlled by the interactions of proteins and mineral surfaces.

Rock and mineral surfaces are described by surface energy. Surface energy is a thermodynamic construct defined as the amount of work required to form more of a surface. Surface energy can be divided into van der Waals, Lewis acid, and Lewis base components. The ability to predict the magnitude of surface energy components is valuable in understanding species behavior. Surface energy is controlled by three master variables: surface chemistry, surface morphology, and surface coatings. While the surface energy of a number of minerals and aggregates has been characterized, there has not yet been a comprehensive study of the surface energies of a variety of the most common minerals and aggregates using consistent methodology. In addition there has

not yet been a study of the effect of these three master variables on surface energies of natural minerals and rocks.

This study measured the surface energy of 22 common minerals and 7 aggregates. The samples' bulk and surface chemistries were characterized with wavelength and energy dispersive spectra analyses on an electron microprobe and x-ray photoelectron spectroscopy. The XPS was also used to quantify the organic and inorganic coatings on the surfaces. Results showed that van der Waals surface energy is typically between 40 and 60 ergs/cm^2. Polar surface energy varies by 1 to 3 orders of magnitude, and thus is likely the most important component in accounting for changes between natural minerals.

DEDICATION

I would like to dedicate this thesis to my parents for giving me an education and for paying for another one at Texas A&M; my grandparents for their love and support (We miss you Granddad), and my beautiful fiancé Jane Ellen. I love you.

ACKNOWLEDGEMENTS

I would like to thank my committee chair, Dr. Herbert, and my committee members, Dr. Little, Dr. Wade, and Dr. Zhan, for their guidance and support throughout the course of this research. Additionally, I would like to thank Dr. Guillemette for hours and hours of high quality work and help on the electron microprobe and mineral chemistry questions. Thanks also go to Dr. Bhasin for training on the universal sorption device, Dr. Kuo for help with the elemental analysis, Dr. Liang for training on the x-ray photoelectron spectroscopic analyses, and Nathan Gardener for his help with the universal sorption device and all of the headaches therein. Only Nathan and I truly know what that sentence means.

TABLE OF CONTENTS

Page

ABSTRACT…… iii
DEDICATION…… v
ACKNOWLEDGEMENTS…… vi
TABLE OF CONTENTS…… vii
LIST OF FIGURES…… ix
LIST OF TABLES…… xi
CHAPTER
I INTRODUCTION: SURFACE ENERGY OF NATURAL MINERALS.. 1
Geologic and Engineering Processes Impacted by Organic-Rock Interactions …… 1
Surface Energy of Solids …… 3
The Components of Surface Energy …… 5
van der Waals …… 5
Lewis Acid/Base …… 6
Aggregate Surfaces and Factors That Control Surface Energy …… 7
Nonpolar Active Sites on Surfaces …… 7
Polar Actives Sites on Surfaces…… 8
Physical Characteristics…… 9
Organic and Inorganic Coatings …… 10
Measurement of Surface Energy …… 11
History of Surface Energy…… 11
Surface Energy Measurement Methodology …… 12
Research Objectives…… 14
Present Status of Surface Energy Research …… 15
Materials and Methods…… 15
Data Analysis and Error Analysis…… 22
II CONCLUSIONS ON MEASURING THE SURFACE ENERGY OF A VARIETY OF THE MOST COMMON MINERALS…… 24
Introduction …… 24
Materials and Methods…… 28
Pretreatment …… 28
Chemical Characterization …… 29

Page

Universal Sorption Device 37
Quality Assurance/Quality Control 40
Grain Sizes 40
Specific Surface Area 41
Bulk Moisture and Elemental Analysis 42
Data Analysis and Error Analysis 50
Results and Discussion 51
Surface Area and Surface Roughness 53
Surface Energy Results 64
Conclusions 89

REFERENCES 94

APPENDIX A BULK AND SURFACE CHEMISTRY RESULTS 107

APPENDIX B SURFACE ENERGY RESULTS 141

APPENDIX C MINERAL ROUGHNESS RESULTS 169

APPENDIX D RHODOCHROSITE X-RAY IMAGES 177

APPENDIX E XPS PEAK RESULTS 183

VITA 207

LIST OF FIGURES

Page

Figure 1-1	Relationship of Surface Energy to Work	4
Figure 1-2	Low and High Energy Solid Contact Angles	13
Figure 2-1	Rubotherm Column Assembly	38
Figure 2-2	Universal Sorption Device	40
Figure 2-3	Fragment Size Analysis	44
Figure 2-4	Mineral Moisture Percent	49
Figure 2-5	Relationship between Surface Roughness and Surface Area	60
Figure 2-6	Surface Roughness Results	63
Figure 2-7	van der Waals Surface Energy (All)	65
Figure 2-8	van der Waals Surface Energy (Carbonates)	66
Figure 2-9	van der Waals Surface Energy (Common Silicates)	66
Figure 2-10	Lewis Acid Surface Energy (All)	71
Figure 2-11	Lewis Acid Surface Energy (Carbonates)	72
Figure 2-12	Lewis Acid Surface Energy (Sulfates)	73
Figure 2-13	Lewis Acid Surface Energy (Common Silicates)	74
Figure 2-14	Lewis Acid Surface Energy (Clay Minerals)	75
Figure 2-15	Lewis Base Surface Energy (All)	78
Figure 2-16	Lewis Base Surface Energy (Carbonates)	79
Figure 2-17	Effect of Heat on Gypsum Lewis Base Surface Energy	80
Figure 2-18	Total Polar Surface Energy (All)	83
Figure 2-19	Total Surface Energy	84
Figure 2-20	Total Component Surface Energy	85
Figure 2-21	van der Waals Surface Energy per Gram	86
Figure 2-22	Polar Surface Energy per Gram	87
Figure 2-23	Total Surface Energy per Gram	88

Page

Figure 2-24 Effect of Organic Coatings on Carbonate Surface Energy …… 91
Figure 2-25 Effect of Organic Coatings on Lewis Base Surface Energy ……. 92

LIST OF TABLES

Page

Table 1-1	Preliminary Mineral Selection……	16
Table 1-2	Preliminary Aggregate Selection ……...	19
Table 2-1	Surface Energy Literature Values for Reference Vapors ……..	29
Table 2-2	Final Selection of Minerals……	30
Table 2-3	Relative Sensitivity Factors for XPS……..	34
Table 2-4	XPS Peak Positions (eV) by Mineral…….	35
Table 2-5	Atomic Species Tested on XPS …….	36
Table 2-6	Grain Size Analysis……	43
Table 2-7	Sulphanilic Acid Calibration for Elemental Analysis……	45
Table 2-8	Elemental Analysis Results……	46
Table 2-9	Moisture Analysis Prior to Heating ……..	48
Table 2-10	Mineral Surface Functional Groups……	54
Table 2-11	Bulk and Surface Measured Chemical Formulas ……..	56
Table 2-12	Measured Specific Surface Areas ……..	58
Table 2-13	Specific Surface Area Literature Value Comparison ……	59
Table 2-14	Measured Values of Surface Roughness ……...	62
Table 2-15	van der Waals Surface Energy Summary ……..	67
Table 2-16	Lewis Acid Surface Energy Summary ……..	70
Table 2-17	Lewis Base Surface Energy Summary ……..	76
Table 2-18	Polar Surface Energy Summary…….	81

CHAPTER I

INTRODUCTION: SURFACE ENERGY OF NATURAL MINERALS

Geologic and Engineering Processes Impacted by Organic-Rock Interaction

Many geochemical reactions occur at interfaces (BENEDETTI et al., 1994; BENNETT et al., 1996). These interfacial reactions occur in a variety of engineered and natural matrices. Many important reactions take place at rock surfaces such as adsorption, REDOX reactions, biochemical reactions, and phase changes (JOHNSTON, 1996). Interfacial characteristics of rock surfaces at the molecular scale control interactions thereby influencing macroscale phenomena such as wettability, adhesion, friction, surface tension, and surface charge (BOYD and LIVINGSTON, 1942; HARKINS and BOYD, 1942; VAN OSS, 2006). Interfacial geochemical reactions influence a variety of reactions associated with engineering, geological, medical, and biological systems.

One system that is influence by organic-rock interactions is hydrocarbon migration in petroleum reservoirs. Hydrocarbons are primarily nonpolar aromatic carbon chains (SILBERBERG, 2004; SPEIGHT, 1999). Migration of hydrocarbons is controlled by geochemical reactions at pore surfaces of the geologic reservoir as well as conductivity and pore size. Migration is inhibited by retardation through adsorption and absorption on rock surfaces. Sorption, which occurs on rock surfaces, is determined by the rock surface characteristics such as charge and surface morphology (HYNE, 2001; SPEIGHT, 2006). Another geologic and environmental process affected by surface energy is environmental remediation and contaminant transport of nonaqueous phase liquids in hydrologic reservoirs (WAN and WILSON, 1994). Contaminant fate and transport is often controlled by redox reactions within the reservoir (LAGREGA et al., 2000). REDOX reactions occur on surfaces when the geologic media donates or accepts electrons from

---

This thesis follows the style of *Geochimica et Cosmochimica Acta*.

the contaminant. The surface charge of the reservoir also affects the retention of the contaminant plume within the subsurface. Geologic surfaces with high charge to volume ratios, such as clays, will inhibit plume movement while those with less charge will adsorb less material. Therefore; the natures of surfaces determine reactions of contaminants with geologic and engineered materials.

Engineered systems, such as asphalt roadways, are also affected by organic-rock interfacial reactions. Asphalt roadways are under constant deterioration due to a process called moisture damage. Strength and durability of these roadways is contingent on the organic asphalt bonding with introduced aggregates which are mixed with the asphalt. These aggregates do not have clean surfaces. Rather, rocks in the environment will always have organic and inorganic coatings which inhibit simple molecular bonding models. Water, being polar, bonds with the asphalt polar organic functional groups thus reducing adhesion and causing cracking between the aggregates and the asphalt. The surface energy of the asphalts and aggregates has been shown to be a good predictor of bond strength and moisture susceptibility (BHASIN et al., 2007).

Dental research is now becoming aware of the importance of surface energy of enamel and bacteria adsorption (CLINT, 2001). Much research is being done on superhydrophobic surfaces (FENG et al., 2002; NAKAJIMA et al., 1999). These surfaces, either based on morphology or chemistry, do not allow water to wet. Therefore, the liquid stays beaded and rolls off. Medical research has focused on defining the ability of prosthetic devices to adhere to bone tissue.

Geochemical interfacial characteristics play an integral role in biological reactions. Organisms, such as the Water Strider, take advantage of the surface tension of water to move across its surface. Plant leaves often display low surface adhesion so that water can freely flow toward their roots and not remain suspended. Lichens and other attachment organisms take advantage of very high surface energy to strongly adhere to rocks and other surfaces.

Surface Energy of Solids

All solids, liquids, and gases have chemical energy associated with them. Generally, most of the energy is located in the interior except for particles with very small diameters (SHUTTLEWORTH, 1950). However, edges also have energy which exerts forces on neighboring molecules. This surface energy, although generally small, is responsible for many of the behaviors of solids such as surface friction, adsorption of smaller particles, stickiness, etc. as well as many of the properties of liquids such as capillarity, surface tensions, and ability to wet a solid (BOYD and LIVINGSTON, 1942; CARPICK et al., 1996; CLINT, 2001; VAN OSS and GIESE, 1995). Many geochemical reactions are controlled by the interfacial surface energies of the involved media. Surface energy is defined as the work required to make more of a surface (ADAMSON and KLERER, 1977).

The surface energy of a mineral, such as calcite, is the amount of energy required to make more surface of calcite. The relationship between surface energy and work is given in figure 1-1. Conceptually surface energy can be considered as the amount of energy lost when the molecular bonds that are normally filled inside a solid remain unfilled as a result of being at the edge of the solid (BIKERMAN, 1978). In addition to the unfilled bonds, however, the effects of the nonadjacent molecules in the solids must also be considered (FOWKES, 1964; SPELT et al., 1986). These molecules can either be attractive or repulsive; however the surface energy must always be positive. The forces are a function of the specific chemical nature of the material (FOWKES, 1964). Therefore, chemical heterogeneities will create unique surface energies.

For solids the surface energy should not be confused with surface tension (CLINT, 2001). Chemical energy of surfaces has three components: two normal and one shear parallel to the edge (SHUTTLEWORTH, 1950). These components combine to form the total surface stress or surface tension. For a liquid the shear stress is zero because liquids cannot support shear stress. The surface tension of a solid is defined as the total force per unit length that must be applied tangentially to the surface in order that the surface

planes have the same lattice spacing as the underlying solid (SHUTTLEWORTH, 1950). For most solids it is not possible for atoms or molecules to flow (nondiffusionally) from the interior to the surface or vice versa at any detectable rate as happens in liquids. This nonzero shear strength causes the tangential tension to add to the total shear.

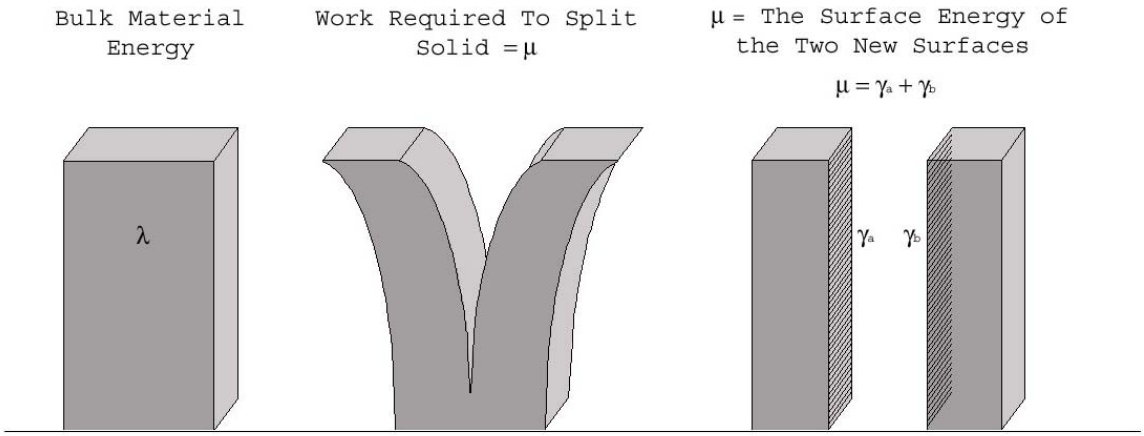

Figure 1-1 Relationship of Surface Energy to Work

Thus, surface tension of solids is a function of all three shear components. Surface tension of solids is related work (Figure 1-1) and to surface energy as:

$$\tau^{S}_{T} = \gamma^{S}_{T} + A(d\gamma^{S}_{T}/dA) \qquad \text{Eq. 1.1}$$

where A is the area of the solid, $d\gamma^{S}_{T}$ is the change in the total surface energy, and dA is the change in area (SHUTTLEWORTH, 1950). The value of surface tension as well as surface energy will vary with crystal direction or edge location for any heterogeneous anisotropic solid. This is especially true for minerals that display strong cleavage such as phyllosilicates. In minerals with strong cleavage the surface area may be dominated by one plane to the extent that the smaller edges can be neglected. It is also possible, however, that the planes with large surface area are relatively inert and the total surface energy be dominated by broken edges. As with liquids the total surface energy can be divided into two components: dispersive or Van der Waals and the polar or acid/base.

$$\gamma^{S}_{T} = \gamma^{S}_{d} + \gamma^{S}_{ab} \qquad \text{Eq. 1.2}$$

$$\gamma^{S}_{d} = \gamma^{S}_{ab} = 2\sqrt{(\gamma^{+}\,\gamma^{-})} \qquad \text{Eq. 1.3}$$

where γ^{S}_{d} is the dispersive surface energy, γ^{S}_{ab} is the polar component of surface energy, γ^{+} is the acid component, and γ^{-} is the base component of the polar contribution (FOWKES, 1964; VAN OSS et al., 1988). The acid/base portion may originate from hydrogen bonding, π-bonding, and acceptor/donor electrostatic interactions (JANCZUK and BIALOPIOTROWICZ, 1988). Hydrogen bonding is probably the most common interaction leading to the acid/base component of free energy of adhesion (GOOD and VAN OSS, 1992).

The Components of Surface Energy

van der Waals

Surface energy components describe the surface characteristics of the investigated material. The components of surface energy control much of the interfacial interactions of that material edge. The chemical components are: the Lifshitz-van der Waals, the electron donor, and the electron acceptor components (VAN OSS et al., 1988; VAN OSS et al., 2001). The Lifshitz-van der Waals component is a grouping of three different interactions: the van der Waals-Keesom, the van der Waals-Debye, and the van der Waals-London force. As Overbeek discovered in 1952 these three forces are additive (OVERBEEK, 1952; VAN OSS, 2006). Therefore, they can be described simply as:

$$\gamma^{S}_{d} = \gamma^{LW} = \gamma^{L} + \gamma^{D} + \gamma^{K} \qquad \text{Eq. 1.4}$$

When all three of these interactions are grouped together like so they collectively become known as Lifshitz-van der Waals interactions. This grouping gives the benefit of easily describing their magnitude, however commonly (as is the case in this research) their respective amounts are not known.

Lewis Acid/Base

In addition to Lifshitz-van der Waals forces the other major component to surface energy is the polar or electron acceptor-donor component. This portion of the surface energy can be up to two orders of magnitude greater than the van der Waals component, however it is strongest at less than ten Å (VAN OSS, 2006). The polar or Lewis acid-base interactions are probably mainly hydrogen donor and hydrogen acceptor reactions (VAN OSS et al., 2001). However, it is more useful to define "polar" more broadly for all electron acceptor-donor interactions. In this way all of the interactions with similar donor/acceptor affects can be measured.

The major difference between Lifshitz-van der Waals interactions and polar interactions is that electron donor-acceptor reactions are not symmetrical as are van der Waals interactions. The molecular polarizabilities and the ionization energies enter the equations for the dispersion (polar) force symmetrically (VAN OSS, 2006). In an electron acceptor/donor relationship this symmetry does not exist. This is because in a strict sense a basic functional group, such as a carboxylic acid, will not interact as a base with another basic entity. One must act as an electron donor and the other must act as an electron acceptor (MCMURRY, 2004). Nondispersive forces only occur when there are complimentary groups present (an electron acceptor and an electron donor in a Lewis sense).

For this reason the duality of electron acceptor-donor interactions must be treated together yet understood separately. For instance, a monopolar substance, such as methyl propyl ketone, has a total polar surface energy of zero because $\gamma^+ = 0$. However, the $\gamma^- \neq 0$. Therefore, methyl propyl ketone can react through polar interactions with any other monopolar substance with an electron acceptor component or with any bipolar substance despite the fact that its polar surface energy is zero. This is just one example of the importance of understanding all of the components of a material's surface free energy if inferences are to be made on the interface reactivity characteristics of that material. Polar interactions must not be confused with electrostatic interactions and must be understood separately. Because of the universality of van der Waals interactions and

the specificity of electron donor-acceptor forces the interpretation of polar components of surfaces and edge sites has the greatest potential.

Aggregate Surfaces and Factors That Control Surface Energy

Nonpolar Active Sites on Surfaces

Chemical surface energy components are located on natural surfaces in sites, commonly termed 'active sites'. These are the positions where sorption occurs. Combining known knowledge of individual mineral surface characteristics to surface energy results can correlate type and density of active surface sorption sites on minerals. The sorption sites on minerals are of varying type (JOHNSTON and E., 2002). There are two major positions that an active site of a mineral can be found. These are on the edges and the basal surfaces. Of these two positions an active site can be either polar or nonpolar.

Nonpolar sites primarily bond with van der Waals components of adsorbates. Nonpolar sites are commonly found on micas, zeolites, kaolinite, serpentine minerals, smectites, and a variety of other silicate minerals. Vermiculites and chlorites have nonpolar sites to a lesser degree (JOHNSTON and E., 2002). Micas and zeolites often have the strongest nonpolar sites. Nonpolar sites are generally found on the neutral siloxane surface of silicates. These surfaces have no charge and no permanent dipole moment. Therefore, they are termed hydrophobic. Because of this hydrophobic nature water has little or no interaction with neutral siloxane surfaces and they are not able to form hydrogen bonds.

Hydrophobic surfaces occur on 2:1 phyllosilicates where no isomorphic substitution has occurred. This is a result of the -2 charge on the oxygen atoms being completely satisfied by neighboring silicon atoms (HUHEEY et al., 1983). Siloxane surfaces act as very weak Lewis bases but are basically inert. Their surface energy is therefore dominated by van der Waals forces. For this reason although water and other polar molecules have a slight affinity for neutral siloxane surfaces nonpolar organic solutes and nonpolar regions of larger biological molecules such as proteins and

enzymes can efficiently bond to this type of surface through van der Waals interactions (JOHNSTON and E., 2002).

Polar Active Sites on Surfaces

Polar active sites on surfaces can be broken down into permanently charged sites, conditionally charged sites, exchangeable metal cations, and exposed uncoordinated metal atoms (JOHNSTON, 1996). Polar sites react with Lewis acid/base components of adsorbates. Polar sites are generally termed hydrophilic as a result of their charge and dipole moments. Conditionally charged sites are pH dependent. Some examples of pH dependent sites are on iron oxides such goethite, aluminum oxides such as gibbsite, manganese oxides such as birnessite, palygorskite and sepiolite, and a large number of other silicate minerals (JOHNSTON and E., 2002). In addition to these kaolinite, serpentine, phyrophyllite, talc, micas, zeolites such as analcime, carbonates, and even titanium and zirconium minerals have some conditionally charges surfaces. Conditionally charged sites are primarily a result of inorganic surface hydroxyl groups. They must always be located on edge sites. The best example of this is gibbsite as explained by Johnston (JOHNSTON and E., 2002).

Permanent charge sites are often found on aluminosilicates such as allophane (contains pH dependent sites as well), micas such as biotite, silicate clays such as montmorillonite (also contain pH dependent sites, and vermiculite, and zeolites. Kaolinite and serpentinites also contain some permanently charged sites (KLEIN, 2002). Constant charged sites are a result of isomorphic substitution and defects within the mineral. Isomorphic substitution is a process where one atom or molecule is replaced by another of similar size. Isomorphous substitution often occurs in either the octahedral or tetrahedral sheets of 2:1 phyllosilicates. This switch is sometimes accompanied by a change in charge by the substituted atom. Constant charge sites are characterized by a permanent negative charge (JOHNSTON, 1996). One example is the substitution of Mg^{2+} for Al^{3+} in the octahedral sheet of layer silicates. Al^{3+} often substitutes for Si^{4+} in the tetrahedral sheet. Both of these result in a gain of one electron. Isomorphic substitution can result in a localized or delocalized charge. Mg^{2+} for Al^{3+} is thought to be delocalized

over approximately nine oxygen atoms on the siloxane surface whereas Al^{3+} for Si^{4+} is more concentrated at around three oxygens (JOHNSTON and E., 2002; SPOSITO, 1984). Closely related to constant charged sites described above are the exchangeable metal cation sites. In this case, however, the metal cation is not replaced by another cation. Instead, the organic solute coordinates directly to the cation occupying the isomorphic substitution site (ISAACSON and SAWHNEY, 1983; JOHNSTON, 1996). One example of this occurrence is when phenols react with exchangeable alkali and alkaline earth metal cations on these sites (JOHNSTON, 1996). The degree of metal-organic solute attraction will be a function of the organic solutes ability to compete for coordination sites around the metal center (ISAACSON and SAWHNEY, 1983).

It is also possible for exchangeable and structural transition metals in their oxidized state to interact directly with organic solutes. These metal cations can act as Lewis acids when they accept electrons from the organic solute (JOHNSTON, 1996; VOUDRIAS and REINHARD, 1986). An example of this reaction is when Cu^{2+} or Al^{3+} interact with reduced aqueous solutes. Cu^{2+} and Al^{3+} are themselves reduced and a radical organic cation is produced on the surface. These last two types of polar active sites are common on clay minerals.

Physical Characteristics

In addition to surface energy being controlled by surface chemistry it is also determined by the physical structure (PONSONNET et al., 2003). The physical characteristics of solids such as surface roughness, grain size, grain shape, porosity, and degree of crystalinity as well as events such as cracking, weathering, fracture, and compaction have a direct impact on the magnitudes of the surface energy components. The actual effect of surface physical structure on surface energy, however, has not been rigorously studied. The dominant control on surface energy is certainly surface area. This is proven by the equation to calculate the equilibrium film pressure by Chibowski (CHIBOWSKI and WAKSMUNDZKI, 1978). Thus, all of the physical characteristics that change surface energy can be thought of in the context of how they change the surface area.

Surface area of minerals can vary wildly depending on grain size and shape. Because surface area increases as grain size becomes smaller minerals and aggregates with smaller grain sizes, especially clay and silt sized, will have larger surface energy than otherwise identical minerals. It has long been known that clays are the most reactive soil texture (SCHAETZL and ANDERSON, 2005). Thus, in order to study surface energy of solids the surface area is usually expressed as specific surface area which is an area per mass or volume parameter. Because surface energy increases as surface area increases effects that cause greater surface area, such as physical weathering, are expected to cause an increase in energy. No systematic study has been performed on surface roughness role in surface energy, however the connection between surface roughness and surface area is clear and would be expected to have similar interplay. The effect of surface roughness on surfaces of equal area has not been systematically researched.

It should also be noted that the physical structure of a solid can inhibit bonding. It is possible for steric hindrances and microtopography to impede adsorption onto some sites even when they are chemically available. If a site is located in a cavity or is surrounded by sorption sites to large molecules it can be effectively blocked from sorption by the presence of these molecules or mineral shape. If a reference vapor is used to calculate energy based on adsorption isotherms the component energy may be larger than measured if the vapor molecules are blocked from sites. Thus, it is seen that surface roughness may also have a negative effect on the measured surface energy. Steric hindrances can be caused by the sorbate themselves as well preventing sorption. Larger adsorbates are more likely to have steric hindrances than smaller sorbates.

Organic and Inorganic Coatings

All surface energy measurements are highly variable based on the surface conditions at the time (PARKS, 1990). Any surface can be altered and thereby change its surface energy (STASZCZUK and BILINSKI, 1987). An example of this is when large organic molecules sorb to phyllosilicates. The organic molecule balances the charges of the polar and nonpolar sites. The interface essentially becomes part of the interior of a

new material comprised of the mineral and the organic molecule (NEU, 1996). The new edge site has very different characteristics than the layered silicate had originally. Smaller changes can also affect the surface energy characteristics. If a metal cation is sorbed from an aqueous solution onto the surface of a mineral it can satisfy a net negative charge imbalance. This reaction causes the electron donor γ^- component to decrease. Conversely a loss of a metal cation leads to an increase in the electron donor component of the surface free energy. In addition the presence of water or other aqueous solution at the interface can greatly affect the surface energy. Most notably the electron acceptor component γ^+ will increase (VAN OSS, 2006). Water also transports various media making sorbate species available to the material surface.

Conditionally charged surfaces are also strongly affected by the external environment. Acidic solution provides excess hydrogen positive charges to the surface of the mineral increasing the electron acceptor component. Basic solutions remove positive charges from the mineral surface causing the electron donor component to increase. Thus, the external environment can alter the surface energy even when coatings do not bond to the surface.

Measurement of Surface Energy

History of Surface Energy

Of the terms surface tension and surface energy the older expression is surface tension. The earliest mention of surface tension was written by an Niccolo Cabeo in 1629 Italy (CABEO, 1629; MILLINGTON, 1945). However, Segner from (then) Hungary wrote the first mathematical description of surface tension in 1751 and is often given the credit for introducing the concept (MILLINGTON, 1945; SEGNER, 1751). Theories that introduced molecular forces as causes of surface tension were published by Young (1805), Laplace (1806), Poisson (1830), Worthington (1884), Bakker (1928), Brown (1947), and Prandtl (1947) (BAKKER, 1928; BROWN, 1947; DE LAPLACE, 1806; POISSON, 1830; WORTHINGTON, 1885; YOUNG, 1805) (PRANDTL, 1947). Surface energy as a concept did not become introduced until Gauss in 1830(GAUSS, 1830). Gibbs discovered

in 1876 that the surface tension and the surface energy of a solid are not generally equal and that both vary with crystal face and direction (GIBBS, 1876; SHUTTLEWORTH, 1950). Rayleigh then discovered in 1890 that the surface tension of a one component liquid was equal to its surface energy (RAYLEIGH, 1890a; RAYLEIGH, 1890b; SHUTTLEWORTH, 1950). Modern research has primarily been focused on understanding mathematical relationships for nondispersive (electron donor/acceptor) and dispersive (primarily Van der Waals) forces of two and three phase systems as well as surface molecular reactions of both natural and manmade materials.

Surface Energy Measurement Methodology

The most common method to date for measuring surface energy is by observing the contact angle at a solid/liquid interface. This method takes advantage of the relationship between cohesion and adhesion. The cohesion of the liquid (bulk chemical energy of the liquid) influences the shape of the droplet into a sphere. The adhesion between the liquid and solid (interfacial surface energy) pulls the droplet toward the solid altering its sphericty. The strength of this force is a factor of gravity and the surface energy of the solid. Therefore, by measuring the contact angle of the interface using a liquid of known cohesion the surface energy components can be quantified (MAKKONEN, 2000; VAN OSS et al., 1988). This is shown in Figure 1-2. Although this technique has been used for quite some time methods used to measure the contact angle are still subject to fierce debate. In addition contact angle measurements rely on a smooth artificial surface for minerals that do not display perfect cleavage in one direction.

Another method to measure surface energy of solid minerals is to use inverse gas chromatography (IGC). IGC has proven to be a useful tool for powdered solids. IGC measures the surface properties of solids by injecting probe vapors of known properties into a chromatographic column. The column is filled with the solid of interest. As Saada explains (SAADA et al., 1995) the retention time and retention volume of the probe vapor will increase with greater affinity between the solid and vapor. The retention volume is the amount of probe vapor needed to push through the column. The reason that retention time and retention volume increase with affinity is that more vapor is needed to make up

for the amount adsorbed onto the surface of the powder solid. The disadvantage of IGC is the unlikelihood of probe vapors coming into contact with all the reactive sites in a packed column. For this reason γ^S_d and γ^S_{ab} are generally considered to be partial rather than mean values of surface energy (PAPIRER et al., 1986).

In addition to Inverse gas chromatography and methods to measure contact angles a technique called 'Thin Layer Wicking' has been used extensively to calculate surface energy of solids. This technique is based on liquid penetration (wicking) into a porous solid that is deposited in a thin layer on a silica plate. Surface energy is calculated by using Washburn's equation to relate the velocity of wicking of the penetrating liquid and changes in surface energy in this process (CHIBOWSKI and GONZALEZ-CABALLERO, 1993). The usefulness of the thin layer wicking method is its reproducibility. The major disadvantage, however, is the preparation of the solid. TLW is best used when a flat plane can be created on the solid. Much discussion has been raised on the validity of thin layer wicking as well as methods that measure liquid contact angles for solids which are not easily made into a flat plane or are not naturally so.

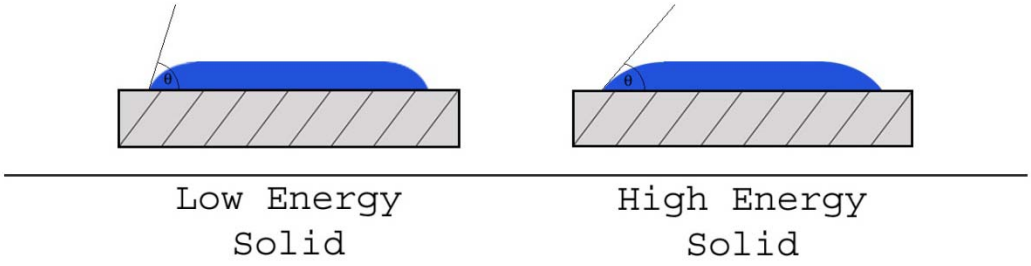

Figure 1-2 Low and High Energy Solid Contact Angles

Each of these techniques requires artificial surfaces created either through cutting or pressing powders (with the exception of very smooth phyllosilicates).However, an artificial surface will not have the same surface energy as the natural surface of the same material. Each of the above controls of surface energy (chemical, physical, and coatings) are changed when an artificial surface is created. Another device, however, is capable of measuring the surface energies of natural rocks and minerals. The universal sorption device (USD) carries the advantage of being a convenient method that can be used on a

routine basis with minimal human biases (BHASIN and LITTLE, 2007; HEFER et al., 2007). The universal sorption device is capable of simultaneously measuring specific surface area and surface energy components (van der Waals, Electron Acceptor, and Electron Donor) of minerals and aggregates. The USD is most effective for high-energy solids. The USD takes advantage of gas adsorption characteristics of selected solvents. The selected solvents have known surface tensions (surface energies). This method indirectly measures the surface free energy of minerals and aggregates based on the work of adhesion of the solvent vapor onto the solid. The selected vapors are n-hexane, Methyl propyl ketone/2-Pentanone, and water vapor.

The USD is made from a Rubotherm magnetic suspension balance system, computer, Rubotherm system software, SEMS (Surface Energy Measurement System, software developed by Bhasin and Little (BHASIN and LITTLE, 2007)) software, temperature control unit, laboratory vacuum, vacuum regulator, pressure transducer, vapor containers, and a vacuum dissector. The magnetic suspension coupling enables accurate measurement of mass without the balance coming into direct contact with the sample or vapors in the sorption cell. The Rubotherm magnetic suspension balance has the ability to measure a sample mass up to 200 g with an accuracy of 10^{-5} g (CHENG, 2002). This is easily sufficient for precise measurements of surface energy (CHENG, 2002). The SEMS software regulates the vapor pressure in the sorption cell and acquires mass, pressure, and temperature data as the test progresses. The mineral sample cage is made of a fine aluminum mesh screen. The surface tensions of the vapors were found in the literature and are recorded in the following table (VAN OSS et al., 1988). The following are the data obtained from the literature for the surface energy components of the reference vapors.

Research Objectives

Environmental reactions occur at interfaces. Interfacial characteristics, such as surface energy, control these reactions. However, there is not currently a comprehensive study of natural mineral and aggregate surface energies. Calculating the free surface

energy of a variety of common minerals and characterized aggregates comprised of those minerals will provide valuable information into organic rock interactions as well as aid in the development of a predictive model for aggregate surface energy based on mineralogy. The surface energy components (van der Waals, electron donor, and electron acceptor) of the minerals determine the ideal complimentary adsorbent, and environmental reactions primarily take place on surfaces. Therefore, surface energy is a valuable predictor of earth material's chemical behavior in both aqueous and nonaqueous systems.

The goals of this research were as follows:

1. Quantify the surface energy of a variety of the most common minerals and rocks as well as their component surface energies (dispersive, electron donor, and electron acceptor) using the Universal sorption device.
2. Develop a model for why minerals have quantified surface energy components (example: arrangement of atoms, types of active sites, etc.).
3. Develop a model for predicting aggregate bulk surface energies based on mineral composition. Test validity of $\gamma^{\mathrm{Aggregates}_{\mathrm{T}}} = \Sigma(\gamma^{\mathrm{Mineral}_{\mathrm{T}}} \bullet \mathrm{SA}) + \sigma$ equation as a predictive model. Where γ is measured in ergs/cm^2 and the surface area for each mineral is given as a percent of total of the aggregate total area.

Present Status of Surface Energy Research

Materials and Methods

The method to establish the pure phase minerals' surface energies involves using a new device called the Universal sorption device (USD)(BHASIN and LITTLE, 2007; BHASIN et al., 2007). The minerals and aggregates initially chosen are on Table 1-1 and 1-2. This device carries the advantage of being a convenient method that can be used on a routine basis with minimal biases. Before performing the test pure phase mineral samples will be purchased or obtained. These pure phase minerals will be well characterized using an electron microprobe. This characterization involves establishing the mineralogy and purity of each mineral as well as the surface characteristics.

Table 1-1 Preliminary Mineral Selection

Minerals	Group	Formula	Importance	Acquisition
Andesine	Tectosilicate	$Na_{(70-50\%)}Ca_{(30-50\%)}(Al,Si)AlSi_2O_8$	Dominant feldspar in andesite. Minor in granite and metamorphic rocks.	TAMU Collection
Albite	Tectosilicate	$NaAlSi_3O_8$	Found in granite and metamorphic rocks	Maine
Augite	Inosilicate	$(Ca,Na)((Mg,Fe,Al)(Si,Al)_2O_6$	An important rock-forming mineral in many igneous rocks, especially in gabbros and basalts. Augite is also found in hydrothermal metamorphic rocks.	TAMU Collection
Bassanite	Sulfate	$CaSO_4 \bullet 0.5H_2O$	Form of gypsum formed in arid landscapes	RNG Collection
Biotite	Phyllosilicate	$K(Mg,Fe)_3(AlSi_3O_{10})(OH)_2$	Common rock forming mineral present in most igneous rocks and both regional and contact	TAMU Collection
Calcite	Carbonate	$CaCO_3$	Common in sedimentary, metamorphic and igneous rocks.	Mexico
Cerussite	Carbonate	$PbCO_3$	An ore of lead	Tsumeb, Namibia
Dolomite	Carbonate	$CaMg(CO_3)_2$	A common sedimentary rock-forming mineral, dolomitic limestone.	RNG Collection

Table 1-1 Continued

Minerals	Group	Formula	Importance	Acquisition
Gypsum	Sulfate	$CaSO_4•_2H2O$	Common mineral found in arid landscapes	RNG Collection
Hematite	Iron Oxide	Fe_2O_3	Formed as a secondary weathering mineral in soils.	RNG Collection
Ilmenite	Iron Titanium Oxide	$FeTiO_3$	Common oxide in igneous environments	RNG Collection
Kaolinite	Clay	$Al_2Si_2O_5(OH)_4$	Common clay found in variety of soils and aggregates	RNG Collection
Quartz	Tectosilicate	SiO_2	Most abundant mineral of the crust; ubiquitous in all environments	Arkansas
Labradorite	Tectosilicate	$Ca_{(50-70\%)}Na_{(50-30\%)}(Al,Si)AlSi_2O_8$	Labradorite is a common feldspar.	Naim, Labrador
Microcline	Tectosilicate	$KAlSi_3O_8$	Common feldspar found in granites	TAMU Collection
Montmorillonite	Clay	$(Na,Ca)(Al,Mg)_6(Si_4O_{10})_3(OH)_6$	Common clay found in variety of soils and aggregates	RNG Collection
Muscovite	Phyllosilicate	$KAl_2(AlSi_3O_{10})(F,OH)_2$	Common silicate in igneous, sedimentary, and metamorphic environments.	RNG Collection

Table 1-1 Continued

Minerals	Group	Formula	Importance	Acquisition
Olivine (Forsterite)	Nesosilicate	$(Mg,Fe)_2SiO_4$	Found in ultramafic igneous rocks and marbles that formed from metamorphosed impure limestones.	San Carlos, Arizona
Rhodochrosite	Carbonate	$MnCO_3$	Minor ore of manganese.	RNG Collection
Siderite	Carbonate	$FeCO_3$	Common mineral found in sedimentary formations.	Idaho

Table 1-2 Preliminary Aggregate Selection

List of Aggregates				
Reference Aggregates	**Group**	**Rock Type**	**Minerals**	**Acquisition**
Lithonia Granite	RA	Granite & Basalt	Quartz, Microcline, Plagioclase, Biotite, Muscovite, Iron Oxides, Augite	SHRP
Granite	RB	Diorite	Quartz, Plagioclase, Hornblende, Biotite, Microcline	SHRP
Limestone	RC	Limestone	Calcite, Dolomite, Quartz	SHRP
Limestone	RD	Shaly Limestone	Calcite, Dolomite, Quartz	SHRP
Basalt	RK	Basalt	Iron Oxides, Plagioclase, Augite, Muscovite, Olivine, Iddingsite, Quartz, Microcline, Chert	SHRP
Gulf Coast Gravel	RL	Chert, Limestone, Granite, Misc.	Quartz, Ilmenite, Chalcedony, Calcite, Dolomite, Calcite, Microcline, Plagioclase, Ilmenite, Leucoxene, Muscovite, Iron Oxides	SHRP
Martin Marietta Sandstone	M.M.S.	Sandstone	Quartz, Feldspars, Calcite, Dolomite	SHRP

In order to establish a model for predicting aggregate bulk surface energies based on mineralogical composition well characterized aggregates were chosen. These aggregates are part of the Strategic Highway Research Program Materials reference Library. The aggregates have previously been tested on the USD and their surface energies have been published (BHASIN and LITTLE, 2007) in the literature. The list of preliminary aggregates and minerals is given in table 1-1 and 1-2. The aggregates and minerals were characterized in the same way on the electron microprobe with the

aggregates also being analyzed of the percent surface area that was covered with each mineral. The microprobe analyses will include multiple X-ray maps of each sample, back scatter electron images of each sample, and wavelength dispersive quantitative analyses of the exact chemical nature of each sample. The aggregates are included in the following chart. The minerals were chosen to compare well with the mineralogy of these aggregates.

Pretreatment

After the minerals were characterized they were be crushed with a stainless steel impact mortar to be retained by a #8 (2.36 mm) sieve and passed through a #4 (4.74 mm) ASTM standard sieve. This method was chosen as opposed to saws and pressed powders to mimic natural erosion by breaking along cleavage or fracturing. After the samples were crushed they were be washed with reverse osmosis water to remove large particles and then with distilled water. The minerals were then placed in an oven (Fisher Isotemp 200 series) at 75-80°C for at least one day. The samples were then allowed to cool for one hour and then were carried to the USD. They were not placed in a dessicator to cool so that they would continue to closely model minerals in the environment.

Universal Sorption Device

After the samples were oven dried approximately 20 to 25 grams will be placed in the sample cage, and the sample column is closed. The sample and sample column are then brought to vacuum (< 0.05 mbars) and hot degassed at 60°C for at least two hours. Next, the Rubotherm magnetic suspension balance is run continuously (autobalance) until the readings remain stable within 0.001g. When the analytical balance remains consistently stable n-hexane is introduced into the sample chamber. Hexane has no electron acceptor or electron donor components; therefore it only exerts van der Waals forces onto the mineral sample. For this reason, hexane can be used to calculate the van der Waals component for the mineral surface energy. The sample is then exposed to ten equal increments of partial vapor pressure from vacuum to saturation vapor pressure. After each increment the adsorbed mass is recorded to plot the isotherm after it reaches

equilibrium (BHASIN and LITTLE, 2007). The equation used to calculate the van der Waals component is:

$$\gamma^{Mineral}_{LW} = (\pi^{Mineral}_{Hex} + 2\gamma^{Total}_{Hex})^2/(4\gamma_{LW,Hex}) \quad \text{Eq. 1.5}$$

where $\gamma^{Mineral}_{LW}$ is the dispersive component of the mineral, $\pi^{Mineral}_{Hex}$ is the equilibrium film pressure of hexane on the mineral, γ^{Total}_{Hex} is the total surface tension (surface free energy) of the vapor hexane, and $\gamma_{LW,Hex}$ is the dispersive component of the surface tension of hexane (ZETTLEMOYER, 1969).

When the sample has reached equilibrium it is degassed, and the process is repeated with methyl propyl ketone as the reference vapor and a new 20-25g of sample. The equilibrium film pressure for MPK is calculated from the specific surface area measured with n-hexane and the MPK adsorption data. Methyl propyl ketone is monopolar and has zero γ^+ term. Thus, from the MPK adsorption isotherm and the dispersive component calculated from n-hexane the γ^+ can be calculated. The equation used to calculate the electron acceptor component is:

$$\gamma^{Mineral,+} = (\pi^{Mineral}_{MPK} + 2\gamma^{Mineral}_{MPK} - \sqrt{(\gamma^{MPK}_{LW} \bullet \gamma^{Mineral}_{LW})^2}/4\gamma^{-}_{MPK} \quad \text{Eq. 1.6}$$

where $\gamma^{Mineral,+}$ is the acid portion of the nondispersive (polar) component of the mineral, $\pi^{Mineral}_{MPK}$ is the equilibrium film pressure of Methyl propyl ketone (MPK) on the solid, $\gamma^{Mineral}_{MPK}$ is the total surface tension of MPK, $\gamma^{Mineral}_{MPK}$ is the dispersive component of the vapor(MPK), and γ^{-}_{MPK} is the base component of MPK.

Thus, the only unknown variable is the base component in this equation. After MPK has reached equilibrium the chamber is degassed and another 20-25g of sample is introduced and run through the same series of steps. This time water vapor is used as the reference solvent. Water vapor is bipolar and has all three components to surface tension. Therefore, it can be used to calculated the remaining variable, γ^-. After the equilibrium film pressure is calculated from the specific surface area under n-hexane. The equation used to calculate the electron donor component is:

$$\gamma^{Mineral,-} = (\pi^{Mineral}{}_{Wat} + 2\gamma^{Mineral}{}_{Wat} - 2\sqrt{(\gamma^{Mineral}{}_{LW} \bullet \gamma^{LW}{}_{Wat})} - 2\sqrt{(\gamma^{Mineral,+} \bullet \gamma^{-}{}_{Wat})^2}/4\gamma^{+}{}_{Wat}$$

Eq. 1.7

where $\gamma^{Mineral,-}$ is the base component of the surface energy of the mineral, $\pi^{Mineral}{}_{Wat}$ is the equilibrium film pressure of water vapor on the solid, $\gamma^{Total}{}_{Wat}$ is the total surface tension of water vapor, $\gamma^{LW}{}_{Wat}$ is the dispersive component of water vapor, $\gamma^{-}{}_{Wat}$ is the base component of the surface energy of water vapor, and $\gamma^{+}{}_{Wat}$ is the acid component of water vapor.

Data Analysis & Error Analysis

The surface energy components of the rocks and minerals are in units of energy per unit area (ergs/cm^2) so that the measurements will be normalized from variations in surface area. Surface area is calculated based the adsorption of n-hexane as a specific surface area, which is on a per gram basis. Several assumptions must be made in order to calculate the surface area. First, hexane is assumed to form a monolayer across the surface so that no hexane molecules will lay on top of each other and that there will be no gaps between molecules (BHASIN and LITTLE, 2007). Also, a hexane molecule is assumed to be 56.2Å^2. This number is from the literature as a best fit with laboratory data rather than based on molecular geometry (MCCLELLAN and HARNSBERGER, 1967). Hexane is expected to lie down on its long axis rather than across the short axis. Any crevices smaller than a hexane molecule will not be added to the total, however because the molecules will "lay across" the opening. This method carries similar difficulties and assumptions as the common use of N^2 to calculate surface areas, and has been shown to correlate well with N^2 measurements for the same materials (BHASIN and LITTLE, 2007). The three equations used to calculate the surface energy components are interdependent and therefore error from one carries over to the others. For this reason the error cannot be estimated based on the variance between film pressures. Therefore, the Delta method will be utilized with the software 'R' to estimate the standard error for each of the

components separately. One disadvantage is that the delta method assumes normality. This may be a correct assumption, but with only twelve data points for each sample it cannot be proven.

The most important contribution to "error" for this research is almost certainly natural heterogeneity. The mineral samples purchased are pure phase or near pure phase, however even among these samples there are likely significant differences between fragments. The aggregates are expected to display far greater heterogeneities than the minerals. Therefore, much of the variation between samples is likely not error, but rather the result for real differences between fragments and test runs.

CHAPTER II

CONCLUSIONS ON MEASURING THE SURFACE ENERGY OF A VARIETY OF THE MOST COMMON MINERALS

Introduction

Adhesion is the tendency of dissimilar molecules to maintain intimate contact. Adhesion impacts interfacial phenomena in a range of geologic systems such as: mineral surfaces and organic liquids and biofilms (HUTTENLOCH et al., 2001; ISAACSON and SAWHNEY, 1983; JOHNSTON, 1996; JURA and HARKINS, 1944; TICKNOR et al., 1996), remediation of nonaqueous-phase liquid contaminants such as trichloroethylene or methyl *tert* -butyl ether (SPARKS, 2005; STENSTRÖM and KJELLEBERG, 1985; ZIELKE and PINNAVAIA, 1988), the migration of petroleum in sedimentary basins (BARKER, 1980; BENNER and BARTEL, 1941; EVDOKIMOV et al., 2001; GONZALEZ and MOREIRA, 1991), bacterial affinity for mineral surfaces (CLINT and WICKS, 2001; EDWARDS and RUTENBERG, 2001; LOWER and TADANIER, 2000; LUTTGE et al., 2005), formation of superhydrophobic surfaces (FENG et al., 2008; MICHIELSEN and LEE, 2007; NOSONOVSKY and BHUSHAN, 2008), and implant technology on the human muscular-skeletal system (BUCCI-SABATTINI et al.; DELIGIANNI et al., 2001; KHANG et al., 2008; PEARCE et al., 2008)

Adhesion involving geologic materials is controlled by the interfacial characteristics of rocks and minerals, specifically the surface energy of natural minerals and rocks. Surface energy is a thermodynamic construct defined as the work necessary to form unit area of surface by a process of division (PARKS, 1990; SHUTTLEWORTH, 1950). Surface energy of natural substances can be divided into two major components: van der Waals and polar forces. Van der Waals forces are present in all molecules to varying degrees. Polar forces are found where electron donor/electron acceptor interactions take place. The chemical components are: the Lifshitz-van der Waals, the electron donor, and the electron acceptor components (VAN OSS et al., 1988; VAN OSS et

al., 2001). The Lifshitz-van der Waals component is a grouping of three different interactions: the van der Waals-Keesom, the van der Waals-Debye, and the van der Waals-London force. As Overbeek discovered in 1952 these three forces are additive (OVERBEEK, 1952; VAN OSS, 2006). Therefore, they can be described simply as:

$$\gamma^{LW} = \gamma^{L} + \gamma^{D} + \gamma^{K} \qquad \text{Eq. 2.1}$$

where γ^{L}, γ^{D}, and γ^{K} are the London, Debye, and Keesom interactions respectively. When all three of these interactions are grouped together they collectively become known as Lifshitz-van der Waals interactions.

In addition to Lifshitz-van der Waals forces the other major component to surface energy is the polar or electron acceptor-donor component. This portion of the surface energy can be up to two orders of magnitude greater than the van der Waals component, however it is strongest at less than ten Å (VAN OSS, 2006). The polar component of surface energy is quantified in Good-van Oss Theory (vOGT) as (VAN OSS et al., 1988):

$$\gamma^{S}_{ab} = 2\sqrt{(\gamma^{+}\,\gamma^{-})} \qquad \text{Eq. 2.2}$$

where γ^{S}_{ab} is the total polar component, γ^{+} is the Lewis acid component, and γ^{-} is the Lewis base component. Fowkes showed that the total surface energy of a solid is a sum of the two components (FOWKES, 1964):

$$\gamma^{T} = \gamma^{LW} + \gamma^{S}_{ab} \qquad \text{Eq. 2.3}$$

Therefore, combining these equations gives the total surface energy as:

$$\gamma^{T} = \gamma^{LW} + 2\sqrt{(\gamma^{+}\,\gamma^{-})} \qquad \text{Eq. 2.4}$$

The polar or Lewis acid-base interactions are probably mainly hydrogen donor and hydrogen acceptor reactions (VAN OSS et al., 2001). However, it is more useful to define "polar" more broadly for all electron acceptor-donor interactions. In this way all of the interactions with similar donor/acceptor affects can be measured. The major difference between Lifshitz-van der Waals interactions and polar interactions is that electron donor-acceptor reactions are not symmetrical as are van der Waals interactions. The molecular polarizabilities and the ionization energies enter the equations for the dispersion (polar) force symmetrically (VAN OSS, 2006). In an electron acceptor/donor

relationship this symmetry does not exist. This is because in a strict sense a basic functional group, such as a carboxylic acid, will not interact as a base with another basic entity. One must act as an electron donor and the other must act as an electron acceptor (McMurry, 2004). Nondispersive forces only occur when there are complimentary groups present (an electron acceptor and an electron donor in a Lewis sense). For this reason the duality of electron acceptor-donor interactions must be treated together yet understood separately. For instance, a monopolar substance, such as methyl propyl ketone, has a total polar surface energy of zero because $\gamma^+ = 0$. However, $\gamma^- = 0$. Therefore, methyl propyl ketone can react through polar interactions with any other monopolar substance with an electron acceptor component or with any bipolar substance despite the fact that its polar surface energy is zero.

We theorize that surface energy of natural minerals is controlled by three master variables that describe the chemical properties of rock and mineral surface: i). Surface chemical composition of the rock or mineral, ii). surface morphology, and iii). surface coatings. Natural mineral surfaces have a variety of types of chemically reactive sites. These sites include: nonpolar active sites on low changed minerals, polar surfaces such as permanently charged, and conditionally charged Lewis acid/base sites (Johnston 2002). These sites have important chemical characteristics that determine their reactivity. The type and magnitude of these sites is described by the individual surface energy components (Costanzo et al., 1990; Fowkes, 1972; Janczuk and Bialopiotrowicz, 1988). Thus, the surface energy of minerals is determined by the types of sites on the surface. The ability to predict the magnitude of these components (and subcomponents), as a function of mineral and rock chemical properties, is valuable in predicting the dominant interfacial reactions that control adhesion between different chemical species and rock or mineral surfaces in a wide range of systems.

Surface roughness is a molecular scale feature that can also affect the surface energy of natural minerals (Boyd and Livingston, 1942). Surface roughness is a measure of deviation from ideality in structure (Whitehouse, 1994). Two surfaces of identical area and chemistry but different surface roughness can have very different

surface energies (ERBIL, 2003; FENG et al., 2002; MIWA et al., 2000). To date no systematic study has been performed on the effect of surface roughness on natural mineral surface energies. Current research on superhydrophobic surfaces, however has made the importance of structure on surface energy clear.

The ability of surface coatings to alter the surface energy of solids has been well documented (CALLOW and FLETCHER, 1994; ISTA et al., 2004; LOWER and TADANIER, 2000; STASZCZUK and BILINSKI, 1987). Coatings essentially create new surfaces when they adsorb and create a separate phase (FOWKES and HARKINS, 1940). Coatings can be organic and inorganic. Practically no surface in the natural environment is without surface coatings. Thus, surface energy measurements of minerals and aggregates which attempt to present "clean" surfaces may have little or no correlation to geologic materials in the natural environment.

While surface energy is a thermodynamic construct, the actual value for a specific mineral or rock surface is dependent on the method used. The surface energy of a number of minerals and aggregates have been characterized using a range of techniques such as: thin layer wicking (TLW) (CHIBOWSKI and GONZALEZ-CABALLERO, 1993; KARAGÜZEL et al., 2005; LOBATO et al., 2006), inverse gas chromatography (IGC) (KUBILAY et al., 2006; LAZAREVIC et al., 2009; PERRUCHOT et al., 2006), gravimetric sorption techniques (CHIBOWSKI and STASZCZUK, 1988; PUGH and STENIUS, 1985; VISWANATH and RAVISHANKAR, 2008), and contact angles (GOEBEL et al., 2004; HELMY et al., 2007; SHANG et al., 2009). These techniques may not be comparable based on the multiplicity of preparation procedures. Contact angle studies, in particular, have been the subject of rigorous analytical and methodological debate (CHIBOWSKI and PEREA-CARPIO, 2002; DELLA VOLPE and SIBONI, 1997; KWOK, 1999; MAKKONEN, 2000; VAN OSS, 2006) .There has not yet been a comprehensive study of the surface energies of a variety of the most common minerals and aggregates using consistent methodology. In addition there has not yet been a study of the effect of these three master variables on surface energies of natural minerals and rocks.

We are addressing the question by measuring the surface energy of 22 common minerals using a universal sorption device (USD) (BHASIN and LITTLE, 2007; CHENG, 2002a; LITTLE and BHASIN, 2007). The USD, which uses the reference vapors listed in Table 2-,1 simultaneously measures the surface energy of each of the sides of mineral fragments. The probe vapors are listed in table 2-1. The device does not require the surfaces to be artificially created as thin layer wicking and contact angle measurements do. Contact angle measurements, for instance, required use of a diamond saw or other cutting device to achieve a very smooth flat surface thus altering the surface characteristics. The surface energies were broken down into van der Waals, Lewis Acid, and Lewis Base components. The samples' bulk and surface chemistries were characterized with wavelength and energy dispersive spectra (WDS & EDS) analyses on an electron microprobe and x-ray photoelectron spectroscopy (XPS). The XPS was also used to quantify the organic and inorganic coatings on the mineral and surfaces. The surface morphology was analyzed for roughness with processing software on SEM images. The analyses highlighted the importance of all three master variables (surface chemistry, surface coatings, and surface morphology) in the type and magnitude of surface energy of natural minerals and rocks in the environment.

Materials and Methods

Pretreatment

The sample pretreatment was designed to alter the chemical and physical characteristics of the samples as little as possible. The purpose of this was to provide data values and comparisons of samples as closely as possible to their environmental states. The samples were originally washed with reverse osmosis water as opposed to distilled water to remove large particles and minimize surface reactions. The samples were crushed with a stainless steel impact mortar to

Table 2-1 Surface Energy Literature Values for Reference Vapors

Surface Energy Components of Reference Vapors				
Probe Vapor	γ^{VDW} ergs/cm^2	γ^{+} ergs/cm^2	γ^{-} ergs/cm^2	γ^{Total} ergs/cm^2
n-hexane	18.4	0.0	0.0	18.4
Methyl Propyl Ketone	24.7	0.0	19.6	24.7
Water Vapor	21.8	25.5	25.5	72.8

γ^{VDW}= van der Waals, γ^{+} = Lewis Acid Component, γ^{-} = Lewis Base Component

be retained by a #8 (2.36 mm) sieve and passed through a #4 (4.74 mm) ASTM standard sieve. This method was chosen as opposed to saws and pressed powders to mimic natural erosion by breaking along cleavage or fracturing. After the samples were crushed they were be washed with reverse osmosis water again to remove large particles. The minerals were then placed in an oven (Fisher Isotemp 200 series) at 75-80°C for at least one day. This temperature was chosen to minimally alter mineral structure while removing some surface volatiles. The samples were allowed to cool for one hour and then were carried to the instrument to be analyzed. They were not placed in a dessicator to cool so that they would continue to closely model minerals in the environment.

Chemical Characterization

The purpose of the chemical characterization was to analyze the chemical properties of representative minerals given in Table 2-2. This was done using an electron microprobe to obtain quantitative elemental analyses of individual minerals and X-ray elemental distribution maps as well as BSE (back-scattered electron) images for the bulk composition. The surface composition was analyzed with an X-Ray Photoelectron Spectrometer. Elemental composition and crystallographic structure control the concentration and chemistry of surface functional groups on the mineral surfaces. The complex arrangement of atoms in well-crystallized silicate, carbonate and oxide minerals are expected to yield very different surface bonds then would be present in an amorphous supercooled liquid such as a glass.

Table 2-2 Final Selection of Minerals

List of Minerals				
Minerals	**Group**	**Formula**	**Importance**	**Acquisition**
Andesine	Tectosilicate	$Na_{(70-50\%)}Ca_{(30-50\%)}(Al,Si)AlSi_2O_8$	Dominant feldspar in andesite. Minor in granite and metamorphic rocks.	TAMU Collection
Albite	Tectosilicate	$NaAlSi_3O_8$	Found in granite and metamorphic rocks	Maine
Augite	Inosilicate	$(Ca,Na)((Mg,Fe,Al)(Si,Al)_2O_6$	An important rock-forming mineral in many igneous rocks, especially in gabbros and basalts. Augite is also found in hydrothermal metamorphic rocks.	TAMU Collection
Bassanite	Sulfate	$CaSO_4 \bullet 0.5H_2O$	Form of gypsum formed in arid landscapes	RNG Collection
Biotite	Phyllosilicate	$K(Mg,Fe)_3(AlSi_3O_{10})(OH)_2$	Common rock forming mineral present in most igneous rocks and both regional and contact	TAMU Collection
Calcite	Carbonate	$CaCO_3$	Common in sedimentary, metamorphic and igneous rocks.	Mexico
Cerussite	Carbonate	$PbCO_3$	An ore of lead	Tsumeb, Namibia

Table 2-2 Continued

Minerals	Group	Formula	Importance	Acquisition
Dolomite	Carbonate	$CaMg(CO_3)_2$)	A common sedimentary rock-forming mineral, dolomitic limestone.	RNG Collection
Gypsum	Sulfate	$CaSO_4•_2H2O$	Common mineral found in arid landscapes	RNG Collection
Hematite	Iron Oxide	Fe_2O_3	Formed as a secondary weathering mineral in soils.	RNG Collection
Ilmenite	Iron Titanium Oxide	$FeTiO_3$	Common oxide in igneous environments	RNG Collection
Kaolinite	Clay	$Al_2Si_2O_5(OH)_4$	Common clay found in variety of soils and aggregates	RNG Collection
Quartz	Tectosilicate	SiO_2	Most abundant mineral of the crust; ubiquitous in all environments	Arkansas
Labradorite	Tectosilicate	$Ca_{(50-70\%)}Na_{(50-30\%)}(Al,SI)AlSi_2O_8$	Labradorite is a common feldspar.	Naim, Labrador
Microcline	Tectosilicate	$KAlSi_3O_8$	Common feldspar found in granites	TAMU Collection
Montmorillonite	Clay	$(Na,Ca)(Al,Mg)_6(Si_4O_{10})_3(OH)_6$	Common clay found in variety of soils and aggregates	RNG Collection
Muscovite	Phyllosilicate	$KAl_2(AlSi_3O_{10})(F,OH)_2$	Common silicate in igneous, sedimentary, and metamorphic environments.	RNG Collection

Table 2-2 Continued

Minerals	Group	Formula	Importance	Acquisition
Olivine (Forsterite)	Nesosilicate	$(Mg,Fe)_2SiO_4$	Found in ultramafic igneous rocks and marbles that formed from metamorphosed impure limestones.	San Carlos, Arizona
Rhodochrosite	Carbonate	$MnCO_3$	Minor ore of manganese.	RNG Collection
Siderite	Carbonate	$FeCO_3$	Common mineral found in sedimentary formations.	Idaho

X-Ray Photoelectron Spectrometer

After the samples cooled one to four randomly selected fragments were taken to the X-Ray Photoelectron Spectroscope (XPS) for surface chemistry analysis. The XPS used is a Kratos Axis Ultra Imaging X-ray photoelectron spectrometer capable of detecting chemical variations of the upper 14 nanometers on a spot size of approximately 400 X 700 microns. The XPS is capable of measuring atomic percents of surface elements with an atomic mass greater than helium. Oxidation state was well as certain types of bonds can be differentiated through this technique. The relative sensitivity factors used are listed in Table 2-3.

The samples were placed in the XPS and pumped to 10^{-8} to 10^{-9} Torr. Each fragment was then irradiated with soft X-Ray photons (1-2 keV) using a monochromatic aluminum Kα X-ray source, and the instrument measures the energies of excited photoelectrons. The binding energy is then recorded along with the counts per second. The binding energy is then calculated according to the equation:

$$E_{Binding} = E_{Photon} - (E_{Kinetic} + \rho) \qquad \text{Eq. 2.5}$$

where E_{Photon} is the energy of the X-ray photos used, $E_{Kinetic}$ is the kinetic energy of the electron measured, and ρ is the work function (minimum energy needed to remove an electron from a solid) of the spectrometer. The XPS then plots a spectrum of the number of electrons detected (counts per second) and binding energy. Each of the elements of interest was then correlated with particular binding energies based on literature values. The elemental binding energies and the elements quantified for each mineral are listed in tables 2-4 and 2-5. The number of counts is proportional to the amount (atomic concentration) of the species; however each species must be corrected with a relative sensitivity factor (RSF). The RSF values chosen are in table 2-3.

Electron Microprobe

An electron microprobe was used to obtain quantitative elemental analyses of individual minerals and X-ray elemental distribution maps as well as BSE (back-scattered electron) images. The electron microprobe is a Cameca SX50 equipped with 4 wavelength-dispersive (WDS) X-ray spectrometers, PGT energy-dispersive X-ray system and cathodoluminescence detector. WDS was used to establish the bulk chemistry of the minerals. Each of the samples was tested on at least 25 individual data points in order to minimize sampling error. In addition to mineral chemistry, the microprobe BSE images provided valuable information on the homogeneity of the mineral samples. The microprobe analyses were also used to choose the wavelength spectra needed for the XPS based on the measured bulk chemistries.

Table 2-3 Relative Sensitivity Factors for XPS

Relative Sensitivity Factors	
Mg 2p	0.168
Al 2p	0.190
C 1s	0.280
Si 2p	0.328
S 2p	0.668
O 1s	0.780
F 1s	1.000
Na 1s	1.685
K 2p	1.466
Ca 2p	1.830
Ti 2p	2.001
Mn 2p	2.660
Fe 2p	2.960
Pb 4f	8.329

Table 2-4 XPS Peak Positions (eV) by Mineral

Sample	Na 1s	Fe 2p	F 1s	Mn 2p	O 1s	Ti 2p	Ca 2p	C 1s	K 2p	S 2p	Pb 4f	Si 2p	Al 2p	Mg 2p
Carbonates														
Calcite (1)	--	--	--	--	530.35	--	346.15	288.90	--	--	--	--	--	--
Dolomite (1)	--	--	--	--	530.55	--	346.45	284.30	--	--	--	--	--	49.55
Cerussite (2)	--	--	--	642.85	529.10	--	345.00	282.95	--	--	137.10	--	--	--
Rhodochrosite (2)	--	707.65	--	640.70	529.35	--	345.05	283.00	--	--	--	--	--	48.65
Siderite (2)	--	709.05	--	--	530.50	--	348.50	284.10	--	--	--	--	--	49.65
Avg.	--	708.35	--	641.78	529.97	--	346.23	284.65	--	--	137.10	--	--	49.28
Sulfates														
Gypsum (1)	--	--	--	--	531.15	--	347.25	284.40	--	168.75	--	--	--	--
Bassanite (1)	--	--	--	--	531.15	--	347.15	284.50	--	168.75	--	--	--	--
Avg.	--	--	--	--	531.15	--	347.20	284.45	--	168.75	--	--	--	--
Silicates														
Olivine (1)	--	708.20	--	640.00	530.10	--	--	284.40	--	--	--	101.40	--	49.80
Augite (4)	1068.75	709.78	--	638.90	529.65	--	345.88	283.30	--	--	--	101.20	73.60	50.23
Hornblende (1)	1069.90	710.80	684.20	--	530.70	458.20	346.90	284.40	292.50	--	--	102.30	74.30	50.10
Biotite (1)	1070.55	709.88	684.20	640.55	530.65	457.95	--	284.30	292.90	--	--	102.10	73.75	53.05
Muscovite (1)	1069.40	710.88	688.00	--	530.80	--	346.90	284.30	292.50	--	--	102.10	74.20	--
Microcline (2)	1069.95	--	--	--	530.80	--	--	284.30	292.25	--	--	102.10	73.95	--
Albite (1)	1068.70	--	--	--	529.50	--	--	282.80	--	--	--	100.90	72.60	--
Labradorite (1)	1070.40	--	--	--	531.00	--	347.40	284.40	292.70	--	--	102.30	74.10	--
Avg.	1069.66	709.91	685.47	639.82	530.40	458.08	346.77	284.03	292.57	--	--	101.80	73.79	50.79
Oxides														
Quartx (1)	--	--	--	--	531.45	--	--	284.10	--	--	--	102.75	--	--
Hematite (4)	--	710.05	--	--	529.25	--	--	283.95	--	--	--	101.68	--	--
Ilmenite (4)	--	710.80	--	--	530.40	--	--	284.40	--	--	--	--	--	--
Avg.	--	710.43	--	--	530.37	--	--	284.15	--	--	--	102.21	--	--
Clays														
Mont. (2)	--	711.28	--	--	530.20	--	348.05	283.15	--	--	--	101.40	73.05	48.40
Kaolinite (2)	--	716.93	--	--	531.60	--	--	284.85	--	--	--	103.00	74.70	--
Avg.	--	714.10	--	--	530.90	--	348.05	284.00	--	--	--	102.20	73.88	48.40
Avg. (Total)	1069.89	710.49	685.47	640.60	530.59	458.08	347.08	284.33	292.84	168.75	137.10	102.18	73.99	50.53

Table 2-5 Atomic Species Tested on XPS

Mineral	**# of Tests**	**Atomic Species**
Albite	1	Na 1s, O 1s, C 1s, K 2p*, Si 2p, Al 2p
Bassanite	1	O 1s, Ca 2p, C 1s, S 2p
Calcite	1	O 1s, Ca 2p, C 1s
Dolomite	1	Fe 2p*, O 1s, Ca 2p, C 1s, Mg 2p, Mn 2p*
Gypsum	1	O 1s, Ca 2p, C 1s, S 2p
Hornblende	1	Na 1s, Fe 2p, O 1s, Ca 2p, C 1s, K 2p**, Si 2p, Al 2p, Mg 2p, Ti 2p, F 1s**, Mn 2p
Labradorite	1	Na 1s, Fe 2p*, O 1s, Ca 2p, C 1s, K 2p*, Si 2p, Al 2p, Ba 4d*
Muscovite	1	Na 1s*, Fe 2p**, O 1s, Ca 2p, C 1s, K 2p, Si 2p, Al 2p, Ba 4d, F 1s**, Mg 2p*, Ti 2p*
Olivine	1	Fe 2p, O 1s, C 1s, Si 2p, Mg 2p, Mn 2p*
Quartz	1	O 1s, C 1s, Si 2p
Biotite	2	Na 1s*, Fe 2p**, O 1s, C 1s, K 2p, Si 2p, Al 2p, Mg 2p, Ti 2p**, Mn2p*, F 1s**
Cerussite	2	Pb 4f, Fe 2p**, O 1s, Ca 2p*, C 1s, Mg 2p, Mn 2p**
Hematite	2	Fe 2p, O 1s, C 1s, Si 2p**
Ilmenite	2	Fe 2p, O 1s, C 1s, Mg 2p*, Ti 2p, Mn 2p**
Kaolinite	2	Fe 2p, O 1s, C 1s, Si 2p, Al 2p
Microcline	2	Na 1s**, O 1s, C 1s, K 2p, Si 2p, Al 2p
Montmorillonite	2	Na 1s, Fe 2p, O 1s, Ca 2p, C 1s, Si 2p, Al 2p, Mg 2p, Mn 2p
Rhodochrosite	2	Pb 4f*, Fe 2p**, O 1s, Ca 2p*, C 1s, Mg 2p, Mn 2p
Siderite	2	Fe 2p, O 1s, Ca 2p*, C 1s, Mg 2p, Mn 2p**
Andesine	4	Na 1s, Fe 2p*, O 1s, Ca 2p, C 1s, K 2p*, Si 2p, Al 2p
Augite	4	Na 1s**, Fe 2p, O 1s, Ca 2p, C 1s, Si 2p, Al 2p, Mg 2p, Mn 2p*

* = Expected to be <1% atomic composition

** = Expected to be 1– 5% atomic composition

Universal Sorption Device

The universal sorption device was used to measure the surface energy components of the mineral samples. After the samples were oven dried approximately 20 to 25 grams were placed in the sample cage, and the sample column was closed. The sample and sample column were then brought to vacuum (< 0.05 mbars) and hot degassed at 60°C for at least two hours. Next, the Rubotherm magnetic suspension balance was run continuously (autobalance) until the readings remain stable within 0.001g. When the analytical balance remained consistently stable n-hexane was introduced into the sample chamber. The column assembly and the layout of the USD are shown in Figures 2-1 and 2-2. Hexane has no electron acceptor or electron donor components; therefore it only exerts van der Waals forces onto the mineral sample. For this reason, hexane can be used to calculate the van der Waals component for the mineral surface energy. The sample was then exposed to ten equal increments of partial vapor pressure from vacuum to saturation vapor pressure. After each increment the adsorbed mass is recorded to plot the isotherm after it reaches equilibrium (BHASIN and LITTLE, 2007). The equation used to calculate the van der Waals component is:

$$\gamma^{Mineral}{}_{LW} = (\pi^{Mineral}{}_{Hex} + 2\gamma^{Total}{}_{Hex})^2/(4\gamma_{LW,Hex}) \qquad \text{Eq. 2.6}$$

where $\gamma^{Mineral}{}_{LW}$ is the dispersive component of the mineral, $\pi^{Mineral}{}_{Hex}$ is the equilibrium film pressure of hexane on the mineral, $\gamma^{Total}{}_{Hex}$ is the total surface tension (surface free energy) of the vapor hexane, and $_{LW,Hex}$is the dispersive component of the surface tension of hexane (ZETTLEMOYER, 1969).

When the sample has reached equilibrium it is degassed, and the process is repeated with methyl propyl ketone as the reference vapor and a new 20-25g of sample. The equilibrium film pressure for MPK is calculated from the specific surface area measured with n-hexane and the MPK adsorption data. Methyl propyl ketone is monopolar and has zero γ^+ term. Thus, from the MPK adsorption isotherm and the dispersive component calculated from n-hexane the γ^+can be calculated.

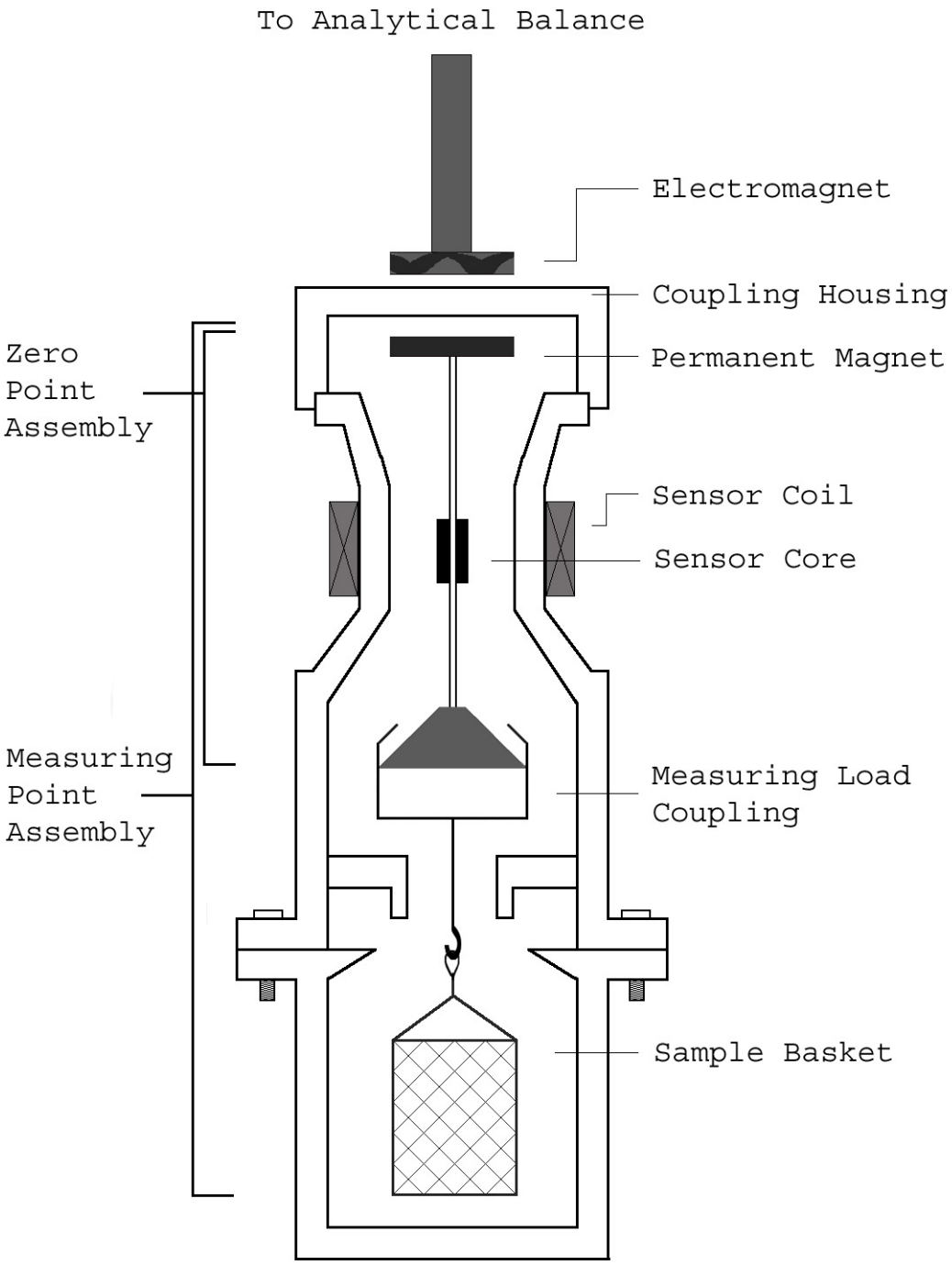

Figure 2-1 Rubotherm Column Assembly

The equation used to calculate the electron acceptor component is:

$$\gamma^{Mineral,+} = (\pi^{Mineral}_{MPK} + 2\gamma^{Mineral}_{MPK} - \sqrt{(\gamma^{MPK}_{LW} \bullet \gamma^{Mineral}_{LW})^2}/4\gamma^{-}_{MPK} \quad \text{Eq. 2.7}$$

where $\gamma^{Mineral,+}$ is the acid portion of the nondispersive (polar) component of the mineral, $\pi^{Mineral}_{MPK}$ is the equilibrium film pressure of Methyl propyl ketone (MPK) on the solid, γ^{-}_{MPK} is the total surface tension of MPK, γ^{MPK}_{LW} is the dispersive component of the vapor(MPK), and γ^{-}_{MPK} is the base component of MPK.

Thus, the only unknown variable is the base component in this equation. After MPK has reached equilibrium the chamber is degassed and another 20-25g of sample is introduced and run through the same series of steps. This time water vapor is used as the reference solvent. Water vapor is bipolar and has all three components to surface tension. Therefore, it can be used to calculated the remaining variable, γ^{-}. After the equilibrium film pressure is calculated from the specific surface area under n-hexane. The equation used to calculate the electron donor component is:

$$\gamma^{Mineral,-} = (\pi^{Mineral}_{Wat} + 2\gamma^{Mineral}_{Wat} - 2\sqrt{(\gamma^{Mineral}_{LW} \bullet \gamma^{LW}_{Wat})} - 2\sqrt{(\gamma^{Mineral,+} \bullet \gamma^{-}_{Wat})^2}/4\gamma^{+}_{Wat}$$

Eq. 2.8

where $\gamma^{Mineral,-}$ is the base component of the surface energy of the mineral, $\pi^{Mineral}_{Wat}$ is the equilibrium film pressure of water vapor on the solid, γ^{Total}_{Wat} is the total surface tension of water vapor, γ^{LW}_{Wat} is the dispersive component of water vapor, γ^{-}_{Wat} is the base component of the surface energy of water vapor, and γ^{+}_{Wat} is the acid component of water vapor.

Therefore, n-hexane was chosen to calculate the dispersive component of the surface energy. The work of adhesion is related to film pressure as:

$$W_A = \pi^{Mineral}_{V} + 2\gamma^{Total}_{V} \quad \text{Eq. 2.9}$$

$$W_A = 2\sqrt{(\gamma^{Mineral}{}_{LW} \bullet \gamma_{LW,V})} + 2\sqrt{(\gamma^{Mineral,+} \bullet \gamma^{-}{}_{V})} + 2\sqrt{(\gamma^{Mineral,-} \bullet \gamma^{+}{}_{V})} \quad \text{Eq. 2.10}$$

Therefore, all three of the unknown variables can be quantified using known data from the literature for the reference vapors and the calculated equilibrium film pressures.

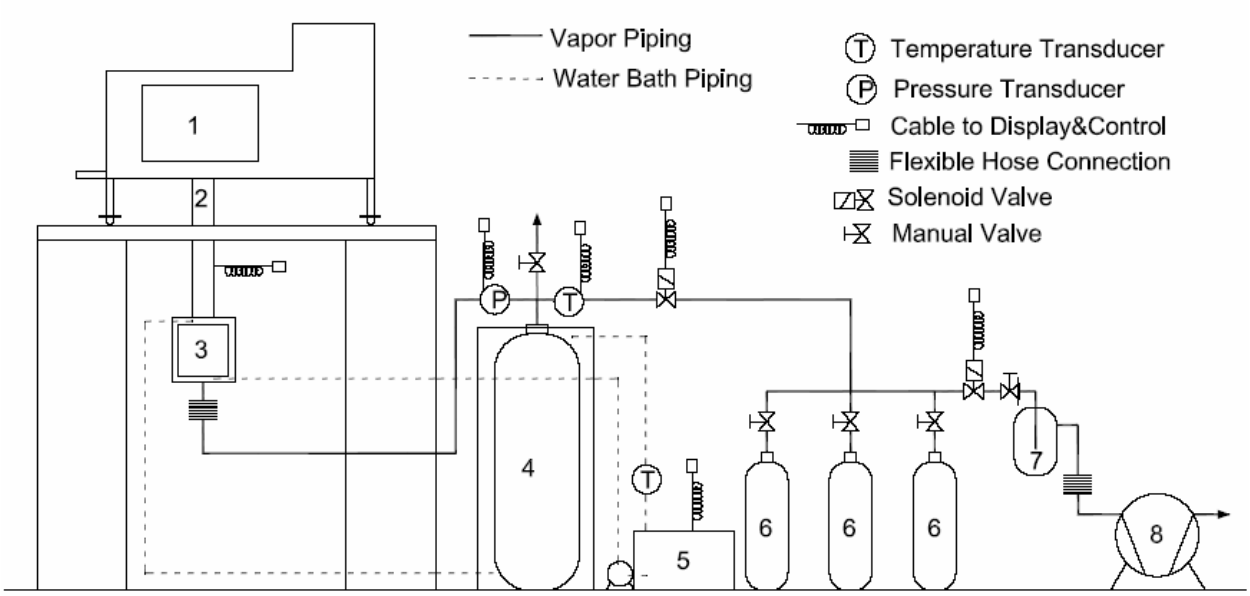

Figure 2-2 Universal Sorption Device (Bhasin 2006)

1. Microbalance 2. Magnetic suspension 3. Sample cell
4. Buffer Tank containers 5. Water bath 6. Probe liquid
7. Knock out tank 8. Vacuum pump

Quality Assurance/Quality Control

Grain Sizes

Each of the minerals were obtained or purchased in as few pegmatitic grains as possible. Some of the samples were from one large rock while others were from several small rocks of similar genesis. This process reduces heterogeneity. Samples were

fragmented with an impact mortar to fall between and number 4 and number 10 sieve. Care was taken to keep fragments similar in size.

Specific Surface Area

Measuring specific surface area (SSA) of minerals and aggregates is a function of density, surface morphology, size and type probe vapor, and grain size. SSA is measured in area per unit mass. Although seeming independent of grain size SSA varies based on this parameter (WHITE and BRANTLEY, 2003). Because surface energy is dependent on SSA then, it was important to maintain quality on the fragment sizes used in the USD. Quality assurance was performed by taking a random subset of mineral fragments used in the surface energy analysis for each mineral and quantitatively measuring area, perimeter length, major and minor axis length, and deviation from sphericity of each fragment. Measurements were taken with NIH software. The samples were then weighed and estimated heights were calculated based on average density. Finally the average weight was calculated based on the number of fragments. The data is listed in Table 2-6 and Figure 2-3.

The majority of the minerals had major axis lengths of .66 to .91 cm and minor axis lengths of .40 to .56 cm. These fall into the data cloud in the center of the fragment size analysis graph. The gypsum fragments were the largest grouping. These fragments were used for gypsum, hot gypsum, and bassanite. Fragment sizes for these three should be assumed to be equal. The major axis, minor axis, and estimated height were 1.3, 0.69, and 0.25 cm with standard deviations of 0.44, 0.27, and 0.25 cm. Biotite and muscovite were also outside of the data cloud because of the irregularity of phyllosilicate cleavage. Biotite and muscovite were very similar to each other. Biotite average dimensions were 1.06, 0.69, and 0.06 cm. Muscovite average dimensions were 1.25, 0.86, and 0.04 cm. Difficulties preparing the siderite fragments also placed the fragments size just outside the data cloud. This was based on the desire to have no oxidized surface analyzed in the sorption device for this mineral. The sample obtained had visible oxidation on the outside. After fragmentation with the impact mortar tweezers were used to separate fragments with oxidation on any surface. This caused the sample to be broken to smaller

sizes to remove all oxidation while having enough sample left for analysis. This effect does not appear to be large however with siderite having average dimensions of .33, 0.21, and 0.46 cm.

Bulk Moisture and Elemental Analysis

Bulk Properties

Surface energy is a characteristic that is affected by the interior as well as the exterior features of the solid (SHUTTLEWORTH, 1950). Van der Waals interactions, which are dependent on molecular weight, exert forces up to ℓ^{-2} where ℓ is equal to the diameter of the atomic particle (HAMAKER, 1937; NAPPER, 1983). In the case of solid minerals this force can equal up to a few tens of angstroms because of the additive nature of van der Waals forces (NAPPER, 1983). This extends the effect several unit cells into the mineral structure. Lewis acid-base components of surface energy do not exert forces as far as van der Waals. Polar components are strongest at less than ten angstroms (VAN OSS, 2006). Polar forces may be shorter range than van der Waals components, but they can exert forces up to two orders of magnitude greater (VAN OSS, 2006).

Table 2-6 Grain Size Analysis

Mineral		Area			(Major Axis)/(Minor Axis)			Estimated Height		
Feldspars	# Frag	Avg.	St. Dev.	95% CI	Avg.	St. Dev.	95% CI	Avg.	St. Dev.	95% CI
Albite	96	0.313	0.201	0.27 - 0.35	1.989	0.857	1.82 - 2.16	0.241	0.169	0.21 - 0.27
Labradorite	179	0.222	0.133	0.20 - 0.24	1.681	0.47	1.61 - 1.75	0.155	0.086	0.14 - 0.17
Microcline	114	0.215	0.183	0.18 - 0.25	1.844	0.668	1.72 - 1.97	0.156	0.114	0.14 - 0.18
Sulfates	# Frag	Avg.	St. Dev.	95% CI	Avg.	St. Dev.	95% CI	Avg.	St. Dev.	95% CI
Gypsum	38	0.768	0.434	0.63 - 0.91	1.998	0.597	1.81 - 2.19	0.252	0.393	0.13 - 0.38
Carbonates	# Frag	Avg.	St. Dev.	95% CI	Avg.	St. Dev.	95% CI	Avg.	St. Dev.	95% CI
Calcite	134	0.254	0.202	0.22 - 0.29	1.695	0.599	1.59 - 1.80	0.287	0.281	0.24 - 0.33
Dolomite	43	0.422	0.224	0.36 - 0.49	1.656	0.387	1.54 - 1.77	0.245	0.153	0.20 - 0.29
Siderite	39	0.058	0.033	0.05 - 0.07	1.621	0.488	1.47 - 1.77	0.458	0.29	0.37 - 0.55
Phyllosilicates	# Frag	Avg.	St. Dev.	95% CI	Avg.	St. Dev.	95% CI	Avg.	St. Dev.	95% CI
Biotite	104	0.609	0.291	0.55 - 0.66	1.62	0.549	1.51 - 1.73	0.064	0.341	0.00 - 0.13
Muscovite	54	0.908	0.499	0.78 - 1.04	1.602	0.554	1.45 - 1.75	0.038	0.079	0.02 - 0.06
Montmorillonite	30	0.478	0.536	0.29 - 0.67	1.669	0.463	1.50 - 1.84	0.66	0.84	0.36 - 0.96
Kaolinite	51	0.378	0.444	0.26 - 0.50	1.533	0.277	1.46 - 1.61	0.428	0.324	0.34 - 0.52
Other Silicates	# Frag	Avg.	St. Dev.	95% CI	Avg.	St. Dev.	95% CI	Avg.	St. Dev.	95% CI
Quartz	97	0.319	0.259	0.27 - 0.37	1.667	0.579	1.55 - 1.78	0.203	0.16	0.17 - 0.24
Hornblende	40	0.308	0.255	0.23 - 0.39	1.728	0.533	1.56 - 1.89	0.317	0.164	0.27 - 0.37
Olivine	36	0.377	0.153	0.33 - 0.43	1.385	0.248	1.30 - 1.47	0.271	0.188	0.21 - 0.33
Augite	87	0.329	0.195	0.29 - 0.37	1.714	0.725	1.56 - 1.87	0.282	0.632	0.15 - 0.41

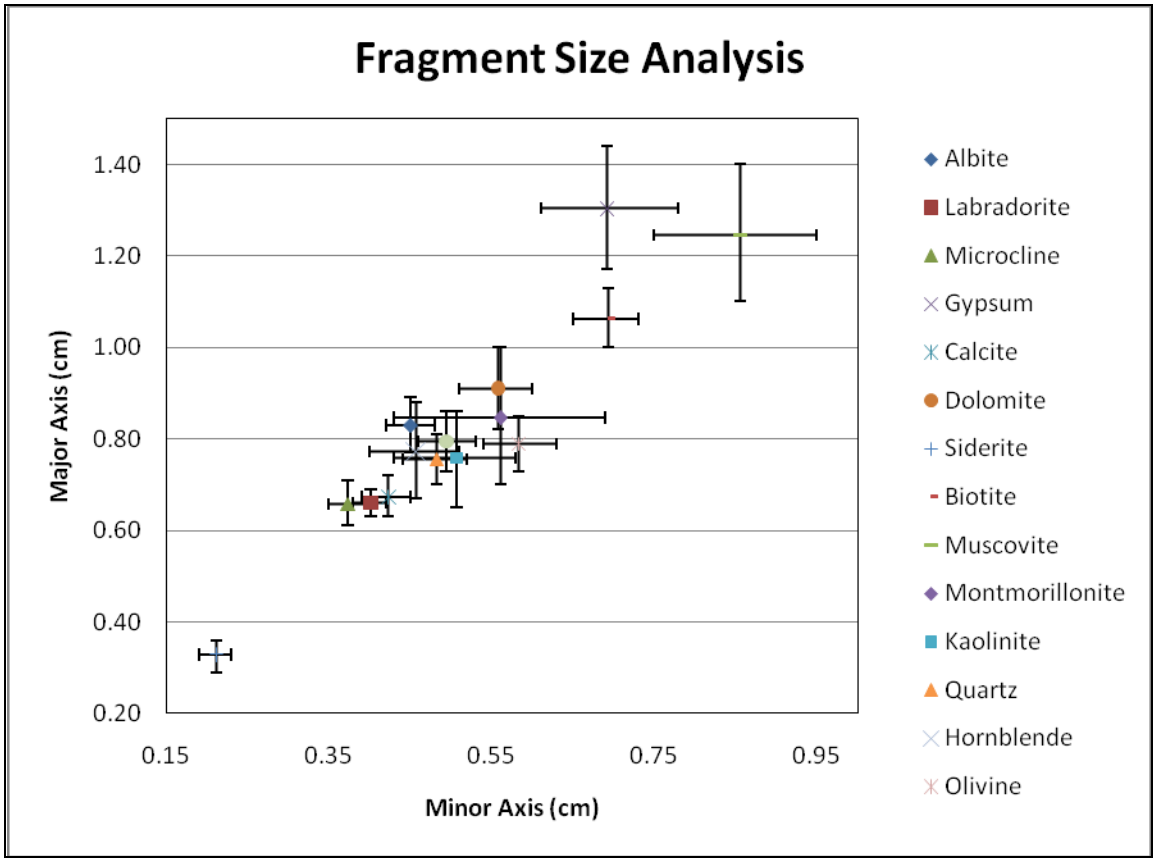

Figure 2-3 Fragment Size Analysis

Elemental Analysis

Elemental analyses were performed on the bulk properties of the minerals. Measurements were achieved by crushing the samples below a number 35 standard sieve and placing them in an oven for 24 hours at 75°C. The samples were then placed in a dessicator and percent nitrogen, sulfur, and carbon was measured with an Elementar Analyzer. Sulphanilic acid was used to establish the calibration curve at .072, .56, 1.04, 1.6, and 2.6 mg. Sulphanilic acid composition was measured at 8.09% nitrogen, 41.61% carbon, and 18.5% sulfur. The Sulphanilic Acid calibration is shown in Table 2-7. Montana soil standards reference material (SRM) 2711 was used for quality control every 25 samples. Results are shown in Table 2-8.

Table 2-7 Sulphanilic Acid Calibration for Elemental Analysis

Sulphanilic Acid Calibration						
Weight (mg)	N% Perc1	C% Perc2	S% Perc3	N Peak Area1	C Peak Area2	S Peak Area3
0.192	8.09	41.61	18.5	555	2025	266
0.443	8.09	41.61	18.5	1285	4592	718
0.997	8.09	41.61	18.5	2936	10298	1826
1.684	8.09	41.61	18.5	4906	17379	3266
2.881	8.09	41.61	18.5	8336	29584	5470

Blanks were placed after each Montana soil standard to allow venting of residual material from the standard and the previous samples. All samples were analyzed in quadruplicate unless otherwise noted. Detection limits were set at 0.01 N%, 0.018% C, and 0.01 S% based on the calibration curve used for these analyses, however personal experience on this device has shown that these detection limits are conservative. The minerals were washed with distilled (DO) and reverse osmosis (RO) water prior to crushing to remove large particles on the surface. After crushing, the minerals were separated and three batches were made for all. Batch number one was placed in consecutive hydrochloric acid solutions until effervescence ceased. Batch one was performed in quadruplicate and placed in the oven. Batch two was placed in consecutive hydrochloric acid solutions in quadruplicate and not placed in the oven. Batch three was not placed in acid solutions or in the oven. This was done to quantify organic carbon and carbonate carbon in the samples. Results are listed in the following tables. No nitrogen was measured above detection limits in any of the samples. Measurements below detection limits are listed in red. Both carbon and sulfur were present above detection limits in most samples. Carbon to nitrogen ratios are listed for comparison. However, C/N ratios are not quantitatively reliable based on the low amount of nitrogen in the samples.

Table 2-8 Elemental Analysis Results

Minerals	Run	Wt (mg)	N%	C%	S%	C/N
Hematite	1	89.077	0.001	0.002	0.012	5.94
Hematite	2	59.076	0.001	0.025	0.059	18.784
Hematite	3	84.897	0.001	0.019	0.05	20.633
Avg.			0.001	0.015	0.040	15.119
Quartz	1	62.897	0.001	0.002	0.033	2.812
Quartz	2	73.47	0.003	0.02	0.033	7.131
Quartz	3	91.359	0.002	0.015	0.021	9.122
Avg.			0.002	0.012	0.029	6.355
Microcline	1	91.824	0.001	0.016	0.020	13.148
Microcline	2	67.395	0.001	0.017	0.021	15.005
Microcline	3	79.065	0.002	0.016	0.013	10.335
Avg.			0.001	0.016	0.018	12.829
Olivine	1	91.786	0.001	0.022	0.007	24.489
Olivine	2	82.067	0.001	0.001	0.005	2.07
Olivine	3	69.317	0.001	0.026	0.007	20.502
Avg.			0.001	0.017	0.007	15.687
Hornblende	1	82.281	0.001	0.094	0.015	63.199
Hornblende	2	76.551	0.001	0.107	0.038	77.376
Hornblende	3	84.784	0.002	0.109	0.027	49.421
Avg.			0.002	0.103	0.027	63.332
Albite	1	87.918	0.001	0.020	0.010	16.371
Albite	2	70.555	0.001	0.018	0.009	19.619
Albite	3	73.501	0.001	0.002	0.007	16.902
Avg.			0.001	0.013	0.009	17.631
Andesine	1	69.474	0.001	0.03	0.020	54.433
Andesine	2	68.88	0.001	0.032	0.024	35.905
Andesine	3	72.031	0.001	0.038	0.024	63.656
Avg.			0.001	0.034	0.023	51.331
Montmorillonite	1	68.635	0.003	0.032	0.014	10.018
Montmorillonite	2	68.606	0.001	0.033	0.019	29.959
Montmorillonite	3	67.901	0.004	0.03	0.018	7.787
Avg.			0.003	0.032	0.017	15.921
Muscovite	1	61.628	0.019	0.206	0.023	10.762
Muscovite	2	40.462	0.024	0.179	0.025	7.571
Avg.			0.015	0.139	0.022	11.418

Table 2-8 Continued

Bulk Carbon				
Mineral	Runs	Organic Carbon		
		Avg. %	St. Dev.	CV%
Hematite	3	0.015	0.012	78.76
Quartz	3	0.012	0.009	75.67
Microcline	3	0.016	0.001	4.37
Olivine	2	0.024	0.003	11.68
Hornblende	3	0.103	0.008	8.04
Albite	3	0.013	0.01	74.91
Andesine	3	0.034	0.004	13.09
Montmorillonite	3	0.032	0.002	5.47
Muscovite	2	0.193	0.019	9.83
Biotite	1	0.001	-	-

Moisture Content

The percent moisture of the bulk samples was also measured. Each of the samples was crushed below a number 10 sieve, and some of the samples were additionally crushed below a number 35 sieve. The samples were placed on Al trays and the tray and the wet samples were weighed. The samples were then placed in the oven at 75°C. After 24 hours the samples were taken out and allowed to cool in a dessicator. The dry sample and the tray were then weighed and the percent moisture was calculated based on the following equation:

$$\% \text{ Moisture} = (M_{Wet} - M_{Dry})/(M_{Dry}) \bullet 100 \qquad \text{Eq. 2.11}$$

where M_{Wet} is equal to the wet mass and M_{Dry} is equal to the dry mass. The percent moisture is recorded in the following table. After the samples were weighed they were then placed on a countertop for 48 hours and reweighed. This was to measure the surface moisture and particle attraction rebound. Rebound was calculated via the reverse equation of percent moisture. Comparisons were then made between rebound and the polar surface energy component measured on the USD. Results are listed in Table 2-9 and Figure 2-4.

Table 2-9 Moisture Analysis Prior to Heating

Moisture Percent											
Sample	Less Than # 35 Sieve (Grams)				Less Than # 10 Sieve (Grams)				Rebound After 48 Hours (Grams)		
	Wt. Wt.	Dry Wt	Moisture %	Rank	Wt. Wt.	Dry Wt	Moisture %	Rank	Wt. Wt.	Dry Wt	Moisture %
Minerals											
Montmorillonite	1.541	1.2576	22.53%	1	4.4207	3.7624	17.50%	1	4.2549	3.7624	11.57%
Muscovite	0.1765	0.1726	2.26%	5	3.0925	2.9922	3.35%	2	3.093	2.9922	3.26%
Kaolinite	--	--	--	--	3.0999	3.0747	0.82%	3	3.0875	3.0747	0.41%
Augite	--	--	--	--	0.6224	0.6218	0.10%	4	0.6219	0.6218	0.02%
Andesine	3.0908	3.082	0.29%	9	5.9209	5.9174	0.06%	5	5.9198	5.9174	0.04%
Labradorite	--	--	--	--	6.0818	6.0794	0.04%	6	6.0803	6.0794	0.01%
Albite	3.0646	2.9469	3.99%	3	4.1682	4.1666	0.04%	7	4.1672	4.1666	0.01%
Gypsum	--	--	--	--	5.8908	5.889	0.03%	8	5.8895	5.889	0.01%
Biotite	0.1759	0.1544	13.92%	2	3.6753	3.6742	0.03%	9	3.6748	3.6742	0.02%
Microcline	2.9024	2.8867	0.54%	7	7.6993	7.6974	0.02%	10	7.6981	7.6974	0.01%
Hornblende	3.7731	3.7515	0.58%	6	16.0974	16.0936	0.02%	11	16.096	16.0936	0.01%
Siderite	--	--	--	--	7.311	7.3096	0.02%	12	7.3102	7.3096	0.01%
Hematite	0.4901	0.4731	3.59%	4	6.9849	6.9836	0.02%	13	6.9841	6.9836	0.01%
Rhodochrosite	--	--	--	--	7.5917	7.5905	0.02%	14	7.5908	7.5905	0.00%
Quartz	3.3603	3.35	0.31%	8	7.4678	7.4667	0.01%	15	7.4674	7.4667	0.01%
Ilmenite	--	--	--	--	6.7055	6.7046	0.01%	16	6.7055	6.7046	0.01%
Calcite	--	--	--	--	5.0155	5.0153	0.00%	17	5.0158	5.0153	0.01%
Cerussite	--	--	--	--	8.4208	8.4211	0.00%	18	8.4216	8.4211	0.01%

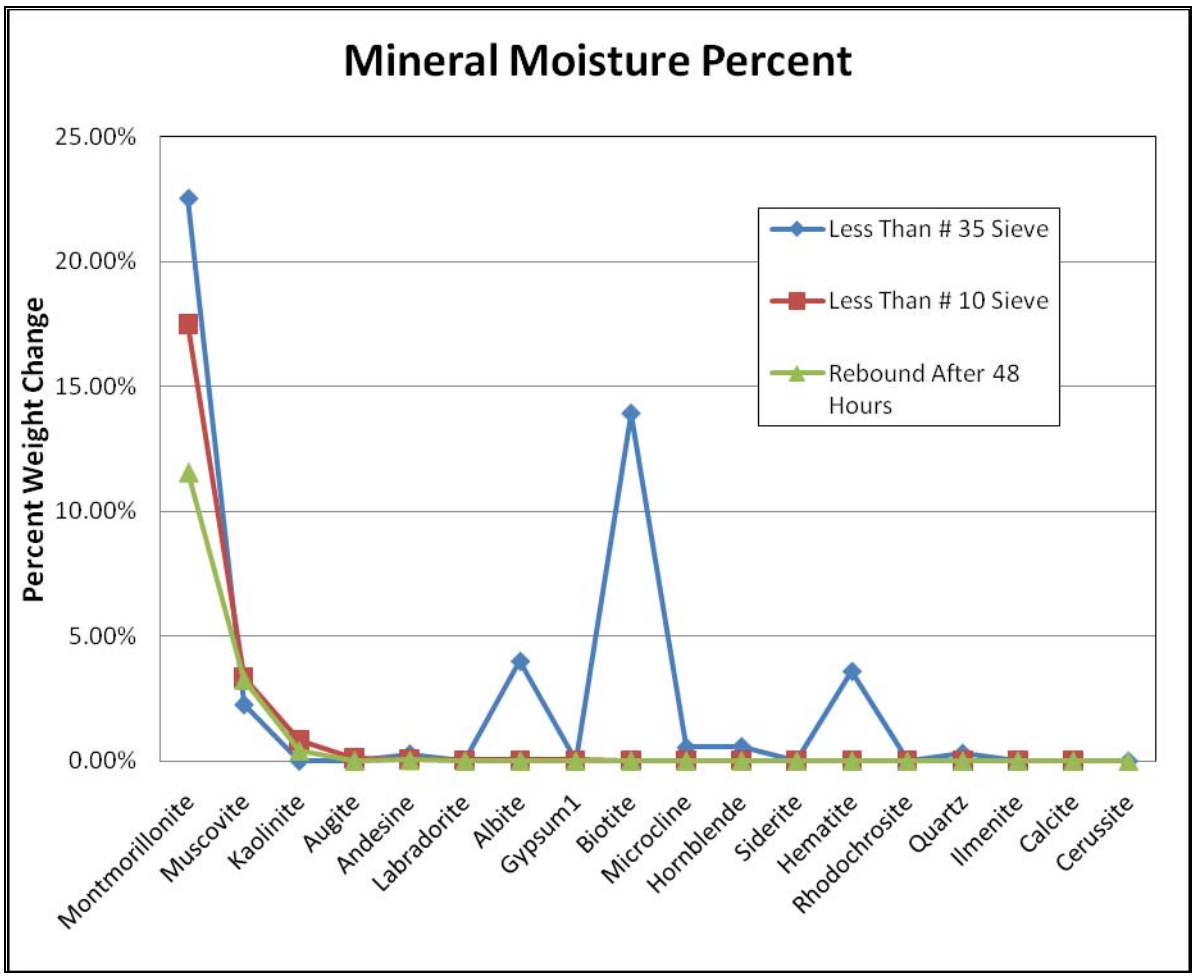

Figure 2-4 Mineral Moisture Percent

Data Analysis and Error Analysis

The surface energy components of the rocks and minerals are in units of energy per unit area (ergs/cm^2) so that the measurements will be normalized from variations in surface area. Surface area is calculated based the adsorption of n-hexane as a specific surface area, which is on a per gram basis. Several assumptions must be made in order to calculate the surface area. First, hexane is assumed to form a monolayer across the surface so that no hexane molecules will lay on top of each other and that there will be no gaps between molecules (BHASIN and LITTLE, 2007). Also, a hexane molecule is assumed to be 56.2Å^2. This number is from the literature as a best fit with laboratory data rather than based on molecular geometry (MCCLELLAN and HARNSBERGER, 1967). Hexane is expected to lie down on its long axis rather than across the short axis. Any crevices smaller than a hexane molecule will not be added to the total, however because the molecules will "lay across" the opening.

This method carries similar difficulties and assumptions as the common use of N^2 to calculate surface areas, and has been shown to correlate well with N^2 measurements for the same materials (BHASIN and LITTLE, 2007).

The three equations used to calculate the surface energy components are interdependent and therefore error from one carries over to the others. For this reason the error cannot be estimated based on the variance between film pressures. Therefore, the Delta method will be utilized with the software 'R' to estimate the standard error for each of the components separately. One disadvantage is that the delta method assumes normality. This may be a correct assumption, but with only twelve data points for each sample it cannot be proven.

The most important contribution to "error" for this research is almost certainly natural heterogeneity. The mineral samples purchased are pure phase or near pure phase, however even among these samples there are likely significant differences between fragments. Therefore, much of the variation between samples is likely not error, but rather the result for real differences between fragments and test runs.

Results and Discussion

Surface energy is believed to be controlled by surface chemistry, surface morphology, and surface coatings (CHURAEV, 1995; FENG et al., 2002; VAN OSS and GIESE, 1995). This research hopes to elucidate the interrelationships of these three master controls on mineral and aggregate surface energy. The electron microprobe, elemental analyzer, and x-ray photoelectron spectroscopy were used to characterize the bulk and surface chemistry of the minerals. From this data the molar ratios of all the major elements in the chemical structure as well as organic and inorganic coatings were quantified. In this way, the effect of surface chemical groups on the measured surface energy of each component can be compared across mineral and aggregate groups.

To date, measuring surface morphology in a quantifiable manner has not been successful. Atomic force microscopy is too delicate a technique to measure the morphology of natural minerals and aggregates. Imaging scanners appear to do an adequate job of measuring two-dimensional surface roughness up to tens of micrometers. Surface energy, however, is a molecular-scale three-dimensional attribute which is at the Angstrom level. SEM images are capable of giving a qualitative estimate of surface roughness at close to these scales. Currently, the techniques being used to estimate roughness factors for SEM images in the Advanced Characterization of Infrastructure Materials laboratory at Texas A&M University are providing some initial data that may prove valuable to understanding the role between surface roughness and surface energy.

The universal sorption device was used to measure the surface energy components of each of the minerals listed in the initial sections. The components measured were nonpolar van der Waals interactions which included Keesom, Debye, and London forces and polar energy including Lewis acids and bases. The Lewis acid and base components combine to form the total polar surface energy. These components are thought to react with oppositely charged sites on probe vapors. In order to evaluate this reaction the hard/soft acid base concept was utilized. This concept compares acids and

bases based on size, charge density, and polarizability. Hard acids and bases are those which are small, have a high charge, and are weakly polarizable. Soft species are those which are the opposite: large, low charge, and are strongly polarizable.
The sites on the minerals were classified based on this concept in the following table. Cations and anions were separated into hard, borderline, and soft species. Hard acids were delineated with a charge to radius ratio greater than or less than two. Hard acid sites on minerals are expected to react strongly with hard base sites on interacting solids, liquids, and gases. Accordingly, soft species are expected to react with their corresponding soft species.

The idea can then be projected to evaluating entire surfaces in a comparative if not quantitative manner. For example, consider two similar species: calcite ($CaCO_3$) and siderite ($FeCO_3$). Calcite and siderite have similar structures (Hexagonal, 3bar 2/m) and chemical formulas. Fe^{2+} and Ca^{2+} have the same charge, however divalent iron is known to be a harder Lewis acid than calcium. Thus, each of the surfaces of siderite are more hard than the calcite surfaces. One must be careful, however, not to overextend the usefulness of this approach. Other factors certainly play a role in the proclivity of a surface to gain or donate electrons which is what Lewis acidity and basicity is actually characterizing. Describing the hardness/softness of a surface may turn out to be a useful rubric for determining the dominant surface energy characteristic of a particular sample. In other words, if the measurement of surface energy among a group of minerals correlates well with the expected hardness/softness then this may be the determining variable for that group. The surface functional groups of mineral groups are listed in Table 2-10 and the chemistry results are shown in Table 2-11.

In a more quantifiable manner, the Lewis acidity/basicity of a surface is essentially being measured by the universal sorption device. Thus, the calculated polar component, such as the base component, is expected to be proportional to the actual surface electron donicity. Thus, if the measurement of a sample's surface energy polar component does not correspond with the expected hardness/softness comparison of

another mineral then it is possible that some other factor (surface coatings, surface morphology) is a more dominant control.

Surface Area and Surface Roughness

The surface area of minerals and aggregates are highly variable. The specific surface area of minerals and aggregates are important characteristics because the variations are as much as 3 or 4 orders of magnitude. Surface energy itself only varies about one order of magnitude. Thus, a mineral that has a low surface energy but a very high specific surface area, such as a clay, will have more of an environmental influence than one with high surface energy but very low SSA. Non-clay minerals average approximately 0.17 m^2/g. Clay minerals, however average 16.91 square meters per gram of mineral. Two charts are below depicting the surface energy on a per gram basis of each of the minerals. These show that although the surface energy of kaolinite and montmorillonite may be lower the actual effect of clay sized grains is much larger because of the increased surface area and surface area to volume ratio. The surface energy of montmorillonite and kaolinite on a per gram basis are three orders of magnitude larger than most of the other minerals. The specific surface area results are shown in Table 2-12 and 2-13. The relationship between surface area and surface roughness is illustrated in Figure 2-5.

Table 2-10 Mineral Surface Functional Groups

Minerals	Nonpolar	Polar						
	Siloxane Surface	Permanently Charged Sites	Conditionally Charged Sites					
			Acid			Base		
			Hard	Border	Soft	Hard	Border	Soft
Carbonates								
Calcite	--	--	Ca^{2+}	--	--	CO_3^{2-}	--	--
Dolomite	--	--	Ca^{2+}, Mg^{2+}	--	--	CO_3^{2-}	--	--
Siderite	--	--	Ca^{2+}, Mg^{2+}	Fe^{2+}	--	CO_3^{2-}	--	--
Cerussite	--	--	Ca^{2+}, Mg^{2+}	Pb^{2+}	--	CO_3^{2-}	--	--
Rhodo-chrosite	--	--	Ca^{2+}, Mg^{2+} Mn^{2+}	Fe^{2+}	--	CO_3^{2-}	--	--
Sulfates								
Gypsum	--	--	Ca^{2+}	--	--	SO_4^{2-}, H_2O	--	--
Bassanite	--	--	Ca^{2+}	--	--	SO_4^{2-}, H_2O	--	--
Phyllosilicates								
Biotite	--	AlO_4^{3}- (T), MgO_3^{4-} (O), FeO_3^{4-}? (O)	Mg^{2+}, Mn^{3+}?, Ti^{4+}, Si^{4+}, Al^{3+}, K^{+}, Mn^{2+}	Fe^{2+}	--	SiO_4^{4-}, AlO_3^{3-}, OH^-,F^-	--	--
Muscovite	--	AlO_4^{5-} (T), FeO_5^{4-}? (O)	Ca^{2+}, Al^{3+}, Fe^{3+}?, Si^{4+}, K^{+}, Na^{+}	Fe^{2+}	--	SiO_4^{4-}, AlO_3^{3-}, OH^-,F^-	--	--
Phyllosilicate Clays								
Montmor-illonite	$(SiO_2)^0$	AlO_4^{5-} (T), MgO_3^{4-}? (O)	Ca^{2+}, Al^{3+}, Mg^{2+}, Na^{+}	--	--	SiO_4^{4-}, AlO_3^{3-}, H_2O, OH^-	--	--
Kaolinite	$(SiO_2)^0$	AlO_4^{5-} (T)	Al^{3+}	--	--	SiO_4^{4-}, AlO_3^{3-}, H_2O, OH^-	--	--

Table 2-10 Continued

Minerals	Nonpolar	Polar						
	Siloxane Surface	Permanently Charged Sites	Conditionally Charged Sites					
			Acid			Base		
			Hard	Border	Soft	Hard	Border	Soft
Tecto & Inosilicates								
Microcline	--	--	Al^{3+}, K^{+}, Na^{+}	--	--	SiO_4^{4-}, AlO_4^{5-}	--	--
Albite	--	--	Na^{+},Al^{3+}	--	--	SiO_4^{4-}, AlO_4^{5-}	--	--
Labradorite	--	--	Ca^{2+}, Al^{3+}, Na^{+}	--	--	SiO_4^{4-}, AlO_4^{5-}	--	--
Andesine	--	--	Ca^{2+}, Al^{3+}, Na^{+}	--	--	SiO_4^{4-}	--	--
Inosilicates								
Hornblende	--	--	Ca^{2+}, Mg^{2+}, Fe^{3+}?	Fe^{2+}	--	$Si_4O_{11}^{6-}$, OH^{-}	--	--
Augite	--	--	Ca^{2+}, Mg^{2+}, Si^{4+}	Fe^{2+}	--	SiO_3^{2-}	--	--
Nesosilicates								
Olivine	--	--	Mg^{2+},Si^{4+}, Mn^{2+}	Fe^{2+}	--	SiO_4^{4-}	--	--
Oxides								
Quartz	--	--	--	--	--	SiO_4^{4-}	--	--
Hematite	--	--	Fe^{3+}	--	--	--	--	--
Ilmenite	--	--	Fe^{3+}, Ti^{4+}	Fe^{2+}	--	--	--	--
Hard, Soft, & Borderline associations according to (Pearson, 1968a; Pearson, 1968b)								

Table 2-11 Bulk and Surface Measured Chemical Formulas

Bulk and Surface Chemical Formulas			
Mineral	**Ideal Formula**	**XPS Measured Formula**	**WDS Measured Formula**
Carbonates			
Calcite	$CaCO_3$	$Ca_{1.11}C_{1.42}O_3$	$CaCO_3$
Dolomite	$CaMg(CO_3)_2$	$Ca_{1.32}Mg_{.624}(C_{3.57}O_3)_2$	$CaMg_{0.98}Fe_{0.01}(CO_3)_2$
Siderite	$FeCO_3$	$Ca_{0.15}Mg_{0.078}Fe_{0.22}C_{0.49}O_3$	$Ca_{0.02}Mg_{0.3}Fe_{1.64}CO_3$
Cerussite	$PbCO_3$	$Pb_{.61}Mn_{.17}Ca_{.01}C_{.65}O_3$	$Pb_{.998}CO_3$
Rhodochrosite	$MnCO_3$	$Mg_{.83}Mn_{.32}Ca_{.06}Fe_{.03}C_{.98}O_3$	$Mn_{.75}Fe_{.16}Ca_{.05}Mg_{.03}CO_3$
Sulfates			
Gypsum	$CaSO_4 \cdot 2H_2O$	$Ca_{1.05}S_{1.0}O_4$	$CaSO_4$
Bassanite	$CaSO_4 \cdot 0.5H_2O$	$Ca_{1.03}S_{.99}O_4$	$CaSO_4$
Phyllosilicates			
Biotite	$K(Mg,Fe)_2(AlSi_3O_{10})(F,OH)_2$	$K_{.48}(Mg_{1.18},Fe_{.31},Mn_{.07},Ti_{.04})_2(Al_{.74}Si_{2.1}O_{10})F_{.43}$	$K_{1.92}(Mg_{1.62}Fe_{1.08}Mn_{.05}Ti_{.12})_2(Al_{2.04}Si_6O_{10})(F_{1.62},OH_X)$
Muscovite	$KAl_2(AlSi_3O_{10})(F,OH)_2$	$K_{.68}Al_{1.44}Na_{.17}Fe_{.04}Ca_{.17}(Al_{.72}Si_{2.03}O_{10})F_{.59}$	$K_{1.78}Al_{3.84}Na_{.21}Fe_{.13}Mg_{.05}(Al_{1.92}Si_{06.07}O_x)F_{.44}$
Phyllosilicate Clays			
Montmorillonite	$(Na,Ca)_{0.33}(Al,Mg)_2(Si_4O_{10})(OH)_2$	$Ca_{.39}(Al_{1.26},Mg_{.23})_2Si_{3.62}O_{10}$	$Ca_{0.2}(Al_{.65}Mg_{.275}Fe_{.05})_2Si_{3.65}O_{10}$
Kaolinite	$Al_2Si_2O_5(OH)_4$	$Al_{1.06}Si_{1.2}O_5$	$Al_{2.9}Si_{2.8}O_5$

Table 2-11 Continued

Mineral	Ideal Formula	XPS Measured Formula	WDS Measured Formula
Tecto & Inosilicates			
Microcline	$KAlSi_3O_8$	$K_{.41}Na_{.41}Al_{2.61}Si_{1.85}O_8$	$K_{.79}Na_{.22}Al_{1.03}Si_{2.97}O_8$
Albite	$NaAlSi_3O_8$	$Na_{.77}Al_{1.35}Si_{3.43}O_8$	$Na_{.96}K_{.01}Al_{1.03}Si_{2.98}O_8$
Labradorite	$Ca_{(.50-.70)}Na_{(.50-.30)}(Al,Si)AlSi_2O_8$	$(Ca_{.3}Na_{.28})Al_{1.36}Si_{2.96}O_8$	$Ca_{.50}Na_{.45}K_{.03}(Al_{1.49}Si_{2.46})O_8$
Andesine	$Na_{(.70-.50)}Ca_{(.30-.50)}(Al,Si)AlSi_2O_8$	$(Ca_{.31}Na_{.68}K_{.03})(Si_{.68}Al_{.44})_4O_8$	$Na_{.49}Ca_{.45}Al_{1.47}Si_{2.53}O_8$
Inosilicates			
Hornblende	$Ca_2(Mg,Fe,Al)_5(Al,Si)_8O_{22}(OH)_2$	$Ca_{1.11}Na_{.80}K_{.03}(Mg_{.63},Fe_{.08},Al_{.65})_5(Al_{1.04},Si_{1.07})O_{22}$	$Ca_{1.02}Na_{1.73}K_{.26}(Mg_{.48},Mn_{.03}Fe_{0.46},Al_{.42})_5(Al_{.67},Si_{7.11})_8O_{22}H_2$
Augite	$(Ca,Mg,Fe)SiO_3$	$(Ca_{.74},Na_{.14})(Mg_{.57},Fe_{.08},Al_{.06})(Al_{.10},Si_{.60})_2O_6$	$(Ca_{.89}Na_{.10}Mg_{.48}Mn_{.03}Fe^{2+}_{.35}Fe^{3+}_{.13}Al_{.07})Si_{1.95}O_6$
Nesosilicates			
Olivine	$(Mg,Fe)_2SiO_4$	$(Mg_{.71},Mn_{.01},Fe_{.02})_2Si_{1.06}O_4$	$(Mg_{.89-.91},Fe_{.08-.10})_2Si_{1.00-1.01}O_4$
Oxides			
Quartz	SiO_2	$Si_{1.03}O_2$	SiO_2
Hematite	Fe_2O_3	$Fe_{.23}O_3$ + .53M Silicate	$Fe_{1.97}O_3$
Ilmenite	$FeTiO_3$	$Mg_{.53}Mn_{.14}Fe_{.07}Ti_{.06}O_3$	$Fe^{2+}_{.84}Fe^{3+}_{.16}Ti_{.93}Mn_{.07}Mg_{.01}O_3$

Table 2-12 Measured Specific Surface Areas

Specific Surface Area Averages		
Probe Vapor	Non-clay Minerals	Clay Minerals
Hexane (39Å^2)	0.12	11.74
Hexane (56Å^2)	0.17	16.91
MPK (35Å^2)	0.03	2.07
Water (5Å^2)	0.09	-0.22
Water (10Å^2)	0.15	-0.37

Table 2-13 Specific Surface Area Literature Value Comparison

Specific Surface Area Literature Values					
Sample	Measured Values	Literature Values			
Minerals	m^2/gm	m^2/gm	m^2/gm	m^2/gm	m^2/gm
Augite	0.027				
Hematite	0.045	4.5[31]	3.2[32]		
Quartz	0.055	0.07[9]	0.17[12]	0.20[15]	0.01[23]
Dolomite	0.063	0.70[18]	1.4[21]	0.14[22]	
Biotite	0.064	1.75[9]	9.1[11]	1.22[13]	1.11[23]
Siderite	0.067				
Hornblende	0.092	0.44[2]	0.58[12]		
Andesine	0.097	0.5[25]			
Ilmenite	0.105				
Muscovite	0.115	3.4[14]	1.4[15]		
Microcline	0.117	0.13[8]	0.11[9]	0.53[12]	0.26[13]
Rhodochrosite	0.174				
Albite	0.193	0.185[2]	0.24[9]	0.20[15]	0.21[24]
Labradorite	0.273	0.141[2]	0.03[26]	0.12[27]	0.20[28]
Calcite	0.282	0.45[16]	0.56[17]	0.37[17]	0.36[17]
Olivine	0.293	0.27[2]			
Hot Gypsum	0.362				
Gypsum	0.383	0.5[29]	3.3[30]		
Bassanite	0.484				
Kaolinite	10.530	15.5[1]	16[3]	26[4]	11.72[5]
Montmorillonite	23.297	30.7[6]	34[7]	20[20]	31.82[23]

Sources: 1: (NELSON and HENDRICKS, 1943); 2: Average from (BRANTLEY and MELLOTT, 2000); 3: (KAISER and GUGGENBERGER, 2003); 4: (THENG et al., 1999); 5: (BAUER and BERGER, 1998); 6: (STUCKI et al., 2002); 7: (METZ et al., 2005); 8: (CLOW and DREVER, 1996); 9: (STENSTRÖM and KJELLEBERG, 1985); 10: Aquifer material similar to aggregate (BENNETT et al., 1996); 11: (JOZEFACIUK and BOWANKO, 2002); 12: (WHITE et al., 1996); 13: (WALLANDER and WICKMAN, 1999); 14: (CASERI et al., 1992); 15: (ARNOLD et al., 2001); 16: (WALTER and MORSE, 1984); 17: (HONJO and EREZ, 1978); 18: (WALKER et al., 2003); 20: (KREBS et al., 1999); 21: (PROCHASKA and ZOUBOULIS, 2006); 22: (KARACA et al., 2006); 24: Averages and single values from (WHITE and BRANTLEY, 2003); 25: (SIEGAL and PFANNKUCH, 1984); 26: (BENEDETTI et al., 1994); 27: (KENOYER and BOWSER, 1992); 28: (TAYLOR et al., 2000); 29: Average from (HIRAO et al., 2009); 30: (OKAZAKI and YAMAZAKI, 1981); 31: (DOS SANTOS AFONSO and STUMM, 1992); 32: (PAVLOVIC and BRANDAO, 2003)

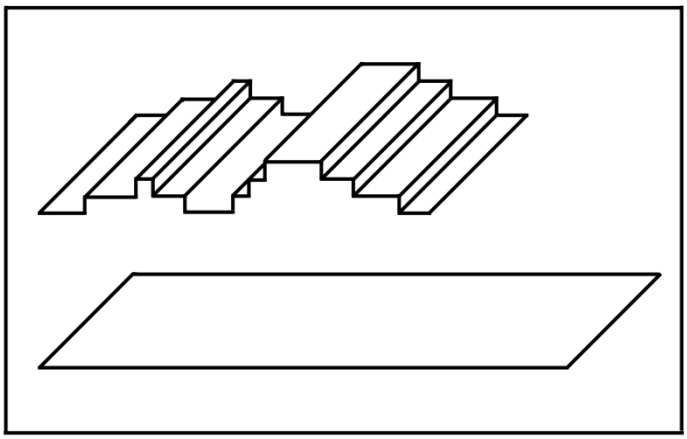

Figure 2-5 Relationship between Surface Roughness and Surface Area

Surface roughness is a measure of surface texture. Surface texture may be an important component of surface energy (BECKER et al., 2001). Generally it is measured as deviation from an ideal structure. Macroscale structures with high roughness have increased friction. It is unclear what role molecular scale roughness plays on surface energy. Molecular scale roughness may increase the number of unfilled bonds on the surface by decreasing the number of neighbor molecules. The schematic drawing above represents two surfaces of equal surface area and specific surface area. The corner molecules lack two neighbor molecules increasing their free energy. Large macromolecules also may not be able to fit into valley regions.

Profilometery is a useful technique in measuring surface roughness. These devices use a thin tip on a cantilever which taps the surface measuring the x, y, and z change. One such device, an Atomic Force Microscope (AFM), was attempted. Unfortunately, the natural mineral surfaces were too rough, and use would have damaged the tip. For this reason this technique was abandoned. Several software programs were then used on Scanning Electron Microscope (SEM) images to measure surface roughness. Unfortunately, to date none have had the computing power capable of measuring the complex three dimensional frameworks.

In the absence of other data a scanning imager was used to measure the length two dimensional edges of the mineral fragments relative to their axial lengths. This was accomplished by scanning the fragments used in the USD and converting the images to absolute black and white. The images were canned at 1200 DPI. Next, NIH image software was used to measure the length of the edges and the major and minor axes. Several different measures of roughness were used. First, the length of the major axis to the area was measured. Next, a two dimensional roughness factor was calculated using the following equation (WHITE and BRANTLEY, 2003):

$$\lambda = (\rho \bullet D \bullet SSA)/6 \qquad \text{Eq. 2.12}$$

where λ = surface roughness (unitless), ρ = density, D = grain diameter, and SSA is equal to the specific surface area measured with the USD. This roughness factor assumes grain diameters to be spheres. For this reason, the variance from sphericity was calculated to determine relevance of the equation. Albite, bassanite, and gypsum showed the greatest deviation from sphericty (1.14, 1.13, and 1.13 respectively). In addition a three dimensional roughness factor was calculated by weighing the samples and dividing by the density and number of fragments to get an average height. This assumes straight perpendicular edges. The above equation was then recalculated for the third dimension. This technique does not appear to corroborate well with surface energy measurements. One possible reason is the dominance of the specific surface area in the calculations. The variance in fragment size and shape was not as large as the variance between specific surface areas. SSA varied by as much as four orders of magnitude. In addition the three dimensional roughness factor measured nothing different from the two dimensional factor except some degree of height difference which was also negated by the much large SSA variability.

Lastly, surface roughness, as it applies to surface energy, is a molecular scale variable. The scanners maximum precision was 1200 DPI which translates to a precision of approximately 21.15 μm. A hexane molecule used to measure surface area is 56 $Å^2$ or 56 X 10^{-8} μm^2. Therefore, the measurements were not at coincidental scales necessary for meaningful results. The test results are shown in Table 2-14 and Figure 2-6.

Table 2-14 Measured Values of Surface Roughness

Surface Roughness Measurements											
Carbonate	Length/ Area	St Dev.	Co. Var.	2D SR	St. Dev.	Co. Var.	3D SR	St. Dev.	Co. V.	areaC/ areaM	St Dev.	Co. Var.
Calcite	11.08	4.99	0.45	697.98	274.51	0.39	587.04	121.09	0.21	1.08	0.11	0.10
Dolomite	7.69	2.30	0.30	218.28	61.40	0.28	169.77	28.74	0.17	1.07	0.06	0.06
Siderite	20.66	6.67	0.32	117.65	35.20	0.30	144.90	23.11	0.16	1.07	0.08	0.08
Feldspar												
Albite	10.10	3.53	0.35	540.64	180.02	0.33	428.35	84.19	0.20	1.14	0.17	0.15
Labradorite	10.60	2.87	0.27	651.76	191.66	0.29	497.89	98.17	0.20	1.08	0.08	0.08
Microcline	11.93	4.18	0.35	257.70	99.47	0.39	197.84	53.86	0.27	1.11	0.13	0.12
Clay Minerals												
Kaolinite	9.67	3.72	0.38	28873.23	14773.14	0.51	25753.66	6991.58	0.27	1.05	0.28	0.26
Montmorillonite	9.69	5.83	0.60	54906.99	29558.10	0.54	53774.76	18645.72	0.35	1.08	0.08	0.08
Phyllosilicates												
Biotite	7.39	7.56	1.02	288.08	79.14	0.27	199.03	51.22	0.26	1.07	0.10	0.09
Muscovite	6.39	4.24	0.66	568.56	178.98	0.31	385.92	111.35	0.29	1.07	0.10	0.09
Other Silicates												
Augite	9.75	5.31	0.54	99.35	32.38	0.33	80.72	29.11	0.36	1.09	0.14	0.13
Hornblende	9.51	2.82	0.30	300.89	117.13	0.39	252.38	56.02	0.22	1.09	0.10	0.09
Quartz	9.73	3.60	0.37	150.82	55.52	0.37	117.07	29.09	0.25	1.08	0.11	0.10
Olivine	7.59	2.46	0.32	1101.45	246.70	0.22	879.43	84.25	0.10	1.03	0.03	0.03
Sulfates												
Bassanite	7.62	5.59	0.73	2197.62	710.59	0.32	1650.16	311.38	0.19	1.13	0.11	0.10
Gypsum	7.62	5.59	0.73	1737.66	561.87	0.32	1304.79	246.21	0.19	1.13	0.11	0.10

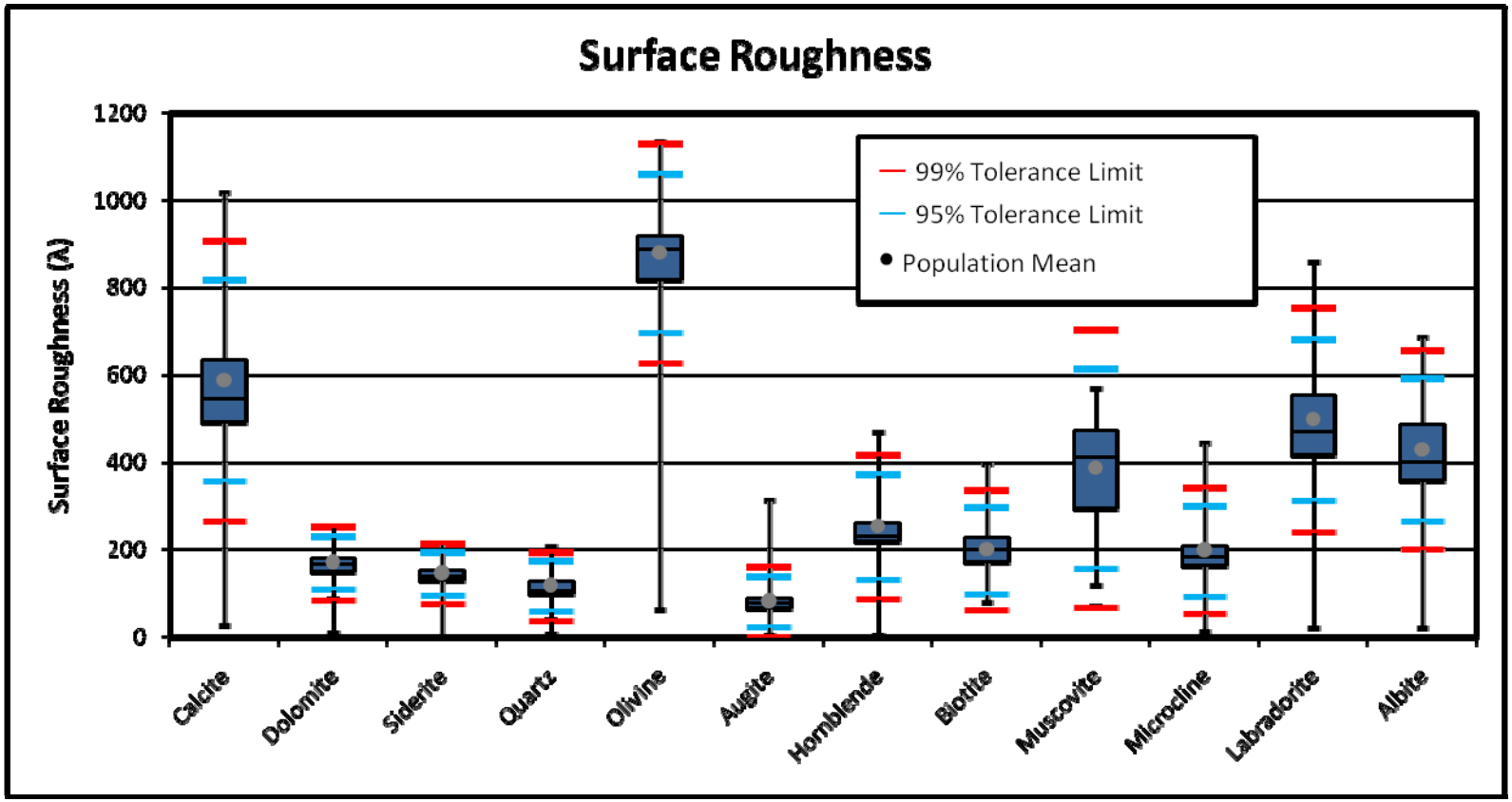

Figure 2-6 Surface Roughness Results

Surface Energy Results

Surface energy is the excess energy of solids compared to the bulk. The results given by the universal sorption device are averages of all of the sides of the minerals rather than a measurement of any given individual side such as an edge site or the octahedral layer. These results are given for natural minerals which have not been subjected to strong acids to remove surface coatings. These minerals were fragmented with an impact mortar in order to mimic natural physical weathering processes. Thus, this data set is a measurement of real conditions. These conditions are inherently complex and heterogeneous despite efforts to simplify the measured systems by using pure phase minerals, heating samples, and using reproducible methods.

van der Waals

The van der Waals component of surface energy is an additive measure of Keesom, Debye, and London forces (Eq. 2.1) (OVERBEEK, 1952). These forces are produced by dipole-dipole interactions and induced dipole interactions. Thus, a single molecule and multiple molecules have van der Waals interactions. Van der Waals interactions are generally weaker than electrostatic interactions, however they influence interactions over longer distances (VAN OSS, 2006). The van der Waals surface energy results are shown in Figures 2-6 through 2-9.

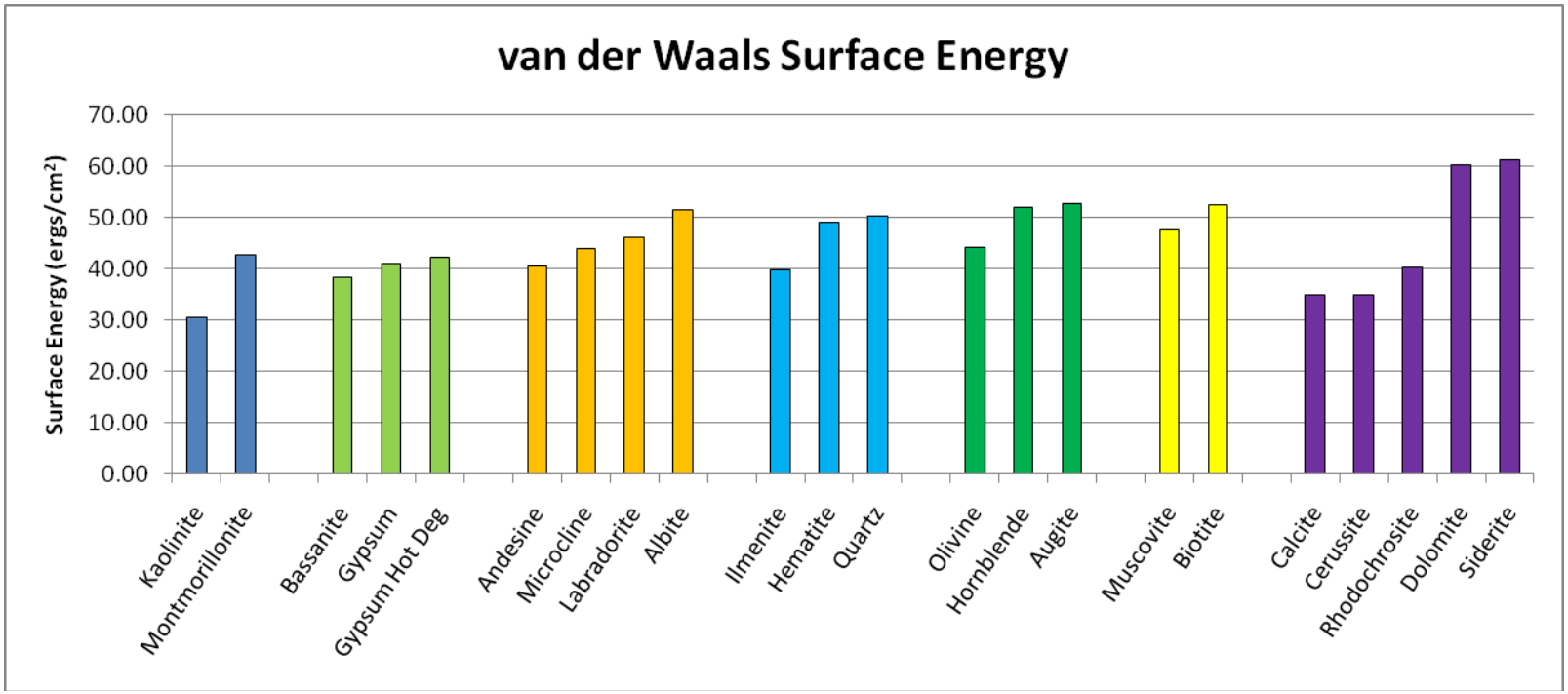

Figure 2-7 van der Waals Surface Energy (All)

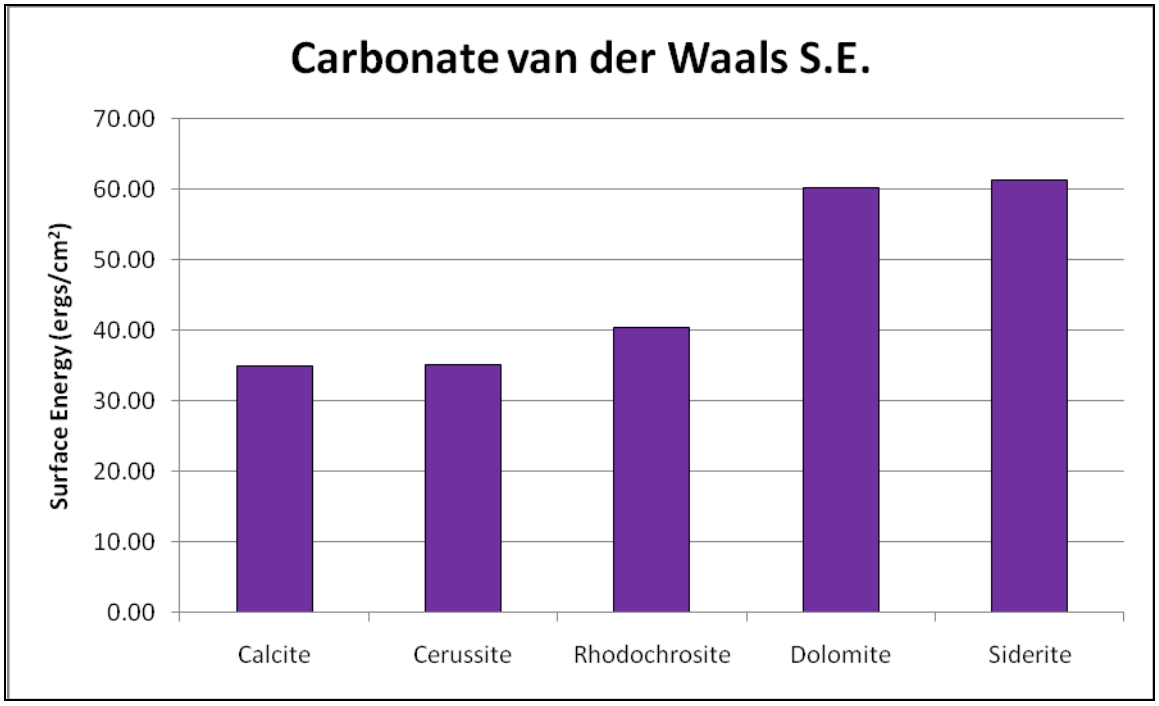

Figure 2-8 van der Waals Surface Energy (Carbonates)

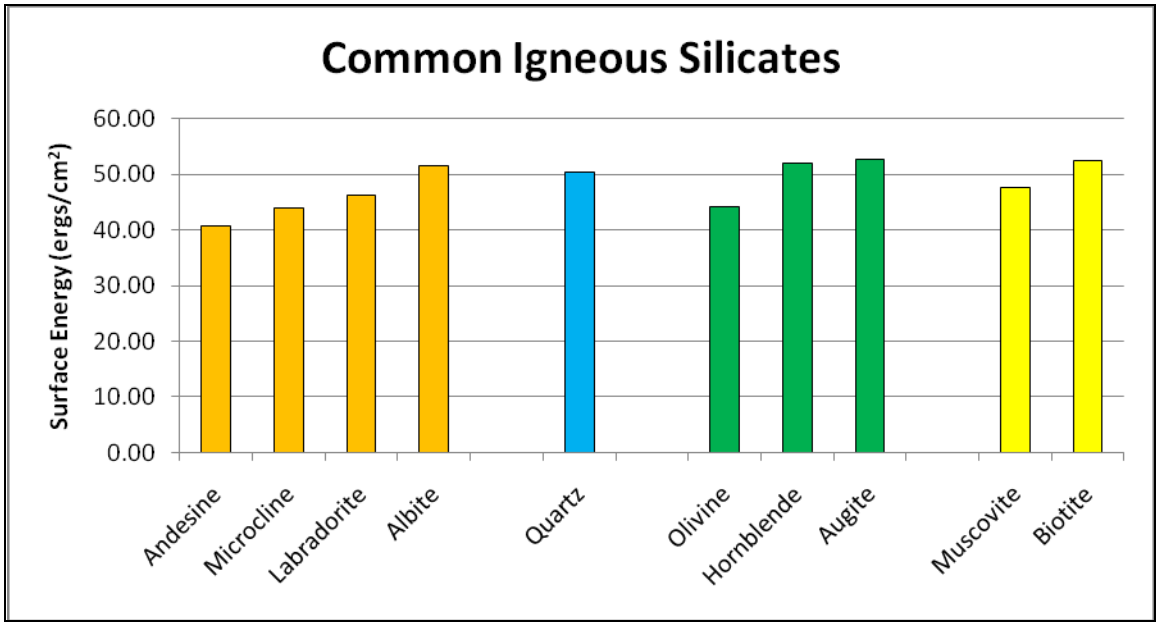

Figure 2-9 van der Waals Surface Energy (Common Silicates)

Overall there was less variation in the van der Waals interactions than in the polar interactions. The average coefficient of variation for all mineral groups was 13.06%. The total range varied from 30.48 for kaolinite and 61.39 ergs/cm^2 for siderite. It is difficult to draw to many conclusions based on the van der Waals measurements. A t-test was not performed between mineral groups based on the limited number of samples in each grouping. The van der Waals surface energy results are listed in Table 2-15.

Table 2-15 van der Waals Surface Energy Summary

van der Waals Summary			
Group	Average ergs/cm^2	St. Dev. ergs/cm^2	Co. Var. ergs/cm^2
Clay Minerals	36.66	8.74	23.84%
Sulfates	40.54	2.05	5.06%
Feldspars	45.61	4.59	10.06%
Oxides	46.36	5.76	12.42%
Carbonates	46.40	13.36	28.79%
Neso/Inosilicates	49.59	4.71	9.50%
Phyllosilicates	50.03	3.50	7.00%

The mean for the 22 minerals was 45.33 with a variance of 62.46 ergs/cm^2. The mean for the 7 aggregates was 50.87 with a variance of 14.70 ergs/cm^2. The two tailed p-value between the mineral dataset and the aggregate dataset yields a confidence of 84% that the null hypothesis is false. Thus, the two datasets are not statistically different at a 90% confidence. By contrast a t-test comparing silicates and carbonates yields confidence of 71%. The carbonates are, therefore, only statistically different at a 70%

confidence. These statistics may not seem large. However, for natural specimens the author interprets these as important differences.

Lewis Acid/Base

In addition to Lifshitz-van der Waals forces the other major component to surface energy is the polar or electron acceptor-donor component. Van Oss states that polar surface energies can be up to two orders of magnitude greater than nonpolar interactions. This was true of this dataset as well. No values were two orders of magnitude, but some values such as augite were close(VAN OSS, 2006). The polar or Lewis acid-base interactions are probably mainly hydrogen donor and hydrogen acceptor reactions (VAN OSS et al., 2001). However, it is more useful to define "polar" more broadly for all electron acceptor-donor interactions. In this way all of the interactions with similar donor/acceptor affects can be measured.

It is important to remember in interpreting the polar surface energies that the major difference between Lifshitz-van der Waals interactions and polar interactions is that electron donor-acceptor reactions are not symmetrical as van der Waals interactions are. The molecular polarizabilities and the ionization energies enter the equations for the dispersion (polar) force symmetrically (i.e. it doesn't make a difference what the partner is) (VAN OSS, 2006). In an electron acceptor/donor relationship this symmetry does not exist. This is because in a strict sense a basic functional group, such as a carboxylic acid, will not interact as a base with another basic entity. One must act as an electron donor and the other must act as an electron acceptor (MCMURRY, 2004). Nondispersive forces only occur when there are complimentary groups present (an electron acceptor and an electron donor in a Lewis sense).

For this reason the duality of electron acceptor-donor interactions must be treated together yet understood separately. For instance, a monopolar substance, such as methyl propyl ketone, has a total polar surface energy of zero because $\gamma^+ = 0$. However, the $\gamma^- \neq 0$. Therefore, methyl propyl ketone can react through polar interactions with any other monopolar substance with an electron acceptor component or with any bipolar substance despite the fact that its polar surface energy is zero. This is just one example

of the importance of understanding all of the components of a material's surface free energy if inferences are to be made on the interface reactivity characteristics of that material. Polar interactions must not be confused with electrostatic interactions and must be understood separately. Because of the universality of van der Waals interactions and the specificity of electron donor-acceptor forces the interpretation of polar components of surfaces and edge sites has the greatest potential.

Lewis Acid Component: The acid surface energy is the smallest component of natural minerals and aggregates. Normal values range from very close to zero to 4 or 5 ergs/cm^2 for minerals as shown in Table 2-16 and Figures 2-10 through 2-14. An interesting phenomenon that has been clearly seen in many surface energy measurements is the near zero values of the γ^+ component for nearly all dry solid surfaces. van Oss describes this, *"Virtually all dry solid surfaces of polar compounds are monopolar electron donors which manifest a sizeable* γ^- *and a* γ^+ *which is very small"* (VAN OSS, 2006). Van Oss goes on to explain, *"The reason for* γ^- *monopolarity in dried state is that their excess electron donicity over electron acceptivity causes, upon drying, a neutralization of all* γ^+ *by the excess* γ^-*, so that on a dried surface one measures only residual* γ^-*."* Generally in the literature the measured values of γ^+ on dried solid surfaces is credited to hydration or residual wetness. These same substances often show dipolarity in aqueous solutions. For this reason the γ^+ variable must be considered to be the most vulnerable to differences in sample preparation. Care was taken to maintain methodological approach for all mineral samples.

Table 2-16 Lewis Acid Surface Energy Summary

Lewis Acid Summary			
Group	Average ergs/cm^2	St. Dev. ergs/cm^2	Co. Var. ergs/cm^2
Phyllosilicates	0.31	0.34	109.91%
Carbonates	0.63	0.61	97.61%
Sulfates	0.97	0.59	60.34%
Feldspars	0.72	0.73	100.75%
Oxides	1.07	1.55	144.40%
Clay Minerals	3.29	2.43	74.02%
Neso/Inosilicates	3.72	4.32	116.30%

However, each of the samples experienced atmospheric conditions for a small period of time between the oven and the universal sorption device testing. Highly absorbent minerals are expected to regain more of their electron acceptivity within that timeframe. For this reason it may be important to normalize acid surface energy components when comparing datasets to remove sample preparation variance.

The average acid component for all minerals was 1.39 ergs/cm^2. Performing a t-test analysis on minerals showed no significant difference between the datasets. This reinforces the conclusion that the acid component is a method preparation dependent variable. Coefficients of variation ranged from 60.34% for sulfates to 184.7% for aggregates. The average coefficient of variation for all groups was 111%. Based on an analysis of literature values and this research a normal range for acid surface energies of natural minerals is likely in the range of 0.01 to 4 ergs/cm^2 after heating to 75°C.

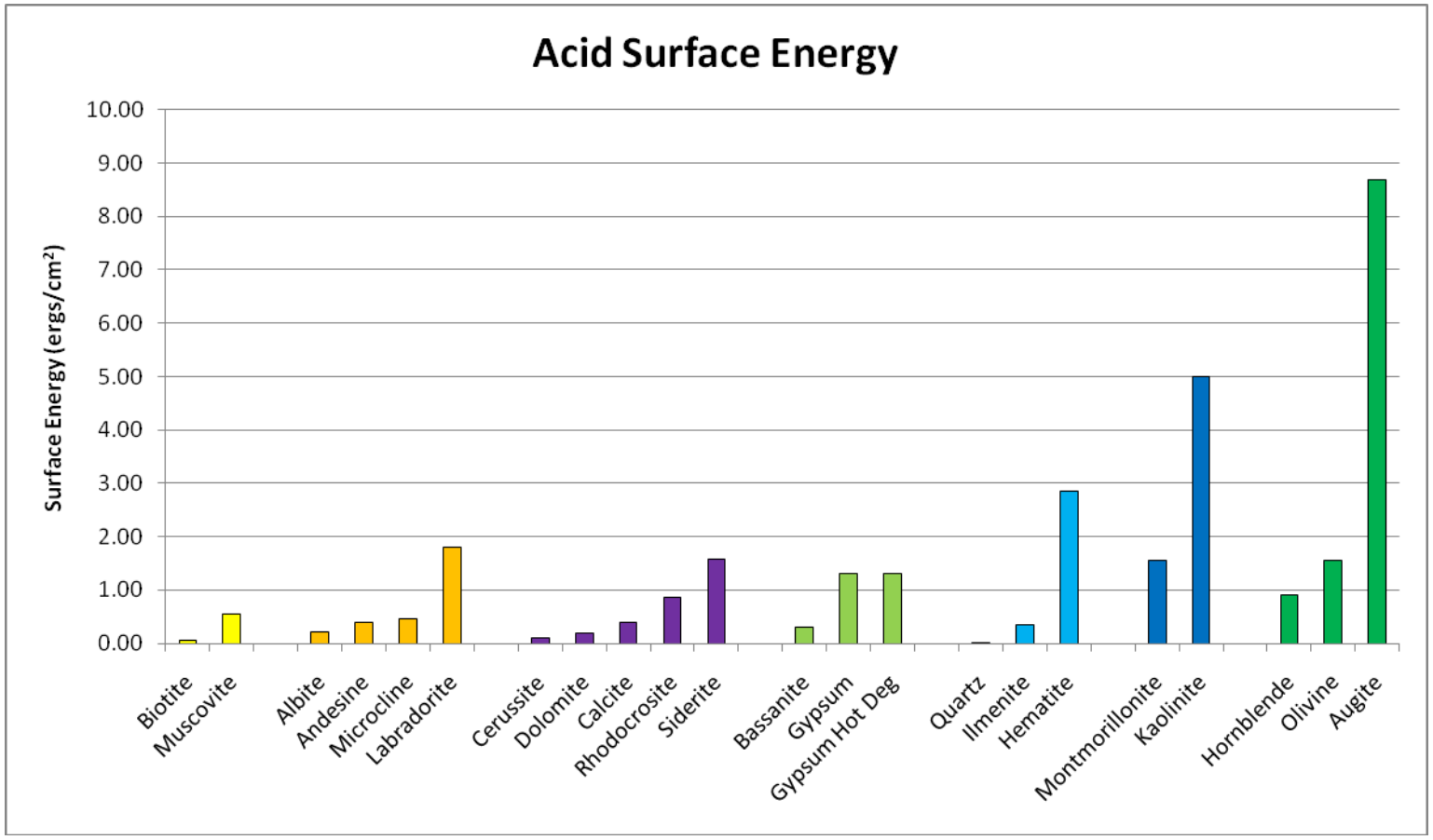

Figure 2-10 Lewis Acid Surface Energy (All)

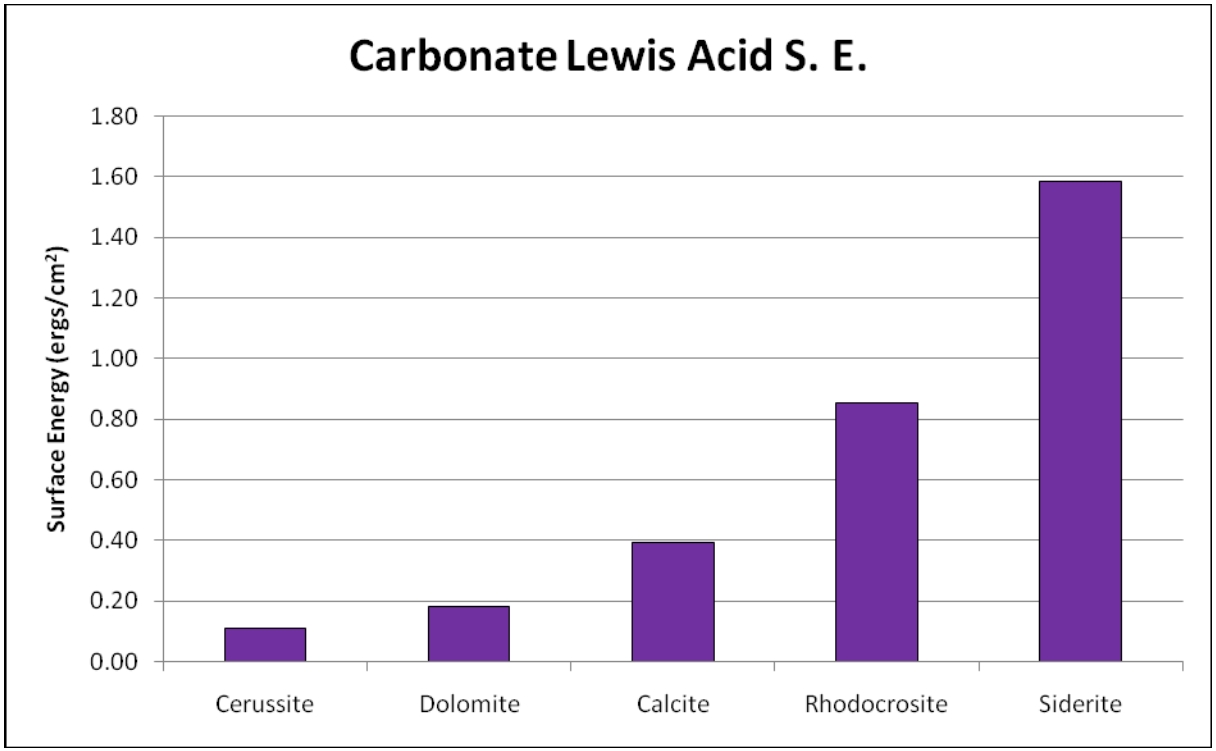

Figure 2-11 Lewis Acid Surface Energy (Carbonates)

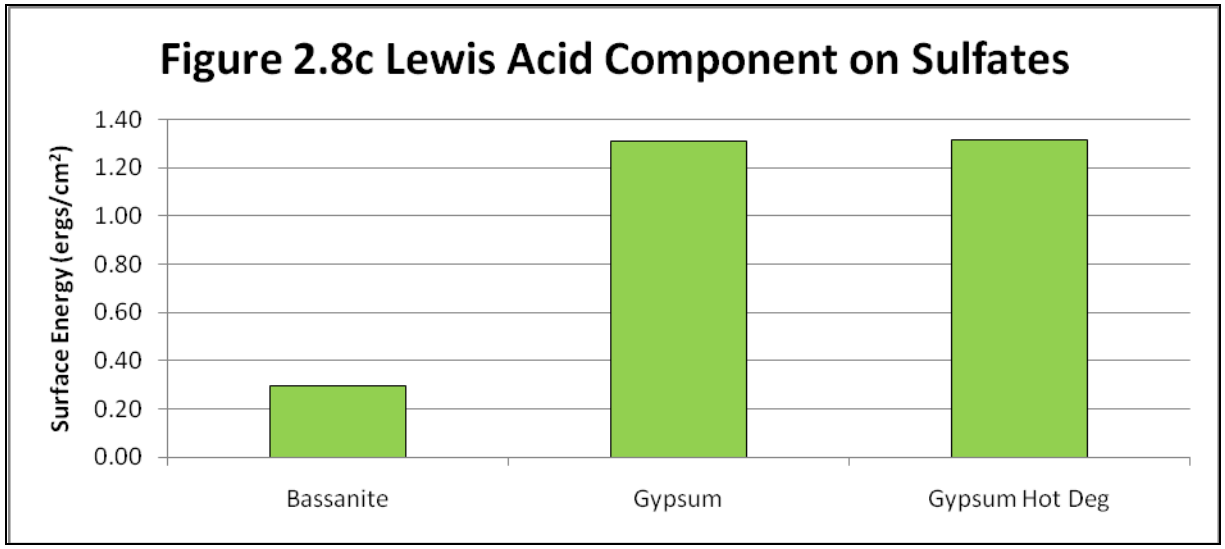

Figure 2-12 Lewis Acid Surface Energy (Sulfates)

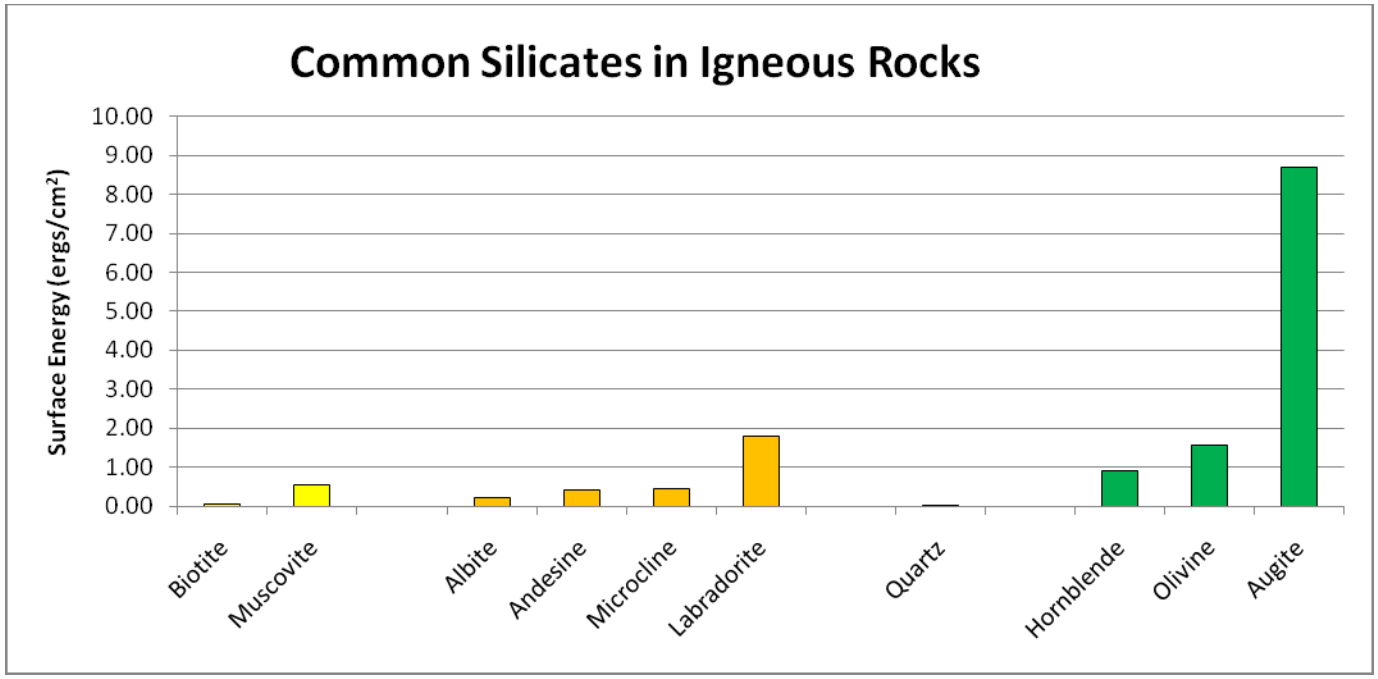

Figure 2-13 Lewis Acid Surface Energy (Common Silicates)

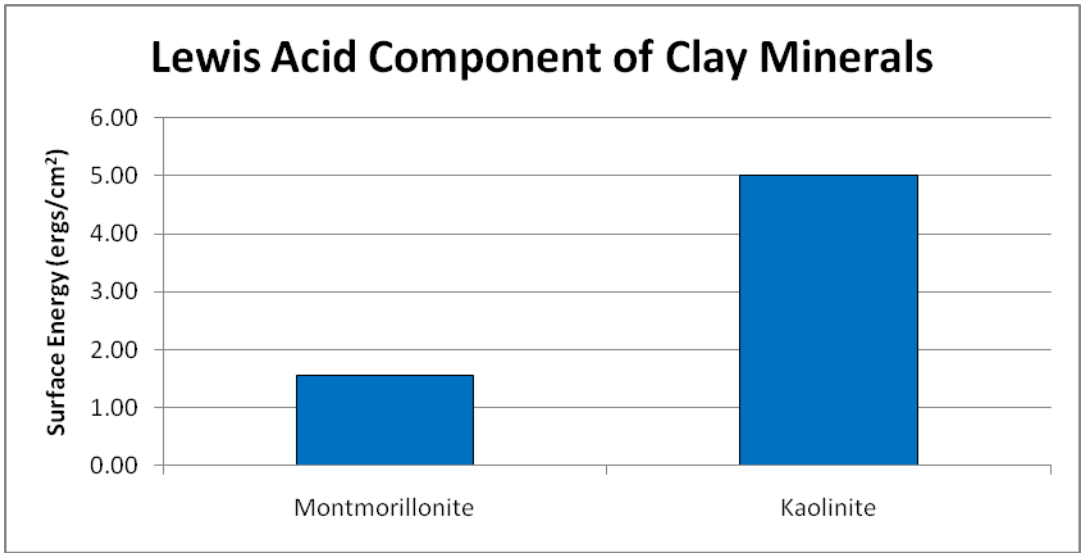

Figure 2-14 Lewis Acid Surface Energy (Clay Minerals)

Lewis Base Component: The base component is the most variable of the three portions of surface energy. Measurements range from 3890.33 for augite to 57.52 ergs/cm^2 for olivine as shown in Table 2-17 and Figures 2-15 through 2-17. The Lewis base component tends to dominate polar surface energies of dry surfaces because the electron donicity neutralizes the electron acceptivity.

Table 2-17 Lewis Base Surface Energy Summary

Lewis Base Summary			
Group	Average ergs/cm^2	St. Dev. ergs/cm^2	Co. Var. ergs/cm^2
Clay Minerals	80.22	0.31	0.39%
Carbonates	339.55	318.79	93.88%
Oxides	413.99	126.89	30.65%
Phyllosilicates	677.33	187.58	27.69%
Sulfates	1063.05	1708.68	160.73%
Feldspars	1161.51	1735.08	149.38%
Neso/Inosilicates	1762.24	1951.16	110.72%

The average Lewis base surface energy for all minerals was 798.94 ergs/cm^2 with a median of 342, and the average for aggregates was less at 569.07 ergs/cm^2 with a median of 469. This was the only surface energy component that the aggregates were not the highest average category. Coefficients of variation were generally similar to Lewis acid coefficients. The clay minerals had the lowest at less than one percent while the sulfates had the highest at 160.73%. The average coefficient of variation was 78.41% for all groups. The 95% confidence interval for all minerals was 307.55 - 1290.33 ergs/cm^2. Computing a t-test showed no significant difference between minerals. The highest and lowest values were, in fact, in one single grouping (Neso/Inosilicates).

The Lewis base surface energy component is the most important contributor to surface reactivity with polar sites. It is difficult to establish trends, however, because of the large variation between values across mineral groups and within groups. If augite, andesine, and bassanite are taken out of the dataset the average for all minerals becomes 362.91 ergs/cm^2. This is a decrease of 45% based on removing only 14% of the dataset. The coefficient of variation between all groups then becomes 52.06%. Bassanite is likely a correct figure based on the preparation procedures. Augite and andesine may need to be reevaluated on the USD to verify the accuracy of these measurements.

Total Polar Component: The polar surface energy component is the most important component for comparing surface characteristics of minerals based on its larger variation than van der Waals and the ubiquitous nature of electron donor/acceptor interactions. The total polar surface energy is computed based on equation 2.4. The results are shown in Table 2-18. The polar surface energies ranged from 1.2 for RA Granite to 367.78 ergs.cm^2 for augite. The average coefficient of variation for all groups was 84.78%. The 95% confidence interval range for all minerals was 16.86 to 79.61 ergs/cm^2.

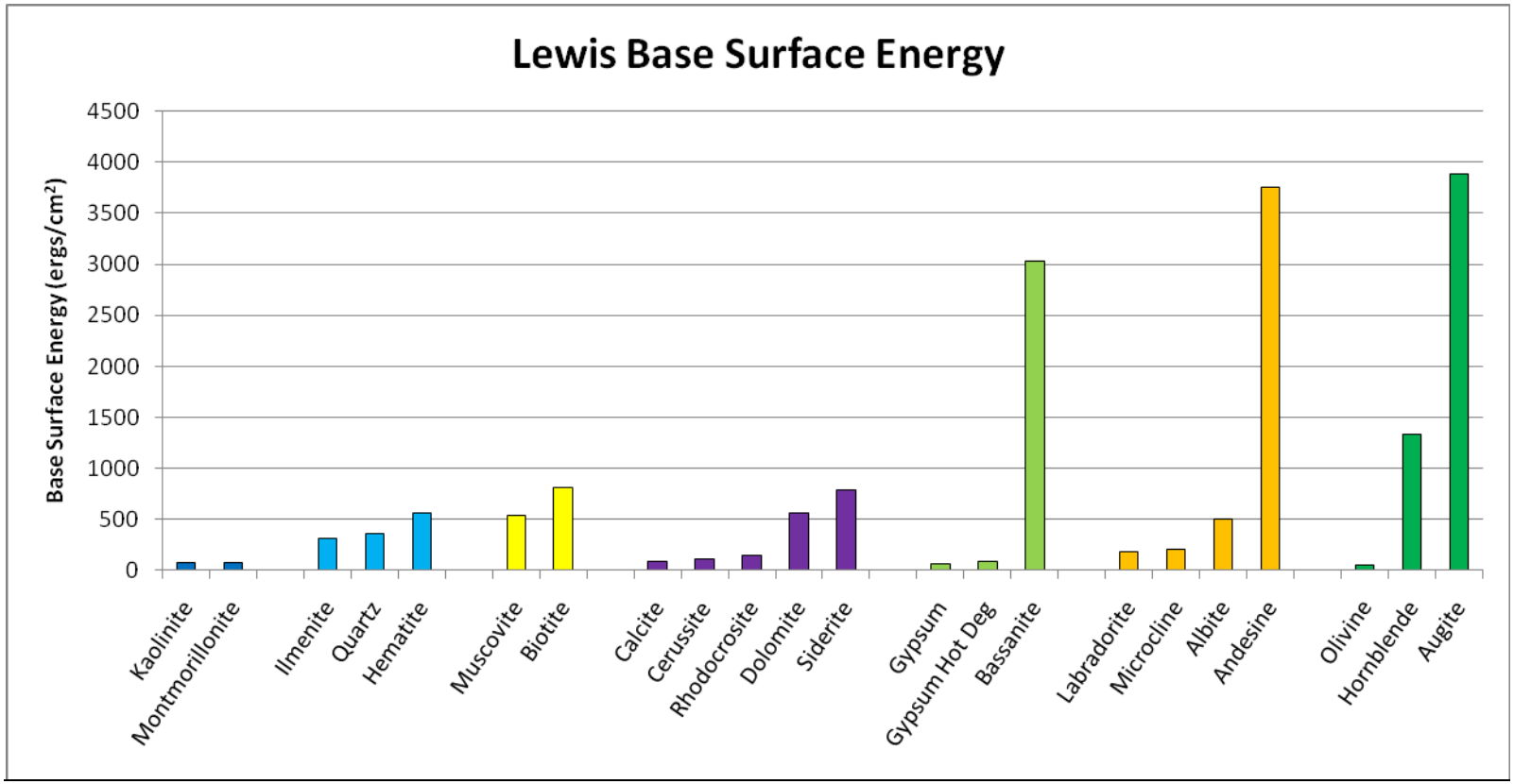

Figure 2-15 Lewis Base Surface Energy (All)

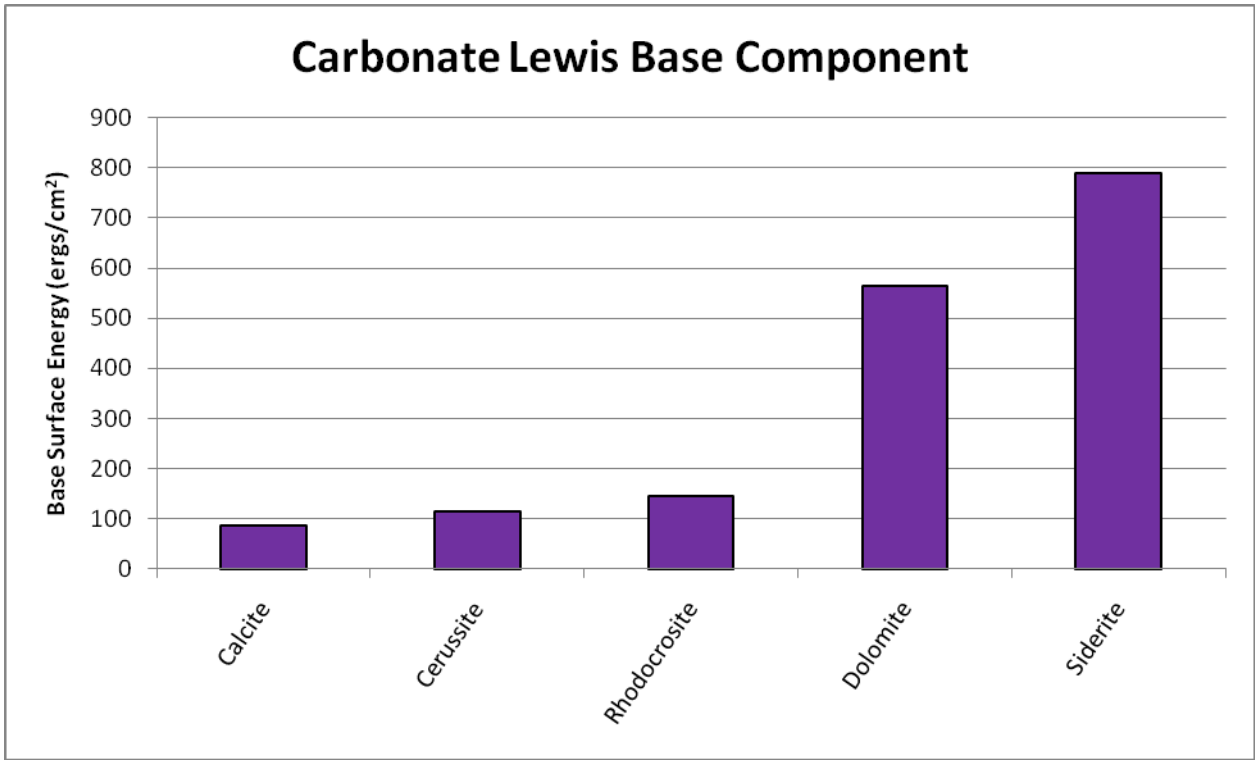

Figure 2-16 Lewis Base Surface Energy (Carbonates)

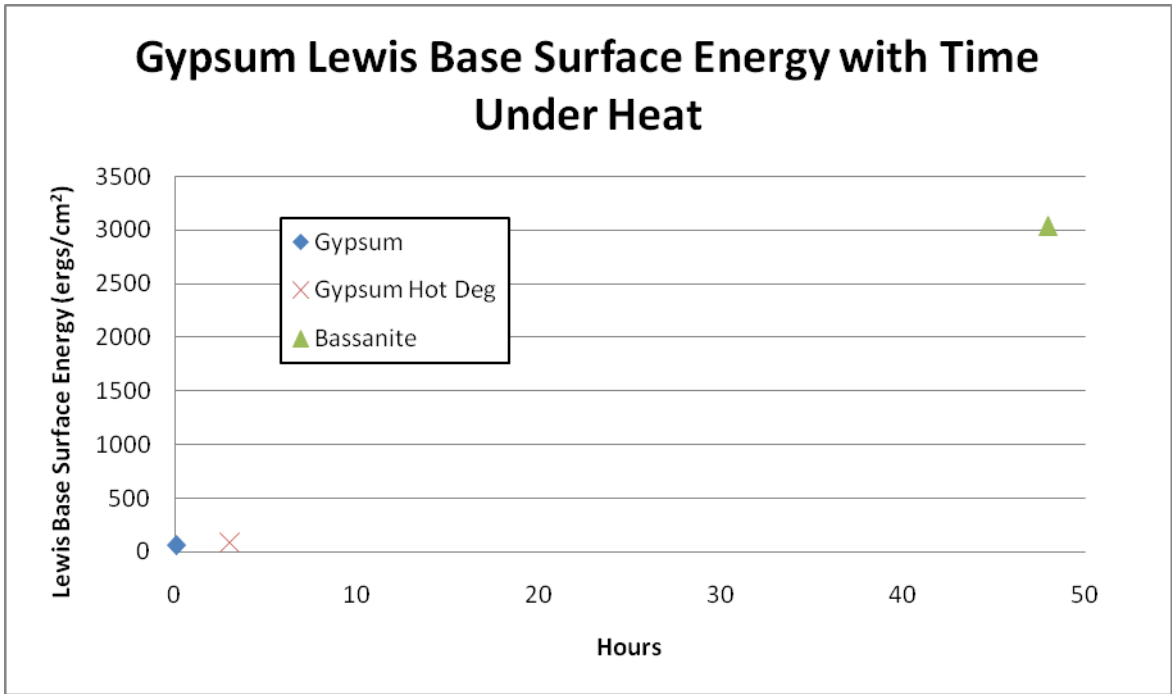

Figure 2-17 Effect of Heat on Gypsum Lewis Base Surface Energy

Table 2-18 Polar Surface Energy Summary

Polar Surface Energy Summary			
Group	Average ergs/cm^2	St. Dev. ergs/cm^2	Co. Var. ergs/cm^2
Carbonates	26.41	25.59	96.88%
Phyllosilicates	24.71	13.87	56.12%
Clay Minerals	31.23	12.43	39.79%
Sulfates	33.30	23.08	69.30%
Oxides	35.33	39.36	111.41%
Feldspars	38.74	27.11	69.97%
Neso/Inosilicates	152.12	188.49	123.91%

The hard/soft acid base concept (HSAB) was used to evaluate and compare the polar surface energy components within classes. The carbonates' surface hardness was calculated, and the results were plotted against the polar surface energy. There does appear to be a correlation with an R^2 of .56. However, a better fit is between the moles of organic carbon measured on the surface with XPS as compared with the polar surface energy. Thus, carbonate polar energy seems to be heavily influenced by surface coatings. It can be argued, however that the organic carbon is not the cause of the surface energy, but rather a result of the surface chemistry which is being measured. This could be validated by a comparison of these same carbonate minerals if the organic coatings were removed. Acid solvents cannot be used to carbonates. A heating process may drive much of the organic carbon into the interior of the mineral rather than volatilizing all of it. Further study could elucidate important controls on the surface energy of carbonates. Phyllosilicates also showed some correlation with the HSAB comparison. No conclusions can be draw based on the limited dataset. However, again there is a comparison that fits the data with the moles of organic carbon on the surface measured by XPS and the polar surface energy. If more phyllosilicates are measured will the hypothesis hold that the surface is influenced by the hardness and polarity/magnitude of the surface coatings? The polar surface energy of feldspars does not continue to follow this trend. A poor correlation is seen with the surface hardness; however no correlation is seen with organic

carbon coating. The surfaces of complex tectosilicates such as feldspars may be heavily influenced by surface morphology.

The polar surface energy of the gypsum was seen to increase with heating. The hot gypsum was not heated long enough to remove any compositional waters. For this reason the hot gypsum should be more similar to gypsum than to bassanite. This is exactly what is seen. The bassanite polar surface energy is approximately three times higher than gypsum. Bassanite does not return to gypsum under atmospheric conditions; however the removal of water does present a strong affinity for regaining the lost water as outersphere complexes. Thus, the bassanite has a strong polar affinity. The results are shown in Figures 2-18.

Total Surface Energy

Combining known knowledge of individual mineral surface characteristics to surface energy results can correlate type and density of active surface sorption sites. The total surface energy is essentially that surface's affinity for adsorption. Higher van der Waals components correspond with affinity for reaction with nonpolar species. If a mineral or aggregate has a high polar component it will 'want' to bond with species of high polar energy. Therefore, the total surface energy is less important than the magnitudes of the respective components for predicting interactions. The results are shown in Figures 2-19 through 2-23.

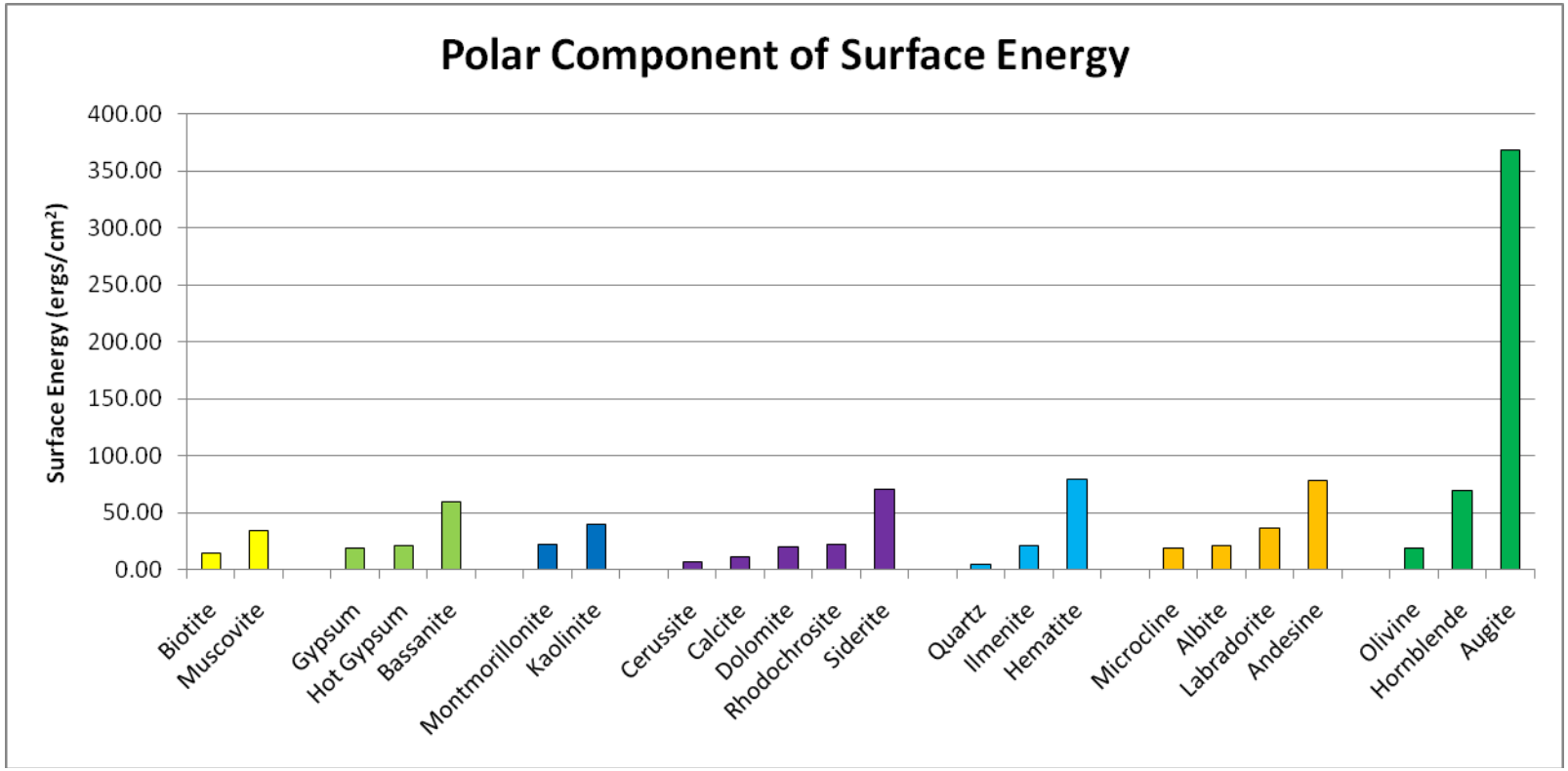

Figure 2- 18 Total Polar Surface Energy (All)

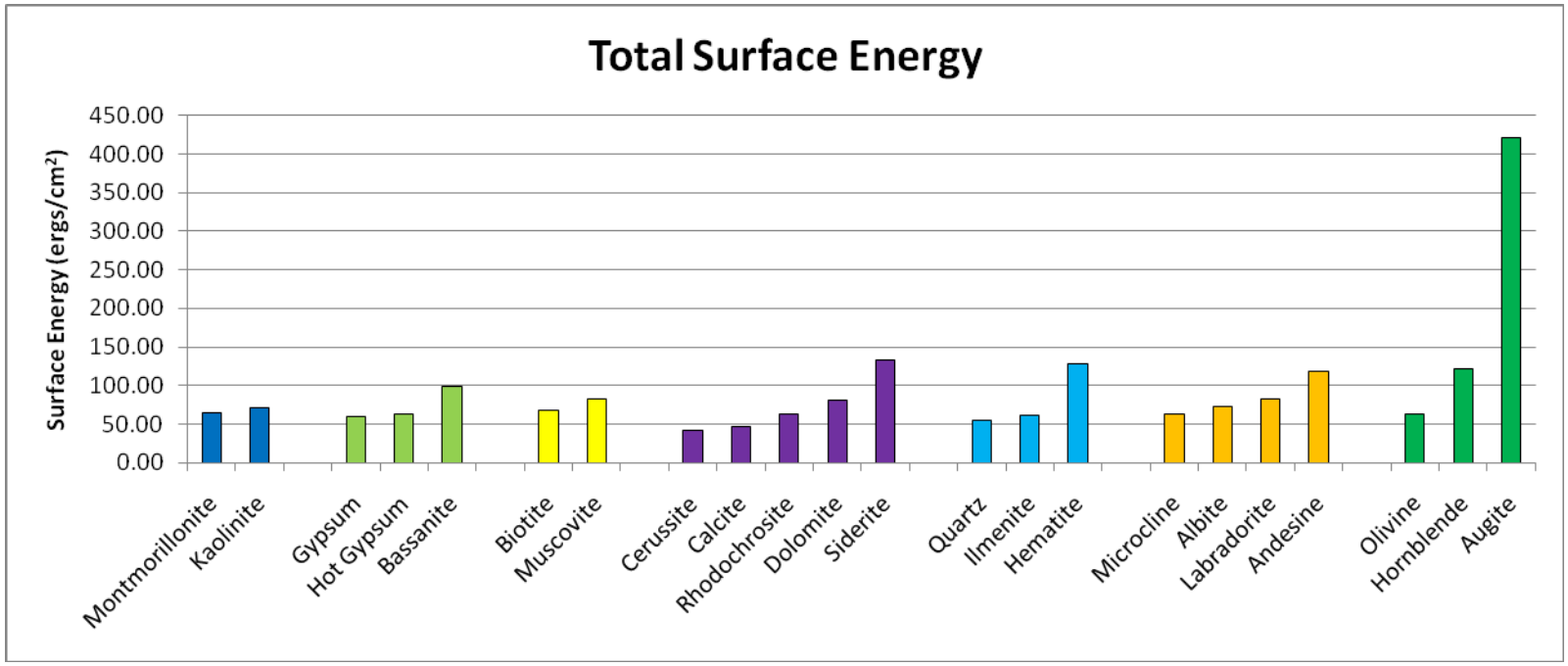

Figure 2-19 Total Surface Energy

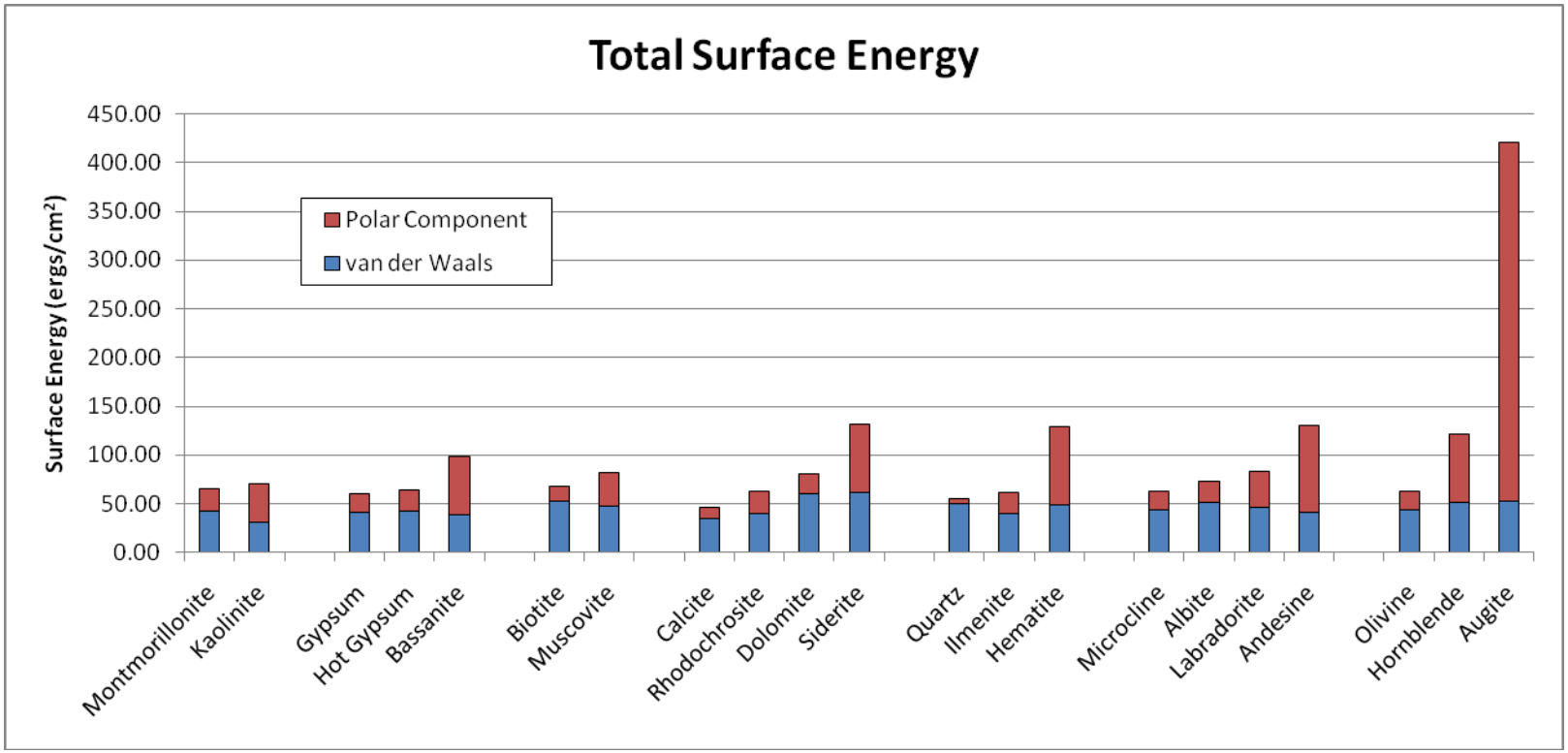

Figure 2-20 Total Component Surface Energy

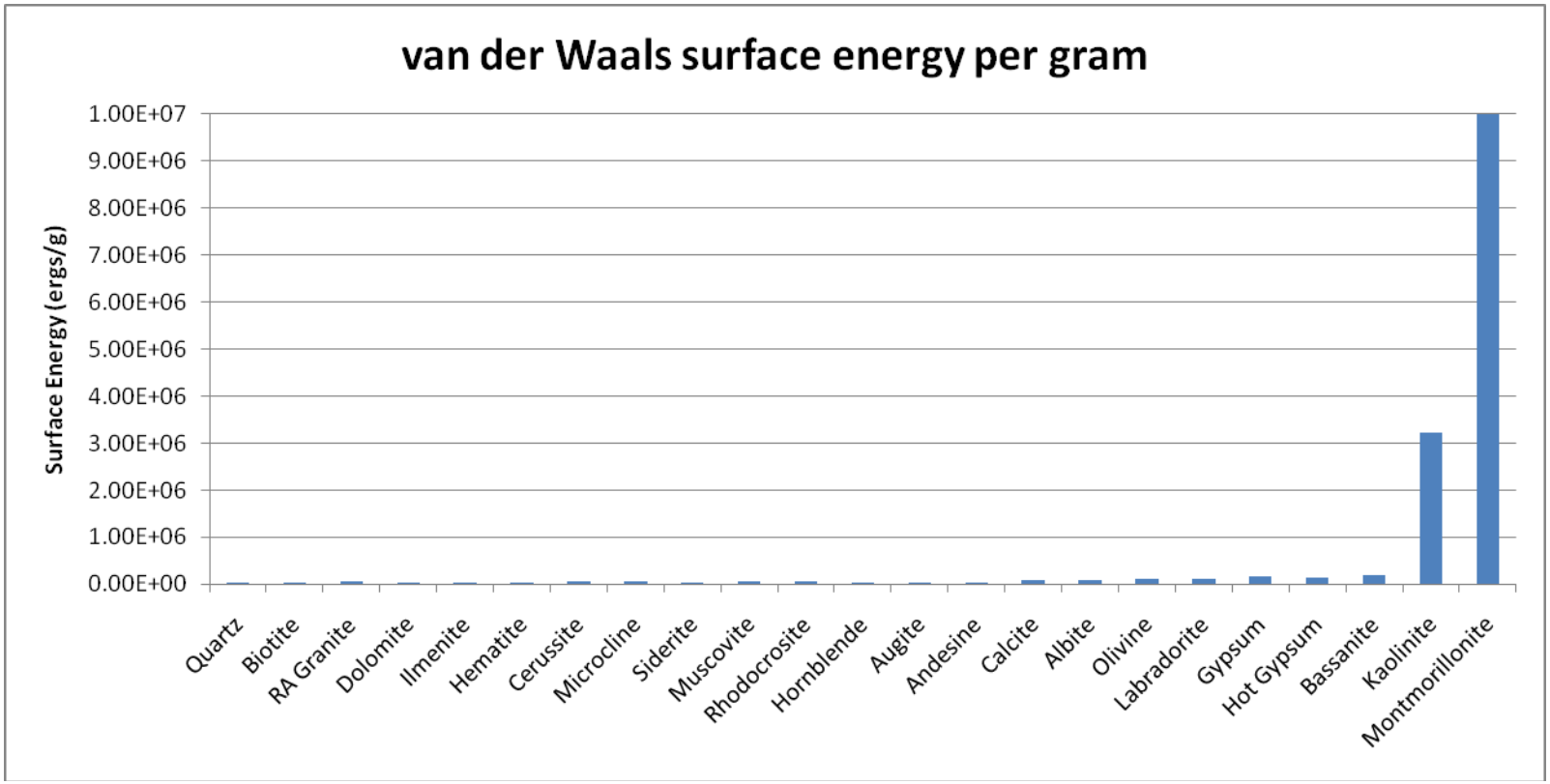

Figure 2-21 van der Waals Surface Energy per Gram

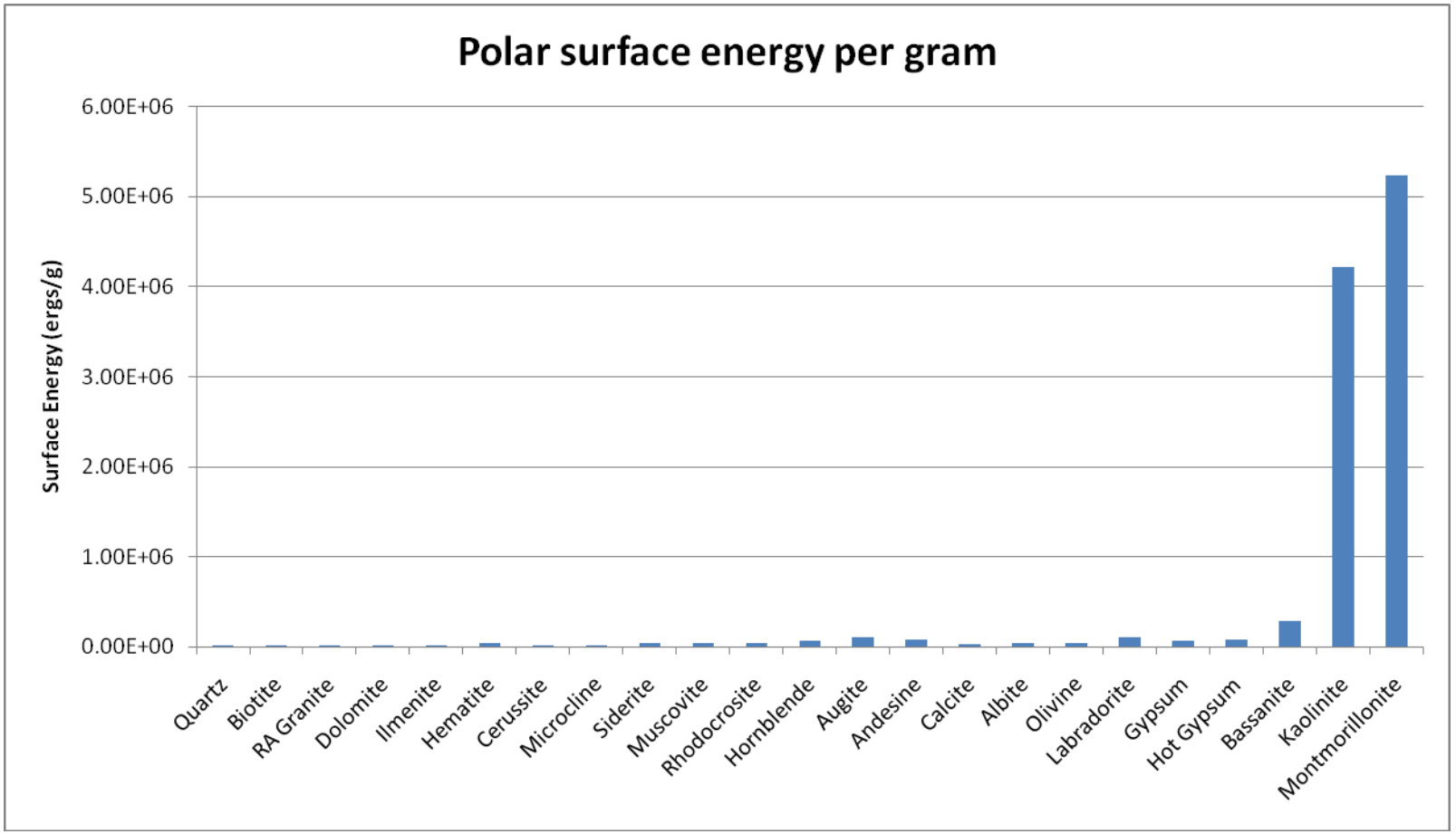

Figure 2-22 Polar Surface Energy per Gram

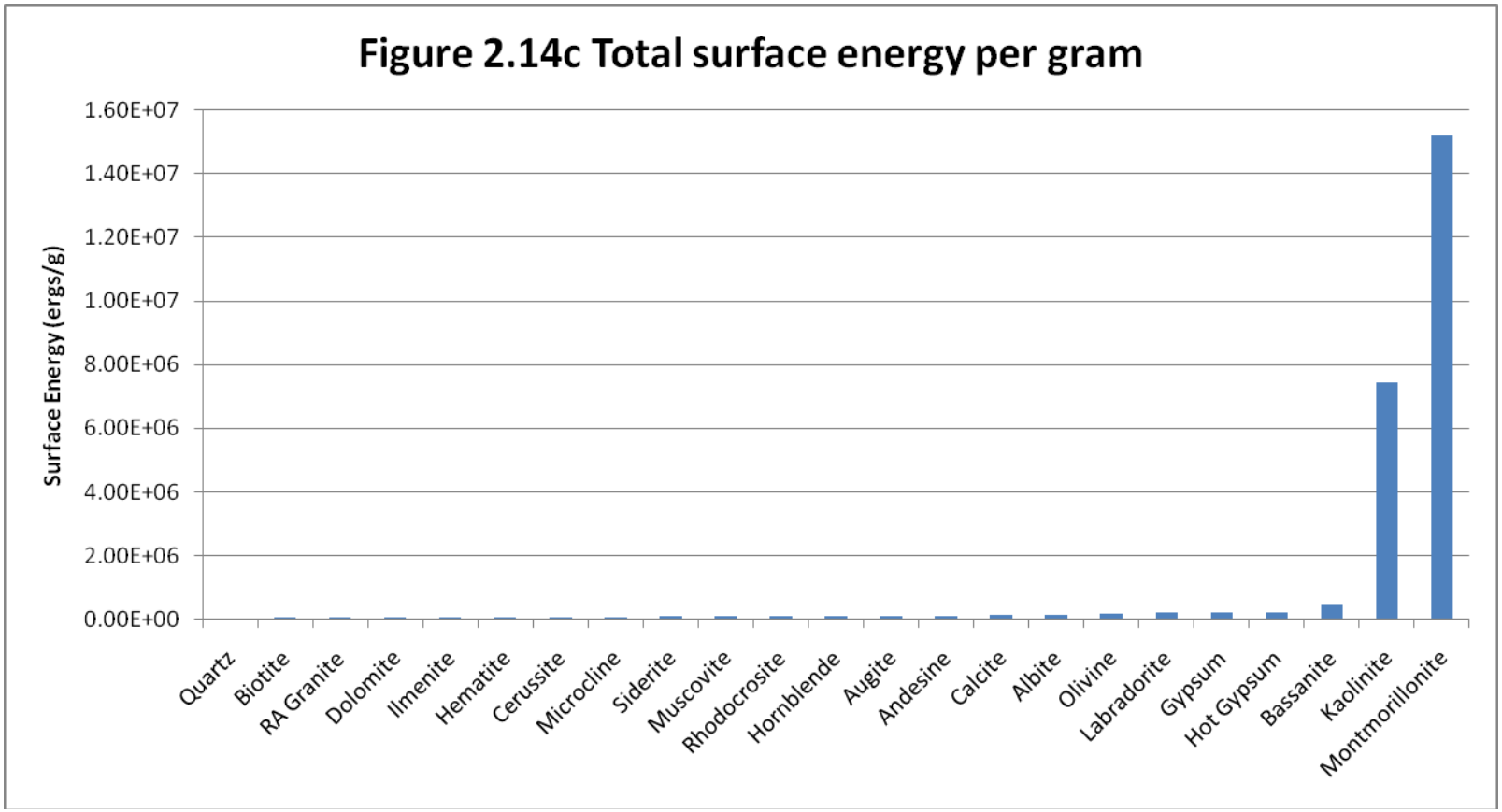

Figure 2-23 Total Surface Energy per Gram

Conclusions

In the current research the major difficulty is in understanding the complex interrelationship between the three master variables of surface energy: surface chemistry, surface morphology, and surface coatings. The current paradigm is to separate these three variables and analyze them independently. This is primarily due to difficulties in methodology. Surface energy cannot be directly measured unless the substance is a liquid or a gas. Thus, proxies such as adsorption of well characterized compounds, must be used. Additionally, current research on the relationship between surface energy and surface chemistry focuses on chemical and structural functional groups as active sites (ph dependent, siloxane cavities, etc.) This functionalist approach is useful to understand interfacial reactions, however it stops short of explaining the magnitude or strength of these sites. Rather, active site research describes affinity between species. Surface coatings affect surface energy of solids in, perhaps a less well known manner. It is obvious that sorption affects electrostatic interactions. It less well known how much sorption affects the surface energy of solids. This gap in knowledge again springs from methodology on the part of measuring surface energy. Good-van Oss theory states that the total surface energy is the sum of the polar and nonpolar components (VAN OSS, 2006). Does adsorption of a polar solvent then alter the polar component only? How then is the effect quantified? Additionally, the role of surface morphology in surface energy is the least well known of the three master variables. The importance of structure on adhesion has been shown best through the creation of superhydrophobic surfaces. These surfaces may be chemically very reactive, however the structure or roughness will not allow adhesion to take place. It the role of roughness only important for certain morphologies or does it always play a role in surface energy? Can the affect of morphology on surface adhesion be quantified?

An additional complexity lies in the desire to understand these interrelationships for natural minerals rather than artificially created laboratory systems which have no real correlation to natural systems. Natural minerals are chemically heterogeneous, have

irregular surfaces, and are generally coated with organics and inorganics. For this reason this project chose to simplify the systems without taking away their relevance to natural media. This was accomplished by obtaining chemically homogeneous minerals then producing new faces through mineral cleavage and fracture. The samples maintained their relevance to natural media in two ways. First, the samples were not subjected to harsh chemical treatments in order to 'clean' the surfaces. Second, the method of creating new surfaces mimicked natural physical erosion. This was important because previous contact angle measurements, inverse gas chromatographic methods, and thin layer wicking each rely on the production of artificial surfaces or pressed powders. In addition the USD creates an average of all the surfaces on the measured samples instead of one unique face followed by another unique face.

In comparing measurements it is most useful to compare each of the mineral classes separately. For this the reader is referred to the individual sections on each group. However, several general conclusions can be made. First,

- Organic coatings appear to make the most impact when the amount becomes great enough to be considered as a separate phase.

This is most evident in the comparison of carbonates. The hard/soft acid/base (HSAB) concept appears to hold true for the samples until the amount of organic carbon on the surface increases significantly. The siderite sample (4.4 moles of organic carbon) appears to have enough organic coating to have established a separate phase. None of the other carbonate samples had as much organic carbon (1.07, 1.95, 0.92, and 1.46 moles). However, a weak positive trend can also be seen when all of the Lewis Base component surface energies are plotted against moles of surface organics. This leads to the second observation:

- Organic coatings may increase the Lewis base component.

By comparing each of the individual mineral groups there is no noticeable pattern that arises from the magnitude of the organic material on the surface with van der Waals and Lewis Acid as shown in Figures 2-24 and 2-25. However, when comparing all of the groups together there appears to an increase in Lewis base surface energy with

organic coatings. A weak linear correlation exists among each of the mineral groups between Lewis basicity and total organic carbon. This might show that surface coatings always play a role in surface energy, but are additionally affected by other variables. If a strong correlation was seen then it could be argued that organic coatings are a dominant control on Lewis Basicity. This, however was not seen.

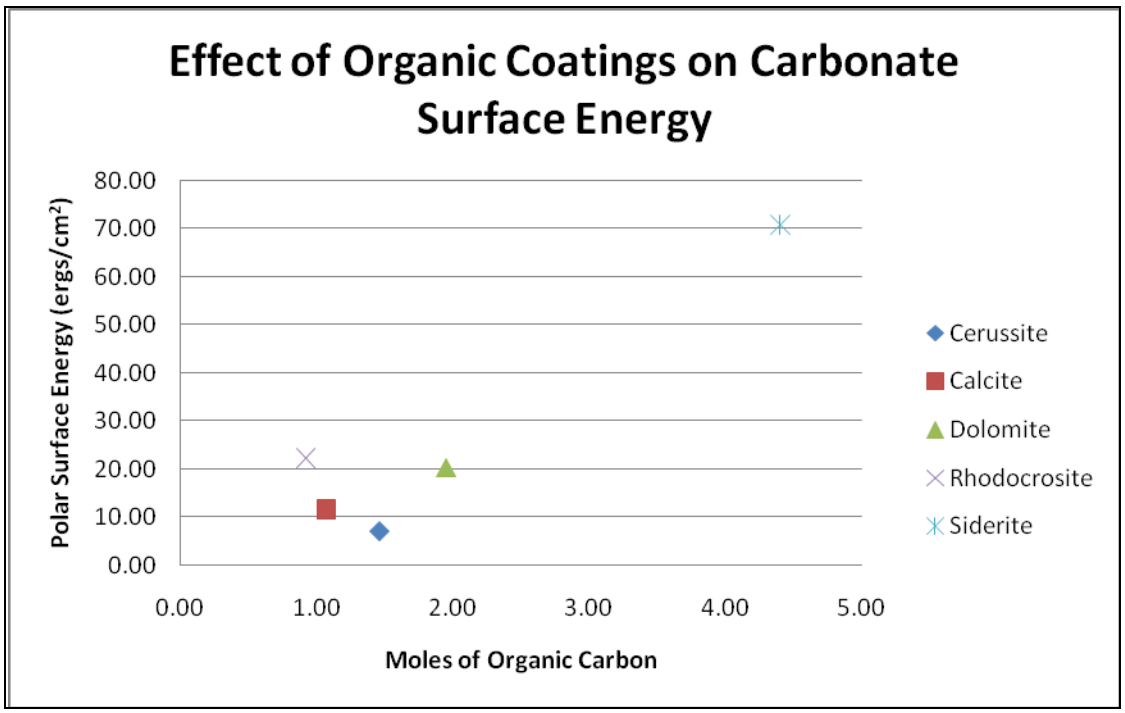

Figure 2-24 Effect of Organic Coatings on Carbonate Surface Energy

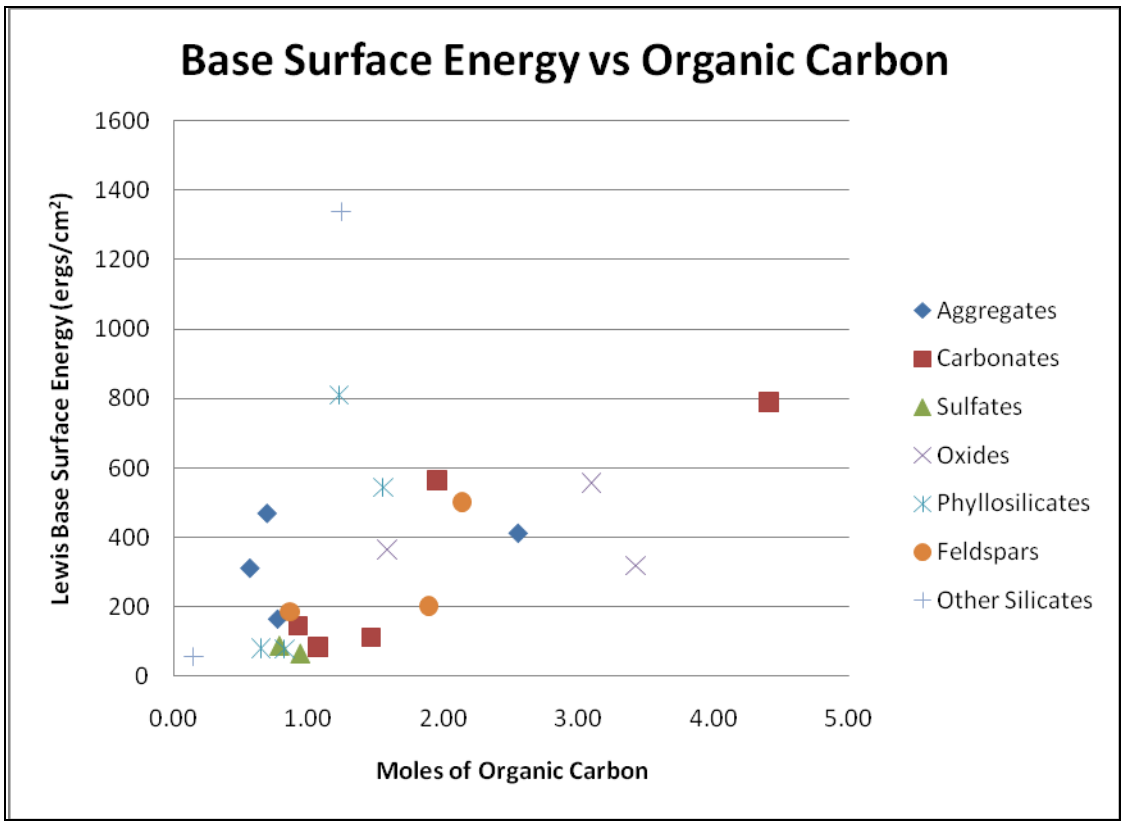

Figure 2-25 Effect of Organic Coatings on Lewis Base Surface Energy

Thirdly,

- X-ray photoelectron spectroscopic methods used to measure surface chemistry appear to correlate well with electron microprobe measurements.

A comparison was made in Table 2-11 of the ideal, XPS measured surface chemistry, and the microprobe measured bulk chemistry. The results correlated very well between the two methods indicating that XPS is a reliable technique that can be used to measure surface chemical compositions. XPS is also very useful because of the lack of penetration of the X-Rays into the bulk material. This is useful for artificial samples where the surface chemistry is often different from the bulk chemistry. Fourth,

- The universal sorption device specific surface area calculations correlate well with literature values for similar minerals.

Bhasin (BHASIN and LITTLE, 2007; CHENG, 2002b) found that a good correlation exists between aggregate SSA measurements of n-Hexane adsorption and BET nitrogen adsorption. This research (Table 2-13) found that results compared well with published values for similar minerals. This may be evidence that the assumption of n-Hexane preferentially laying along its long axis is correct. Next,

- Surface roughness/morphology appears to play an important role in the overall surface energy of minerals.
- A knowledge gap exists between the relationship between surface roughness and surface energy.

This project did not always draw clear relationships between surface chemistry and surface energy. This may be caused by inaccurate descriptions of surface chemistries or surface coatings. The tight correlation between XPS and electron microprobe tends to discredit this possibility however. Additionally, measured values of organic and inorganic coatings varied between minerals while keeping accuracy between samples of the same mineral. The capability of XPS to accurately characterize surface chemistries of natural minerals appears to be highly reliable. Another possibility may be that a model for understanding the relationship between surface chemistry and adhesion of probe vapors simply does not yet exist. This is probably not true. Most likely the surface roughness of the minerals is playing an important role in the adhesion of the reference vapors.

REFERENCES

Adamson, A. W. and Klerer, J., 1977. Physical chemistry of surfaces. *Journal of the Electrochemical Society* **124**, 192C.

Arnold, T., Zorn, T., Zänker, H., Bernhard, G., and Nitsche, H., 2001. Sorption behavior of U (VI) on phyllite: experiments and modeling. *Journal of Contaminant Hydrology* **47**, 219-231.

Bakker, G., 1928. Wien-Harms Handbook on Experimental Physics, 6. Akademische Verlags- gesellschaft, Leipzig, Germany

Barker, C., 1980. Primary migration: the importance of water-mineral-organic matter interactions in the source rock. *Problems of petroleum migration: AAPG Studies in Geology* **10**, 19-31.

Bauer, A. and Berger, G., 1998. Kaolinite and smectite dissolution rate in high molar KOH solutions at 35 and 80 C. *Applied Geochemistry* **13**, 905-916.

Becker, U., Rosso, K. M., and Hochella, M. F., 2001. The proximity effect on semiconducting mineral surfaces: a new aspect of mineral surface reactivity and surface complexation theory? *Geochimica et Cosmochimica Acta* **65**, 2641-2649.

Benedetti, M. F., Menard, O., Noack, Y., Carvalho, A., and Nahon, D., 1994. Water-rock interactions in tropical catchments: field rates of weathering and biomass impact. *Chemical Geology* **118**, 203-220.

Benner, F. C. and Bartel, F. E., 1941. The effect of polar impurities upon capillary and surface phenomena in petroleum production. *Drilling and Production Practice* **6**, 41-341.

Bennett, P. C., Hiebert, F. K., and Choi, W. J., 1996. Microbial colonization and weathering of silicates in a petroleum-contaminated groundwater. *Chemical Geology* **132**, 45-53.

Bhasin, A. and Little, D. N., 2007. Characterization of aggregate surface energy using the universal sorption device. *Journal of Materials in Civil Engineering* **19**, 634-641.

Bhasin, A., Little, D. N., Vasconcelos, K. L., and Masad, E., 2007. Surface free energy to identify moisture sensitivity of materials for asphalt mixes. *Transportation Research Record* **2001**, 37-45.

Bikerman, J. J., 1978. Surface energy of solids. *Topics in Current Chemistry* **77**, 1-66.

Boyd, G. E. and Livingston, H. K., 1942. Adsorption and the energy changes at crystalline solid surfaces. *Journal of the American Chemical Society* **64**, 2383-2388.

Brantley, S. L. and Mellott, N. P., 2000. Surface area and porosity of primary silicate minerals. *American Mineralogist* **85**, 1767-1783.

Brown, R. C., 1947. The fundamental concepts concerning surface tension and capillarity. *Proceedings of the Physical Society* **59**, 429-448.

Bucci-Sabattini, V., Cassinelli, C., Coelho, P. G., Minnici, A., Trani, A., and Ehrenfest, D. M. D., 2010. Effect of titanium implant surface nanoroughness and calcium phosphate low impregnation on bone cell activity in vitro. *Oral Surgery, Oral Medicine, Oral Pathology, Oral Radiology and Endodontology* **109**, 217-224.

Cabeo, N., 1629. Confutatur Gilberti opinio de electricis atractionibus & cur humida, bullm in aqua, & alia confluant, hanc yore non esse electrieam atraetionem. *Philosophia Magnetica, Ferrara* **lib. ii**.

Callow, M. E. and Fletcher, R. L., 1994. The influence of low surface energy materials on bioadhesion--a review. *International Biodeterioration & Biodegradation* **34**, 333-348.

Carpick, R. W., Agrait, N., Ogletree, D. F., and Salmeron, M., 1996. Measurement of interfacial shear (friction) with an ultrahigh vacuum atomic force microscope. *Journal of Vacuum Science & Technology* **14**, 1289-1295.

Caseri, W. R., Shelden, R. A., and Suter, U. W., 1992. Preparation of muscovite with ultrahigh specific surface area by chemical cleavage. *Colloid & Polymer Science* **270**, 392-398.

Cheng, D., 2002a. Thesis, Surface Free Energy of Asphalt-aggregate System and Performance Analysis of Asphalt Concrete Based on Surface Free Energy, Texas A&M University, College Station.

Chibowski, E. and Gonzalez-Caballero, F., 1993. Theory and practice of thin-layer wicking. *Langmuir* **9**, 330-340.

Chibowski, E. and Perea-Carpio, R., 2002. Problems of contact angle and solid surface free energy determination. *Advances in Colloid & Interface Science* **98**, 245-264.

Chibowski, E. and Staszczuk, P., 1988. Determination of surface free energy of kaolinite. *Clays and Clay Minerals* **36**, 455-461.

Chibowski, E. and Waksmundzki, A., 1978. A relationship between the zeta potential and surface free energy changes of the sulfur/n-Heptane-Water system. *Journal of Colloid & Interface Science* **66**, 213-219.

Churaev, N. V., 1995. Contact angles and surface forces. *Advances in Colloid & Interface Science* **58**, 87-118.

Clint, J. H., 2001. Adhesion and components of solid surface energies. *Current Opinion in Colloid & Interface Science* **6**, 28-33.

Clint, J. H. and Wicks, A. C., 2001. Adhesion under water: surface energy considerations. *International Journal of Adhesion and Adhesives* **21**, 267-273.

Clow, D. W. and Drever, J. I., 1996. Weathering rates as a function of flow through an alpine soil. *Chemical Geology* **132**, 131-141.

Costanzo, P. M., Giese, R. F., and Van Oss, C. J., 1990. Determination of the acid-base characteristics of clay mineral surfaces by contact angle measurements-implications for the adsorption of organic solutes from aqueous media. *Journal of Adhesion Science and Technology* **4**, 267-275.

de Laplace, P. S., 1806. Mechanique Celeste. *Supplement to Book* 10. Hilliard , Gray, Little, and Wilkins Publishers, Boston, MA, 1929

Deligianni, D. D., Katsala, N. D., Koutsoukos, P. G., and Missirlis, Y. F., 2001. Effect of surface roughness of hydroxyapatite on human bone marrow cell adhesion, proliferation, differentiation and detachment strength. *Biomaterials* **22**, 87-96.

Della Volpe, C. and Siboni, S., 1997. Some reflections on acid-base solid surface free energy theories. *Journal of Colloid & Interface Science* **195**, 121–136.

Deng, Y. and Dixon, J.B., 2002. Soil mineralogy with environmental applications. (eds. J. B. Dixon and D.G. Schulze) *Soil Organic Matter and Organic Minerals Interactions*. Soil Science Society of America, Inc., Madison, WI

Dos Santos Afonso, M. and Stumm, W., 1992. Reductive dissolution of iron (III)(hydr) oxides by hydrogen sulfide. *Langmuir* **8**, 1671-1675.

Edwards, K. J. and Rutenberg, A. D., 2001. Microbial response to surface microtopography: the role of metabolism in localized mineral dissolution. *Chemical Geology* **180**, 19-32.

Erbil, H. Y., 2003. Transformation of a simple plastic into a superhydrophobic surface. *Science* **299**, 1377-1380.

Evdokimov, I. N., Eliseev, N. Y., and Eliseev, D. Y., 2001. Rheological evidence of structural phase transitions in asphaltene-containing petroleum fluids. *Journal of Petroleum Science and Engineering* **30**, 199-211.

Feng, L., Li, S., Li, Y., Li, H., Zhang, L., Zhai, J., Song, Y., Liu, B., Jiang, L., and Zhu, D., 2002. Super-hydrophobic surfaces: from natural to artificial. *Advanced Materials* **14**, 1857-1860.

Feng, L., Zhang, Y., Xi, J., Zhu, Y., Wang, N., Xia, F., and Jiang, L., 2008. Petal effect: A superhydrophobic state with high adhesive force. *Langmuir* **24**, 4114-4119.

Fowkes, F. M., 1964. Attractive forces at interfaces. *Industrial & Engineering Chemistry* **56**, 40-52.

Fowkes, F. M., 1972. Donor-acceptor interactions at interfaces. *The Journal of Adhesion* **4**, 155-159.

Fowkes, F. M. and Harkins, W. D., 1940. The state of monolayers adsorbed at the interface solid-aqueous solution. *Journal of the American Chemical Society* **62**, 3377-3386.

Gauss, C. F., 1830. *Werke:* vol. 3. Teubner, Germany.

Gibbs, J. W., 1876. *Collected Works and Commentary*. Yale University Press, New Haven, 1936.

Goebel, M. O., Bachmann, J., Woche, S. K., Fischer, W. R., and Horton, R., 2004. Water potential and aggregate size effects on contact angle and surface energy. *Soil Science Society of America Journal* **68**, 383-393.

Gonzalez, G. and Moreira, M. B. C., 1991. The wettability of mineral surfaces containing adsorbed asphaltenes. *Colloids and Surfaces* **58**, 293-302.

Good, R. J. and van Oss, C. J., 1992. The modern theory of contact angles and the hydrogen bond components of surface energies.(eds, Malcolm E. Schrader and Loeb, G. I.) *Modern approaches to wettability: theory and applications*. Plenum Press, New York.

Gregg, S. J. and Sing, K. S. W., 1967. *Adsorption, Surface Area and Porosity*. Academic Press, New York.

Hamaker, H. C., 1937. The London-van der Waals attraction between spherical particles. *Physica* **4**, 1058-1072.

Harkins, W. D. and Boyd, G. E., 1942. The binding energy between a crystalline solid and a liquid: the energy of adhesion and emersion. Energy of emersion of crystalline powders. II. *Journal of the American Chemical Society* **64**, 1195-1204.

Hefer, A. W., Little, D. N., and Herbert, B. E., 2007. Bitumen surface energy characterization by inverse gas chromatography. *Journal of Testing and Evaluation* **35**, 233.

Helmy, A. K., de Bussetti, S. G., and Ferreiro, E. A., 2007. The surface energy of palygorskite. *Powder Technology* **171**, 126-131.

Honjo, S. and Erez, J., 1978. Dissolution rates of calcium carbonate in the deep ocean; an in-situ experiment in the North Atlantic Ocean. *Earth Planetary Science Letters* **40**, 287–300.

Huheey, J. E., Keiter, E. A., Keiter, R. L., and Medhi, O. K., 1983. *Inorganic Chemistry:Principles of Structure and Reactivity*. Harper & Row, New York.

Huttenloch, P., Roehl, K. E., and Czurda, K., 2001. Sorption of nonpolar aromatic contaminants by chlorosilane surface modified natural minerals. *Environmental Science & Technology* **35**, 4260-4264.

Hyne, N. J., 2001. *Nontechnical Guide to Petroleum Geology, Exploration, Drilling, and Production*. Pennwell Publishing, Nashua, NH.

Isaacson, P. J. and Sawhney, B. L., 1983. Sorption and transformation of phenols on clay surfaces: effect of exchangeable cations. *Clay Minerals* **18**, 253-265.

Ista, L. K., Callow, M. E., Finlay, J. A., Coleman, S. E., Nolasco, A. C., Simons, R. H., Callow, J. A., and Lopez, G. P., 2004. Effect of substratum surface chemistry and surface energy on attachment of marine bacteria and algal spores. *Applied and Environmental Microbiology* **70**, 4151-4157.

Janczuk, B. and Bialopiotrowicz, T., 1988. Components of surface free energy of some clay minerals. *Clays and Clay Minerals* **36**, 243-248.

Johnston, C. T., 1996. Sorption of organic compounds on clay minerals. *Clay Minerals Society, CMS Workshop Lectures.*

Johnston, C. T. and E., T., 2002. Surface chemistry of soil minerals. (eds. S. B. Dixon and D. G. Schulze), *Soil Mineralogy with Environmental Applications*. Soil Science Society of America, Inc. Madison, WI.

Jozefaciuk, G. and Bowanko, G., 2002. Effect of acid and alkali treatments on surface areas and adsorption energies of selected minerals. *Clays and Clay Minerals* **50**, 771-783.

Jura, G. and Harkins, W. D., 1944. Surfaces of solids. XI. Determination of the decrease (p) of free surface energy of a solid by an adsorbed film. *Journal of the American Chemical Society* **66**, 1356-1362.

Kaiser, K. and Guggenberger, G., 2003. Mineral surfaces and soil organic matter. *European Journal of Soil Science* **54**, 219-236.

Karaca, S., Gürses, A., Ejder, M., and Açikyildiz, M., 2006. Adsorptive removal of phosphate from aqueous solutions using raw and calcinated dolomite. *Journal of Hazardous Materials* **128**, 273-279.

Karagüzel, C., Can, M. F., Sönmez, E., and Çelik, M. S., 2005. Effect of electrolyte on surface free energy components of feldspar minerals using thin-layer wicking method. *Journal of Colloid & Interface Science* **285**, 192-200.

Kenoyer, G. J. and Bowser, C. J., 1992. Groundwater chemical evolution in a sandy silicate aquifer in Northern Wisconsin. *Water Resources Research* **28**, 591-600.

Khang, D., Lu, J., Yao, C., Haberstroh, K. M., and Webster, T. J., 2008. The role of nanometer and sub-micron surface features on vascular and bone cell adhesion on titanium. *Biomaterials* **29**, 970-983.

Klein, C., 2002. *Mineral Science*. John Wiley & Sons, Inc., San Francisco, CA.

Krebs, R., Gupta, S. K., Furrer, G., and Schulin, R., 1999. Gravel sludge as an immobilizing agent in soils contaminated by heavy metals: a field study. *Water, Air, & Soil Pollution* **115**, 465-479.

Kubilay, Gürkan, R., Savran, A., and Yalcinkaya, Z., 2006. Determination of the surface properties of untreated and chemically treated kaolinites by inverse gas chromatography. *Colloid Journal* **68**, 274-284.

Kwok, D. Y., 1999. The usefulness of the Lifshitz–van der Waals/acid–base approach for surface tension components and interfacial tensions. *Colloids and Surfaces A: Physicochemical and Engineering Aspects* **156**, 191-200.

LaGrega, M. D., Buckingham, P. L., and Evans, J. C., 2000. *Hazardous Waste Management*. McGraw-Hill Science/Engineering/Math, New York.

Lazarevic, S., Radovanovic, Z., Veljovic, D., Onjia, A., Janackovic, D., and Petrovic, R., 2009. Characterization of sepiolite by inverse gas chromatography at infinite and finite surface coverage. *Applied Clay Science* **43**, 41-48.

Little, D. N. and Bhasin, A., 2007. Exploring Mechanism of Healing in Asphalt Mixtures and Quantifying its Impact, *Self Healing Materials*. Springer, Amsterdam, The Netherlands.

Lobato, E., Zhang, J., Yildirim, I., Yoon, R. H., and Yordan, J., 2006. Characterization of Surface Free Energies of Talc Powders Using the Thin Layer Wicking Technique. *Functional Fillers and Nanoscale Minerals: New Markets/New Horizons*, SME Annual Meeting,101-114.

Lower, S. K. and Tadanier, C. J., 2000. Measuring interfacial and adhesion forces between bacteria and mineral surfaces with biological force microscopy. *Geochimica et Cosmochimica Acta* **64**, 3133-3139.

Luttge, A., Zhang, L., and Nealson, K. H., 2005. Mineral surfaces and their implications for microbial attachment: results from Monte Carlo simulations and direct surface observations. *American Journal of Science* **305**, 766.

Makkonen, L., 2000. On the methods to determine surface energies. *Langmuir* **16**, 7669-7672.

McClellan, A. L. and Harnsberger, H. F., 1967. Cross-sectional areas of molecules adsorbed on solid surfaces. *Journal of Colloid & Interface Science* **23**, 577–599.

McMurry, J., 2004. *Organic Chemistry*. Thomson Brooks/Cole, Belmont, CA.

Metz, V., Raanan, H., Pieper, H., Bosbach, D., and Ganor, J., 2005. Towards the establishment of a reliable proxy for the reactive surface area of smectite. *Geochimica et Cosmochimica Acta* **69**, 2581-2591.

Michielsen, S. and Lee, H., 2007. Design of a superhydrophobic surface using woven structures. *Langmuir* **23**, 6004-6010.

Millington, E. C., 1945. Theories of cohesion in the seventeenth century. *Annals of Science* **5**, 253-269.

Miwa, M., Nakajima, A., Fujishima, A., Hashimoto, K., and Watanabe, T., 2000. Effects of the surface roughness on sliding angles of water droplets on superhydrophobic surfaces. *Langmuir* **16**, 5754-5760.

Nakajima, A., Fujishima, A., Hashimoto, K., and Watanabe, T., 1999. Preparation of transparent superhydrophobic boehmite and silica films by sublimation of aluminum acetylacetonate. *Advanced Materials* **11**, 1365-1368.

Napper, D., 1983. Polymeric stabilization of colloid dispersions. Colloid Science, Academic Press, London.

Nelson, R. A. and Hendricks, S. B., 1943. Specific surface of some clay minerals, soils, and soil colloids. *Soil Science* **56**, 285-296.

Neu, T. R., 1996. Significance of bacterial surface-active compounds in interaction of bacteria with interfaces. *Microbiology and Molecular Biology Reviews* **60**, 151-166.

Nosonovsky, M. and Bhushan, B., 2008. Biologically inspired surfaces: broadening the scope of roughness. *Advanced Functional Materials* **18**, 843-855.

Okazaki, S. and Yamazaki, M., 1981. The character of acid sites on the gypsum surface. *Bulletin of the Chemical Society of Japan* **54**, 436-440.

Overbeek, J., 1952. Electrochemistry of the double layer. *Colloid Science* **1**, 115-193.

Papirer, E., Roland, P., Nardin, M., and Balard, H., 1986. Variation of the surface energy characteristics of mica(muscovite) upon grinding. *Journal of Colloid & Interface Science* **113**, 62-66.

Parks, G. A., 1990. Surface energy and adsorption at mineral/water interfaces; an introduction. *Reviews in Mineralogy and Geochemistry* **23**, 133-175.

Pavlovic, S. and Brandao, P. R. G., 2003. Adsorption of starch, amylose, amylopectin and glucose monomer and their effect on the flotation of hematite and quartz. *Minerals Engineering* **16**, 1117-1122.

Pearce, A. I., Pearce, S. G., Schwieger, K., Milz, S., Schneider, E., Archer, C. W., and Richards, R. G., 2008. Effect of surface topography on removal of cortical bone screws in a novel sheep model. *Journal of Orthopaedic Research* **26**, 1377-1383.

Pearson, R. G., 1968. Hard and soft acids and bases, HSAB part I, fundamental principals. *Journal of Chemical Education* **45**, 581-587.

Perruchot, C., Chehimi, M. M., Vaulay, M. J., and Benzarti, K., 2006. Characterisation of the surface thermodynamic properties of cement components by inverse gas chromatography at infinite dilution. *Cement and Concrete Research* **36**, 305-319.

Poisson, 1827. Memoirs de l'academie des Sciences (volume 33)

Ponsonnet, L., Reybier, K., Jaffrezic, N., Comte, V., Lagneau, C., Lissac, M., and Martelet, C., 2003. Relationship between surface properties (roughness, wettability) of titanium and titanium alloys and cell behaviour. *Materials Science & Engineering: C* **23**, 551-560.

Prandtl, L., 1947. Zum Wesen der Oberflächenspannung. *Annalen der Physik* **436**, 59-64.

Prochaska, C. A. and Zouboulis, A. I., 2006. Removal of phosphates by pilot vertical-flow constructed wetlands using a mixture of sand and dolomite as substrate. *Ecological Engineering* **26**, 293-303.

Pugh, R. and Stenius, P., 1985. Solution chemistry studies and flotation behaviour of apatite, calcite and fluorite minerals with sodium oleate collector. *International Journal of Mineral Processing* **15**, 193-218.

Rayleigh, L., 1890a. On the tension of water surfaces, clean and contaminated, investigated by the method of ripples. *Philosophical Magazine* **30**, 386-100.

Rayleigh, L., 1890b. On the theory of surface forces. *Philosophical Magazine* **30**, 285-98.

Saada, A., Papirer, E., Balard, H., and Siffert, B., 1995. Determination of the surface properties of illites and kaolinites by inverse gas chromatography. *Journal of Colloid & Interface Science* **175**, 212-218.

Schaetzl, R. and Anderson, S., 2005. *Soils Genesis and Geomorphology*. Cambridge University Press, Cambridge, United Kingdom

Segner, 1751. De figuris superficierum fluidarum. *Commentarii Soc. Regiae* **1,** 301-372

Shang, J., Flury, M., Harsh, J., and Zollars, R., 2009. Contact angles and surface free energies of aluminosilicate clays as affected by relative humidity and exchangeable cations. *Colloids and Surfaces A: Physicochemical and Engineering Aspects* **353**, 1-10.

Shuttleworth, R., 1950. The surface tension of solids. *Proceedings of the Physical Society Section A* **63**, 444-457.

Siegal, D. and Pfannkuch, H. O., 1984. Silicate mineral dissolution at pH 4 and near standard temperature and pressure *Geochemica Cosmochemica Acta* **48**, 197-201.

Silberberg, M., 2004. Chemistry: the molecular nature of matter and change. McGraw-Hill, New York

Sparks, D. L., 2005. Toxic metals in the environment: The role of surfaces. *Elements* **1**, 193-197.

Speight, J., 2006. *The Chemistry and Technology of Petroleum*. CRC Press. Boca Raton, Fl.

Speight, J. G., 1999. The chemical and physical structure of petroleum: effects on recovery operations. *Journal of Petroleum Science and Engineering* **22**, 3-15.

Spelt, J. K., Absolom, D. R., and Neumann, A. W., 1986. Solid surface tension: The interpretation of contact angles by the equation of state approach and the theory of surface tension components. *Langmuir* **2**, 620-625.

Sposito, G., 1984. *The Surface Chemistry of Soils*. Oxford University Press, London

Staszczuk, P. and Bilinski, B., 1987. Investigations of water film properties on barite surface containing preadsorbed tetradecylammonium hydrochloride(TDACl). *Thermochimica acta* **122**, 363-376.

Stenström, T. A. and Kjelleberg, S., 1985. Fimbriae mediated nonspecific adhesion of Salmonella typhimurium to mineral particles. *Archives of microbiology* **143**, 6-10.

Stucki, J. W., Lee, K., Zhang, L., and Larson, R. A., 2002. Effects of iron oxidation state on the surface and structural properties of smectites. *Pure and Applied Chemistry* **74**, 2145-2158.

Taylor, A. S., Blum, J. D., and Lasaga, A. C., 2000. The dependence of labradorite dissolution and Sr isotope release rates on solution saturation state. *Geochimica et Cosmochimica Acta* **64**, 2389-2400.

Theng, B. K. G., Ristori, G. G., Santi, C. A., and Percival, H. J., 1999. An improved method for determining the specific surface areas of topsoils with varied organic

matter content, texture and clay mineral composition. *European Journal of Soil Science* **50**, 309-316.

Ticknor, K. V., Vilks, P., and Vandergraaf, T. T., 1996. The effect of fulvic acid on the sorption of actinides and fission products on granite and selected minerals. *Applied Geochemistry* **11**, 555-565.

van Oss, C. J., 2006. *Interfacial Forces in Aqueous Media*. CRC Press, Taylor and Francis Group. Boca Raton, Fl.

Van Oss, C. J. and Giese, R. F., 1995. The hydrophilicity and hydrophobicity of clay minerals. *Clays and Clay Minerals* **43**, 474-477.

Van Oss, C. J., Good, R. J., and Chaudhury, M. K., 1988. Additive and nonadditive surface tension components and the interpretation of contact angles. *Langmuir* **4**, 884-891.

van Oss, C. J., Wu, W., Docoslis, A., and Giese, R. F., 2001. The interfacial tensions with water and the Lewis acid-base surface tension parameters of polar organic liquids derived from their aqueous solubilities. *Colloid Surf. B-Biointerfaces* **20**, 87-91.

Viswanath, B. and Ravishankar, N., 2008. Controlled synthesis of plate-shaped hydroxyapatite and implications for the morphology of the apatite phase in bone. *Biomaterials* **29**, 4855-4863.

Voudrais, E. A. and Reinhard, M., 1986. Abiotic organic reactions at mineral surfaces *Geochemical Processes at Mineral Surfaces*. **323**, 462-486.

Walker, G. M., Hansen, L., Hanna, J. A., and Allen, S. J., 2003. Kinetics of a reactive dye adsorption onto dolomitic sorbents. *Water Research* **37**, 2081-2089.

Wallander, H. and Wickman, T., 1999. Biotite and microcline as potassium sources in ectomycorrhizal and non-mycorrhizal Pinus sylvestris seedlings. *Mycorrhiza* **9**, 25-32.

Walter, L. M. and Morse, J. W., 1984. Reactive surface area of skeletal carbonates during dissolution--effect of grain size. *Journal of Sedimentary Petrology* **54**, 1081-1090.

Wan, J. and Wilson, J. L., 1994. Visualization of the role of the gas-water interface on the fate and transport of colloids in porous media. *Water Resources Research* **30**, 11-24.

White, A. F., Blum, A. E., Schulz, M. S., Bullen, T. D., Harden, J. W., and Peterson, M. L., 1996. Chemical weathering rates of a soil chronosequence on granitic alluvium: I. Quantification of mineralogical and surface area changes and calculation of primary silicate reaction rates. *Geochimica et Cosmochimica Acta* **60**, 2533-2550.

White, A. F. and Brantley, S. L., 2003. The effect of time on the weathering of silicate minerals: why do weathering rates differ in the laboratory and field? *Chemical Geology* **202**, 479-506.

Whitehouse, D. J., 1994. *Handbook of Surface Metrology*. Taylor & Francis, London.

Worthington, A. M., 1885. Error involved in Quincke's Method of calculating surface tensions from dimensions of flat drops and bubbles. *Proceedings of the Physical Society of London* **20**, 51-66.

Young, T., 1805. An essay on the cohesion of fluids. *Philosophical Transactions of the Royal Society of London* **95**, 65-87.

Zettlemoyer, A. C., 1969. Hydrophobic surfaces. *Journal of Colloid & Interface Science* **28**, 343-369.

Zielke, R. C. and Pinnavaia, T. J., 1988. Modified clays for the adsorption of environmental toxicants: binding of chlorophenols to pillared, delaminated, and hydroxy-interlayered smectites. *Clays and Clay Minerals* **36**, 403–408.

APPENDIX A
BULK AND SURFACE CHEMISTRY RESULTS

Carbonates

Five carbonates were chosen for analysis. These were calcite, cerussite, dolomite, rhodochrosite, and siderite. These have ideal chemistries of $CaCO_3$, $PbCO_3$, $CaMg(CO_3)_2$, $MnCO_3$, and $FeCO_3$ respectively. Carbonate structure is built on the anionic $(CO_3)^{2-}$ complex. For charge neutrality in an ideal system metal cations carry a charge of 2+. The anionic complex is strongly bonded and does share oxygens (KLEIN, 2002). For these reasons the carbonate class is an excellent choice for studying variations in surface energy based on chemistry.

Organic Carbon on Carbonate Samples

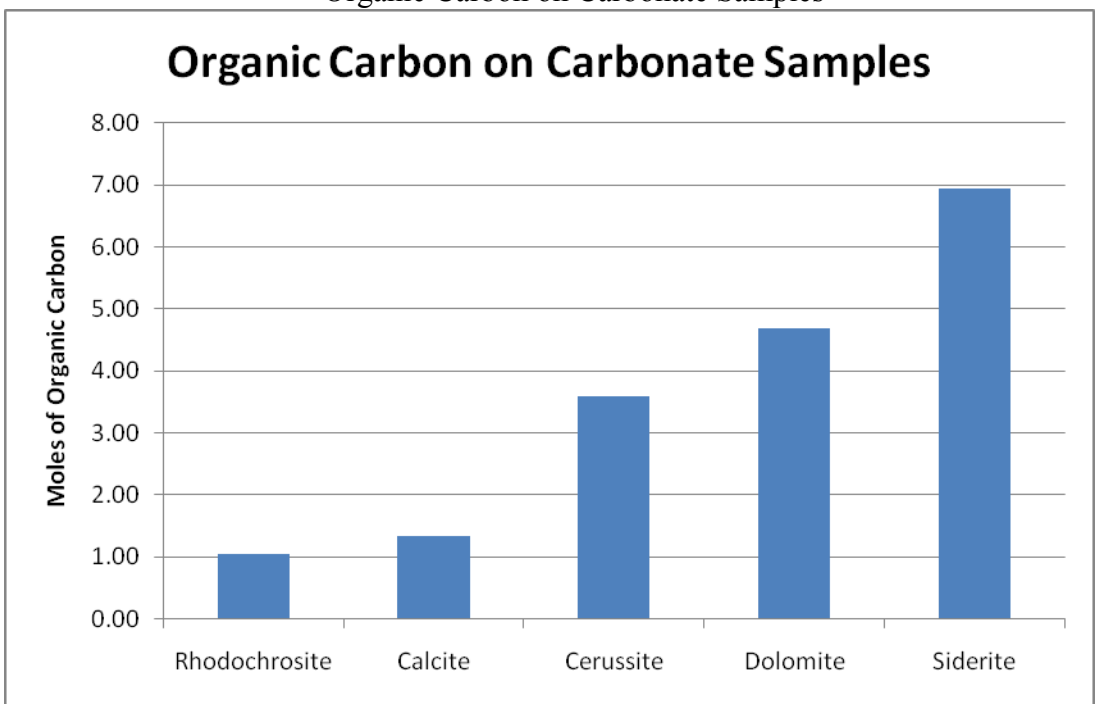

Calcite, rhodochrosite, and siderite are hexagonal $R\bar{3}c$ minerals. All three of these minerals have perfect cleavage in $10\bar{1}1$. Dolomite is in space group $R\bar{3}$. The

structure is very similar to calcite except that Ca and Mg layers alternate along the C axis. Thus, the structure is intermediate between calcite ($CaCo_3$) and magnesite ($MgCO_3$), however solid solution does not exists between the two (KLEIN, 2002). At low temperatures both Ca and Mg occupy structurally distinct positions. The surface chemistry of dolomite therefore, is a combination of the two distinct endmembers.

By comparing the microprobe data and the XPS it was seen that the surface was enriched in calcium relative to the bulk chemistry. The calcite sample was pure phase and is seen to be ideal at detection limits for both methods. Siderite had very little calcium in either position however; the surface composition was considerably higher than the bulk composition. Dolomite continued this trend having a surface to bulk ratio of 34:25 or 1.36. The surface calcium can be attributed to structural or surface contamination. By analyzing the samples it was seen to be both as discussed in the following sections.

Carbonates: Calcite

Calcite Surface Chemistry

Measurement	O 1s	Ca 2p	C 1s	C (Adven)	C (Carb)
Position BE (eV)	530.35	346.15	288.90	284.44	288.82
FWHM (eV)	1.79	1.70	1.58	1.46	1.41
Raw Area (CPS)	30374.40	24220.60	8916.30	6317.77	6704.95
Atomic Conc %	43.57	16.15	40.28	19.53	20.73
Mass Conc. %	38.13	35.41	26.46	12.83	13.62
Moles	2.38	0.88	2.20	1.07	1.13

The calcite sample is pure phase with no detectable (no peak) magnesium, iron, manganese or other elements which commonly substitute in solid solution. It has the least organic carbon on the surface (1.07 moles) of the carbonates. The ideal formula for

calcite is $CaCO_3$. The bulk formula measured with WDS was $CaCO_3$ as well with calcium having a standard deviation of 0.0016.

The surface chemistry measured with XPS was $Ca_{1.11}C_{1.42}O_3$ indicating that oxygen is limiting at the surface. The calcite surface is dominated by partially charged sites. Ca^{2+} will act as a soft Lewis acid on the surface. CO_3^{2-} will act as a hard Lewis base on the surface. The calcium was enriched at the surface relative to the bulk composition. 1.34 moles of organic carbon were measured on the surface.

Carbonates: Dolomite

Dolomite Surface Energy

Measurement	O 1s	Ca 2p	C 1s	C (Adven)	C (Carb)	Mg 2p
Position BE (eV)	530.55	346.45	284.30	289.01	284.42	49.55
FWHM (eV)	1.84	1.75	1.68	1.42	1.22	1.61
Raw Area (CPS)	24042.60	12543.00	10095.90	9777.81	5202.37	452.30
Atomic Conc %	37.27	9.04	49.40	32.24	17.16	4.29
Mass Conc. %	36.00	21.87	35.83	23.38	12.44	6.29
Moles	2.25	0.55	2.98	1.95	1.04	0.26

The dolomite sample is near pure phase with approximately 1:1 ratio of Ca to Mg. The ideal formula of dolomite is $CaMg(CO_3)_2$. The bulk formula was measured as a $Ca_1Mg_{0.98}Fe_{0.01}(CO_3)_2$ indicating iron is a minor component. Thus, Ca:Mg+Fe is approximately 1:1. Calcium and iron each had a standard deviation of .01 and magnesium had a standard deviation of .02.

Because of the relative purity of calcite and dolomite only one fragment was used for each XPS analysis. The surface composition was measured as $Ca_{1.32}Mg_{.62}(C_{3.57}O_3)_2$. The dolomite has a Ca:Mg ratio at the surface of 1:0.47 or approximately 2 to 1. Therefore, magnesium and oxygen are limited on the surface as compared to the bulk. The surface chemistry of dolomite is dominated by pH dependent sites. Mg^{2+} and Ca^{2+}

are the main acidic functional groups. Magnesium is a harder Lewis acid than calcium. Pure phase dolomite is, therefore, expected to be harder than calcite based on the increased substitution of magnesium. 4.68 moles of organic carbon were on the surface of the dolomite sample.

Carbonates: Siderite

Siderite is an iron carbonate with an ideal formula of $FeCO_3$. The siderite sample showed considerable oxidation and surface weathering when collected. Therefore, when the sample was crushed only the inner fragments without oxidation were chosen to be cleaned and used for analyses. The bulk formula measured on the electron microprobe was $Ca_{0.02}Mg_{0.3}Fe_{1.64}CO_3$ indicating that the sample has significant amounts of magnesium and minor amounts of calcium. The ratio of Fe:Mg is approximately 5.5:1. Because of the heterogeneity of the sample two fragments were used to evaluate the surface chemistry on the XPS. The surface chemical formula was measured as $Ca_{0.15}Mg_{0.07}Fe_{0.22}C_{0.49}O_3$ or $Ca_{.3}Mg_{.16}Fe_{.45}CO_{6.1}$ indicating that the surface is deficient in magnesium, iron, and inorganic carbon as compared to the bulk. Thus, the ratio of Fe:Mg:Ca at the surface is 1:0.36:0.67. The iron had a standard deviation of .08, and the magnesium and calcium had 0.0002 and 0.1. The organic carbon film on the surface was measured as 6.94 moles. This is the most organic carbon of all three carbonates. The siderite surface is dominated by pH dependent sites. Fe^{2+}, Mg^{2+}, and Ca^{2+} are the dominant acidic functional groups. Iron 2+ is the hardest acid of the metals. Therefore, siderite has the hardest surface of the carbonate samples. CO_3^{2-} again is the main basic functional group. Carbonate will act as a hard Lewis base.

Carbonates: Rhodochrosite

Rhodochrosite was imaged with 6-four millimeter images. The bulk chemistry of the rhodochrosite sample was measured as $Mn_{.75}Fe_{.16}Ca_{.05}Mg_{.03}CO_3$. Banding was seen alternating between calcium and magnesium on all of the fragments. This banding was also evident from color variations on the sample when first purchased. The surface composition was measured as $Mg_{.83}Mn_{.32}Fe_{.03}C_{.98}O_{3.}$ The XPS position for both fragments landed on a magnesium band. This is the reason for the high magnesium

content in the composition. Iron was depleted at the surface compared to the bulk. The surface organic carbon measured 1.04 moles. This was the least organic carbon on the carbonate samples.

Siderite Surface Chemistry

Measurement	Statistic	Fe 2p	O 1s	Ca 2p	C 1s	C 1s (Adven)	C 1s (Carb)	Mg 2p
Position BE (eV)	Average	709.05	530.50	348.50	284.10	284.15	288.15	49.65
	St. Dev.	0.71	0.21	2.47	0.14	--	--	0.28
	Cf. Var.	0.10%	0.04%	0.71%	0.05%	--	--	0.59%
FWHM (eV)	Average	4.34	2.14	1.83	1.58	1.28	1.38	1.46
	St. Dev.	0.22	0.11	0.06	0.07	--	--	0.14
	Cf. Var.	5.15%	5.35%	3.13%	4.60%	--	--	9.29%
Raw Area (CPS)	Average	5313.10	17681.25	1933.50	13884.55	18315.55	1285.40	80.35
	St. Dev.	3052.58	168.36	1953.74	2267.48	--	--	1.34
	Cf. Var.	57.45%	0.95%	101.05%	16.33%	--	--	1.67%
Atomic Concentration (%)	Average	2.07	27.64	1.47	68.06	63.60	4.46	0.77
	St. Dev.	1.34	2.18	1.54	5.12	--	--	0.06
	Cf. Var.	64.72%	7.88%	104.86%	7.52%	--	--	7.35%
Mass Concentration (%)	Average	7.77	30.44	3.90	56.61	52.89	3.72	1.29
	St. Dev.	4.54	0.07	3.96	8.57	--	--	0.01
	Cf. Var.	58.43%	0.23%	101.53%	15.14%	--	--	0.55%
Moles	Average	0.14	1.90	0.10	4.71	4.40	0.31	0.05
	St. Dev.	0.08	0.00	0.10	0.71	0.64	0.07	0.00
	Cf. Var.	58.43%	0.23%	101.53%	15.14%	14.64%	22.08%	0.55%

Rhodochrosite Surface Chemistry

Measurement	Statistic	Fe 2p	O 1s	Ca 2p	C 1s	C (Adven)	C (Carb)	Mg 2p	Mn 2p
Position BE (eV)	Average	707.65	529.35	345.05	283.00	284.49	289.00	47.15	639.20
	St. Dev.	0.49	0.07	0.07	0.00	0.01	0.04	0.21	0.14
	Cf. Var.	0.07%	0.01%	0.02%	0.00%	0.00%	0.01%	0.45%	0.02%
FWHM (eV)	Average	4.33	2.57	2.63	2.48	--	--	2.84	3.81
	St. Dev.	0.30	0.05	0.05	0.07	--	--	0.00	0.03
	Cf. Var.	6.91%	1.79%	1.99%	2.73%	--	--	0.15%	0.74%
Raw Area (CPS)	Average	1268.70	26306.90	1237.05	6477.40	42562.10	40383.65	1461.25	9400.40
	St. Dev.	207.04	3369.86	446.11	422.57	1763.74	5948.26	135.27	874.69
	Cf. Var.	16.32%	12.81%	36.06%	6.52%	4.14%	14.73%	9.26%	9.30%
Atomic Concentration (%)	Average	0.62	47.71	0.93	32.37	--	--	13.33	5.04
	St. Dev.	0.14	3.28	0.28	4.04	--	--	0.44	0.17
	Cf. Var.	22.81%	6.88%	30.41%	12.48%	--	--	3.29%	3.37%
Mass Concentration (%)	Average	1.90	41.81	2.04	21.33	--	--	17.76	15.18
	St. Dev.	0.45	2.24	0.59	2.98	--	--	0.32	0.28
	Cf. Var.	23.82%	5.36%	29.12%	13.96%	--	--	1.79%	1.82%
Moles	Average	0.04	2.61	0.05	1.78	0.92	0.86	0.73	0.28
	St. Dev.	0.01	0.14	0.01	0.25	0.21	0.04	0.01	0.01
	Cf. Var.	14.78%	5.36%	29.12%	13.96%	22.99%	4.27%	1.79%	1.82%

Rhodochrosite WDS Results

Rhodochrosite WDS Measurements														
Element	Fragment 1		Fragment 2		Fragment 3		Fragment 4		Fragment 5		Fragment 6		Averages	
	Avg..	St. Dev.	Avg..	St. Dev.	Avg..	St. Dev.	Avg..	St. Dev.	Avg..	St. Dev.	Avg..	St. Dev.	Avg..	St. Dev.
Cationic Values Calibrated for 6 Oxygens														
Mn	1.50	0.01	1.52	0.03	1.48	0.03	1.47	0.01	1.51	0.02	1.48	0.02	1.50	0.02
Fe	0.35	0.01	0.32	0.03	0.29	0.02	0.30	0.02	0.36	0.01	0.31	0.03	0.32	0.02
Ca	0.08	0.01	0.10	0.02	0.14	0.03	0.13	0.02	0.06	0.01	0.12	0.03	0.10	0.02
Mg	0.06	0.01	0.05	0.03	0.08	0.01	0.08	0.01	0.05	0.01	0.08	0.01	0.07	0.01
Pb	0.00	0.00	0.00	0.00	0.00	0.00	0.00	0.00	0.00	0.00	0.00	0.00	0.00	0.00
Sr	0.00	0.00	0.00	0.00	0.00	0.00	0.00	0.00	0.00	0.00	0.00	0.00	0.00	0.00
Ba	0.00	0.00	0.00	0.00	0.00	0.00	0.00	0.00	0.00	0.00	0.00	0.00	0.00	0.00

Cerussite WDS Results

Cerussite WDS Measurements											
Element	Group 1	Group 2	Group 3	Group 4	Group 5	Group 6	Group 7	Group 8	Group 9	Group 10	Average
	Avg..	Avg..	Avg..	Avg..	Avg..	Avg..	Avg..	Avg..	Avg..	Avg..	
Cationic Values Calibrated for 6 Oxygens											
Pb	2.00	1.99	2.00	2.00	2.00	2.00	2.00	2.00	2.00	2.00	2.00
Ca	0.00	0.01	0.00	0.00	0.00	0.00	0.00	0.00	0.00	0.00	0.00
Mg	0.00	0.00	0.00	0.00	0.00	0.00	0.00	0.00	0.00	0.00	0.00
Sr	0.00	0.00	0.00	0.00	0.00	0.00	0.00	0.00	0.00	0.00	0.00
Mn	0.00	0.00	0.00	0.00	0.00	0.00	0.00	0.00	0.00	0.00	0.00
Fe	0.00	0.00	0.00	0.00	0.00	0.00	0.00	0.00	0.00	0.00	0.00
Ba	0.00	0.00	0.00	0.00	0.00	0.00	0.00	0.00	0.00	0.00	0.00

Carbonates: Cerussite

WDS analyses on the cerussite sample measured the molar values for 10 data point groupings of three. The ratios were calibrated for 6 oxygens in the chemical structure. Lead, calcium, magnesium, strontium, manganese, iron, and barium were measured. The sample chemistry was found to be $PbCO_3$ with amounts of calcium and barium at just above detection limits. Thus, the sample is very close to ideal chemistry in the bulk composition.

The surface composition measured on the XPS was $Pb_{.61}Mn_{.17}C_{.65}O_3$ with 3.58 moles of organic carbon. Because no manganese was measured by the electron microprobe the Mn is not expected to be structural. Calcium was measured just above detection limits. The coefficient of each of the major elements was less than 10%.

Cerussite Surface Chemistry

Measurement	Statistic	O 1s	Ca 2p	C 1s	C 1s (Adven)	C 1s (Carb)	Mn 2p	Pb 4f
Position BE (eV)	Average	529.10	345.00	282.95	284.50	288.70	642.85	137.10
	St. Dev.	0.14	0.71	0.07	0.02	0.03	0.07	0.00
	Cf. Var.	0.03%	0.20%	0.02%	0.01%	0.01%	0.01%	0.00%
FWHM (eV)	Average	2.54	1.14	2.48	--	--	5.21	2.40
	St. Dev.	0.04	1.14	0.07	--	--	0.02	0.05
	Cf. Var.	1.39%	99.53%	2.68%	--	--	0.41%	2.18%
Raw Area (CPS)	Average	13108.30	337.20	7857.25	61667.65	22643.67	2492.65	28554.10
	St. Dev.	1534.78	20.79	1610.58	12354.99	2673.54	723.44	6663.00
	Cf. Var.	11.71%	6.17%	20.50%	20.03%	11.81%	29.02%	23.33%
Atomic Concentration (%)	Average	34.48	0.37	56.17	--	--	1.91	7.07
	St. Dev.	2.12	0.04	1.55	--	--	0.22	0.40
	Cf. Var.	6.15%	11.47%	2.76%	--	--	11.51%	5.60%
Mass Concentration (%)	Average	19.65	0.54	24.00	--	--	3.72	52.10
	St. Dev.	1.75	0.08	0.01	--	--	0.33	1.51
	Cf. Var.	8.92%	14.54%	0.03%	--	--	8.74%	2.89%
Moles	Average	1.23	0.01	2.00	1.46	0.54	0.07	0.25
	St. Dev.	0.11	0.00	0.00	0.03	0.03	0.01	0.01
	Cf. Var.	8.92%	14.54%	0.03%	2.22%	5.25%	8.74%	2.89%

Sulfates

Sulfates: Gypsum & Bassanite

The gypsum and bassanite samples are the same original sample. The bassanite sample was placed in the oven at 65°C for two weeks to remove 1.5 H_2O molecules per unit. This was done to compare the differences in surface energy with the universal sorption device.

Gypsum Surface Chemistry

Measurement	O 1s	Ca 2p	C 1s	C (Adven)	C (Carb)	S 2p
Position BE (eV)	531.15	347.25	284.40	282.94	286.36	168.75
FWHM (eV)	2.06	1.91	1.91	1.98	1.00	2.43
Raw Area (CPS)	35671.80	20099.60	4503.00	6395.40	479.88	6360.70
Atomic Conc %	52.29	13.70	20.84	19.39	1.45	13.17
Mass Conc. %	40.65	26.67	12.16	11.31	0.85	20.52
Moles	2.54	0.67	1.01	0.93	0.08	0.64

Gypsum has an ideal formula of $CaSO_4 \cdot 2H_2O$. The two sulfate samples were the only evaluated of all aggregates and minerals with detected sulfur. At this time neither gypsum nor bassanite have been run on the electron microprobe. Therefore, no bulk chemistry has been established. The surface chemical formula was measured on the XPS as $Ca_{1.05}S_{1.0}O_4$. Thus, the surface chemistry is very similar to the pure phase mineralogy of gypsum with the exception of surface coatings. The sample has .93 moles of organic carbon and .08 moles of carbonate carbon on the surface. Both likely affect the surface energy of the sample. Water molecules cannot be measured on the XPS because of the vacuum necessary. For this reason the number of waters in the unit formula cannot be verified.

Bassanite Surface Chemistry

Measurement	O 1s	Ca 2p	C 1s	C (Adven)	C (Carb)	S 2p
Position BE (eV)	531.15	347.15	284.50	283.16	287.00	168.75
FWHM (eV)	1.83	1.72	2.12	2.03	1.43	2.29
Raw Area (CPS)	41161.70	23047.90	4181.30	5940.93	452.69	7299.30
Atomic Conc %	60.33	15.70	19.35	17.98	1.37	15.11
Mass Conc. %	41.76	27.22	10.06	9.34	0.71	20.96
Moles	2.61	0.68	0.84	0.78	0.06	0.65

Bassanite has an ideal formula of $CaSO_4 \bullet .5H_2O$. The surface chemistry of the sample was measured as $Ca_{1.03}S_{.99}O_4$ indicating that the surface chemistry of the bassanite is also similar to the pure phase mineralogy. The oven removed some of the organic carbon from the surface. The sample had .78 moles as compared to .93 moles on the gypsum. The carbonate carbon was roughly equal on the two samples at .06 and .08 moles. The surface chemistry of the sulfates will also be dominated by conditionally charged sites. Ca^{2+} will act as a Lewis acid. SO_4^{2-} and H_2O are the main basic functional groups. Each of these is considered a hard base.

Phyllosilicates

Phyllosilicates: Biotite

Biotite is a 2:1 layered silicate ideally having one quarter of the Si^{4+} tetrahedral sites occupied by Al^{3+}. This substitution causes a net excess of one negative charge per formula unit. This negative charge is balanced by monovalent cations, such as K^+, that occupy space between two 2:1 layers. The ideal formula for biotite is $K(Mg,Fe)_2(AlSi_3O_{10})(F,OH)_2$. The bulk formula of the biotite sample was measured one the electron microprobe as, $K_{.96}(Mg_{.81}Fe_{.54}Mn_{.02}Ti_{.06})_2(Al_{1.02}Si_3O_{10})(F_{.81},(OH)_X)$. Potassium ranged from .92 to 1.00 moles and had a standard deviation of .02. Magnesium ranged from .77 to .89 with a standard deviation of .06 moles. Iron ranged from .46 to .58 and had a standard deviation of .05 moles. Manganese ranged from .02 to .03 moles and titanium ranged from .1 to .14 moles. Aluminum ideal exists in 1:3 ratio

Biotite Surface Chemistry

Measurement	Statistic	Na 1s	Fe 2p	O 1s	C 1s	C 1s (Adven)	C 1s (Carb)	K 2p	Si 2p	Al 2p	Mg 2p	Ti 2p	Mn 2p	F 1s
Position BE (eV)	Avg.	1070.5	709.88	530.65	284.30	283.04	286.18	292.90	102.10	73.75	53.05	457.95	640.55	684.20
	St. Dev.	1.20	0.42	0.07	0.14	--	--	0.14	0.28	0.07	4.03	0.21	0.07	0.00
	Cf. Var.	0.11%	0.06%	0.01%	0.05%	--	--	0.05%	0.28%	0.10%	7.82%	0.05%	0.01%	0.00%
FWHM (eV)	Avg.	0.37	4.44	2.33	1.79	1.99	1.78	1.51	1.89	1.61	2.48	1.85	3.04	1.78
	St. Dev.	0.08	0.08	0.16	0.05	--	--	0.07	0.08	0.12	1.31	0.34	0.62	0.06
	Cf. Var.	21.3%	1.85%	7.08%	2.72%	--	--	4.77%	4.16%	7.28%	52.68%	18.28%	20.30%	3.18%
Raw Area (CPS)	Avg	313.85	7579.6	29951.9	5494.5	15066.1	1694.3	2416.0	2081.6	417.0	1158.5	675.40	1407.15	1632.80
	St. Dev.	150.26	471.36	359.21	2173.58	--	--	2135.9	469.02	3.32	66.33	68.17	404.96	1323.28
	Cf. Var.	47.8%	6.22%	1.20%	39.56%	--	--	88.41%	22.53%	0.80%	5.73%	10.09%	28.78%	81.04%
Atomic Concentration (%)	Avg.	0.16	2.71	44.04	25.28	22.72	2.56	2.17	9.28	3.21	10.42	0.40	0.57	1.78
	St. Dev.	0.07	0.29	1.51	8.91	--	--	1.97	2.50	0.17	1.11	0.06	0.14	1.49
	Cf. Var.	44.1%	10.72%	3.44%	35.24%	--	--	91.12%	26.97%	5.29%	10.66%	14.14%	24.81%	84.06%
Mass Concentration (%)	Avg.	0.20	7.81	36.51	15.95	14.34	1.60	4.25	13.40	4.48	13.08	1.00	1.64	1.70
	St. Dev.	0.10	0.30	1.29	6.65	--	--	3.69	2.71	0.07	0.48	0.08	0.51	1.35
	Cf. Var.	49.5%	3.90%	3.52%	41.73%	--	--	86.85%	20.22%	1.58%	3.68%	7.82%	31.04%	79.68%
Moles	Avg.	0.01	0.14	2.28	1.33	1.22	0.14	0.11	0.48	0.17	0.54	0.02	0.03	0.09
	St. Dev.	0.00	0.01	0.08	0.55	0.48	0.02	0.09	0.10	0.00	0.02	0.00	0.01	0.07
	Cf. Var.	49.5%	3.90%	3.52%	41.73%	39.66%	17.19%	86.85%	20.22%	1.58%	3.68%	7.82%	31.04%	79.68%

Muscovite Surface Chemistry

Measurement	Statistic	Na 1s	Fe 2p	O 1s	Ca 2p	C 1s	C (Adven)	C (Carb)	K 2p	Si 2p	Al 2p	F 1s
Position BE (eV)	Average	1069.40	710.88	530.80	346.90	284.30	282.76	285.93	292.50	102.10	74.20	688.00
FWHM (eV)	Average	2.23	0.19	2.26	1.62	1.62	1.58	2.24	1.67	1.86	1.80	2.16
Raw Area (CPS)	Average	1412.20	335.60	30839.80	1085.70	7252.30	19471.88	2953.09	3524.80	2428.90	1271.10	2433.70
Atomic Conc %	Average	0.69	0.11	42.44	0.69	31.51	27.36	4.15	2.89	10.08	9.15	2.42
Mass Conc. %	Average	0.89	0.35	37.80	1.55	21.07	18.58	2.82	6.30	15.76	13.74	2.56
Moles	Average	0.04	0.01	2.36	0.04	1.75	1.55	0.23	0.16	0.56	0.51	0.13

with silicon. The bulk ratio is approximately equal at 1.02:3.00 with aluminum having a range from .97 to 1.06 and a tight standard deviation of .01 moles. Silicon ranged from 2.96 to 3.07 and had a standard deviation of .03 moles. Fluorine average .81 moles and ranged from .73 to .92 moles with a standard deviation of .05 moles.

The surface composition was measured as $K_{.48}(Mg_{1.18}Fe_{.31}Mn_{0.07}Ti_{0.04})_2$-$(Al_{.74}Si_{2.1}O_{10})F_{.43}$ indicating a surface aluminum to silicon ratio of 1.05:3. The ideal formula of biotite has an Al+Si:O (Other than hydroxide ions) ratio of 2:5. The bulk composition ratio was approximately 2:5 and the surface composition was 1.4:5. This is an indication that likely some of the oxygen measured by the XPS was not compositional oxygen. Aluminum ranged from .70 to .74 and silicon ranged from 1.8 to 2.4 moles. The surface was also enriched in magnesium relative to the bulk composition and depleted in iron. Magnesium ranged from 1.14 to 1.2 and iron ranged from .29 to .31 moles. It is unclear why the surface was deficient in potassium as cleavage would be expected along the interlayer and potassium molecules should be well exposed. Phyllosilicates are dominated by polar surface functional groups based on the high charge density of the surface. Biotite will also have permanent charged sites that result from isomorphic cationic substitutions. Constant charged sites occur when Mg^{2+} substitutes for Al^{3+} in the octahedral sheet and Al^{3+} substituting for Si^{4+} in the tetrahedral sheet. This creates a net negative charge. In addition iron can also substitute in the octahedral sheet.

In addition to permanently charged polar sites biotite will also have conditionally charged sites. The dominant hard acid sites will be Mg^{2+}, Ti^{4+}, and possibly Fe^{3+} and Mn^{3+} based on the XPS and microprobe analyses. Fe^{2+} and Mn^{2+} are borderline hard/soft active sites and K^+ is a soft acid site. SiO_4^{4-} and AlO_3^{3-} are the dominant hard base sites on the biotite surface. OH^- is a borderline hard/soft base and F^- sites will be soft Lewis bases.

Phyllosilicates: Muscovite

The ideal formula for muscovite used is $KAl_2(AlSi_3O_{10})(F,OH)_2$. The bulk formula measured by the microprobe was $K_{1.78}Al_{3.84}Na_{.21}Fe_{.13}Mg_{.05}$-

$(Al_{1.92}Si_{6.07}O_{10})(F_{.44}(OH)_X)$. The ratio of Al:Si in the ideal formula is 1:1. The ratio measured for the bulk chemistry of muscovite is 0.95:1. Potassium ranged from 1.74 to 1.91 moles and total aluminum ranging from 5.64 to 5.83 moles. Sodium ranged from .11 to .24 moles while iron and magnesium ranged from .1 to .2 and .04 to .08 moles respectively. Silica ranged from 6.04 to 6.11 moles and fluorine ranged from .37 to .56 moles.

The surface chemistry calculated on the XPS established a formula of $K_{.68}Al_{1.44}Na_{.17}Fe_{.04}Ca_{.17}(Al_{.72}Si_{2.03}O_{10})F_{.59}$ for muscovite. Because of the relative homogeneity of the sample only one fragment was used for the XPS measurement. The potassium, as with biotite, again appears to be depleted at the surface. This is likely due to the interlayer where potassium is located not being close to the surface. The ratio of total Al:Si in this formula is 1.06:1 indicating that the chemical structure for both biotite and muscovite at the surface is close to ideal.

Muscovite will have permanent charged sites just as biotite except the sample had no detectable magnesium. The acid conditionally charged sites will differ somewhat from biotite however. There are expected to be few hard Lewis acid sites except possibly Fe^{3+}. The borderline hard/soft acids are likely to be Fe^{2+} and Ca^{2+} with K^+ and Na^+ as soft acids. The conditionally charged base sites will be similar to biotite having SiO_4^{4-} and AlO_3^{3-} as the dominant hard Lewis base sites and OH^- and F^- sites as borderline soft.

Phyllosilicates: Montmorillonite

Montmorillonite is a 2:1 phyllosilicate similar to biotite and muscovite discussed above. The interlayer contains exchangeable cations such as Ca^{2+} and Mg^{2+}. Smectites, such as montmorillonite, have a charge per formula weight of approximately 0.6 to 0.25. The most important property of the clays for this study is their large surface area to volume ratio. If the surface energy of montmorillonite is equal to a tectosilicate, such as quartz for instance, in a charge unit over area ratio then the surface energy of the clay on a per mass or per volume ratio will be much larger.

The ideal formula for montmorillonite is $(Na,Ca)_{0.33}(Al,Mg)_2(Si_4O_{10})(OH)_2$. The electron microprobe measured the elemental molar ratio and estimated the bulk

composition as $Ca_{0.2}(Al_{.65}Mg_{.28}Fe_{.05})_2Si_{3.65}O_{10}$. The XPS measured surface composition was $Ca_{.39}(Al_{1.26},Mg_{.23})_2Si_{3.62}O_{10}$ making the smectite a calcic montmorillonite. No peak was found at detection limit for iron with the XPS. The surface was enriched in aluminum and calcium relative to the bulk composition. Silicon was virtually the same with 3.62 moles on the surface and 3.65 in the bulk.

Montmorillonite will also have neutral siloxane cavities and permanently charged sites. Conditionally charged acidic sites will be dominated by Mg^{2+} as a hard Lewis acid and Ca^{2+} as a borderline hard/soft site and Na^{+} as a softer acidic site. The basic pH dependent sites will be dominated by SiO_4^{4-}, AlO_3^{3-} and H_2O. Sulfate, aluminate, and water will all act as hard Lewis bases.

Montmorillonite Surface Chemistry

Measurement	Statistic	Fe 2p	O 1s	Ca 2p	C 1s	C (Adven)	C (Carb)	Si 2p	Al 2p	Mg 2p
Position BE (eV)	Average	711.28	530.20	348.05	283.15	283.18	287.25	101.40	73.05	48.40
	St. Dev.	0.00	0.42	1.63	0.21	--	--	0.28	0.07	0.42
	Cf. Var.	0.00%	0.08%	0.47%	0.07%	--	--	0.28%	0.10%	0.88%
FWHM (eV)	Average	0.14	2.50	5.46	2.18	2.07	3.47	2.07	1.89	1.57
	St. Dev.	0.00	0.23	0.07	0.21	--	--	0.14	0.01	0.24
	Cf. Var.	0.00%	9.07%	1.24%	9.70%	--	--	6.60%	0.30%	15.52%
Raw Area (CPS)	Average	140.60	12971.30	1041.85	972.60	2443.36	420.90	1480.55	308.65	86.55
	St. Dev.	0.00	11151.36	760.92	592.56	--	--	1147.71	254.06	59.04
	Cf. Var.	0.00%	85.97%	73.04%	60.92%	--	--	77.52%	82.31%	68.22%
Atomic Concentration (%)	Average	0.05	54.10	2.18	14.78	12.37	2.40	19.58	6.88	2.45
	St. Dev.	0.06	4.82	0.22	3.75	--	--	0.74	0.23	0.40
	Cf. Var.	141.42%	8.91%	10.08%	25.41%	--	--	3.79%	3.29%	16.48%
Mass Concentration (%)	Average	0.14	44.90	4.53	9.21	7.71	1.50	28.52	9.63	3.09
	St. Dev.	0.19	3.94	0.46	2.35	--	--	1.12	0.30	0.51
	Cf. Var.	141.42%	8.77%	10.16%	25.58%	--	--	3.92%	3.08%	16.48%
Moles	Average	0.00	2.81	0.11	0.77	0.64	0.12	1.02	0.36	0.13
	St. Dev.	0.00	0.25	0.01	0.20	0.14	0.06	0.04	0.01	0.02
	Cf. Var.	141.42%	8.77%	10.16%	25.58%	21.20%	47.85%	3.92%	3.08%	16.48%

Phyllosilicates: Kaolinite

Kaolinite is 1:1 dioctahedral phyllosilicate clay containing Al^{3+} in the octahedral and Si^{4+} in the tetrahedral sites. Because of the layer charge neutrality there are little or no exchangeable cations between layers. There is also very little isomorphous substitution causing there to be few expected permanently charged active sites on the surface.

Kaolinite Surface Chemistry

Measurement	Statistic	Fe 2p	O 1s	C 1s	C (Adven)	C (Carb)	Si 2p	Al 2p
Position BE (eV)	Average	716.93	531.60	284.85	283.40	287.36	103.00	74.70
	St. Dev.	9.69	0.00	0.21	--	--	0.00	0.14
	Cf. Var.	1.35%	0.00%	0.07%	--	--	0.00%	0.19%
FWHM (eV)	Average	0.46	2.18	2.23	2.09	2.44	2.01	1.84
	St. Dev.	0.11	0.17	0.17	--	--	0.10	0.06
	Cf. Var.	23.01%	7.73%	7.49%	--	--	4.75%	3.34%
Raw Area (CPS)	Average	366.05	22374.80	2094.95	5400.36	646.45	1788.50	912.30
	St. Dev.	122.26	750.81	104.44	--	--	119.64	9.62
	Cf. Var.	33.40%	3.36%	4.99%	--	--	6.69%	1.05%
Atomic Concentration (%)	Average	0.23	57.01	16.87	15.05	1.82	13.73	12.16
	St. Dev.	0.08	0.81	1.17	--	--	0.65	0.37
	Cf. Var.	34.57%	1.41%	6.96%	--	--	4.74%	3.02%
Mass Concentration (%)	Average	0.68	49.54	11.01	9.82	1.19	20.95	17.83
	St. Dev.	0.21	0.40	0.83	--	--	0.87	0.64
	Cf. Var.	31.20%	0.80%	7.58%	--	--	4.15%	3.61%
Moles	Average	0.01	3.10	0.92	0.82	0.10	0.75	0.66
	St. Dev.	0.00	0.02	0.07	0.05	0.02	0.03	0.02
	Cf. Var.	31.20%	0.80%	7.58%	5.96%	20.95%	4.15%	3.61%

Kaolinite has an ideal formula of $Al_2Si_2O_5(OH)_4$ and most natural kaolinites are close to the ideal formula based on the low amount of substitution. The bulk formula was measured as $Al_{2.9}Si_{2.8}O_5(OH)_X$ and the surface composition was $Al_{1.06}Si_{1.2}O_5(OH)_X$.

Nesosilicates

Nesosilicates: Olivine

Olivine is a common rock forming mineral varying from accessory to main constituent in igneous aggregates (KLEIN, 2002). Olivine is orthorhombic with 2/m2/m2/m crystallography. A complete solid substitution exists between Mg_2SiO_4 (forsterite) and Fe_2SiO_4 (fayalite) giving an ideal composition of $(Mg,Fe)_2SiO_4$. Magnesium rich olivines are more common than iron rich species (KLEIN, 2002).

Olivine Surface Chemistry

Measurement	Fe 2p	O 1s	C 1s	C (Adven)	C (Carb)	Si 2p	Mg 2p	Mn 2p
Position BE (eV)	708.20	530.10	284.40	282.84	286.74	101.40	49.80	640.00
FWHM (eV)	3.60	1.72	1.46	1.49	1.29	1.44	1.18	0.52
Raw Area (CPS)	253.00	7909.00	1199.40	6590.69	866.31	692.70	459.30	96.40
Atomic Conc %	0.37	47.42	22.70	20.06	2.64	12.52	16.84	0.16
Mass Conc. %	1.13	41.65	14.96	13.22	1.74	19.31	22.47	0.48
Moles	0.02	2.60	1.25	0.14	1.10	0.69	0.92	0.01

Bulk composition was measured as $(Mg_{.90},Fe_{.09})_2Si_{1.00}O_{4.00}$ with minor manganese above detection limits. This made the sample $Fo_{91}Fa_{09}$. Although the bulk sample showed only minor manganese the surface measurement showed some manganese enrichment. The XPS elemental composition was $(Mg_{.71},Fe_{0.02},Mn_{0.01})_2Si_{1.06}O_{4.00}$. This makes the surface closer to $Fo_{96}Fa_{03}Te_{01}$. Manganese, however, is still a minor component and likely has little effect on the total surface energy of the sample. The sample being dominant in Mg^{2+} compared to Fe^{2+} makes the surface harder than a predominantly fayalitic olivine. Mg^{2+} will act as a hard Lewis acid and Fe^{2+} as borderline hard/soft. The only hard base site will be SiO_4^{4-}.

Inosilicates

Inosilicates: Augite

Augite is a single chain clinopyroxene where sodium substitutes for calcium and aluminum substitutes for magnesium, iron, and silicon (KLEIN, 2002). Augite is monoclinic with 2/m crystallography. It is commonly very heterogeneous with an ideal formula of $(Ca,Na)(Mg,Fe,Al)(Si,Al)_2O_6$. The bulk compositon was, as expected, very heterogeneous with a measured formula of $(Ca_{.89}Na_{.10})(Mg_{.48}Mn_{03}Fe^{2+}_{.36}Fe^{3+}_{.13}Al_{.07})Si_{1.95}O_{3.00}$. The amount of substitution likely increases bond angle stress. Nonideal bond angles are expected to increase the free energy at the surface as compared with pure phase minerals.

Four augite fragments were analyzed on the XPS. The chemical formula of the surface was measured as $(Ca_{.37},Na_{.07})(Mg_{.29},Fe_{.04},Al_{.10})Si_{1.20}O_{3.00}$. Each of the elements was depleted at the surface. This indicates that carbon (inorganic and organic) was effectively shielding the cations from measurement. 1.7 moles of organic carbon and .29 moles of inorganic carbon were measured on the sample. Only one of the four samples contained manganese above detection limits.

Augite Surface Chemistry

Measurement	Statistic	Na 1s	Fe 2p	O 1s	Ca 2p	C 1s	C (Adven)	C (Carb)	Si 2p	Al 2p	Mg 2p	Mn 2p
Position BE (eV)	Average	1068.75	709.78	529.65	345.88	283.30	284.82	288.38	101.20	73.60	50.23	638.90
	St. Dev.	0.24	0.38	0.17	0.17	0.23	0.15	0.53	0.24	0.57	2.52	319.45
	Cf. Var.	0.02%	0.05%	0.03%	0.05%	0.08%	0.08%	0.08%	0.24%	0.78%	5.02%	
FWHM (eV)	Average	1.65	4.99	2.58	1.75	1.72	1.64	2.79	1.81	2.27	1.92	0.86
	St. Dev.	0.34	1.24	0.34	0.60	0.59	0.49	2.67	0.47	1.65	1.51	--
	Cf. Var.	20.52%	24.88%	13.08%	34.01%	34.20%	34.20%	34.20%	26.07%	72.70%	78.76%	--
Raw Area (CPS)	Average	413.20	559.78	8582.25	2244.28	2330.60	20688.86	4672.18	1032.85	55.35	112.08	249.90
	St. Dev.	275.77	609.51	8982.41	2192.72	2522.31	27520.72	6420.45	932.13	55.21	87.91	--
	Cf. Var.	66.74%	108.88%	104.66%	97.70%	108.23%	108.23%	108.23%	90.25%	99.74%	78.44%	--
Atomic Concentration (%)	Average	0.88	0.63	38.68	4.79	34.69	--	--	15.22	1.38	3.71	0.04
	St. Dev.	0.20	0.12	8.07	0.86	8.12	--	--	2.20	0.30	0.98	0.08
	Cf. Var.	23.06%	18.69%	20.86%	17.97%	23.41%	--	--	14.45%	21.69%	26.51%	
Mass Concentration (%)	Average	1.09	1.91	33.57	10.39	22.79	--	--	23.22	2.02	4.90	0.12
	St. Dev.	0.22	0.38	6.61	1.56	6.06	--	--	3.00	0.44	1.32	0.23
	Cf. Var.	20.47%	19.69%	19.69%	15.02%	26.61%	--	--	12.92%	21.79%	26.97%	200.00%
Moles	Average	0.05	0.03	2.10	0.26	1.90	1.70	0.29	0.83	0.07	0.20	0.00
	St. Dev.	0.01	0.01	0.41	0.04	0.50	0.62	0.06	0.11	0.02	0.05	0.00
	Cf. Var.	20.47%	19.69%	19.69%	15.02%	26.61%	36.22%	22.11%	12.92%	21.79%	26.97%	200.00%

Inosilicates: Hornblende

Hornblende is a double chain monoclinic inosilicate with 2/m crystallography. Hornblende is a common rock forming mineral that is widely distributed on the crust located it igneous, metamorphic, and sedimentary formations. Ideally the elemental formula is $(Ca,Na)_{2\text{-}3}(Mg,Fe,Al)_5(Al,Si)_8O_{22}(OH)_2$. Thus, hornblende and augite both exhibit common heterogeneity based on substitution. Despite the amount of substitution the sample was spatially homogeneous evidenced by the electron microprobe spot sampling.

The bulk formula was measured as $(Ca_{1.02}Na_{1.73}K_{.26})(Mg_{.48}\ Fe_{.46}\ Al_{.42}Mn_{.03}Ti_{.02})_5(Al_{.67},Si_{7.11})_{8.00}O_{22.00}H_{2.00}$. The most variable species were calcium, sodium, potassium, and titanium which ranged from .88-1.06, 1.67-1.92, .19-.28, and .06-.14 moles respectively. Manganese and iron measured 3.98% and 1.18% coefficients of variability yielding little variability. Magnesium, total aluminum and silicon measured 0.85%, 0.99%, and 0.34% coefficients of variation respectively. Thus, over 25 spot samples the spatial variability was small. The average coefficient of variation was 3.98%. For this reason it was decided that one fragment would be sufficient for surface analysis on the XPS.

Calcium XPS Peak Deconvolution

Calcium Peak Deconvolution			
Mineral	Relative Ratios		Interpreted # of Chemical States
	$2p_{1/2}$	$2p_{3/2}$	
Calcite Ca	0.30	0.70	1
Dolomite Ca	0.38	0.62	2
Siderite Ca	0.36	0.64	2
Bassanite Ca	0.30	0.70	1
Gypsum Ca	0.29	0.71	1
Labradorite Ca	0.27	0.73	2
Muscovite Ca	0.27	0.73	2
Hornblende Ca	0.49	0.51	3, 4?

The surface elemental chemistry was $(Ca_{1.11}Na_{.80}K_{.03})$-$(Mg_{.63},Fe_{.08},A_{l.65})_5(Al_{1.04},Si_{1.07})O_{22}$. The bulk Na:Ca ratio was approximately 1:0.6 while

the surface became enriched in Ca yielding a ratio of approximately 1:1.4. The acidity of the surface compared to the bulk composition when Ca^{2+} substitutes for Na^{1+}. However, this increase in calcium may be due to surface calcite. As seen in the table of calcium peak deconvolutions the ideal ratio of Ca $2p_{1/2}$ to Ca $2p_{3/2}$ electron states for calcite is approximately .30 to .70. Two peaks are found on XPS because the electron spin affects the binding energy of the photo-emitted electrons as they are bombarded by the X-rays.

Dolomite and Siderite deviate from ideality because the variance in the type of crystallographic bond. Dolomite is interpreted as calcium bonded to carbonate as well as calcium to carbonate where the bond angle is disrupted due to the presence of an adjacent magnesium. Similarly calcium in siderite is interpreted to not only bond to carbonate but also to bond with carbonate where the bond angle is disrupted due to the presence of an adjacent magnesium or iron. This does not indicate that the ratio of $2p_{1/2}$ to $2p_{3/2}$ changes. Appropriate deconvolution would show two $2p_{1/2}$ peaks and two $2p_{3/2}$ peaks. Calcium, Gypsum and bassanite are expected to each only have one chemical state where calcium is bonded to sulfate. Labradorite has calcium bonded to oxygen in the crystallographic structure, and possibly labradorite has calcite on the surface. This is based on the interpretation of carbon peaks through XPS.

Carbon has two visible peaks at 282.93 and 286.91 electron volts. The peak located at 286 eV is a carbonate peak. Muscovite similarly has two peaks and likely has surface carbonate. Lastly, hornblende deviates strongly from an ideal ratio. This was interpreted as the presence of two peaks not visible in each electron spin configuration. Calcium in hornblende bonds with oxygen and probably has another configuration with oxygen bonds disrupted by nearby sodium. In addition the calcium-oxygen bond angle can be disrupted by substituted aluminum for magnesium and iron. Finally, calcium is probably bonding with carbonate on the surface.

Thus, the hornblende sample has a very diverse surface chemistry with solid substitution in a variety of locations. Surface hard acid sites are Mg^{2+} and possibly Fe^{3+}. Borderline hard/soft Lewis acid sites are Ca^{2+} and Fe^{2+}. Hard basic sites are $Si_4O_{11}^{6-}$ cyclic structures with OH^- available as a borderline hard/soft site.

Tectosilicates

Feldspars consist of a complex structure of $(SiO_2)^0$ tetrahedra and $(AlO_2)^{1-}$ tetrahedral with metal cations incorporated into the network in available voids. Metal cations neutralize the charge when Al^{3+} substitutes for Si^{4+}. When one aluminum substitutes for one silicon then a monovalent atom, such as Na^+ or K^+, can bring charge neutrality. If two adjacent silicons are replaced two aluminums then a divalent molecule such as Mg^{2+} or Ca^{2+} can bring charge neutrality. Feldspar structure is considered packed or sometimes termed "stuffed" derivative of SiO_2 structures because of this substitution (KLEIN, 2002).

Hornblende Surface Chemistry

Measurement	Na 1s	Fe 2p	O 1s	Ca 2p	C 1s	C (Adven)	C (Carb)	K 2p	Si 2p	Al 2p	Mg 2p	Ti 2p	F 1s
Position BE (eV)	1069.90	710.80	530.70	346.90	284.40	282.96	286.57	292.50	102.30	74.30	50.10	458.20	684.20
FWHM (eV)	1.44	4.90	2.37	1.29	1.37	1.34	1.40	1.27	1.73	1.30	1.38	0.46	1.61
Raw Area (CPS)	742.70	556.50	7091.80	761.70	1428.20	7200.96	873.05	160.30	917.50	103.60	164.60	64.30	579.70
Atomic Conc %	1.54	0.78	41.21	2.06	26.20	23.37	2.83	0.56	16.07	3.15	5.85	0.15	2.44
Mass Conc. %	1.87	2.32	34.89	4.36	16.65	14.85	1.80	1.15	23.89	4.49	7.53	0.38	2.46
Moles	0.08	0.04	2.18	0.11	1.39	1.24	0.15	0.03	0.85	0.17	0.31	0.01	0.13

Tectosilicates: Andesine

Andesine has an ideal formula of $Na_{.7-.5}Ca_{.5-.3}Al_{1.4}Si_{2.6}O_8$. The sample was homogeneous and the sample was measured on the electron microprobe at 25 points. These points gave a bulk formula of $Na_{.49}Ca_{.45}Al_{1.47}Si_{2.53}O_8$. This indicated that the andesine was very close to the labradorite region. This meant that the surface chemistry of the andesine sample and the labradorite sample were expected to be similar. When analyzed on the XPS, however the sample was homogeneous across 4 fragments at Ab68An32 with less than 3% potassium. This gave the measured formula of $(Ca_{.31}Na_{.68}K_{.03})(Si_{.68}Al_{.44})_{4.00}O_{8.00}$. 1.23 moles of organic carbon and 0.19 moles of carbonate carbon were measured on the surface.

Andesine Surface Chemistry

Measurement	Statistic	Na 1s	O 1s	Ca 2p	C 1s	C (Adven)	C (Carb)	K 2p	Si 2p	Al 2p
Position BE (eV)	Average	1069.05	529.60	346.45	283.13	284.66	288.80	292.05	100.95	72.98
	St. Dev.	0.10	0.06	0.06	0.05	0.05	0.36	1.44	0.13	0.13
	Cf. Var.	0.01%	0.01%	0.02%	0.02%	0.02%	0.12%	0.49%	0.13%	0.17%
FWHM (eV)	Average	1.59	1.94	1.51	1.39	1.15	1.30	0.85	1.71	1.51
	St. Dev.	0.06	0.04	0.03	0.07	0.04	0.60	0.40	0.05	0.05
	Cf. Var.	3.75%	1.82%	2.12%	4.69%	3.79%	45.86%	47.39%	3.18%	3.00%
Raw Area (CPS)	Average	2793.08	11833.58	1023.80	2249.83	10404.14	1713.29	77.25	1336.08	503.10
	St. Dev.	2097.23	1338.07	360.30	345.34	1335.06	1560.37	18.80	225.70	58.72
	Cf. Var.	75.09%	11.31%	35.19%	15.35%	12.83%	91.07%	24.34%	16.89%	11.67%
Atomic Concentration (%)	Average	3.65	43.58	1.75	26.28	--	--	0.17	14.88	9.69
	St. Dev.	2.62	3.20	0.57	4.32	--	--	0.04	2.49	0.74
	Cf. Var.	71.74%	7.34%	32.54%	16.43%	--	--	24.96%	16.70%	7.63%
Mass Concentration (%)	Average	4.59	37.60	3.76	17.10	--	--	0.36	22.51	14.10
	St. Dev.	3.40	1.83	1.13	3.22	--	--	0.09	3.32	0.76
	Cf. Var.	74.13%	4.86%	29.95%	18.84%	--	--	25.16%	14.75%	5.42%
Moles	Average	0.20	2.35	0.09	1.42	1.23	0.19	0.01	0.80	0.52
	St. Dev.	0.15	0.11	0.03	0.27	0.17	0.16	0.00	0.12	0.03
	Cf. Var.	74.13%	4.86%	29.95%	18.84%	13.71%	81.17%	25.16%	14.75%	5.42%

Tectosilicates: Albite

Albite has an ideal formula of $NaAlSi_3O_8$ however commonly contains some calcium. The bulk chemistry was analyzed at 25 separate datapoints. The sample was homogeneous and the formula was $Na_{.96}Al_{1.03}Si_{2.98}O_{8.00}$ indicating that the albite sample was 98.98% albite endmember, 0.81% orthoclase endmember, and 0.16% anorthite endmember. Coefficients of variation for sodium, aluminum, and silicon were 1.19, 0.61, and 0.18% respectively.

Albite Surface Chemistry

Measurement	Na 1s	O 1s	C 1s	C (Adven)	C (Carb)	Si 2p	Al 2p
Position BE (eV)	1068.70	529.50	282.80	282.87	286.47	100.90	72.60
FWHM (eV)	1.49	1.89	1.31	1.17	1.00	1.54	1.28
Raw Area (CPS)	1701.00	6429.60	2279.80	9955.94	853.48	918.80	210.40
Atomic Conc %	3.35	35.51	39.76	36.62	3.14	15.30	6.08
Mass Conc. %	4.49	33.10	27.82	25.63	2.20	25.03	9.55
Moles	0.20	2.07	2.32	2.13	0.18	0.89	0.35

The surface chemistry was analyzed on one fragment and the surface formula was $Na_{.2}Al_{.35}Si_{.89}O_{2.07}$ which calibrated for 8 oxygens is $Na_{.77}Al_{1.35}Si_{3.43}O_{8.00}$. This indicates that the surface was depleted in sodium and enriched in aluminum and silicon. 2.13 moles of organic carbon and .18 moles of inorganic carbon were on the sample.

Labradorite

The bulk chemistry for labradorite was analyzed with the electron microprobe on 25 individual points. Labradorite has an ideal formula of $Na_{0.4}Ca_{0.6}Al_{1.6}Si_{2.4}O_{8.00}$ where calcium ranges from .5 to .7 and sodium ranges from .3 to .5 moles. The bulk chemistry was measured as $Na_{.45}Ca_{.50}Al_{1.51}Si_{2.50}O_{8.00}$. This indicates that the chemistry is very similar to andesine. The sample was 51.36% anorthite and 46.02% albite. The sample was very homogeneous. All of the coefficients of variation were less than 30%.

The labradorite surface chemistry was measured on one fragment. The surface chemistry was $Na_{.09}Ca_{.10}Al_{.46}Si_{.98}O_{2.64}$. When calibrated for 8 oxygens this formula becomes $Na_{.28}Ca_{.30}Al_{1.39}Si_{2.97}O_8$. The cations sodium and calcium were depleted at the surface

with respect to the bulk chemistry. The ratio of Na:Ca at the surface was .93 and the bulk ratio was .90. Silicon was enriched at the surface. .86 moles of organic carbon and .1 moles of inorganic carbon were measured. This was the least amount of organic carbon of the feldspar samples.

Labradorite Surface Chemistry

Measurement	Na 1s	O 1s	Ca 2p	C 1s	C 1s (Adven)	C 1s (Carb)	K 2p	Si 2p	Al 2p
Position BE (eV)	1070.40	531.00	347.40	284.40	282.93	286.92	292.70	102.30	74.10
FWHM (eV)	1.59	1.93	1.80	1.41	1.27	1.46	1.43	1.72	1.45
Raw Area (CPS)	887.70	8914.30	740.90	977.60	4334.85	486.67	59.00	1103.50	300.40
Atomic Conc %	1.80	50.66	1.96	17.54	15.77	1.77	0.20	18.91	8.93
Mass Conc. %	2.15	42.20	4.08	10.97	10.28	1.15	0.41	27.65	12.54
Moles	0.09	2.64	0.10	0.91	0.86	0.10	0.01	0.98	0.46

Tectosilicates: Microcline

Microcline is has an ideal formula of $KAlSi_3O_8$ with triclinic $\bar{1}$ crystallography. Sodium substitutes for potassium at small amounts. However, sodium identification is usually evidence of intergrown plagioclase crystals within the sample. Two fragments were measured with the XPS. The surface chemistry was measured as $K_{.16}Al_{.98}Si_{.70}O_3$. 1.89 moles of organic carbon and 0.35 moles of inorganic carbon were measured on the surface. Sodium was measured with the highest variations (115.46% coefficient of variation). Potassium and aluminum had 57.16% and 54.22% coefficients of variation respectively. The other elements were under 25% with silicon at 22.96%, carbon at 8.76%, and oxygen at 2.32% coefficient of variation. These deviations were considered low and likely represented natural variations rather than methodological error.
The bulk chemistry was measured as $K_{.79}Al_{1.03}Si_{2.97}O_8$. The sample was 77.97% orthoclase endmember and 21.76% albite endmember. Potassium and silicon were depleted on the surface. This was likely due to shielding due to the adventitious carbon. Microcline was analyzed with 25 individual points.

Microcline Surface Chemistry

Measurment	Statistic	Na 1s	O 1s	C 1s	C 1s (Adven)	C 1s (Carb)	K 2p	Si 2p	Al 2p
Position BE (eV)	Average	1069.95	530.80	284.30	282.85	286.61	292.25	102.10	73.95
	St. Dev.	0.21	0.14	0.14	--	--	0.07	0.00	0.07
	Cf. Var.	0.02%	0.03%	0.05%	--	--	0.02%	0.00%	0.10%
FWHM (eV)	Average	1.55	2.19	1.33	1.21	2.10	1.21	1.58	1.54
	St. Dev.	0.11	0.22	0.02	--	--	0.00	0.06	0.03
	Cf. Var.	6.88%	9.99%	1.38%	--	--	0.18%	3.62%	1.93%
Raw Area (CPS)	Average	915.60	6327.05	2117.20	8651.94	1604.33	549.50	482.30	400.75
	St. Dev.	1043.55	379.79	108.05	--	--	297.27	93.34	229.74
	Cf. Var.	113.97%	6.00%	5.10%	--	--	54.10%	19.35%	57.33%
Atomic Concentration (%)	Average	1.93	36.74	38.87	32.80	6.07	1.92	8.47	12.10
	St. Dev.	2.21	1.34	2.91	--	--	1.07	1.84	6.70
	Cf. Var.	114.97%	3.64%	7.48%	--	--	55.98%	21.71%	55.36%
Mass Concentration (%)	Average	2.56	33.82	26.88	22.67	4.20	4.33	13.71	18.72
	St. Dev.	2.96	0.78	2.35	--	--	2.47	3.15	10.15
	Cf. Var.	115.46%	2.32%	8.76%	--	--	57.16%	22.96%	54.22%
Moles	Average	0.11	2.11	2.24	1.89	0.35	0.11	0.49	0.69
	St. Dev.	0.13	0.05	0.20	0.10	0.09	0.06	0.11	0.38
	Cf. Var.	115.46%	2.32%	8.76%	5.37%	27.06%	57.16%	22.96%	54.22%

Feldspar Bulk Compositions

Mineral	Element	Mean	# Points	St. Dev.	Co. Var.	Range
Cationic Values Calibrated for 8 Oxygens						
Andesine	Na	0.49	25	0.04	7.49%	0.34-0.53
	Al	1.47	25	0.02	1.63%	1.41-1.50
	Si	2.53	25	0.02	0.93%	2.51-2.59
	K	0.03	25	0.05	152.56%	0.01-0.26
	Ca	0.45	25	0.02	4.53%	0.39-0.48
	Fe	0.01	25	0.02	177.14%	0.00-0.10
	Ba	0.00	25	0.00	--	0.00-0.00
Albite	Na	0.96	25	0.01	1.19%	0.94-0.99
	Al	1.03	25	0.01	0.61%	1.02-1.04
	Si	2.98	25	0.01	0.18%	2.97-2.99
	K	0.01	25	0.00	20.83%	0.00-0.01
	Ca	0.00	25	0.00	--	0.00-0.00
	Fe	0.00	25	0.00	--	0.00-0.00
	Ba	0.00	25	0.00	--	0.00-0.00
Labradorite	Na	0.45	25	0.01	2.98%	0.43-0.49
	Al	1.51	25	0.01	0.95%	1.49-1.55
	Si	2.50	25	0.01	0.57%	2.46-2.52
	K	0.03	25	0.01	20.23%	0.02-0.03
	Ca	0.50	25	0.01	2.29%	0.47-0.52
	Fe	0.01	25	0.00	30.10%	0.00-0.01
	Ba	0.00	25	0.00	--	0.00-0.00
Microcline	Na	0.22	25	0.33	153.87%	0.05-0.97
	Al	1.03	25	0.01	0.71%	1.02-1.04
	Si	2.97	25	0.00	0.16%	2.97-2.98
	K	0.79	25	0.35	44.30%	0.00-0.96
	Ca	0.00	25	0.01	250.00%	0.00-0.02
	Fe	0.00	25	0.00	--	0.00-0.00
	Ba	0.00	25	0.00	--	0.00-0.00

Feldspar Bulk Compositions (Continued)					
Mineral	Endmember	Mean	St. Dev.	# Points	Range
Endmember Values					
Andesine	Albite	50.34	3.94	25	34.10-54.60
	Orthoclase	3.26	4.94	25	1.50-26.40
	Anorthite	46.35	2.01	25	39.50-48.40
	Celsian	0.06	0.08	25	0.00-0.20
Albite	Albite	98.98	0.27	25	98.40-99.40
	Orthoclase	0.81	0.19	25	0.60-1.30
	Anorthite	0.16	0.11	25	0.00-0.40
	Celsian	0.06	0.10	25	0.00-0.40
Labradorite	Albite	46.02	1.11	25	43.90-49.20
	Orthoclase	2.46	0.26	25	1.70-2.90
	Anorthite	51.36	1.15	25	47.90-53.50
	Celsian	0.16	0.14	25	0.00-0.50
Microcline	Albite	21.76	34.00	25	5.40-98.50
	Orthoclase	77.97	34.48	25	0.50-94.60
	Anorthite	0.20	0.48	25	0.00-1.70
	Celsian	0.06	0.11	25	0.00-0.30

Oxides

Hematite

Three oxides were included in the dataset: Hematite, Ilmenite, and Quartz. Quartz is alternatively termed as a silicate based on its tectosilicate chemistry and structure. Other oxides are generally accessory minerals in igneous and metamorphic rocks that are relatively hard and dense (KLEIN, 2002). Oxides are also common in soils and sediments. Oxide structures are strongly ionic. All three of the oxide minerals in this dataset are simple oxides, that is, they follow the general structure of having only one nonequivalent metal cation. Hematite and ilmenite have cubic closest packing.

Hematite is hexagonal and $\bar{3}\,2/m$ with an ideal formula of Fe_2O_3. The bulk chemistry was determined with 25 individual data points. The bulk chemical formula

was measured as $Fe_{3.99}O_{6.00}$ or $Fe_{1.99}O_{3.00}$. The standard deviation of iron in the 25 points was less than 1% (.58%). Magnesium, aluminum, and silicon were measured in some of the data points above detection limits (2, 3, and 3 points respectively). The 99% confidence interval for iron ranged from 3.98-4.00 moles per six oxygens.

Hematite Bulk Chemistry

Element	Mean	St. Dev.	Co. Var.	# Points	Range
Cationic Values for 6 Oxygens					
Mg	0.00	0.01	379.09%	25	0.00-0.05
Al	0.00	0.00	500.00%	25	0.00-0.01
Si	0.00	0.01	390.31%	25	0.00-0.06
Ti	0.00	0.00	--	25	0.00-0.00
Ca	0.00	0.00	--	25	0.00-0.00
Fe	3.99	0.02	0.58%	25	3.89-4.00
Mn	0.00	0.00	--	25	0.00-0.00

The surface chemistry measured significant amounts of silicates on the surface that were not removed by washing (.53 moles). These were likely clays that were inside cracks. The formula was measured on four hematite fragments at $Fe_{.23}O_{3.00}$. The imbalance of iron may be due to masking by the organic carbon (3.91 moles) and the silicate.

Oxides: Ilmenite

Ilmenite Bulk Chemistry

Element	Mean	St. Dev.	Co. Var.	# Points	Range
Cationic Values for 6 Oxygens					
Mg	0.02	0.00	10.20%	25	0.01-0.02
Al	0.00	0.00	--	25	0.00-0.00
Si	0.00	0.00	--	25	0.00-0.00
Ti	1.85	0.08	4.35%	25	1.60-1.96
Ca	0.00	0.00	--	25	0.00-0.00
Fe^{2+}	1.68	0.07	4.30%	25	1.47-1.78
Fe^{3+}	0.31	0.16	52.19%	25	0.09-0.80
Mn	0.14	0.01	5.32%	25	0.12-0.16

Ilmenite is also hexagonal but is in space group $\bar{3}$. The stoichiometric ideal formula is $FeTiO_3$, and the composition is 36.8% iron, 31.6% titanium, and 31.6% oxygen (KLEIN, 2002). The structure of ilmenite is similar to hematite with iron and titanium contained in alternating octahedral on each layer along the C-axis. The bulk formula was $Fe_{1.99}Ti_{1.85}Mn_{.14}O_6$ or $Fe_{.99}Ti_{.93}Mn_{.07}O_3$. Divalent iron was 1.68 moles and trivalent iron was .31 moles. Manganese is an important accessory element in the ilmenite sample which is evenly distributed across the sample. The coefficient of variation for manganese was 5.32% with a range of .12 to .16 moles. Magnesium was found in all of the data points above the detection limit (.02 moles ranging from .01-.02). Total iron to titanium was 1.06.

Oxides: Quartz

Quartz is ubiquitous in most terrestrial environments on the earth (KLEIN, 2002). It is a tectosilicate as well as an oxide and is hexagonal in space group 32. It is commonly of high purity. The ideal formula is SiO_2. For 25 data points no other cation other than silicon was found above detection limit. Thus, the chemical formula is SiO_2.

Quartz WDS Results

Quartz Wavelength Dispersive Measurements					
Element	Mean	St. Dev.	Co. Var.	# Points	Range
Cationic Values for 8 Oxygens					
Na	0.00	0.00	--	25	0.00-0.00
Al	0.00	0.00	--	25	0.00-0.00
Si	4.00	0.00	0.00%	25	4.00-4.00
K	0.00	0.00	--	25	0.00-0.00
Ca	0.00	0.00	--	25	0.00-0.00
Fe	0.00	0.00	--	25	0.00-0.00
Ba	0.00	0.00	--	25	0.00-0.00

The quartz sample was obtained from a collector who had cleaned its surface with oxalic acid. This effectively removed all of the inorganic carbon. The surface composition was $Si_{1.37}O_{2.66}$ or $Si_{1.03}O_2$ when calibrated for two oxygens. The oxalic acid did not remove all of the organic carbon (or it reformed after application). 1.58 moles of adventitious carbon were measured on the sample. The sample, therefore, had very similar bulk and surface chemistries except the surface contained organic carbon.

Quartz Surface Chemistry

Measurement	O 1s	C 1s	C (Adven)	C (Carb)	Si 2p
Position BE (eV)	531.45	284.10	282.60	--	102.75
FWHM (eV)	1.73	1.71	1.71	--	1.75
Raw Area (CPS)	38528.50	7243.20	7243.20	--	6612.30
Atomic Conc %	47.37	28.13	28.13	--	24.51
Mass Conc. %	42.48	18.94	18.94	--	38.58
Moles	2.66	1.58	1.58	0.00	1.37

APPENDIX B

SURFACE ENERGY RESULTS

In addition to the samples being measured on three different probe vapors each of these vapors was also used to estimate the specific surface area. These results are given in the table below. Methylpropyl ketone and water each give biased results to SSA. These biases, however, give information on the sample surfaces. Hexane (56$Å^2$) should be considered the least biased and therefore the comparable result across the minerals and aggregates.

The surface energy components of the rocks and minerals were measured in units of energy per unit area (ergs/cm^2) so that the measurements would be normalized from variations in surface area. Surface area was calculated based the adsorption of n-hexane as a specific surface area, which is on a per gram basis. Several assumptions must be made in order to calculate the surface area. First, hexane is assumed to form a monolayer across the surface so that no hexane molecules will lay on top of each other and that there will be no gaps between molecules (BHASIN and LITTLE, 2007). Also, a hexane molecule is assumed to be 56$Å^2$. This number is from the literature as a best fit with laboratory data rather than based on molecular geometry (MCCLELLAN and HARNSBERGER, 1967). Hexane is expected to lie down on its long axis rather than across the short axis. Any crevices smaller than a hexane molecule will not be added to the total, however because the molecules will "lay across" the opening. This method carries similar difficulties and assumptions as the common use of N^2 to calculate surface areas, and has been shown to correlate well with N^2 measurements for the same materials (BHASIN and LITTLE, 2007).

The three equations used to calculate the surface energy components are interdependent and therefore error from one carries over to the others. For this reason the error cannot be estimated based on the variance between film pressures. Therefore, a variation of the Delta method was utilized with the software 'R' to estimate the standard error for each of the components separately. One disadvantage is that the delta method

assumes normality. This likely is a correct assumption, but with only twelve data points for each sample it cannot be proven.

Oxide Measured Specific Surface Areas

Probe Vapor	Quartz	Ilmenite	Hematite
Hexane (39Å^2)	0.04	0.07	0.03
Hexane (56Å^2)	0.06	0.10	0.05
MPK (35Å^2)	0.02	0.01	0.02
Water (5Å^2)	0.02	0.04	0.03
Water (10Å^2)	0.03	0.07	0.04

The most important contribution to "error" in the surface energy measurement of minerals and aggregates is almost certainly natural heterogeneity. The mineral samples purchased are pure phase or near pure phase, however even among these samples there are likely significant differences between fragments. Therefore, much of the variation between samples is likely not error, but rather the result for real differences between fragments and test runs.

Oxides

The oxides measured were quartz (SiO_2), hematite (Fe_2O_3), and ilmenite ($FeTiO_3$). Quartz is also a tectosilicate similar to the feldspars sampled. Specific surface areas for the oxides ranged from .05 to .1 cm^2/g for the standard hexane molecule. 39Å^2 was calculated by Bhasin and Little using the liquid density formula (BHASIN and LITTLE, 2007). However, Bhasin found that using 56.2Å^2, which was a value found in the literature, fit Micrometrics N^2 specific surface area measurements of aggregates more tightly (MCCLELLAN and HARNSBERGER, 1967). The estimated 56.2Å^2 hexane molecule will hereafter be referred to as the standard hexane molecule. Using water as the SSA vapor lowered the measurement slightly. For a 10 square angstrom water molecule the SSA ranged from .03 to .04 cm^2/g. Using MPK as the SSA probe vapor lowered the measurements again to a range of .01 to .02 cm^2/g.

Oxides: Quartz

The quartz van der Waals component measured 50.33 ergs/cm^2 for the standard hexane molecule and 68 ergs/cm^2 for 39Å^2 hexane molecule. The acid component for quartz was close to zero. This measurement was close to the detection limit for the sorption device. This caused the coefficient of variation for the acid component and the total polar component to be much larger than other minerals. The coefficient of variation for the acid component was 471%, and the coefficient for the total polar component was 72.81%. The quartz sample surface energy was controlled by the nonpolar component (fractional polarity of .09). Thus, there were not many unfilled bonds on the surface of the sample.

Quartz Surface Energy Results

Component	SSA Probe Vapor	Surface Energy	CV%
van der Waals	Hexane (56Å^2)	50.33	7.29%
	MPK (35Å^2)	135.89	16.55%
	Water (10Å^2)	81.68	13.76%
Acid Component	Hexane (56Å^2)	0.02	471.48%
	MPK (35Å^2)	0.50	303.47%
	Water (10Å^2)	0.04	650.45%
Base Component	Hexane (56Å^2)	365.00	11.25%
	MPK (35Å^2)	1096.34	18.09%
	Water (10Å^2)	639.91	15.24%
Totals			
Total Polar Component	Hexane (56Å^2)	5.04	72.81%
	MPK (35Å^2)	46.59	74.09%
	Water (10Å^2)	10.70	99.56%
Total Surface Energy	Hexane (56Å^2)	55.37	22.45%
	MPK (35Å^2)	182.48	40.72%
	Water (10Å^2)	92.38	39.60%

Oxides: Hematite

The total surface energy of hematite was measured as 128.81 ergs/cm^2. This was higher than the other oxides. The sample had higher polar surface energy than nonpolar with a fractional polarity of .62. The sample was homogeneous but limited in amount. This caused the confidence interval to be larger than desired. There was enough sample to give an estimate of the magnitudes of the components.

Hematite Surface Energy Results

Component	SSA Probe Vapor	Surface Energy	CV%
van der Waals	Hexane (56Å^2)	48.99	34.58%
	MPK (35Å^2)	153.64	58.41%
	Water (10Å^2)	49.81	35.03%
Acid Component	Hexane (56Å^2)	2.85	147.65%
	MPK (35Å^2)	13.68	201.74%
	Water (10Å^2)	2.93	148.92%
Base Component	Hexane (56Å^2)	558.07	18.18%
	MPK (35Å^2)	2622.24	25.20%
	Water (10Å^2)	572.27	18.35%
Totals			
Total Polar Component	Hexane (56Å^2)	79.82	51.82%
	MPK (35Å^2)	378.76	71.30%
	Water (10Å^2)	81.87	52.27%
Total Surface Energy	Hexane (56Å^2)	128.81	47.93%
	MPK (35Å^2)	532.40	74.26%
	Water (10Å^2)	131.68	48.49%

Oxides: Ilmenite

The ilmenite sample was also limited in quantity; however the homogeneity of the sample (see chemistry section) caused the surface energy measurements to remain

Ilmenite Surface Energy Results

Component	SSA Probe Vapor	Surface Energy	CV%
van der Waals	Hexane (56Å^2)	39.76	4.76%
	MPK (35Å^2)	421.17	11.79%
	Water (10Å^2)	54.26	6.22%
Acid Component	Hexane (56Å^2)	0.35	51.44%
	MPK (35Å^2)	91.44	25.63%
	Water (10Å^2)	1.59	36.83%
Base Component	Hexane (56Å^2)	318.90	3.27%
	MPK (35Å^2)	4263.84	7.29%
	Water (10Å^2)	457.86	4.18%
Totals			
Total Polar Component	Hexane (56Å^2)	21.13	12.97%
	MPK (35Å^2)	1248.81	13.67%
	Water (10Å^2)	53.97	12.40%
Total Surface Energy	Hexane (56Å^2)	60.89	9.47%
	MPK (35Å^2)	1669.98	10.40%
	Water (10Å^2)	108.23	9.75%

tight in range. The total surface energy 95% confidence interval was 49.5-72.2 ergs/cm^2 with a coefficient of variation of 9.47%. The average total surface energy for the standard hexane molecule was 60.89. The nonpolar surface energy was 39.76 was 21.13 ergs/cm^2 giving a fractional polarity of .35. This showed that the sample surface energy was controlled by the nonpolar portion.

Tectosilicates

Four feldspar samples were sampled: microcline, albite, andesine, and labradorite. Microcline is the triclinic potassium rich endmember sometimes known as "Kspar." Albite, andesine, and labradorite are all members of the plagioclase Na-Ca series. Albite has the most sodium (90-100%). Andesine and labradorite are intermediate

composition (50-70 & 30-50% respectively). Feldspars are very common igneous, sedimentary, and metamorphic minerals, and therefore are very important to the study. The specific surface areas of the feldspars ranged from 0.10 to 0.27 cm^2/g.

Feldspar Measured Specific Surface Areas

Probe Vapor	Microcline	Albite	Andesine	Labradorite
Hexane (39$Å^2$)	0.08	0.13	0.07	0.19
Hexane (56$Å^2$)	0.12	0.19	0.10	0.27
MPK (35$Å^2$)	0.02	0.02	0.03	0.03
Water (5$Å^2$)	0.03	0.02	0.22	0.07
Water (10$Å^2$)	0.05	0.04	0.36	0.11

This range was higher than the average of the other mineral groups and very similar to the aggregate specific surface areas. Labradorite had the highest SSA for every reference vapor except water. Water estimated at 5 and 10 square angstroms estimated andesine as the highest.

Tectosilicates: Microcline

The microcline ($KAlSi_3O_8$) was perthitic. Perthitic feldspars are intergrown with sodic alkali feldspar. Perthitic texture and composition is very common in feldspars. The sample was pegmatitic which increased the value of the mineral as a homogeneous sample for measuring the surface energy. Microcline had a large van der Waals component of 44 $ergs/cm^2$, and the polar component was only 19.35. This gave a fractional polarity of .31. The acid component was 0.46 $ergs/cm^2$. This was very close to andesine and albite. The total surface energy was 63.35 $ergs/cm^2$.

Microcline Surface Energy Results

Component	SSA Probe Vapor	Surface Energy	CV%
van der Waals	Hexane (56Å^2)	44.00	10.87%
	MPK (35Å^2)	296.54	23.10%
	Water (10Å^2)	97.69	17.41%
Acid Component	Hexane (56Å^2)	0.46	106.45%
	MPK (35Å^2)	126.92	35.31%
	Water (10Å^2)	6.58	67.30%
Base Component	Hexane (56Å^2)	202.79	13.80%
	MPK (35Å^2)	568.22	46.06%
	Water (10Å^2)	344.17	25.33%
Totals			
Total Polar Component	Hexane (56Å^2)	19.35	38.33%
	MPK (35Å^2)	537.10	40.33%
	Water (10Å^2)	95.16	41.29%
Total Surface Energy	Hexane (56Å^2)	63.35	18.05%
	MPK (35Å^2)	833.64	20.42%
	Water (10Å^2)	192.85	19.81%

Tectosilicates: Albite

Albite Surface Energy Results

Component	SSA Probe Vapor	Surface Energy	CV%
van der Waals	Hexane (56Å^2)	51.57	3.54%
	MPK (35Å^2)	119.96	5.34%
	Water (10Å^2)	66.11	4.15%
Acid Component	Hexane (56Å^2)	0.22	117.34%
	MPK (35Å^2)	0.04	630.09%
	Water (10Å^2)	0.16	182.08%
Base Component	Hexane (56Å^2)	501.69	10.64%
	MPK (35Å^2)	1510.59	14.15%
	Water (10Å^2)	704.58	11.93%
Totals			
Total Polar Component	Hexane (56Å^2)	21.22	35.33%
	MPK (35Å^2)	15.79	94.42%
	Water (10Å^2)	21.51	46.61%
Total Surface Energy	Hexane (56Å^2)	72.79	17.35%
	MPK (35Å^2)	135.76	36.96%
	Water (10Å^2)	87.63	22.62%

The albite sample was pegmatitic and homogeneous. This was displayed in the tight nonpolar surface energy range. The coefficient of variation for the standard hexane molecule was 3.54%. The 95% confidence interval was 48-55.15 ergs/cm^2 with an average of 51.57. The acid component was the lowest of the feldspars (0.22), but the base component was the second highest second to andesine).

Tectosilicates: Labradorite

The chemical composition of labradorite and andesine were very similar ($Na_{.45}Ca_{.50}Al_{1.51}Si_{2.50}O_8$ and $Na_{.49}Ca_{.45}Al_{1.47}Si_{2.53}O_8$ respectively both with minor potassium). Thus, any difference in surface energy might be attributed to other characteristics such as surface coatings or surface morphology. The total

Labradorite Surface Energy Results

Component	SSA Probe Vapor	Surface Energy	CV%
van der Waals	Hexane (56Å^2)	46.21	4.69%
	MPK (35Å^2)	656.29	10.59%
	Water (10Å^2)	107.46	7.45%
Acid Component	Hexane (56Å^2)	1.81	24.89%
	MPK (35Å^2)	273.43	17.20%
	Water (10Å^2)	17.95	19.97%
Base Component	Hexane (56Å^2)	186.54	3.59%
	MPK (35Å^2)	1064.19	12.92%
	Water (10Å^2)	297.28	7.04%
Totals			
Total Polar Component	Hexane (56Å^2)	36.71	9.46%
	MPK (35Å^2)	1078.85	14.91%
	Water (10Å^2)	146.11	11.85%
Total Surface Energy	Hexane (56Å^2)	82.92	6.15%
	MPK (35Å^2)	1735.14	7.79%
	Water (10Å^2)	253.57	6.87%

surface energy was measured at 82.92 ergs/cm^2 with nonpolar and polar surface energies of 46.21 and 36.71. Thus, the fractional polarity was .44. The acid component was much higher than the average for the feldspars (1.81 and .72 ergs/cm^2). The base component, however was the lowest of the feldspars.

Tectosilicates: Andesine

The andesine sample measured the highest total surface energy of the feldspars (129.88 ergs/cm^2). This was mainly due to the polar component measured at 89.24 ergs/cm^2. The fractional polarity was also the highest of the feldspars at .69.

Andesine Surface Energy Results

Component	SSA Probe Vapor	Surface Energy	CV%
van der Waals	Hexane (56Å^2)	40.64	5.32%
	MPK (35Å^2)	127.34	10.07%
	Water (10Å^2)	23.49	1.87%
Acid Component	Hexane (56Å^2)	0.40	57.14%
	MPK (35Å^2)	0.28	231.47%
	Water (10Å^2)	0.45	14.47%
Base Component	Hexane (56Å^2)	3755.04	31.88%
	MPK (35Å^2)	33315.91	35.99%
	Water (10Å^2)	553.10	22.03%
Totals			
Total Polar Component	Hexane (56Å^2)	77.70	42.68%
	MPK (35Å^2)	191.60	91.27%
	Water (10Å^2)	31.42	17.85%
Total Surface Energy	Hexane (56Å^2)	118.35	22.00%
	MPK (35Å^2)	318.94	70.00%
	Water (10Å^2)	54.91	8.00%

Phyllosilicates

Phyllosilicate Measured Specific Surface Areas

Probe Vapor	Biotite	Muscovite	Kaolinite	Montmorillonite
Hexane (39Å^2)	0.04	0.08	7.31	16.17
Hexane (56Å^2)	0.06	0.12	10.53	23.30
MPK (35Å^2)	0.02	0.06	4.58	-0.45
Water (5Å^2)	0.05	0.06	-0.42	-0.02
Water (10Å^2)	0.08	0.10	-0.70	-0.03

Four phyllosilicates were analyzed on the sorption device: biotite, muscovite, kaolinite, and montmorillonite. Two of the minerals were clays (kaolinite, and montmorillonite). These samples were separated from all the other minerals based on their specific surface areas. SSA measurements with the standard hexane molecule were two orders of magnitude higher than the other mineral specimens. Kaolinite SSA was 10.53, and montmorillonite SSA was 23.30. These agreed well with literature values. SSA data for water and MPK for montmorillonite could not be computed based on the computational method. As discussed earlier the SSA is calculated based on the BET equation $A = \left(\frac{n_M \cdot N_0}{M}\right) \cdot \alpha$ where n_M, N_0, M, and α are monolayer capacity of the aggregate surface, Avogadro's number, molecular weight of the probe vapor, and the projected area of a single molecule. n_M is calculated based on the equation $n_M = 1/S + 1$ where S is the slope of the partial pressure isotherm. This is estimated based on the slope and intercept of the best fit line between $\frac{p}{n(p_0-p)}$ versus $\frac{p}{p_0}$ where p, p_0, and n are equal to partial vapor pressure, maximum saturation vapor pressure, and mass of vapor adsorbed. For the case of montmorillonite and kaolinite the large amount of negatively charged area per unit mass causes the y-intercept of the 0-.35 vapor pressure range to increase. This causes the slope of the line to become negative. The best fit line could be estimated based on the .35 to 1.0 vapor pressure range, however the BET equation is not valid for this range (See (GREGG and SING, 1967)).

Phyllosilicates: Montmorillonite

The montmorillonite mineral sample had a nonpolar surface energy of 42.85 ergs/cm^2. This was higher than kaolinite but lower than the two micas. The polar component was 22.45 ergs/cm^2. This was lower than kaolinite and muscovite. The montmorillonite was homogeneous, but very friable. For this reason the sample had to be placed in a specially designed holder cage inside the USD in order to catch the sample if any broke off during adsorption of the probe vapors. The error for the sample reflected the homogeneity. The coefficient of variation of the total surface energy was 10.66% and the 95% confidence interval was 51.65 to 78.94 ergs/cm^2.

Montmorillonite Surface Energy Results

Component	SSA Probe Vapor	Surface Energy	CV%
van der Waals	Hexane (39Å^2)	56.86	11.31%
	Hexane (56Å^2)	42.85	9.04%
Acid Component	Hexane (39Å^2)	4.42	42.19%
	Hexane (56Å^2)	1.57	49.21%
Base Component	Hexane (39Å^2)	64.24	24.60%
	Hexane (56Å^2)	80.43	15.36%
Totals			
Component	Probe Vapor	Surface Energy	CV%
Total Polar Component	Hexane (39Å^2)	33.72	32.22%
	Hexane (56Å^2)	22.45	27.50%
Total Surface Energy	Hexane (39Å^2)	90.58	11.53%
	Hexane (56Å^2)	65.29	10.66%

Phyllosilicates: Kaolinite

It was also necessary to place the kaolinite on the special holder inside the sorption device because of the friable nature of kaolinite. The total surface energy of kaolinite was 70.51 ergs/cm^2. The magnitude was mainly due to the polar component, 40.02 ergs/cm^2. This gave a fractional polarity of .57. Thus, the polar component of kaolinite was similar to montmorillonite, but the nonpolar component was much less. The acid component was higher than the acid component for montmorillonite, but both were higher than the mineral average.

Kaolinite Surface Energy Results

Component	SSA Probe Vapor	Surface Energy	CV%
van der Waals	Hexane (39Å^2)	36.78	4.56%
	Hexane (56Å^2)	30.48	3.48%
	MPK (35Å^2)	50.71	6.20%
Acid Component	Hexane (39Å^2)	8.55	28.56%
	Hexane (56Å^2)	5.01	25.90%
	MPK (35Å^2)	18.15	31.27%
Base Component	Hexane (39Å^2)	73.61	16.61%
	Hexane (56Å^2)	80.00	11.06%
	MPK (35Å^2)	61.96	28.90%
Totals			
Total Polar Component	Hexane (39Å^2)	50.18	21.78%
	Hexane (56Å^2)	40.02	16.92%
	MPK (35Å^2)	67.06	30.06%
Total Surface Energy	Hexane (39Å^2)	86.95	9.73%
	Hexane (56Å^2)	70.51	8.13%
	MPK (35Å^2)	117.77	12.41%

Phyllosilicates: Muscovite and Biotite

Muscovite and biotite are 2:1 phyllosilicates with ¼ of the tetrahedral sites occupied by Al^{3+} instead of Si^{4+}. This charge increase is balanced by monovalent

potassium in the interlayer. The main difference between biotite and muscovite is that biotite is trioctahedral and muscovite is dioctahedral. This means that the hydroxides in the octahedral sheet are balanced by a divalent cation in trioctahedral sheets and a trivalent cation in dioctahedral sheets. This is the reason that biotite is more dense than muscovite (3.09 and 2.82).

Muscovite Surface Energy Results

Component	SSA Probe Vapor	Surface Energy	CV%
van der Waals	Hexane (56Å^2)	47.55	3.09%
	MPK (35Å^2)	79.82	4.25%
	Water (10Å^2)	54.64	3.43%
Acid Component	Hexane (56Å^2)	0.55	44.88%
	MPK (35Å^2)	3.42	31.97%
	Water (10Å^2)	1.02	39.12%
Base Component	Hexane (56Å^2)	544.68	13.02%
	MPK (35Å^2)	1081.38	16.53%
	Water (10Å^2)	658.50	14.11%
Totals			
Total Polar Component	Hexane (56Å^2)	34.52	24.17%
	MPK (35Å^2)	121.65	22.99%
	Water (10Å^2)	51.82	23.50%
Total Surface Energy	Hexane (56Å^2)	82.07	9.99%
	MPK (35Å^2)	201.47	11%
	Water (10Å^2)	106.46	10.27%

Muscovite Surface Energy Results

Component	SSA Probe Vapor	Surface Energy	CV%
van der Waals	Hexane (56Å^2)	52.51	5.60%
	MPK (35Å^2)	159.57	9.06%
	Water (10Å^2)	44.38	4.88%
Acid Component	Hexane (56Å^2)	0.07	181.49%
	MPK (35Å^2)	0.25	267.74%
	Water (10Å^2)	0.12	110.60%
Base Component	Hexane (56Å^2)	809.97	7.46%
	MPK (35Å^2)	3782.68	9.77%
	Water (10Å^2)	613.41	6.87%
Totals			
Total Polar Component	Hexane (56Å^2)	14.90	36.79%
	MPK (35Å^2)	61.56	51.15%
	Water (10Å^2)	17.07	27.56%
Total Surface Energy	Hexane (56Å^2)	67.41	20.55%
	MPK (35Å^2)	221.13	37.86%
	Water (10Å^2)	61.45	15.79%

The total surface energy for muscovite and biotite were 82.07 and 67.41 ergs/cm^2. The nonpolar component was roughly equal with biotite begin slightly higher (47.55 and 52.51), but muscovite had a larger polar component (34.52 to 14.90). The acid component of biotite was the second lowest of the mineral set (.01). This increased the error of this measurement due to its proximity to the detection limit. The coefficient of variation for the acid component of biotite was 181.49%.

Sulfates

Gypsum was acquired for analysis. In order to improve any heterogeneity the bassanite and hot gypsum were prepared from the gypsum sample. After the gypsum was fractured with the impact mortar between a number 4 and 8 sieve 1/3 of the sample was placed in the oven at 75°C for two weeks. When gypsum ($CaSO_4 \bullet 2H_2O$) is heated to

70°C it loses 1.5 waters and becomes Bassanite (commonly known as hemihydrates $CaSO_4 \bullet 0.5H_2O$).

Sulfate Measured Specific Surface Areas

Probe Vapor	Gypsum	Hot Gypsum	Bassanite
Hexane (39Å^2)	0.27	0.25	0.34
Hexane (56Å^2)	0.38	0.36	0.48
MPK (35Å^2)	0.02	0.03	0.13
Water (5Å^2)	0.02	0.03	0.81
Water (10Å^2)	0.03	0.04	1.37

The rest of the sample was placed in a plastic bag and stored. Half of the remaining sample was placed in vacuum and hot degassed in the same manner at the other minerals while the rest was allowed to get to vacuum but not hot degassed. The bassanite measured the highest SSA with all the reference vapor calculations. Hot gypsum measured higher SSA for MPK and both waters indicating higher affinity for polar molecules. The difference was most profound with water. Bassanite SSA for 5 and 10 square angstrom water was approximately 30 times higher than hot gypsum and 40 times higher than gypsum. Gypsum measured higher SSA for both hexane molecular sizes.

Sulfates: Gypsum and Hot Gypsum

As discussed in the chemistry section the gypsum sample was homogeneous and the sample size was over 500 grams. The coefficient of variation for the standard hexane molecule was 1.81% for nonpolar and 8.9% for polar surface energy. The 95% confidence interval for the total surface energy was 56.45 to 62.84 ergs/cm^2. Hot gypsum measured similar results to gypsum. The main differences were increased affinity to polar probe vapors. The polar surface energy of hot gypsum was 21.49 while the polar surface energy for gypsum was 18.52 ergs/cm^2. The fractional polarity was 3% higher.

Gypsum Surface Energy Results

Component	SSA Probe Vapor	Surface Energy	CV%
van der Waals	Hexane (56Å^2)	41.13	1.81%
	MPK (35Å^2)	1811.60	4.92%
	Water (10Å^2)	798.93	4.65%
Acid Component	Hexane (56Å^2)	1.31	14.70%
	MPK (35Å^2)	1037.39	9.41%
	Water (10Å^2)	396.90	9.53%
Base Component	Hexane (56Å^2)	65.47	5.39%
	MPK (35Å^2)	1905.17	19.29%
	Water (10Å^2)	537.53	22.95%
Totals			
Total Polar Component	Hexane (56Å^2)	18.52	8.90%
	MPK (35Å^2)	2811.69	13.47%
	Water (10Å^2)	923.79	14.79%
Total Surface Energy	Hexane (56Å^2)	59.65	2.73%
	MPK (35Å^2)	4623.29	6.80%
	Water (10Å^2)	1722.71	7.00%

Hot Gypsum Surface Energy Results

Component	SSA Probe Vapor	Surface Energy	CV%
van der Waals	Hexane (56Å^2)	42.24	2.28%
	MPK (35Å^2)	1162.13	5.87%
	Water (10Å^2)	492.90	5.42%
Acid Component	Hexane (56Å^2)	1.32	13.47%
	MPK (35Å^2)	574.89	8.70%
	Water (10Å^2)	199.94	8.87%
Base Component	Hexane (56Å^2)	87.66	2.38%
	MPK (35Å^2)	161.65	26.20%
	Water (10Å^2)	10.25	70.20%
Totals			
Total Polar Component	Hexane (56Å^2)	21.49	5.66%
	MPK (35Å^2)	609.70	15.10%
	Water (10Å^2)	90.54	24.95%
Total Surface Energy	Hexane (56Å^2)	63.73	2.76%
	MPK (35Å^2)	1771.83	6.11%
	Water (10Å^2)	583.43	7.15%

Sulfates: Bassanite

Bassanite Surface Energy Results

Component	SSA Probe Vapor	Surface Energy	CV%
van der Waals	Hexane (56Å^2)	38.27	7.83%
	MPK (35Å^2)	129.60	15.92%
	Water (10Å^2)	24.61	3.46%
Acid Component	Hexane (56Å^2)	0.30	90.47%
	MPK (35Å^2)	0.03	1092.69%
	Water (10Å^2)	0.40	27.54%
Base Component	Hexane (56Å^2)	3036.03	29.52%
	MPK (35Å^2)	32170.48	34.03%
	Water (10Å^2)	666.26	22.19%
Totals			
Total Polar Component	Hexane (56Å^2)	59.90	51.68%
	MPK (35Å^2)	60.40	192.83%
	Water (10Å^2)	32.62	24.72%
Total Surface Energy	Hexane (56Å^2)	98.16	29.19%
	MPK (35Å^2)	190.00	174.09%
	Water (10Å^2)	57.23	10.19%

The bassanite sample showed a large increase in polar surface energy (59.90 ergs/cm^2). The van der Waals component was slightly lower than gypsum and hot gypsum. Fewer sample runs were performed on bassanite than the other two sulfates based on time constraints on the universal sorption device. This caused an increase in standard error. The coefficient of variation for the standard hexane molecule was 29.19% for the total surface energy.

Carbonates

Five carbonates were analyzed on the USD: calcite ($CaCO_3$), cerussite ($PbCO_3$), Siderite ($FeCO_3$), Rhodochrosite ($MnCO_3$), and Dolomite ($CaMg(CO_3)_2$). The carbonate series was most useful for comparing surface hardness and softness. This was

accomplished by comparing the surface chemistry of the various cations. The SSA of the carbonates ranged from .06 to .28 cm^2/g for the standard hexane molecule, and .02 to .08 for water. Methylpropyl ketone was very low and did not vary much across the carbonate series.

Carbonate Measured Specific Surface Areas

Probe Vapor	Calcite	Dolomite	Cerussite	Siderite	Rhodochrosite
Hexane (39$Å^2$)	0.20	0.04	0.12	0.05	0.12
Hexane (56$Å^2$)	0.28	0.06	0.17	0.07	0.18
MPK (35$Å^2$)	0.02	0.02	0.00	0.02	0.02
Water (5$Å^2$)	0.01	0.04	0.04	0.05	0.03
Water (10$Å^2$)	0.02	0.06	0.07	0.08	0.05

Carbonates: Calcite and Dolomite

Calcite surface energy was primarily nonpolar with a fractional polarity of .25. The total surface energy was 46.54 $ergs/cm^2$. Dolomite surface energy was also nonpolar with a fractional polarity of .25. Dolomite and calcite differed considerably on the van der Waals component, however with 34.94 and 60.29 $ergs/cm^2$ respectively. The polar surface energy of calcite was 11.6 $ergs/cm^2$ while dolomite was approximately double at 20.28 $ergs/cm^2$.

Calcite Surface Energy Results

Component	SSA Probe Vapor	Surface Energy	CV%
van der Waals	Hexane (56Å^2)	34.94	12.44%
	MPK (35Å^2)	1073.10	39.42%
	Water (10Å^2)	768.57	38.34%
Acid Component	Hexane (56Å^2)	0.40	117.09%
	MPK (35Å^2)	497.31	57.94%
	Water (10Å^2)	332.55	58.32%
Base Component	Hexane (56Å^2)	85.16	11.14%
	MPK (35Å^2)	495.95	87.68%
	Water (10Å^2)	267.74	99.02%
Totals			
Total Polar Component	Hexane (56Å^2)	11.60	36.11%
	MPK (35Å^2)	993.26	71.28%
	Water (10Å^2)	596.78	75.99%
Total Surface Energy	Hexane (56Å^2)	46.54	17.38%
	MPK (35Å^2)	2066.36	32.51%
	Water (10Å^2)	1365.35	33.11%
	MPK (35Å^2)	686.22	23.03%
	Water (10Å^2)	87.77	21.28%

Dolomite Surface Energy Results

Component	SSA Probe Vapor	Surface Energy	CV%
van der Waals	Hexane (56Å^2)	60.29	7.61%
	MPK (35Å^2)	292.95	12.75%
	Water (10Å^2)	63.57	7.86%
Acid Component	Hexane (56Å^2)	0.18	161.29%
	MPK (35Å^2)	11.61	74.61%
	Water (10Å^2)	0.24	147.93%
Base Component	Hexane (56Å^2)	564.05	15.12%
	MPK (35Å^2)	3330.43	23.09%
	Water (10Å^2)	600.66	15.53%
Totals			
Total Polar Component	Hexane (56Å^2)	20.28	49.38%
	MPK (35Å^2)	393.26	41.51%
	Water (10Å^2)	24.19	47.94%
Total Surface Energy	Hexane (56Å^2)	80.57	21.17%
	MPK (35Å^2)	686.22	23.03%
	Water (10Å^2)	87.77	21.28%

Carbonates: Rhodochrosite, Cerussite, and Siderite

Rhodochrosite Surface Energy results

Component	SSA Probe Vapor	Surface Energy	CV%
van der Waals	Hexane (56Å^2)	40.33	4.05%
	MPK (35Å^2)	728.69	10.50%
	Water (10Å^2)	153.80	8.17%
Acid Component	Hexane (56Å^2)	0.86	28.01%
	MPK (35Å^2)	289.16	16.78%
	Water (10Å^2)	31.79	18.09%
Base Component	Hexane (56Å^2)	145.76	7.95%
	MPK (35Å^2)	462.77	49.12%
	Water (10Å^2)	220.22	25.46%
Totals			
Total Polar Component	Hexane (56Å^2)	22.33	14.93%
	MPK (35Å^2)	731.61	28.71%
	Water (10Å^2)	167.34	21.46%
Total Surface Energy	Hexane (56Å^2)	62.66	5.81%
	MPK (35Å^2)	1460.30	14.02%
	Water (10Å^2)	321.14	9.03%

Siderite Surface Energy Results

Component	SSA Probe Vapor	Surface Energy	CV%
van der Waals	Hexane (56Å^2)	61.39	6.94%
	MPK (35Å^2)	313.76	11.62%
	Water (10Å^2)	55.35	6.49%
Acid Component	Hexane (56Å^2)	1.59	55.76%
	MPK (35Å^2)	44.42	39.90%
	Water (10Å^2)	1.09	59.81%
Base Component	Hexane (56Å^2)	789.63	20.21%
	MPK (35Å^2)	5682.12	28.72%
	Water (10Å^2)	686.84	19.24%
Totals			
Total Polar Component	Hexane (56Å^2)	70.80	33.57%
	MPK (35Å^2)	1004.82	33.85%
	Water (10Å^2)	54.68	33.92%
Total Surface Energy	Hexane (56Å^2)	132.18	16.21%
	MPK (35Å^2)	1318.58	18.93%
	Water (10Å^2)	110.03	15.95%

The polar surface energy increased from cerussite, rhodochrosite, to siderite. This increase corresponded with the hard/soft acid base concept. The van der Waals energy was 35.07, 40.33, and 61.39 ergs/cm^2 for cerussite, rhodochrosite, and siderite. Cerussite was limited in sample quantity. For this reason an error analysis could not be performed. The coefficient of variation for the total surface energy of rhodochrosite was 5.81% and 16.21% for siderite. Siderite was the only sample to have a fractional polarity greater than .50.

Cerussite Surface Energy Results

Component	SSA Probe Vapor	Surface Energy
van der Waals	Hexane (56Å^2)	35.07
	MPK (35Å^2)	75352.43
	Water (10Å^2)	153.93
Acid Component	Hexane (56Å^2)	0.11
	MPK (35Å^2)	27805.69
	Water (10Å^2)	18.92
Base Component	Hexane (56Å^2)	113.14
	MPK (35Å^2)	4989.14
	Water (10Å^2)	75.25
Totals		
Total Polar Component	Hexane (56Å^2)	7.04
	MPK (35Å^2)	23556.45
	Water (10Å^2)	75.46
Total Surface Energy	Hexane (56Å^2)	42.11
	MPK (35Å^2)	98908.88
	Water (10Å^2)	229.39

Nesosilicates and Inosilicates

The neso/Inosilicate group had the largest variation in surface energies of any mineral group. Augite had the highest surface energy at 367.78 ergs/cm^2. The fractional polarity was .95. The specific surface areas of this group were modest, however with a range of .03 to .25 cm^2/g. The van der Waals component increase from olivine, hornblende, to augite. The fractional polarity of olivine was .30. Heterogeneity increased from olivine, hornblende, to augite. The heterogeneity of the samples is described in detail in the chemistry section.

Neso/Inosilicate Measured Specific Surface Areas

Probe Vapor	Olivine	Augite	Hornblende
Hexane (39Å^2)	0.17	0.02	0.06
Hexane (56Å^2)	0.25	0.03	0.09
MPK (35Å^2)	0.02	0.04	0.02
Water (5Å^2)	0.01	0.10	0.12
Water (10Å^2)	0.01	0.16	0.21

Olivine Surface Energy Results

Component	SSA Probe Vapor	Surface Energy	CV%
van der Waals	Hexane (56Å^2)	44.17	1.02%
	MPK (35Å^2)	778.10	2.43%
	Water (10Å^2)	778.87	2.43%
Acid Component	Hexane (56Å^2)	1.55	6.24%
	MPK (35Å^2)	345.99	4.18%
	Water (10Å^2)	339.52	3.73%
Base Component	Hexane (56Å^2)	57.52	3.84%
	MPK (35Å^2)	595.24	12.99%
	Water (10Å^2)	587.20	13.01%
Totals			
Total Polar Component	Hexane (56Å^2)	18.87	4.89%
	MPK (35Å^2)	907.63	7.37%
	Water (10Å^2)	893.01	6.96%
Total Surface Energy	Hexane (56Å^2)	63.04	1.31%
	MPK (35Å^2)	1685.73	3.84%
	Water (10Å^2)	1671.88	3.79%

Augite Surface Energy results

Component	SSA Probe Vapor	Surface Energy	CV%
van der Waals	Hexane (56Å^2)	52.67	10.00%
	MPK (35Å^2)	47.45	9.23%
	Water (10Å^2)	24.18	3.12%
Acid Component	Hexane (56Å^2)	8.69	31.25%
	MPK (35Å^2)	7.11	30.26%
	Water (10Å^2)	1.35	16.79%
Base Component	Hexane (56Å^2)	3890.33	21.71%
	MPK (35Å^2)	3116.35	21.23%
	Water (10Å^2)	436.44	13.59%
Totals			
Total Polar Component	Hexane (56Å^2)	367.78	26.05%
	MPK (35Å^2)	297.65	25.35%
	Water (10Å^2)	48.46	15.11%
Total Surface Energy	Hexane (56Å^2)	420.45	16.69%
	MPK (35Å^2)	345.10	15.99%
	Water (10Å^2)	72.64	7.28%

Hornblende Surface Energy Results

Component	SSA Probe Vapor	Surface Energy	CV%
van der Waals	Hexane (56Å^2)	51.92	3.12%
	MPK (35Å^2)	296.85	5.79%
	Water (10Å^2)	31.06	1.78%
Acid Component	Hexane (56Å^2)	0.91	39.73%
	MPK (35Å^2)	43.09	25.58%
	Water (10Å^2)	0.00	436.96%
Base Component	Hexane (56Å^2)	1338.86	9.02%
	MPK (35Å^2)	15399.39	11.88%
	Water (10Å^2)	498.80	6.46%
Totals			
Total Polar Component	Hexane (56Å^2)	69.70	18.93%
	MPK (35Å^2)	1629.22	17.43%
	Water (10Å^2)	1.70	53.15%
Total Surface Energy	Hexane (56Å^2)	121.63	11.75%
	MPK (35Å^2)	1926.07	11.96%
	Water (10Å^2)	32.76	11.48%

APPENDIX C

MINERAL ROUGHNESS RESULTS

Albite Surface Roughness Measurements

96 Fragments	Area (cm^2)	P. Length (cm)	Major (cm)	Minor (cm)	areaC/areaM	Area/(Avg... Area)	Est. Ht. (cm)	Avg. Diameter (3d)
Average	0.313	2.576	0.830	0.450	1.142	1.000	0.241	0.507
Median	0.263	2.422	0.760	0.408	1.082	0.840	0.188	0.471
Q1	0.151	1.868	0.599	0.325	1.025	0.481	0.115	0.424
Q3	0.432	3.292	1.033	0.558	1.160	1.379	0.328	0.574
Minimum	0.046	1.115	0.356	0.142	0.999	0.147	0.059	0.398
Maximum	0.840	4.679	1.951	0.966	1.747	2.684	1.066	0.813
St. Dev.	0.201	0.882	0.317	0.173	0.172	0.642	0.169	0.100
95% CI	0.27 - 0.35	2.40 - 2.75	0.77 - 0.89	0.42 - 0.48	1.11 - 1.18	0.87 - 1.13	0.21 - 0.27	0.49 - 0.53
Coeff. Var.	64.15%	34.25%	38.23%	38.47%	15.05%	64.15%	70.04%	19.65%

Labradorite Surface Roughness Measurements

179 Fragments	Area (cm^2)	P. Length (cm)	Major (cm)	Minor (cm)	areaC/areaM	Area/(Avg. Area)	Est. Ht. (cm)	Avg. Diameter (3d)
Average	0.22	2.02	0.66	0.40	1.08	1.00	0.15	0.41
Median	0.183	1.896	0.617	0.360	1.055	0.825	0.138	0.382
Q1	0.122	1.489	0.469	0.313	1.021	0.548	0.087	0.337
Q3	0.289	2.432	0.806	0.478	1.103	1.303	0.208	0.449
Minimum	0.043	0.882	0.277	0.196	0.999	0.194	0.032	0.319
Maximum	0.791	3.968	1.273	0.792	1.404	3.566	0.591	0.699
St. Dev	0.13	0.60	0.22	0.12	0.08	0.60	0.09	0.08
95% CI	0.20 - 0.24	1.93 - 2.11	0.63 - 0.69	0.38 - 0.42	1.07 - 1.09	0.91 - 1.09	0.14 - 0.17	0.39 - 0.42
Coeff. Var.	60.06%	29.98%	32.89%	30.26%	7.71%	60.06%	55.38%	19.72%

Microcline Surface Roughness measurements

114 Fragments	Area (cm^2)	P. Length (cm)	Major (cm)	Minor (cm)	areaC/areaM	Area/(Avg. Area)	Est. Ht. (cm)	Avg. Diameter (3d)
Average	0.21	2.00	0.66	0.37	1.11	1.00	0.16	0.40
Median	0.165	1.842	0.595	0.349	1.065	0.768	0.126	0.362
Q1	0.103	1.471	0.478	0.279	1.026	0.477	0.094	0.326
Q3	0.222	2.222	0.753	0.429	1.152	1.032	0.201	0.414
Minimum	0.030	0.731	0.213	0.136	1.000	0.140	0.018	0.299
Maximum	1.134	5.138	1.869	0.905	1.910	5.282	0.689	0.886
St. Dev	0.18	0.81	0.28	0.15	0.13	0.85	0.11	0.11
95% CI	0.18 - 0.25	1.86 - 2.15	0.61 - 0.71	0.35 - 0.40	1.09 - 1.13	0.84 - 1.16	0.14 - 0.18	0.38 - 0.42
Coeff. Var.	85.46%	40.52%	42.96%	39.51%	11.68%	85.46%	72.65%	27.23%

Gypsum Surface Roughness Measurements

38 Fragments	Area (cm^2)	P. Length (cm)	Major (cm)	Minor (cm)	areaC/areaM	Area/(Avg. Area)	Est. Ht. (cm)	Avg. Diameter (3d)
Average	0.77	4.23	1.30	0.69	1.13	1.00	0.25	0.75
Median	0.784	4.343	1.373	0.734	1.096	1.020	0.115	0.741
Q1	0.525	3.712	1.083	0.556	1.057	0.684	0.087	0.661
Q3	1.041	5.028	1.552	0.842	1.174	1.355	0.172	0.831
Minimum	0.042	1.400	0.347	0.154	1.001	0.055	0.045	0.517
Maximum	2.000	7.253	2.256	1.342	1.453	2.604	2.146	1.095
St. Dev	0.43	1.36	0.44	0.27	0.11	0.57	0.39	0.14
95% CI	0.63 - 0.91	3.80 - 4.66	1.17 - 1.44	0.61 - 0.78	1.10 - 1.17	0.82 - 1.18	0.13 - 0.38	0.70 - 0.79
Coeff. Var.	56.49%	32.11%	33.37%	38.76%	10.06%	56.49%	156.00%	18.87%

Calcite Surface Roughness Measurements

134 Fragments	Area (cm^2)	P. Length (cm)	Major (cm)	Minor (cm)	areaC/areaM	Area/(Avg. Area)	Est. Ht. (cm)	Avg. Diameter (3d)
Average	0.25	2.04	0.67	0.42	1.08	1.00	0.29	0.46
Median	0.188	1.941	0.616	0.381	1.044	0.741	0.200	0.427
Q1	0.115	1.507	0.486	0.279	1.017	0.452	0.114	0.386
Q3	0.330	2.482	0.859	0.525	1.120	1.301	0.328	0.498
Minimum	0.026	0.681	0.214	0.111	0.999	0.102	0.034	0.364
Maximum	1.097	4.383	1.602	1.125	1.775	4.324	1.477	0.800
St. Dev	0.20	0.80	0.27	0.19	0.11	0.79	0.28	0.10
95% CI	0.22 - 0.29	1.91 - 2.18	0.63 - 0.72	0.39 - 0.45	1.07 - 1.10	0.87 - 1.13	0.24 - 0.33	0.44 - 0.48
Coeff. Var.	79.42%	39.15%	40.37%	44.21%	10.41%	79.42%	98.00%	20.63%

Dolomite Surface Roughness Measurements

43 Fragments	Area (cm^2)	P. Length (cm)	Major (cm)	Minor (cm)	areaC/areaM	Area/(Avg. Area)	Est. Ht. (cm)	Avg. Diameter (3d)
Average	0.42	2.82	0.91	0.56	1.07	1.00	0.24	0.57
Median	0.411	2.845	0.856	0.585	1.057	0.973	0.185	0.551
Q1	0.260	2.271	0.718	0.453	1.028	0.614	0.143	0.495
Q3	0.533	3.132	1.009	0.680	1.102	1.262	0.293	0.598
Minimum	0.108	1.331	0.387	0.275	1.001	0.256	0.073	0.464
Maximum	1.045	4.943	1.697	0.806	1.239	2.474	0.703	0.852
St. Dev	0.22	0.84	0.30	0.15	0.06	0.53	0.15	0.10
95% CI	0.36 - 0.49	2.57 - 3.07	0.82 - 1.00	0.51 - 0.60	1.05 - 1.09	0.84 - 1.16	0.20 - 0.29	0.54 - 0.60
Coeff. Var.	53.09%	29.78%	32.51%	26.66%	5.88%	53.09%	62.58%	16.93%

Siderite Surface Roughness Measurements

39 Fragments	Area (cm^2)	P. Length (cm)	Major (cm)	Minor (cm)	areaC/areaM	Area/(Avg. Area)	Est. Ht. (cm)	Avg. Diameter (3d)
Average	0.06	1.01	0.33	0.21	1.07	1.00	0.46	0.33
Median	0.058	1.015	0.323	0.213	1.041	0.997	0.321	0.311
Q1	0.030	0.761	0.249	0.153	1.019	0.507	0.223	0.295
Q3	0.084	1.187	0.377	0.261	1.088	1.435	0.628	0.347
Minimum	0.016	0.519	0.155	0.102	1.000	0.275	0.147	0.289
Maximum	0.127	1.690	0.628	0.366	1.345	2.183	1.188	0.495
St. Dev	0.03	0.31	0.11	0.07	0.08	0.57	0.29	0.05
95% CI	0.05 - 0.07	0.91 - 1.11	0.29 - 0.36	0.19 - 0.23	1.05 - 1.10	0.82 - 1.18	0.37 - 0.55	0.32 - 0.35
Coeff. Var.	56.73%	30.70%	32.92%	33.43%	7.79%	56.73%	63.34%	15.95%

Biotite Surface Roughness Measurements

104 Fragments	Area (cm^2)	P. Length (cm)	Major (cm)	Minor (cm)	areaC/areaM	Area/(Avg. Area)	Est. Ht. (cm)	Avg. Diameter (3d)
Average	0.61	3.47	1.06	0.69	1.07	1.00	0.06	0.61
Median	0.594	3.437	1.045	0.708	1.035	0.976	0.022	0.602
Q1	0.424	2.923	0.855	0.582	1.011	0.697	0.017	0.517
Q3	0.761	4.030	1.217	0.859	1.085	1.252	0.030	0.689
Minimum	0.004	0.307	0.120	0.039	1.000	0.007	0.009	0.276
Maximum	1.449	6.512	2.612	1.164	1.606	2.383	3.482	1.214
St. Dev	0.29	1.00	0.34	0.21	0.10	0.48	0.34	0.16
95% CI	0.55 - 0.66	3.28 - 3.67	1.00 - 1.13	0.65 - 0.73	1.05 - 1.09	0.91 - 1.09	0.00 - 0.13	0.58 - 0.64
Coeff. Var.	47.75%	28.85%	31.69%	29.58%	9.00%	47.75%	533.66%	25.73%

Muscovite Surface Roughness measurements

54 Fragments	Area (cm^2)	P. Length (cm)	Major (cm)	Minor (cm)	areaC/areaM	Area/(Avg. Area)	Est. Ht. (cm)	Avg. Diameter (3d)
Average	0.91	4.32	1.25	0.86	1.07	1.00	0.04	0.71
Median	0.914	4.670	1.302	0.902	1.040	1.006	0.017	0.758
Q1	0.459	3.124	0.989	0.577	1.009	0.505	0.013	0.543
Q3	1.276	5.327	1.525	1.136	1.079	1.405	0.035	0.873
Minimum	0.027	0.835	0.244	0.143	1.001	0.030	0.008	0.323
Maximum	1.946	6.524	2.118	1.486	1.504	2.143	0.582	1.054
St. Dev	0.50	1.39	0.37	0.34	0.10	0.55	0.08	0.21
95% CI	0.78 - 1.04	3.95 - 4.69	1.15 - 1.35	0.76 - 0.95	1.04 - 1.10	0.85 - 1.15	0.02 - 0.06	0.66 - 0.77
Coeff. Var.	54.94%	32.23%	29.72%	40.07%	9.24%	54.94%	207.40%	28.85%

Montmorillonite Surface Roughness Measurements

30 Fragments	Area (cm^2)	P. Length (cm)	Major (cm)	Minor (cm)	areaC/areaM	Area/(Avg. Area)	Est. Ht. (cm)	Avg. Diameter (3d)
Average	0.48	2.66	0.85	0.56	1.08	1.00	0.66	0.69
Median	0.220	2.089	0.677	0.439	1.055	0.460	0.498	0.573
Q1	0.168	1.688	0.567	0.353	1.028	0.351	0.185	0.535
Q3	0.647	3.620	1.090	0.669	1.113	1.354	0.653	0.743
Minimum	0.026	0.815	0.294	0.101	1.002	0.054	0.055	0.521
Maximum	1.969	6.066	1.879	1.437	1.396	4.123	4.180	1.537
St. Dev	0.54	1.43	0.42	0.35	0.08	1.12	0.84	0.24
95% CI	0.29 - 0.67	2.15 - 3.17	0.70 - 1.00	0.43 - 0.69	1.05 - 1.11	0.60 - 1.40	0.36 - 0.96	0.60 - 0.77
Coeff. Var.	112.33%	53.67%	49.24%	62.81%	7.69%	112.33%	127.23%	34.67%

Kaolinite Surface Roughness Measurements

51 Fragments	Area (cm^2)	P. Length (cm)	Major (cm)	Minor (cm)	areaC/areaM	Area/(Avg. Area)	Est. Ht. (cm)	Avg. Diameter (3d)
Average	0.38	2.43	0.76	0.51	1.05	1.00	0.43	0.56
Median	0.229	2.181	0.651	0.428	1.036	0.606	0.332	0.500
Q1	0.122	1.613	0.521	0.329	1.022	0.323	0.212	0.479
Q3	0.358	2.564	0.826	0.583	1.077	0.947	0.621	0.564
Minimum	0.055	0.967	0.313	0.215	1.001	0.145	0.040	0.462
Maximum	1.885	6.549	1.857	1.352	1.144	4.985	1.365	1.055
St. Dev	0.44	1.31	0.38	0.27	0.04	1.17	0.32	0.15
95% CI	0.26 - 0.50	2.07 - 2.79	0.65 - 0.86	0.43 - 0.58	1.04 - 1.06	0.68 - 1.32	0.34 - 0.52	0.52 - 0.61
Coeff. Var.	117.47%	53.99%	50.57%	53.83%	3.84%	117.47%	75.69%	27.15%

Quartz Surface Roughness measurements

97 Fragments	Area (cm^2)	P. Length (cm)	Major (cm)	Minor (cm)	areaC/areaM	Area/(Avg. Area)	Est. Ht. (cm)	Avg. Diameter (3d)
Average	0.32	2.38	0.75	0.48	1.08	1.00	0.20	0.48
Median	0.221	2.137	0.681	0.422	1.040	0.692	0.180	0.429
Q1	0.154	1.749	0.551	0.349	1.015	0.482	0.113	0.397
Q3	0.354	2.692	0.866	0.568	1.098	1.109	0.260	0.513
Minimum	0.036	0.881	0.254	0.179	0.999	0.113	0.033	0.371
Maximum	1.203	4.739	1.503	1.048	1.681	3.769	1.118	0.848
St. Dev	0.26	0.85	0.28	0.21	0.11	0.81	0.16	0.12
95% CI	0.27 - 0.37	2.21 - 2.55	0.70 - 0.81	0.44 - 0.52	1.06 - 1.10	0.84 - 1.16	0.17 - 0.24	0.46 - 0.50
Coeff. Var.	81.11%	35.64%	37.43%	42.61%	9.73%	81.11%	78.46%	24.85%

Hornblende Surface Roughness Measurements

40 Fragments	Area (cm^2)	P. Length (cm)	Major (cm)	Minor (cm)	areaC/areaM	Area/(Avg. Area)	Est. Ht. (cm)	Avg. Diameter (3d)
Average	0.31	2.33	0.77	0.46	1.09	1.00	0.32	0.52
Median	0.222	2.088	0.655	0.382	1.060	0.719	0.292	0.468
Q1	0.139	1.668	0.575	0.338	1.026	0.449	0.187	0.446
Q3	0.345	2.715	0.870	0.534	1.114	1.120	0.466	0.528
Minimum	0.103	1.435	0.420	0.263	1.001	0.334	0.055	0.436
Maximum	1.169	5.412	2.119	0.864	1.498	3.793	0.625	0.959
St. Dev	0.25	0.91	0.35	0.17	0.10	0.83	0.16	0.11
95% CI	0.23 - 0.39	2.05 - 2.61	0.67 - 0.88	0.40 - 0.51	1.06 - 1.12	0.74 - 1.26	0.27 - 0.37	0.48 - 0.55
Coeff. Var.	82.68%	38.89%	44.76%	36.74%	8.96%	82.68%	51.76%	22.20%

Olivine Surface Roughness Measurements

36 Fragments	Area (cm^2)	P. Length (cm)	Major (cm)	Minor (cm)	areaC/areaM	Area/(Avg. Area)	Est. Ht. (cm)	Avg. Diameter (3d)
Average	0.38	2.53	0.79	0.58	1.03	1.00	0.27	0.55
Median	0.400	2.630	0.801	0.609	1.026	1.061	0.197	0.551
Q1	0.283	2.324	0.697	0.518	1.007	0.751	0.170	0.509
Q3	0.462	2.839	0.899	0.687	1.045	1.227	0.279	0.571
Minimum	0.085	1.258	0.391	0.276	1.001	0.226	0.100	0.470
Maximum	0.786	3.664	1.161	0.862	1.114	2.087	0.928	0.708
St. Dev	0.15	0.56	0.18	0.15	0.03	0.41	0.19	0.05
95% CI	0.33 - 0.43	2.35 - 2.72	0.73 - 0.85	0.54 - 0.63	1.02 - 1.04	0.87 - 1.13	0.21 - 0.33	0.53 - 0.57
Coeff. Var.	40.61%	22.19%	23.18%	25.38%	2.99%	40.61%	69.36%	9.58%

Augite Surface Roughness Measurements

87 Fragments	Area (cm^2)	P. Length (cm)	Major (cm)	Minor (cm)	areaC/areaM	Area/(Avg. Area)	Est. Ht. (cm)	Avg. Diameter (3d)
Average	0.33	2.53	0.79	0.49	1.09	1.00	0.28	0.52
Median	0.291	2.488	0.762	0.477	1.039	0.882	0.165	0.487
Q1	0.160	1.956	0.593	0.360	1.011	0.485	0.104	0.427
Q3	0.461	3.028	0.997	0.623	1.105	1.395	0.299	0.567
Minimum	0.008	0.382	0.120	0.086	0.994	0.024	0.050	0.394
Maximum	0.951	4.555	1.789	0.995	1.807	2.882	5.906	2.037
St. Dev	0.20	0.83	0.30	0.18	0.14	0.59	0.63	0.19
95% CI	0.29 - 0.37	2.35 - 2.71	0.73 - 0.86	0.46 - 0.53	1.06 - 1.12	0.87 - 1.12	0.15 - 0.41	0.48 - 0.56
Coeff. Var.	59.24%	32.98%	37.69%	37.00%	12.76%	59.24%	224.09%	36.06%

APPENDIX D
RHODOCROSITE X-RAY IMAGES

Rhodocrosite X-ray Images

4mm Fragment 1

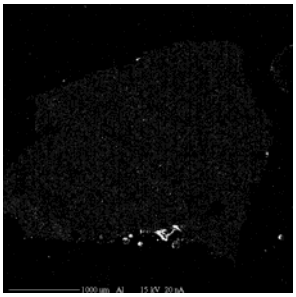

Rhodochrosite 4mm Al

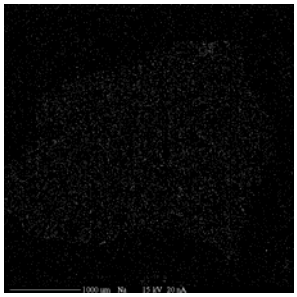

Rhodochrosite 4mm Na

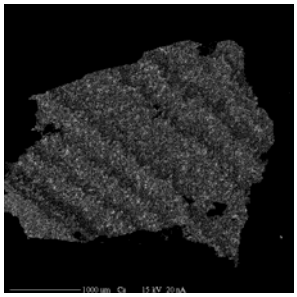

Rhodochrosite 4mm Ca

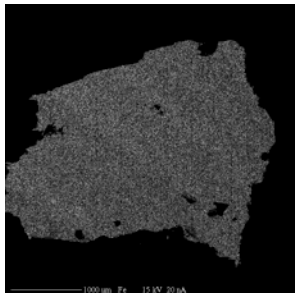

Rhodochrosite 4mm Fe

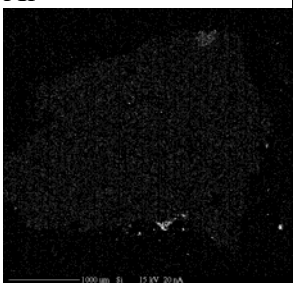

Rhodochrosite 4mm Si

Rhodochrosite 4mm K

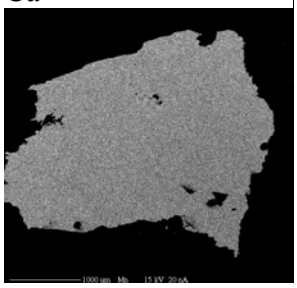

Rhodochrosite 4mm Mn

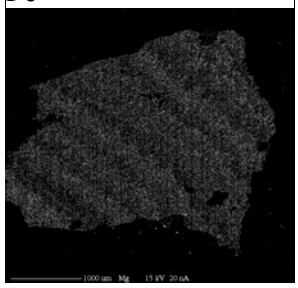

Rhodochrosite 4mm Mg

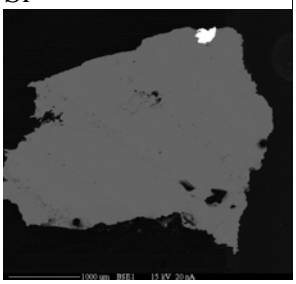

Rhodochrosite 4mm BSE

4mm Fragment 2

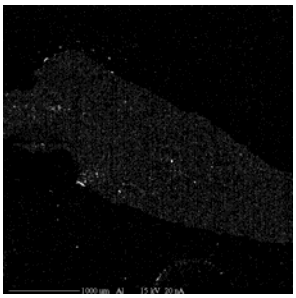

Rhodochrosite 4mm Al

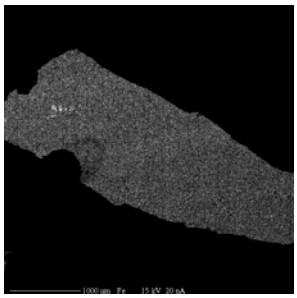

Rhodochrosite 4mm Fe

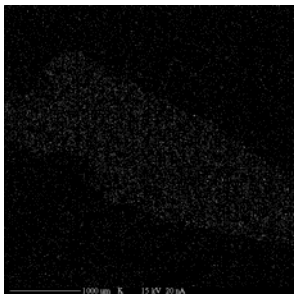

Rhodochrosite 4mm K

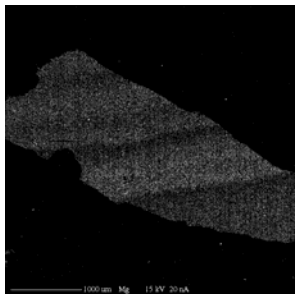

RHODOCHROSITE 4mm

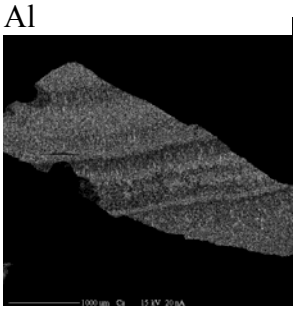

Rhodochrosite 4mm Ca

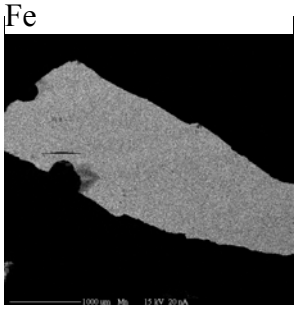

Rhodochrosite 4mm Mn

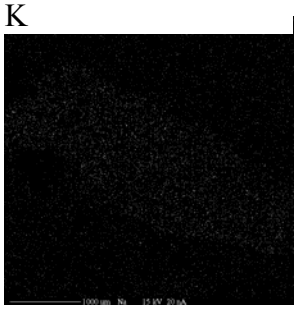

Rhodochrosite 4mm Na

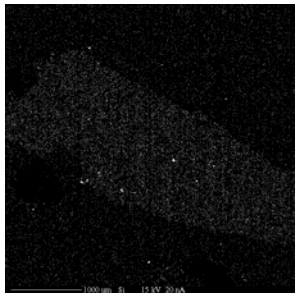

Rhodochrosite 4mm Si

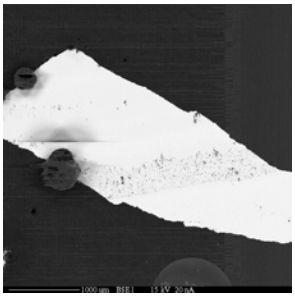

Rhodochrosite 4mm BSE

4mm Fragment 3

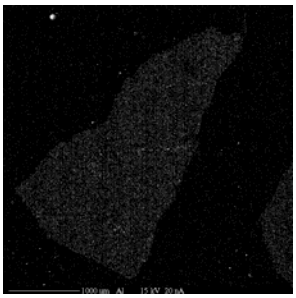

Rhodochrosite 4mm Al

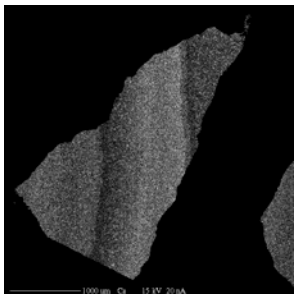

Rhodochrosite 4mm Ca

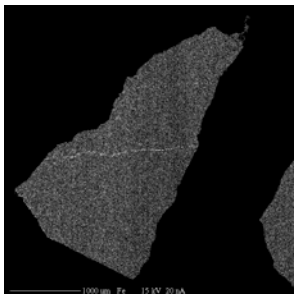

Rhodochrosite 4mm Fe

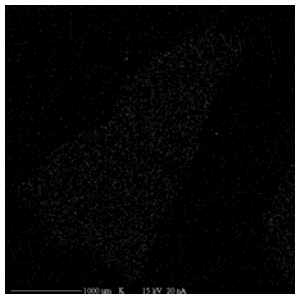

Rhodochrosite 4mm K

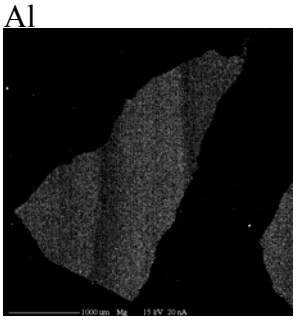

Rhodochrosite 4mm Mg

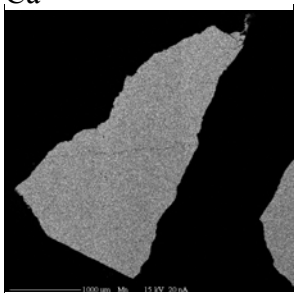

Rhodochrosite 4mm Mn

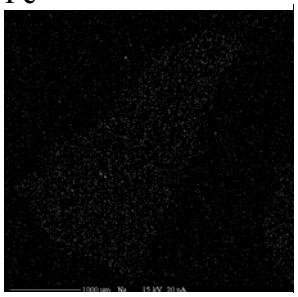

Rhodochrosite 4mm Na

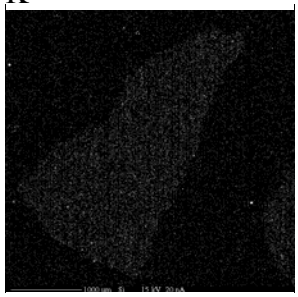

Rhodochrosite 4mm Si

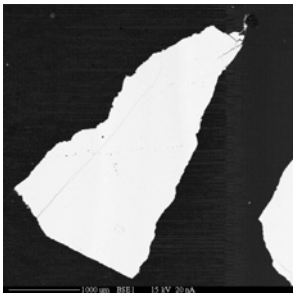

Rhodochrosite 4mm BSE

4mm Fragment 4

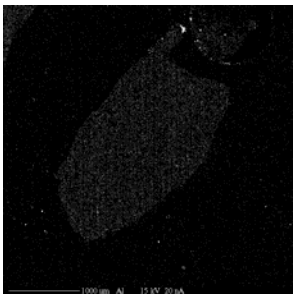

Rhodochrosite 4mm Al

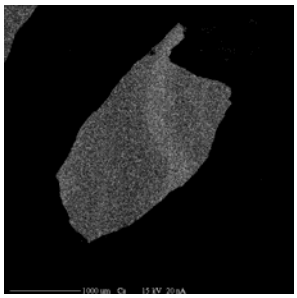

Rhodochrosite 4mm Ca

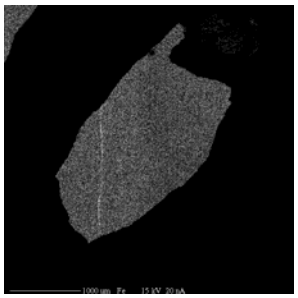

Rhodochrosite 4mm Fe

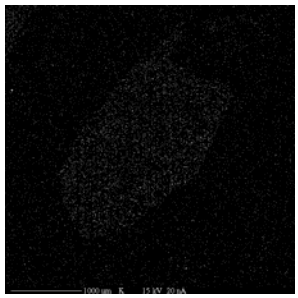

Rhodochrosite 4mm K

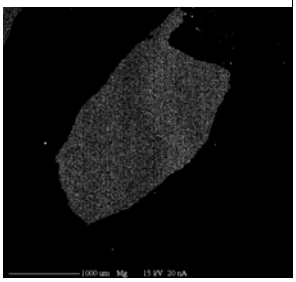

Rhodochrosite 4mm Mg

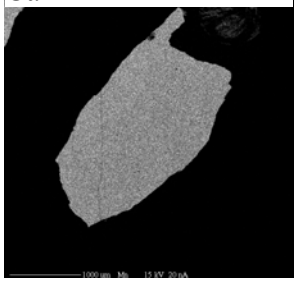

Rhodochrosite 4mm Mn

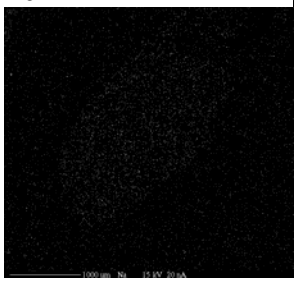

Rhodochrosite 4mm Na

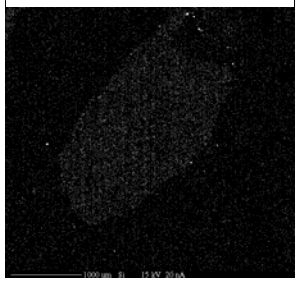

Rhodochrosite 4mm Si

Rhodochrosite 4mm BSE

4mm Fragment 5

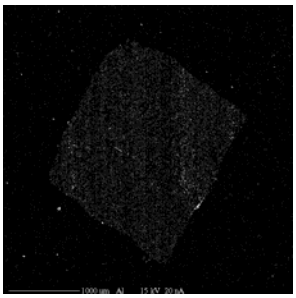

Rhodochrosite 4mm Al

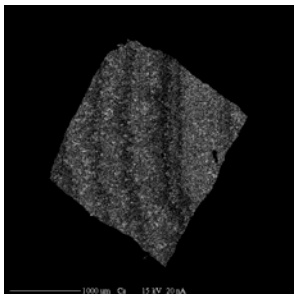

Rhodochrosite 4mm Ca

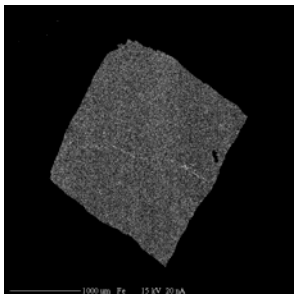

Rhodochrosite 4mm Fe

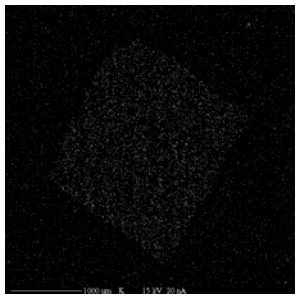

Rhodochrosite 4mm K

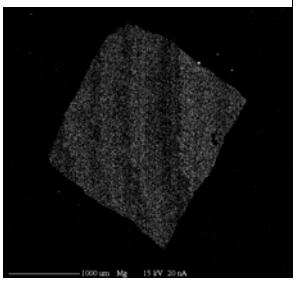

Rhodochrosite 4mm Mg

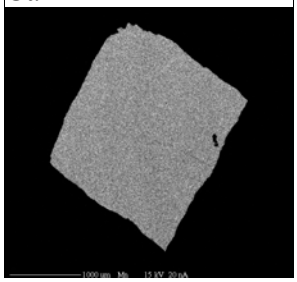

Rhodochrosite 4mm Mn

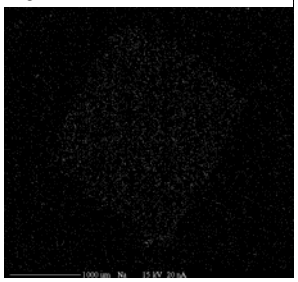

Rhodochrosite 4mm Na

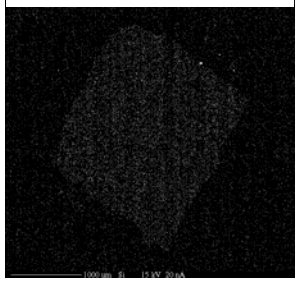

Rhodochrosite 4mm Si

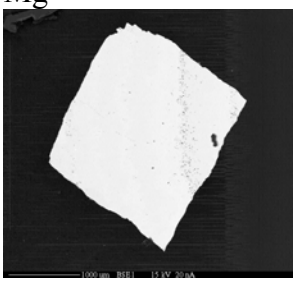

Rhodochrosite 4mm BSE

4mm Fragment 6

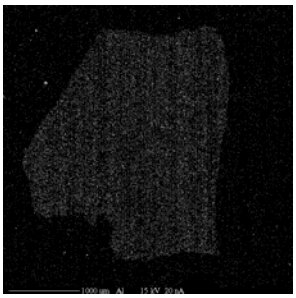

Rhodochrosite 4mm Al

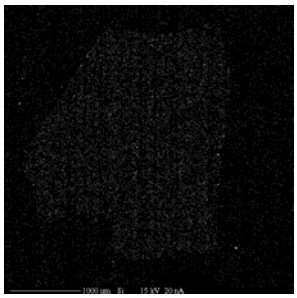

Rhodochrosite 4mm Si

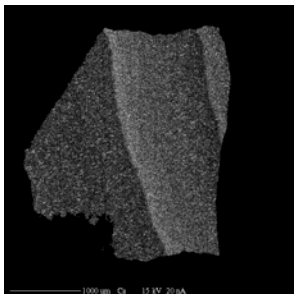

Rhodochrosite 4mm Ca

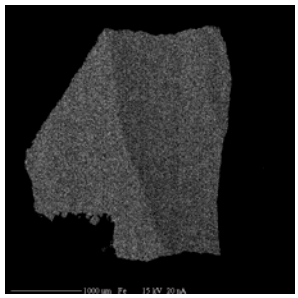

Rhodochrosite 4mm Fe

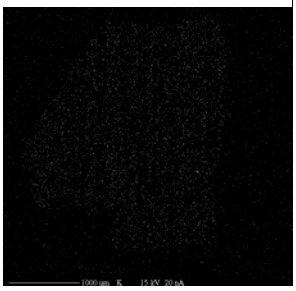

Rhodochrosite 4mm K

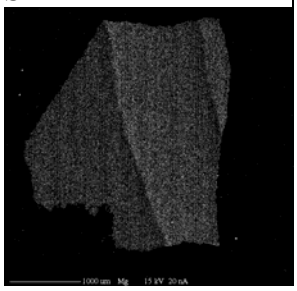

Rhodochrosite 4mm Mg

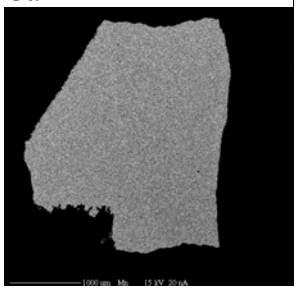

Rhodochrosite 4mm Mn

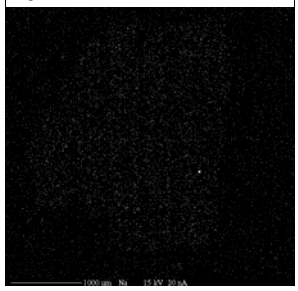

Rhodochrosite 4mm Na

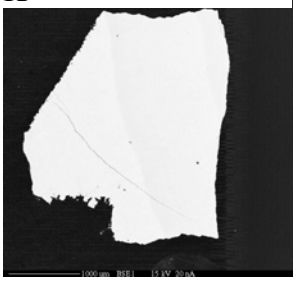

Rhodochrosite 4mm BSE

APPENDIX E

XPS PEAK RESULTS

Andesine XPS Peak Results

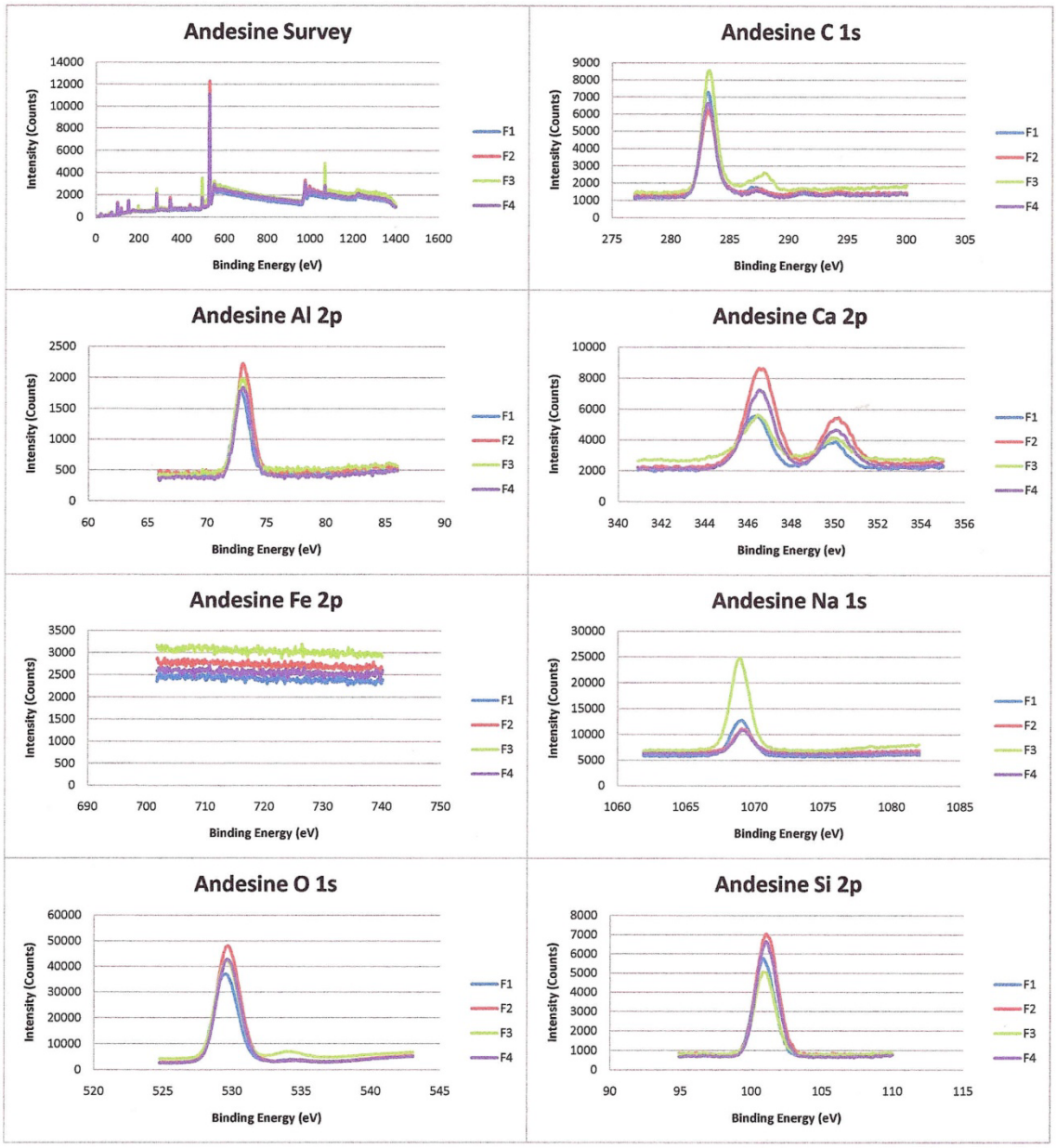

Albite XPS Peaks Results

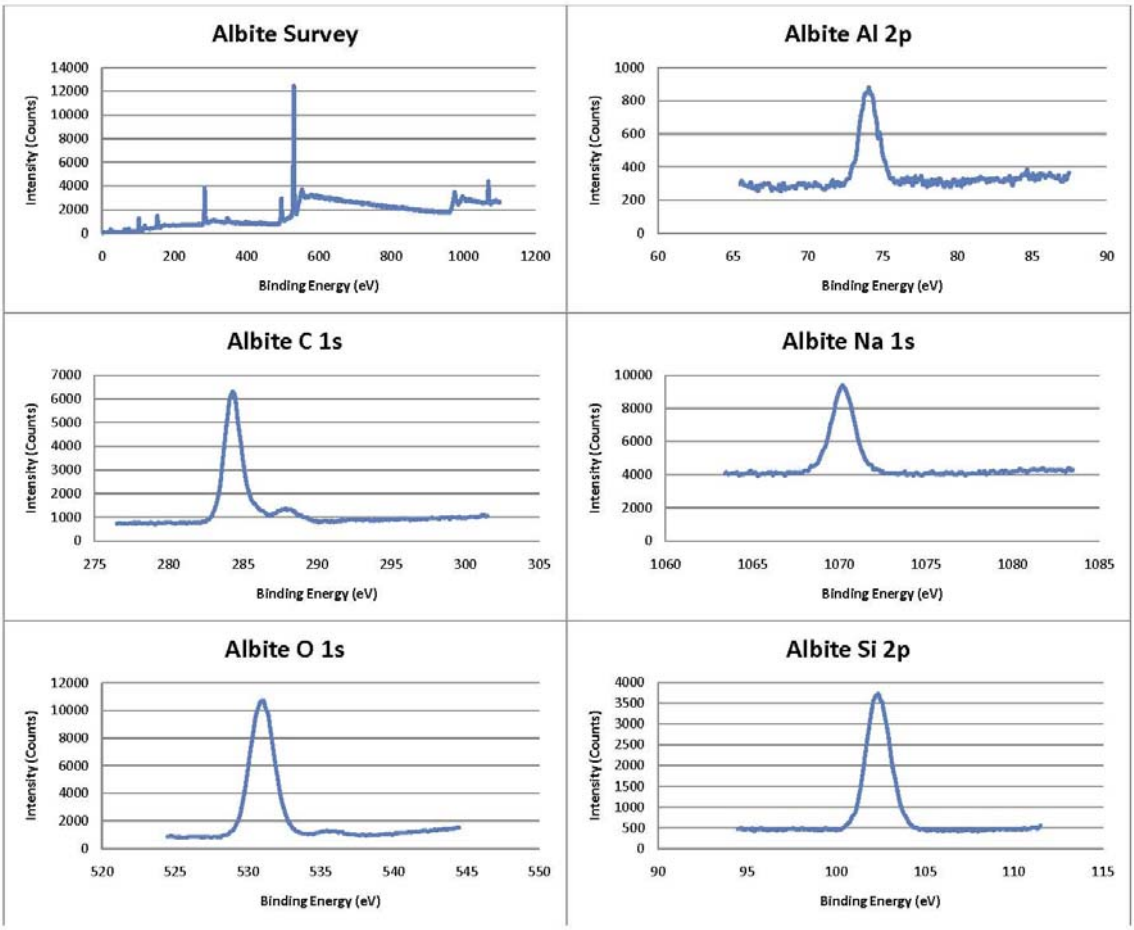

Augite XPS Peak Results

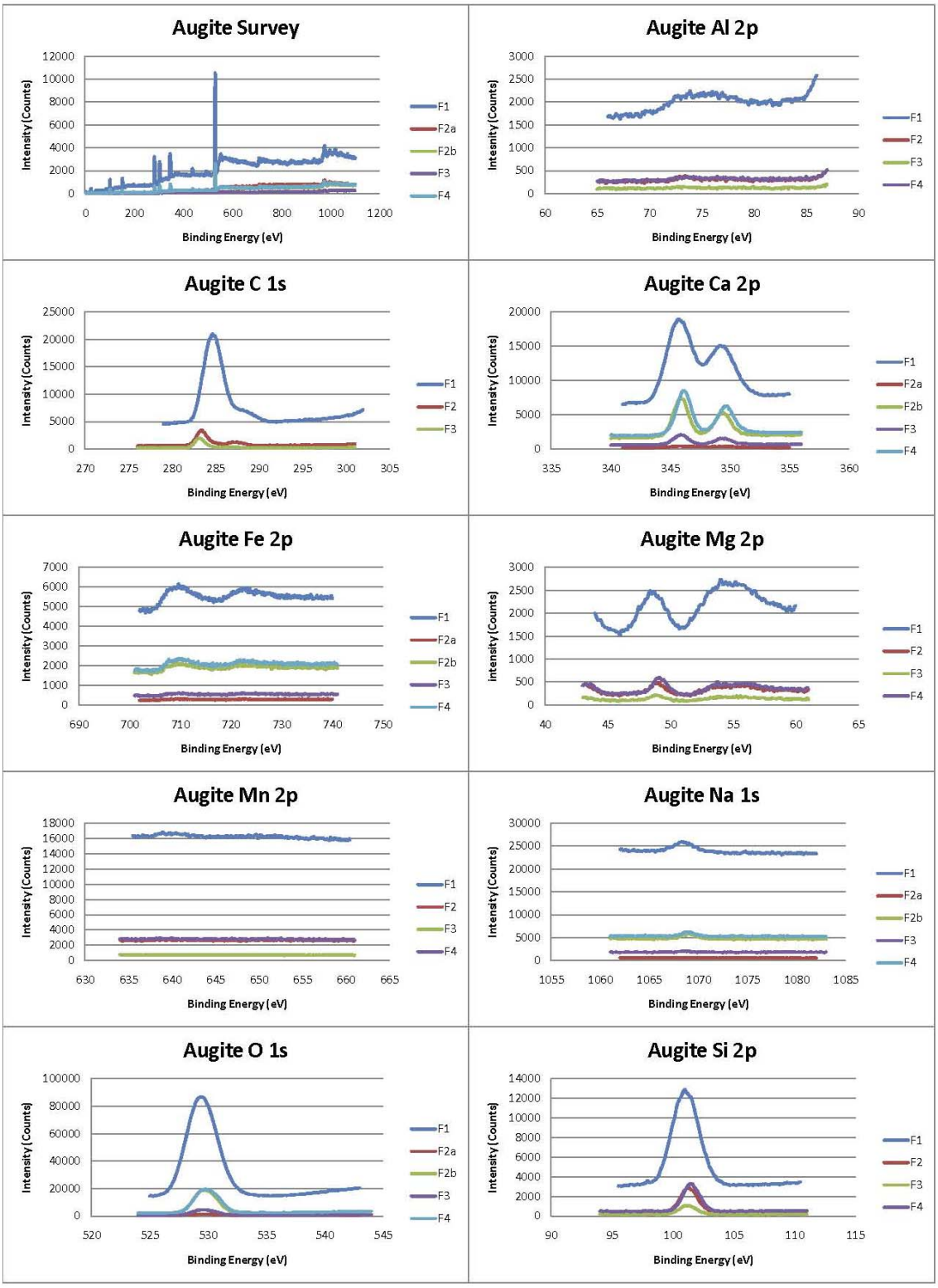

Bassanite XPS Peak Results

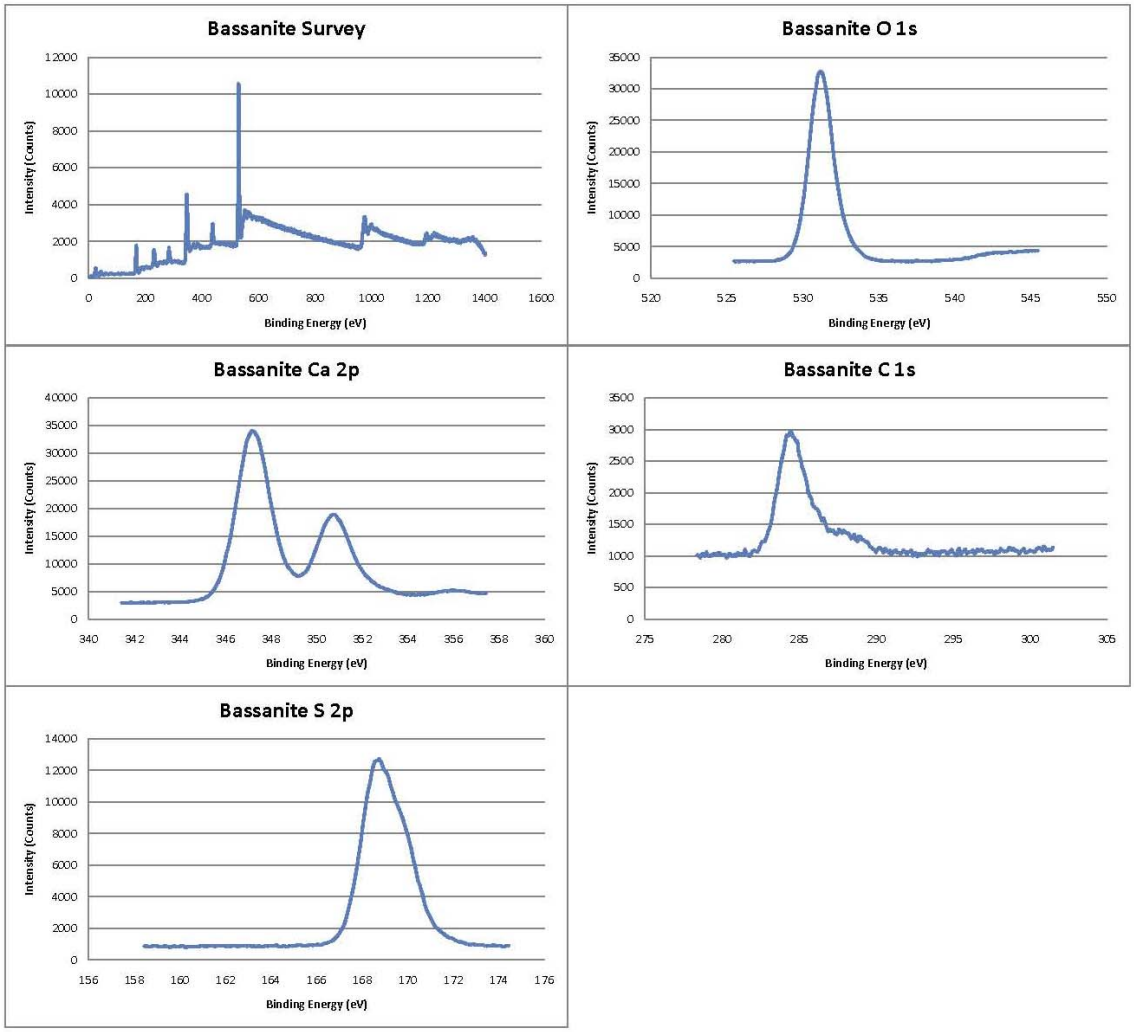

Biotite XPS Peak Results

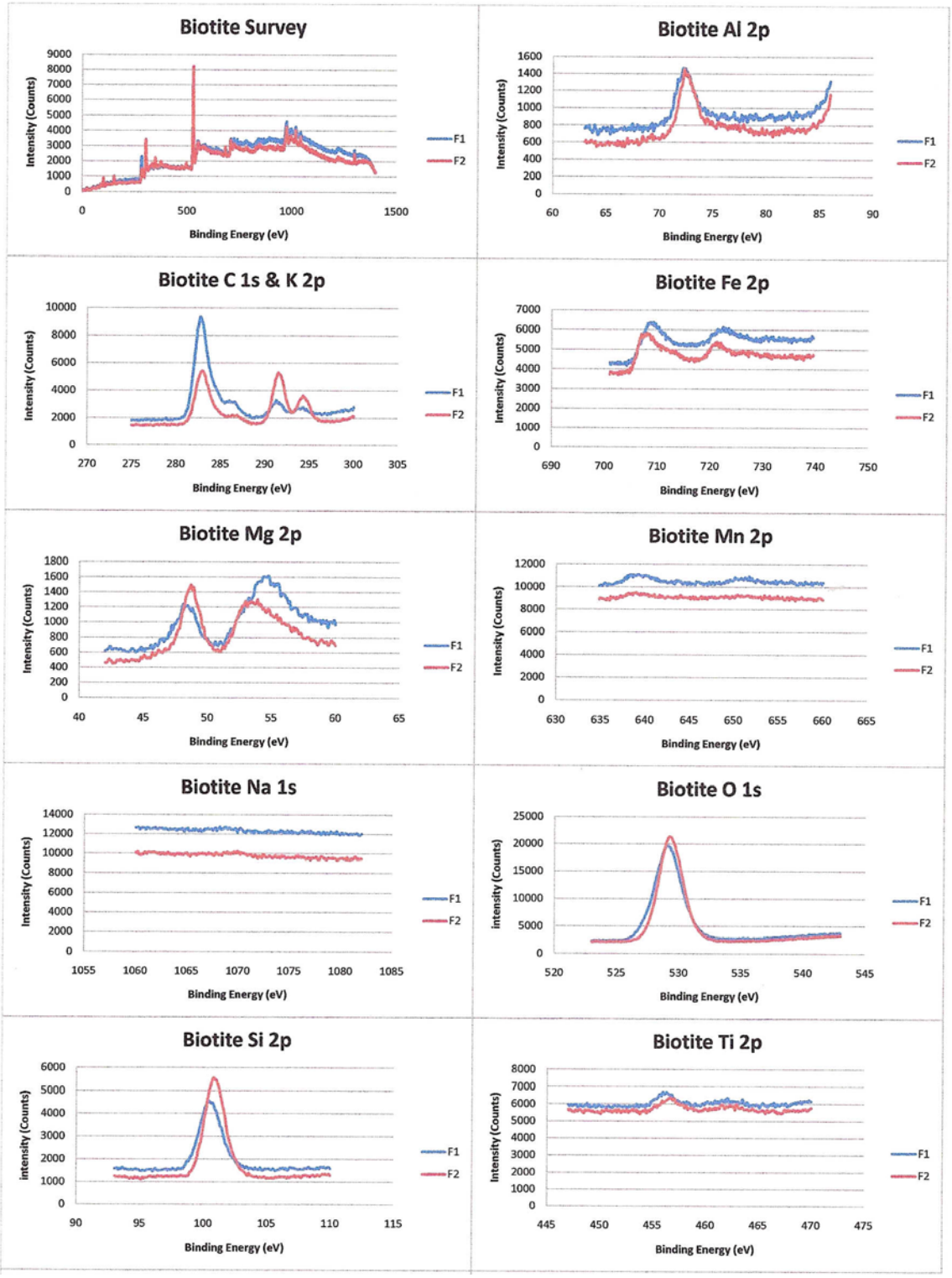

Biotite XPS Peaks Continued

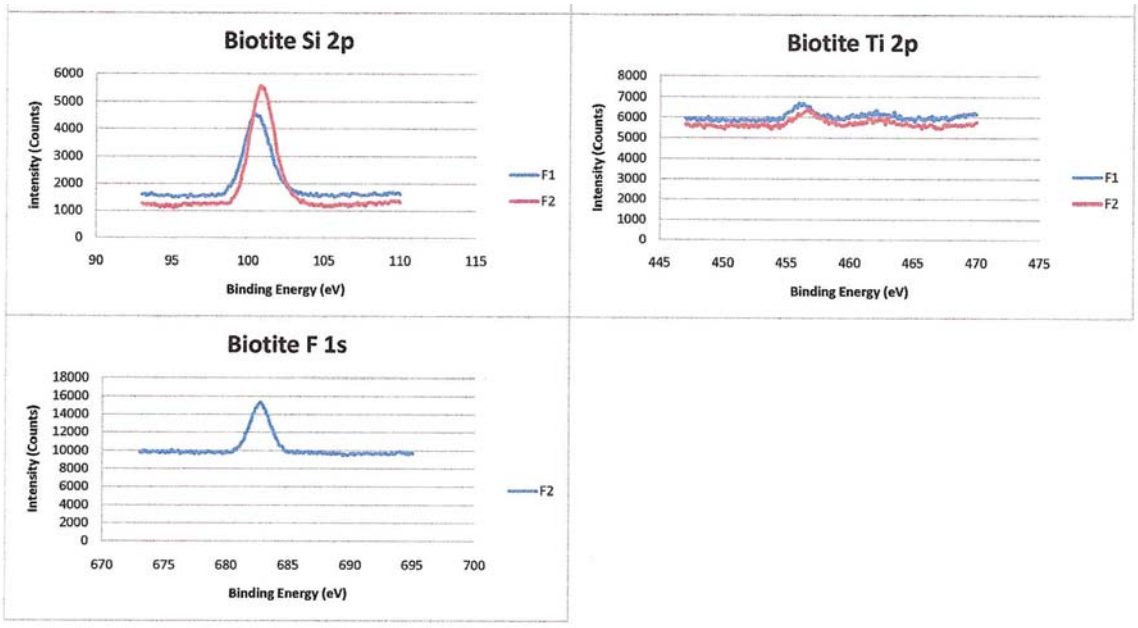

Calcite XPS Peak Results

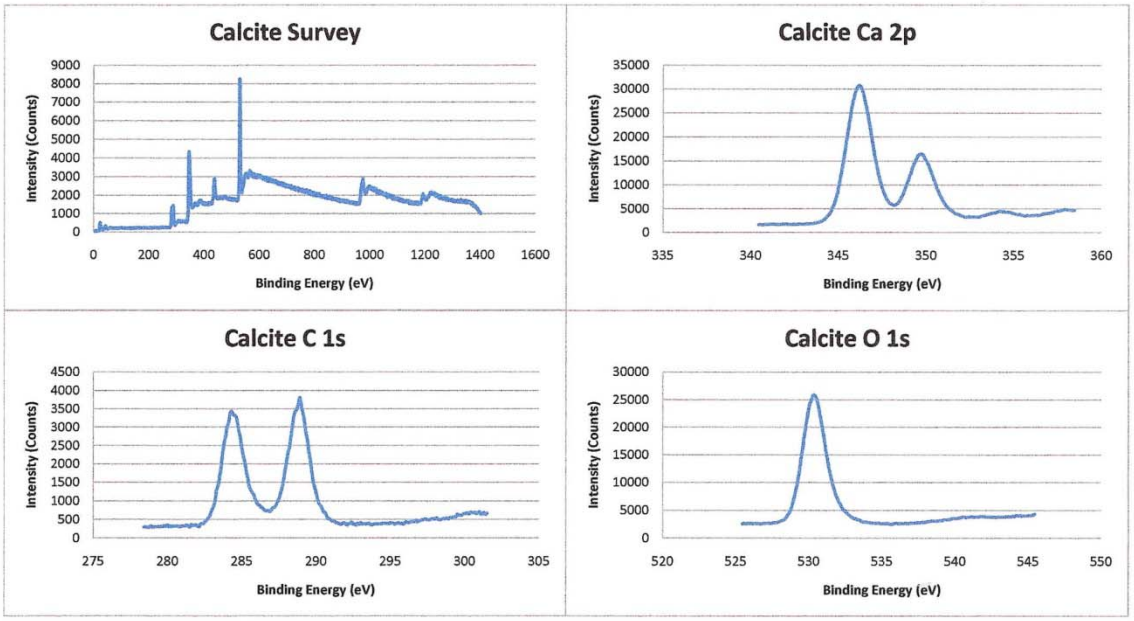

Cerussite XPS Peak Results

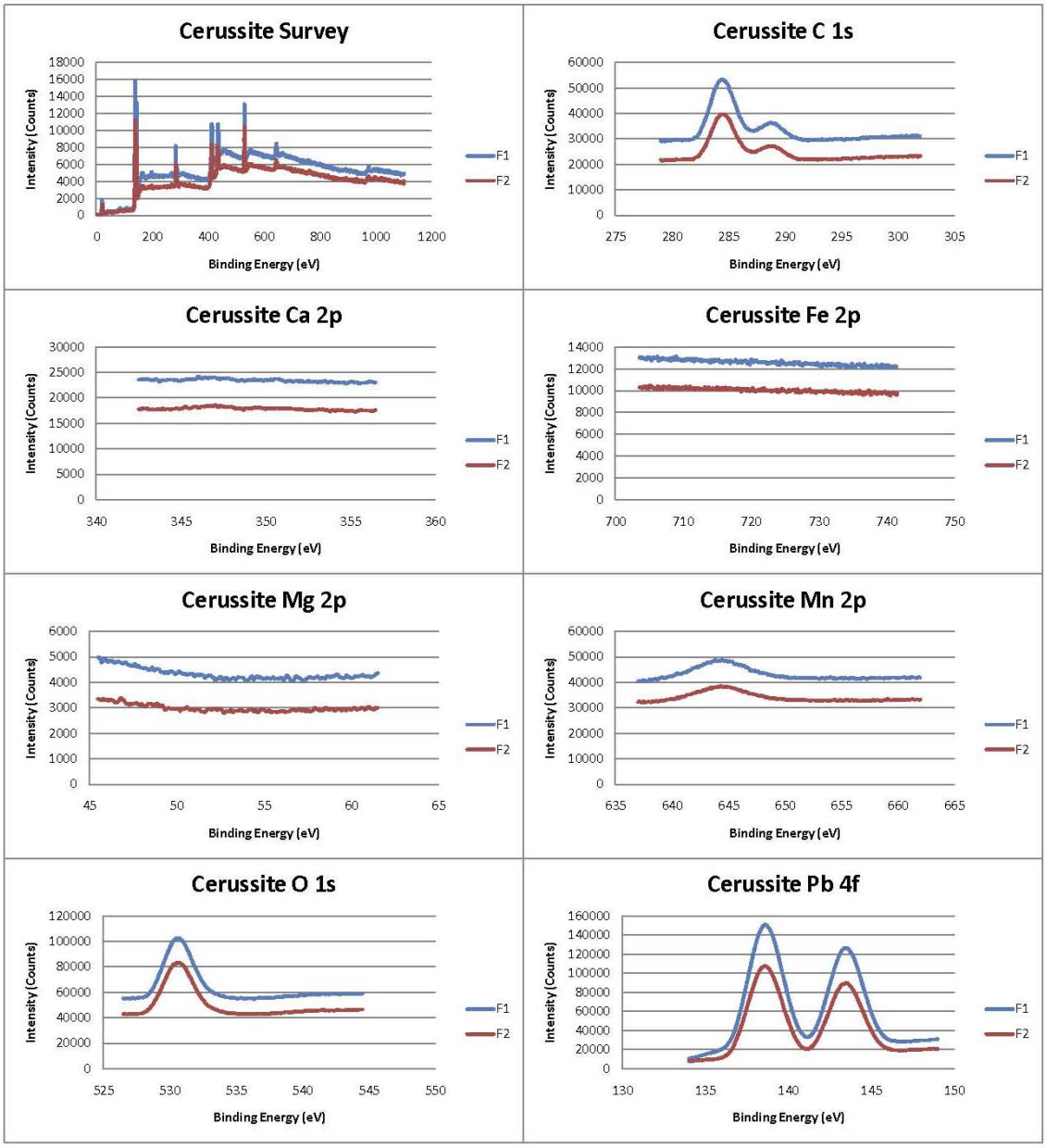

Dolomite XPS Peak Results

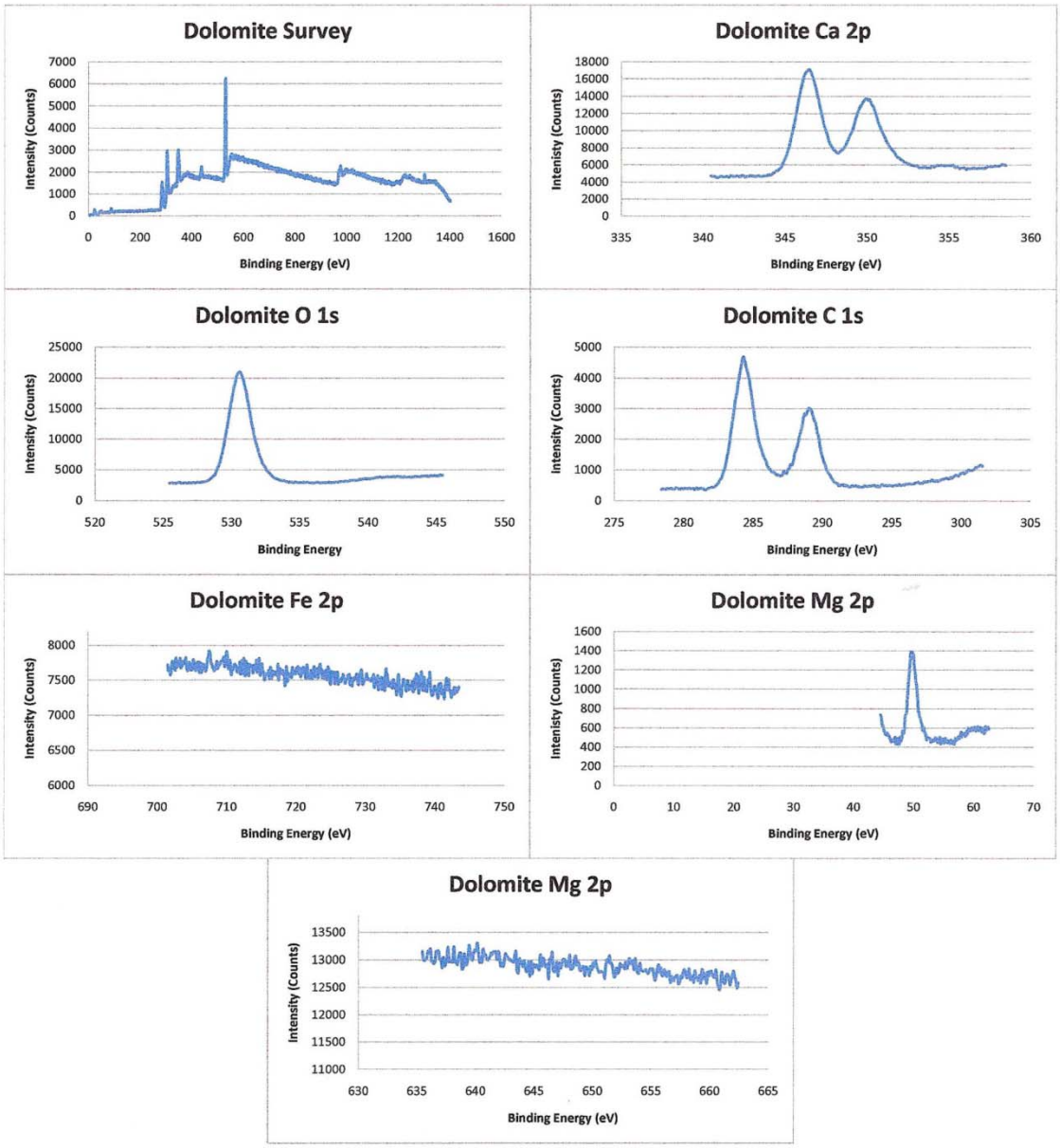

Gypsum XPS Peak Results

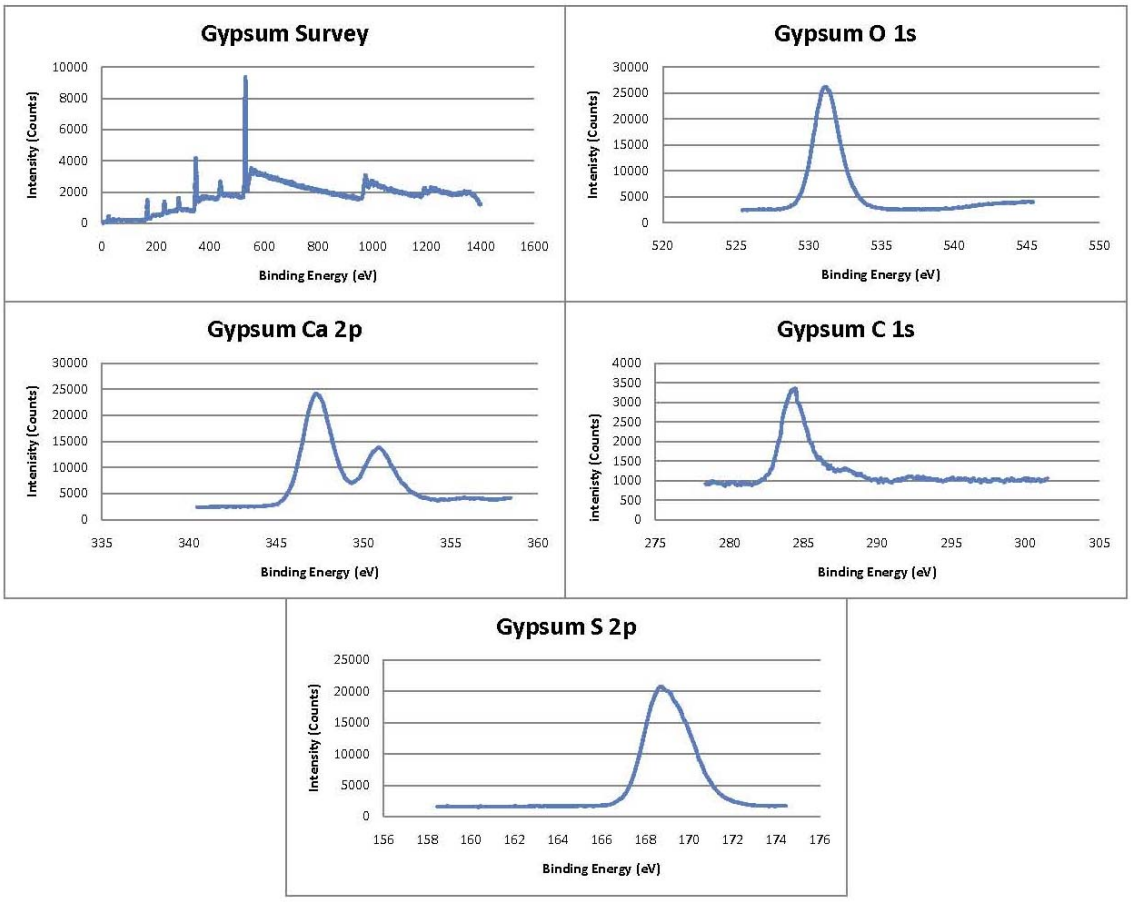

Hematite XPS Peak Results

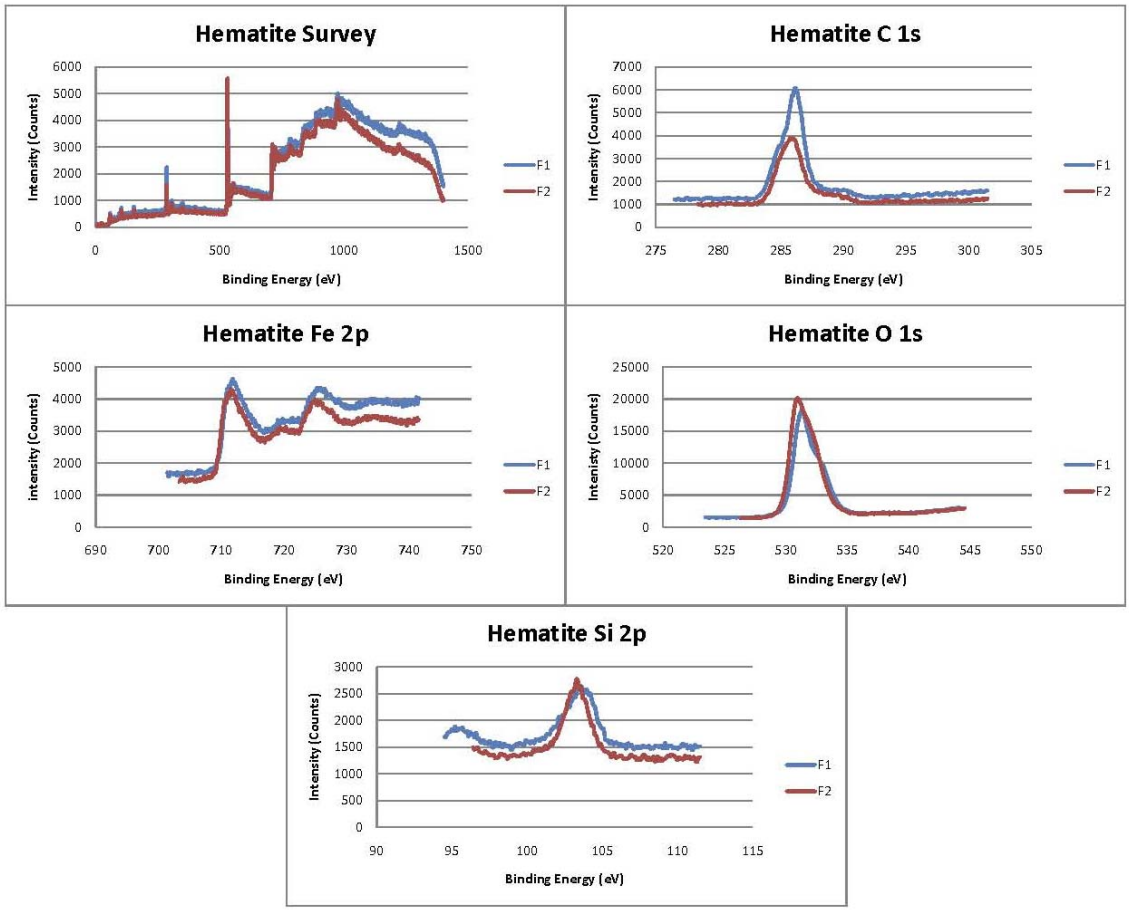

Hornblende XPS Peak Results

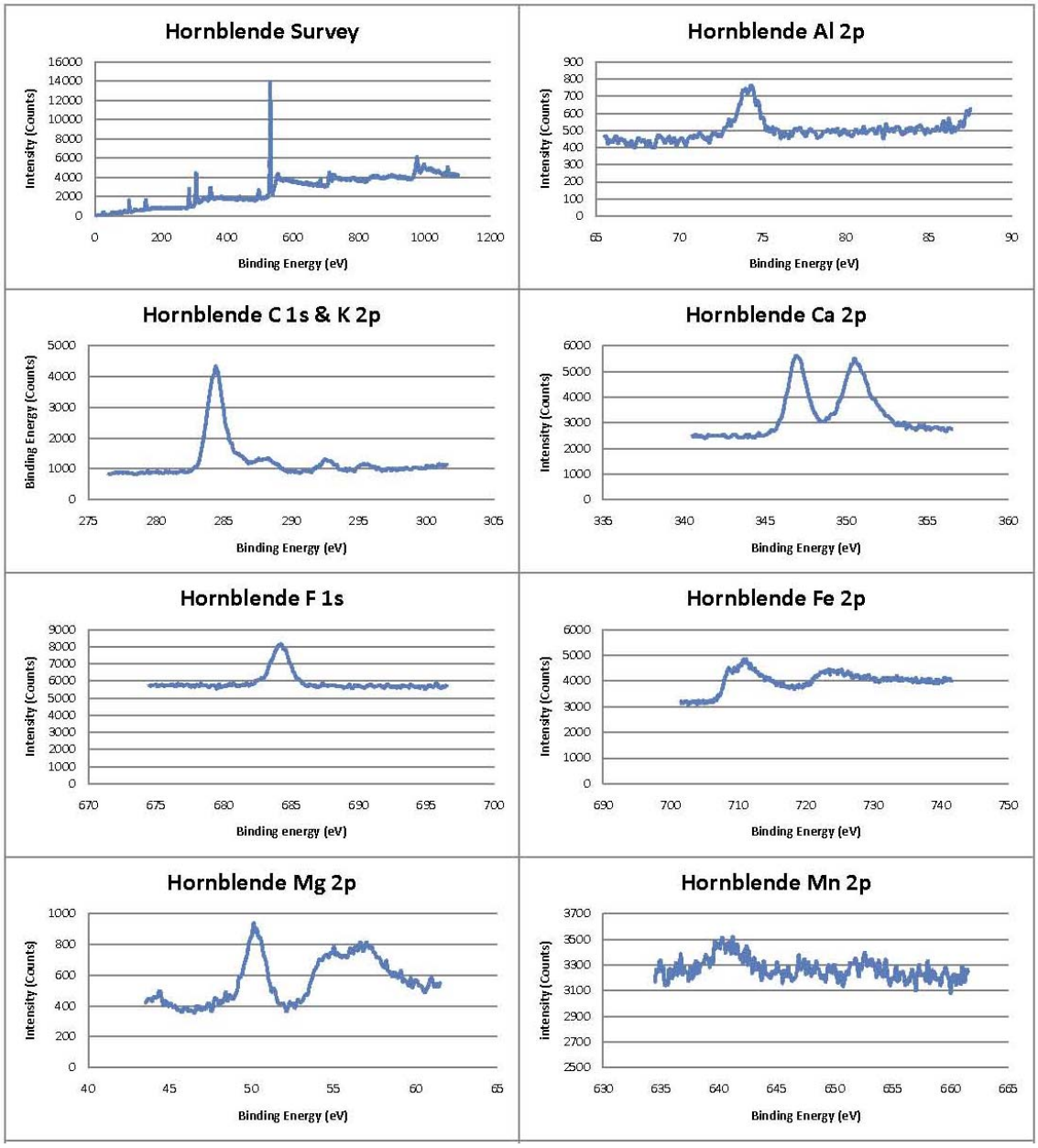

Hornblende XPS Peaks Continued

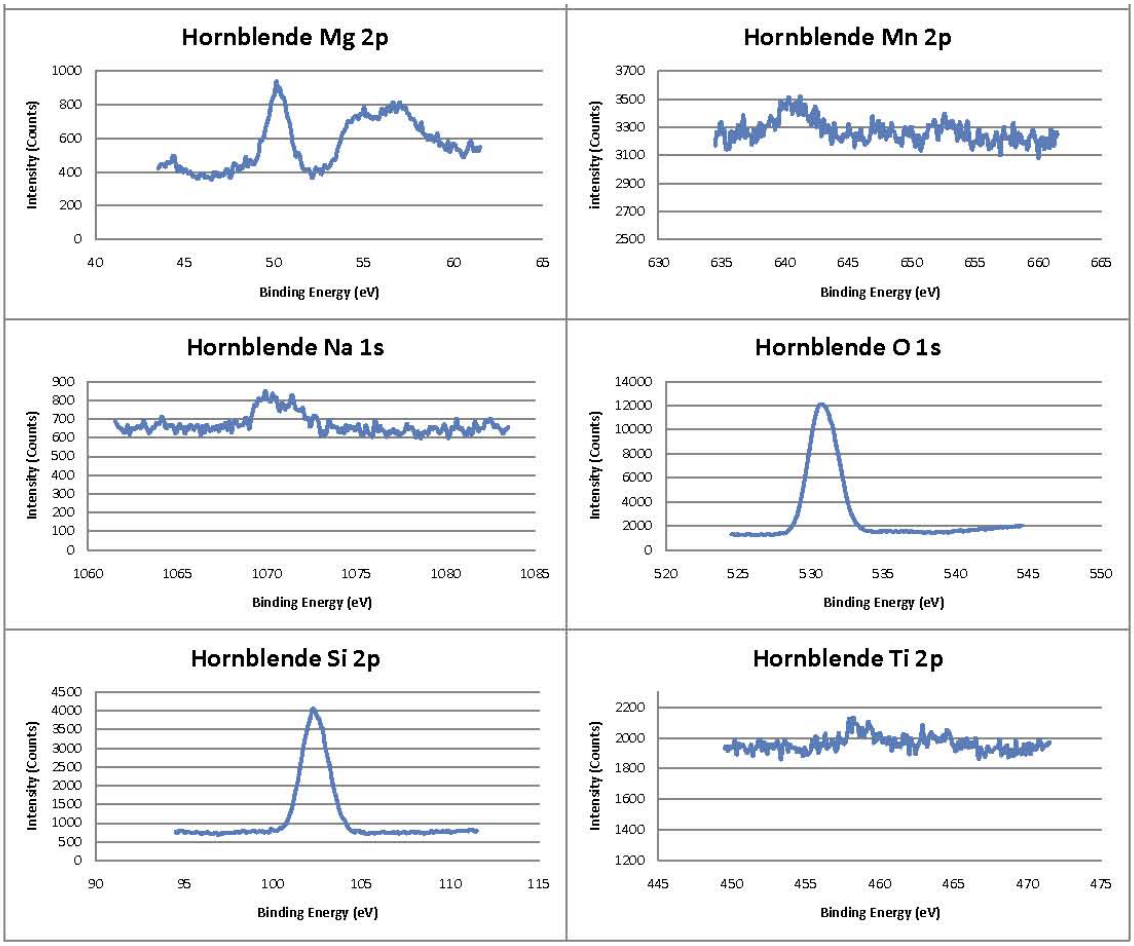

Ilmenite XPS Peak Results

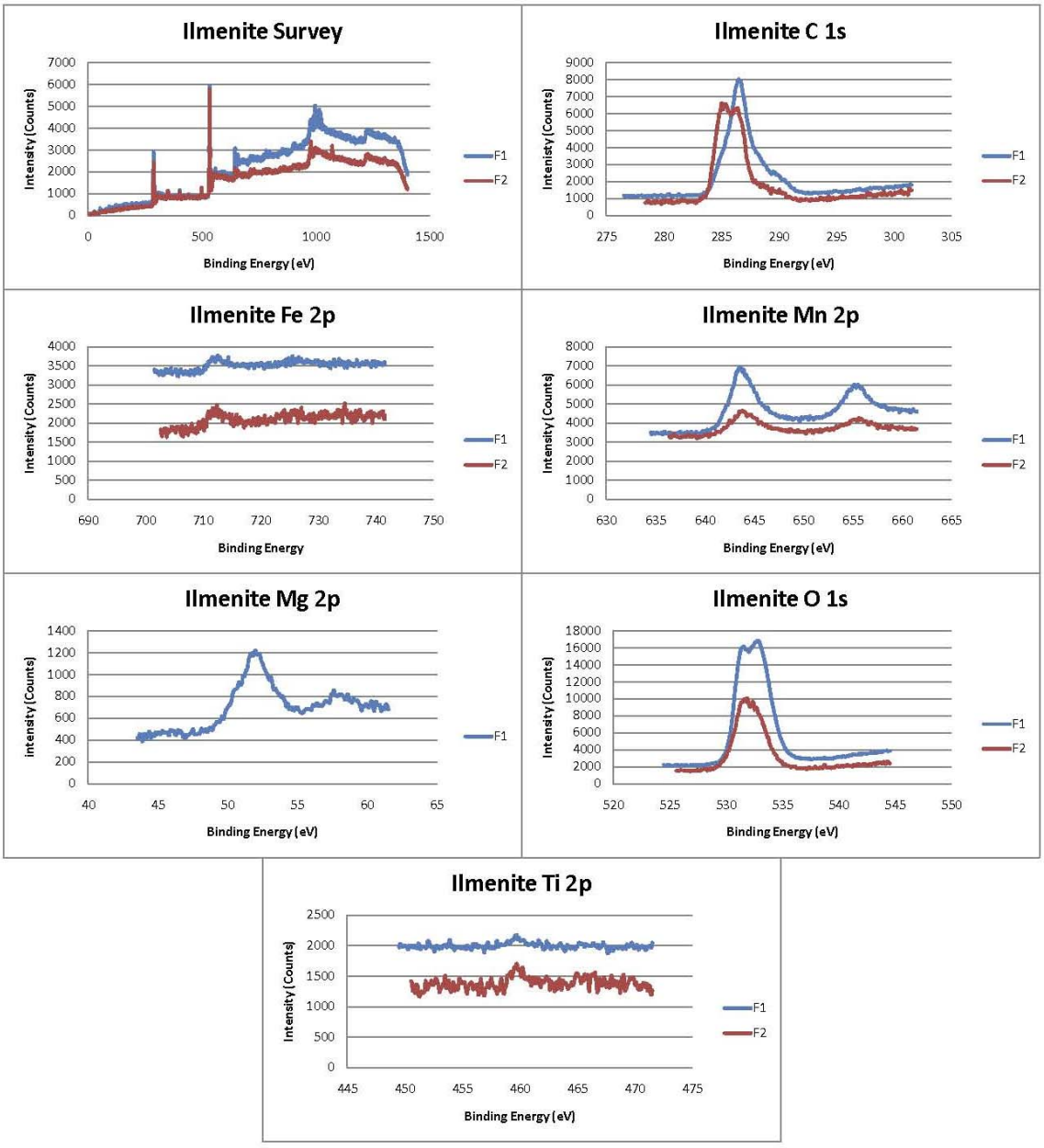

Kaolinite XPS Peak Results

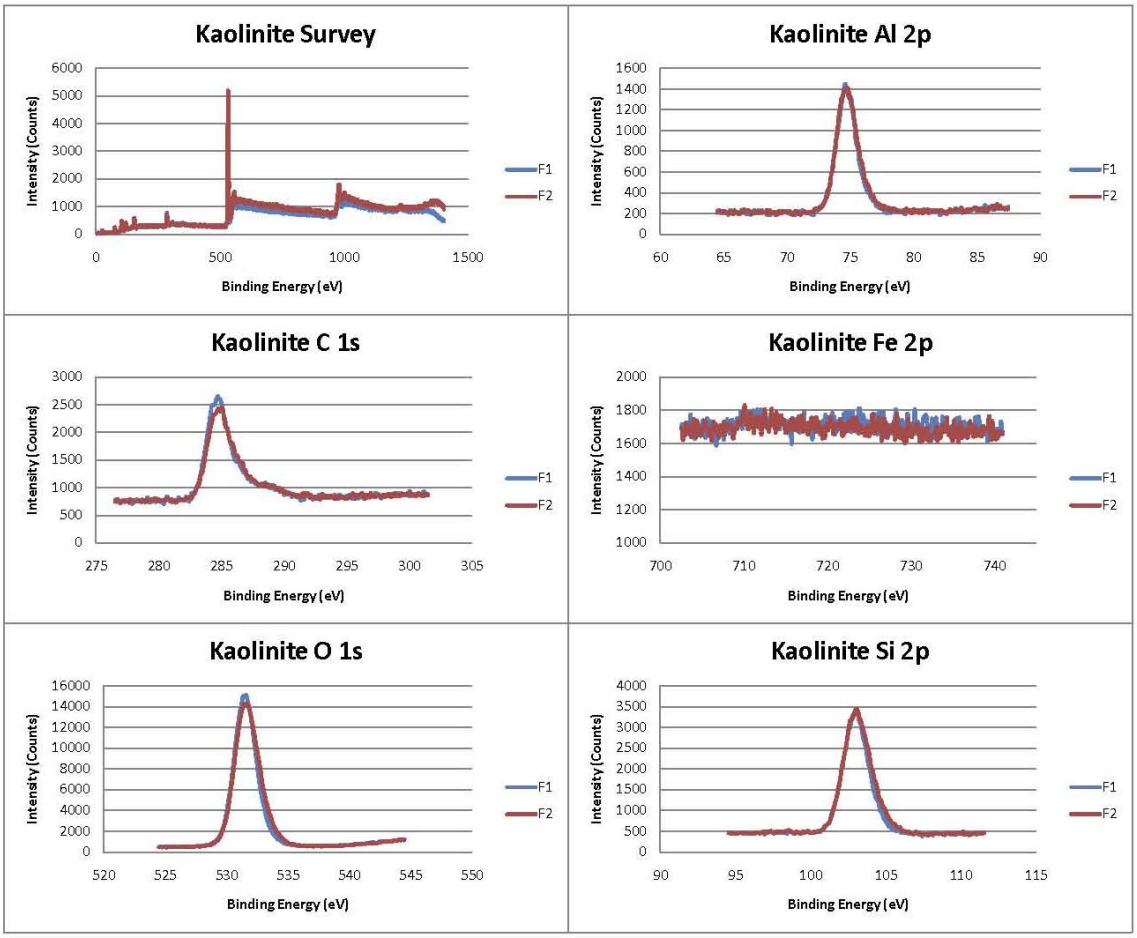

Labradorite XPS Peak Results

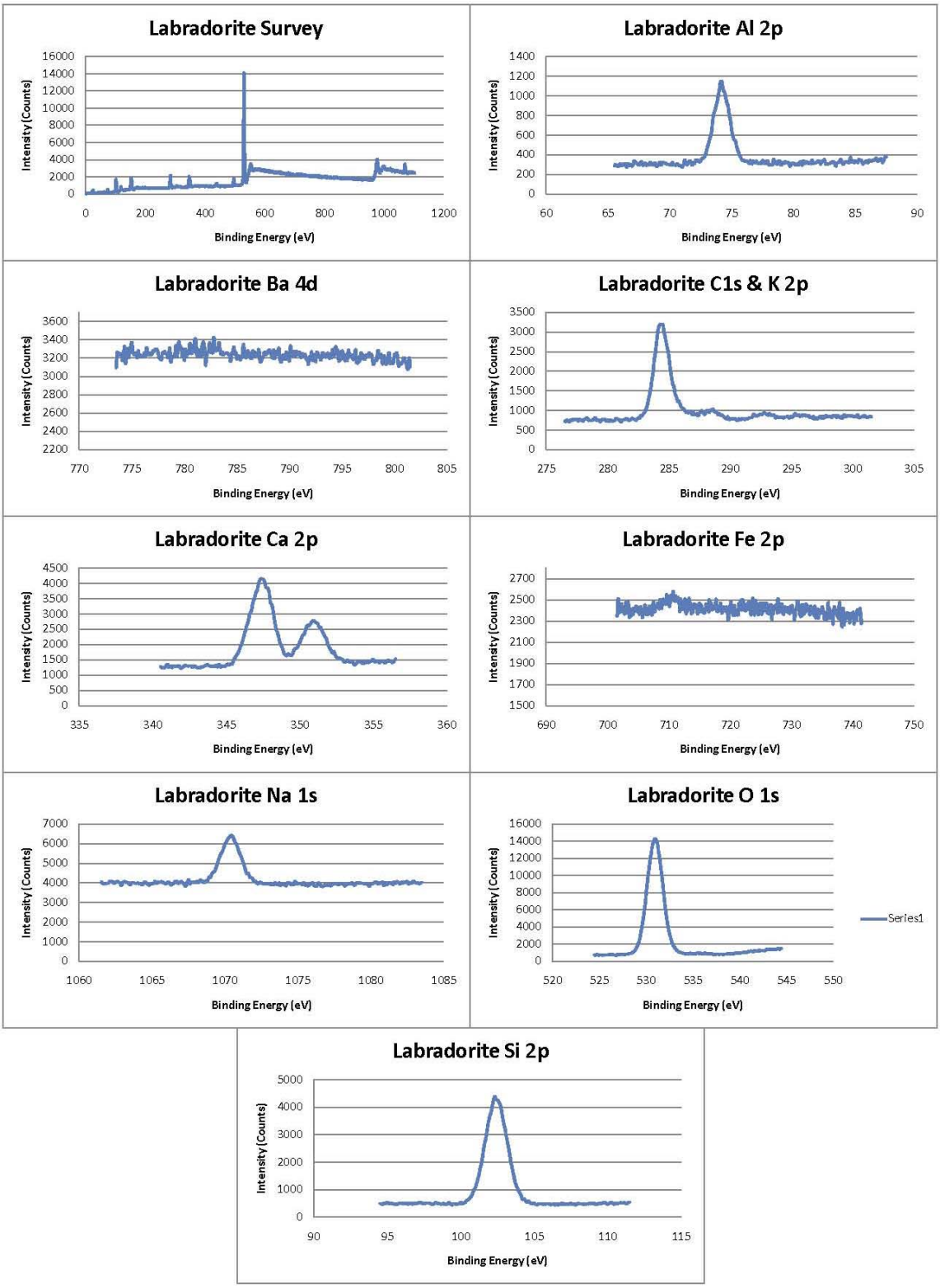

Microcline XPS Peak Results

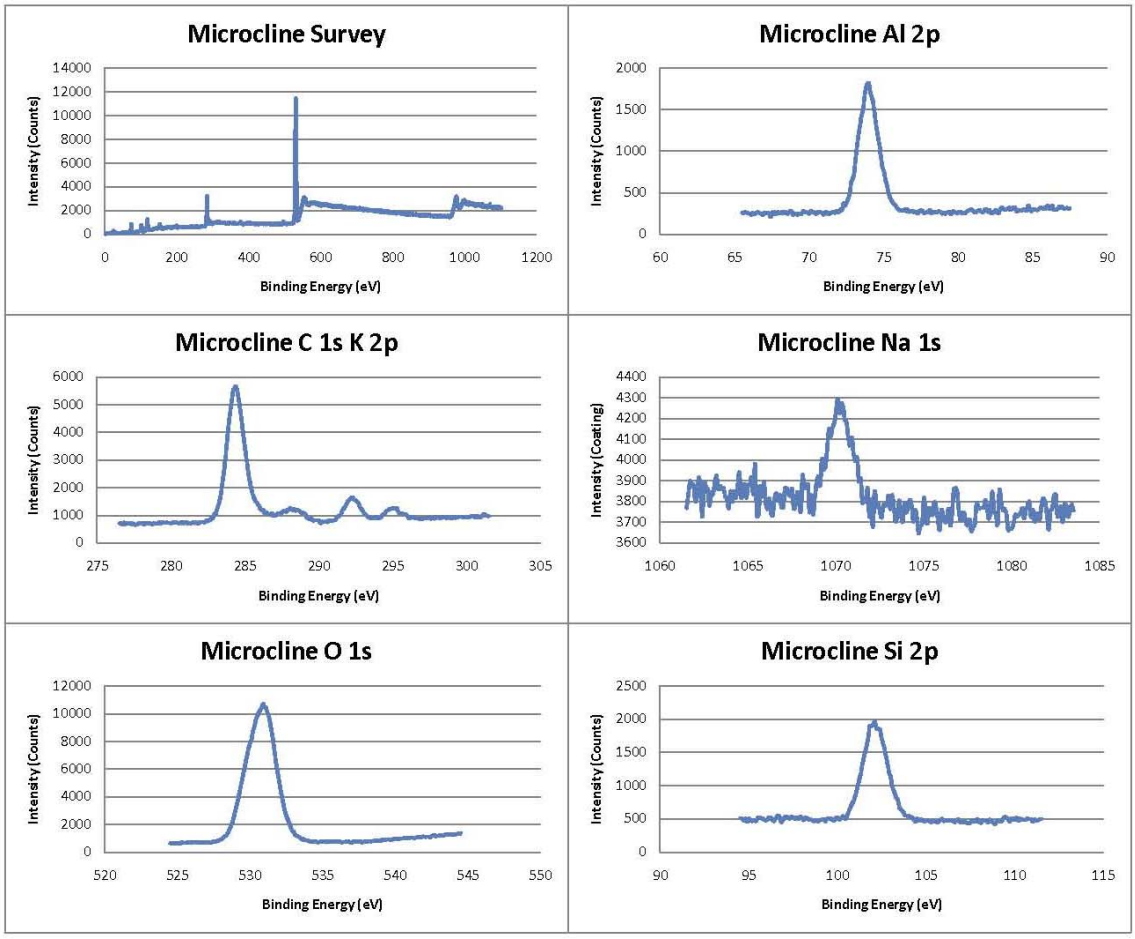

Montmorillonite XPS Peak Results

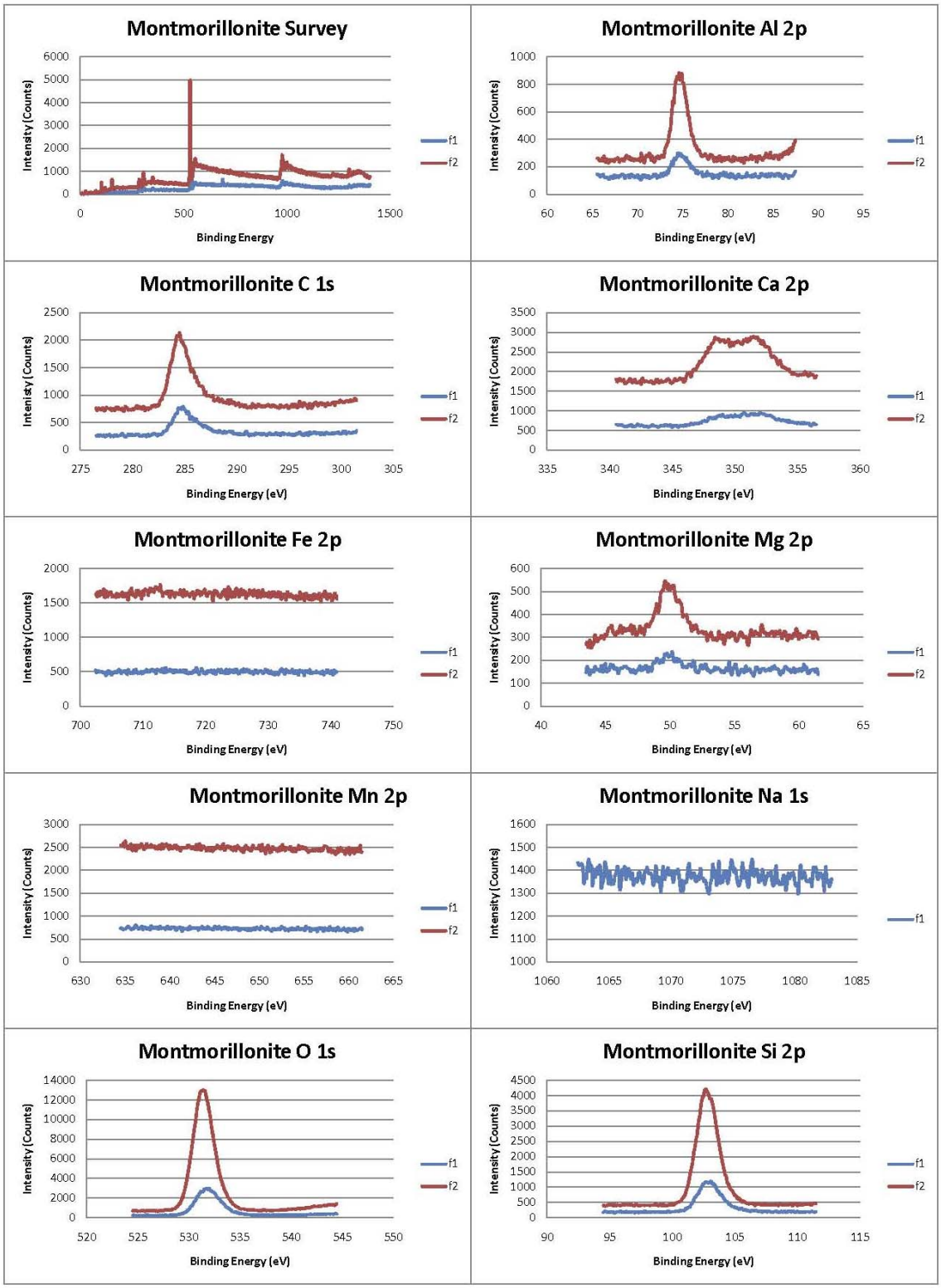

Muscovite XPS Peak Results

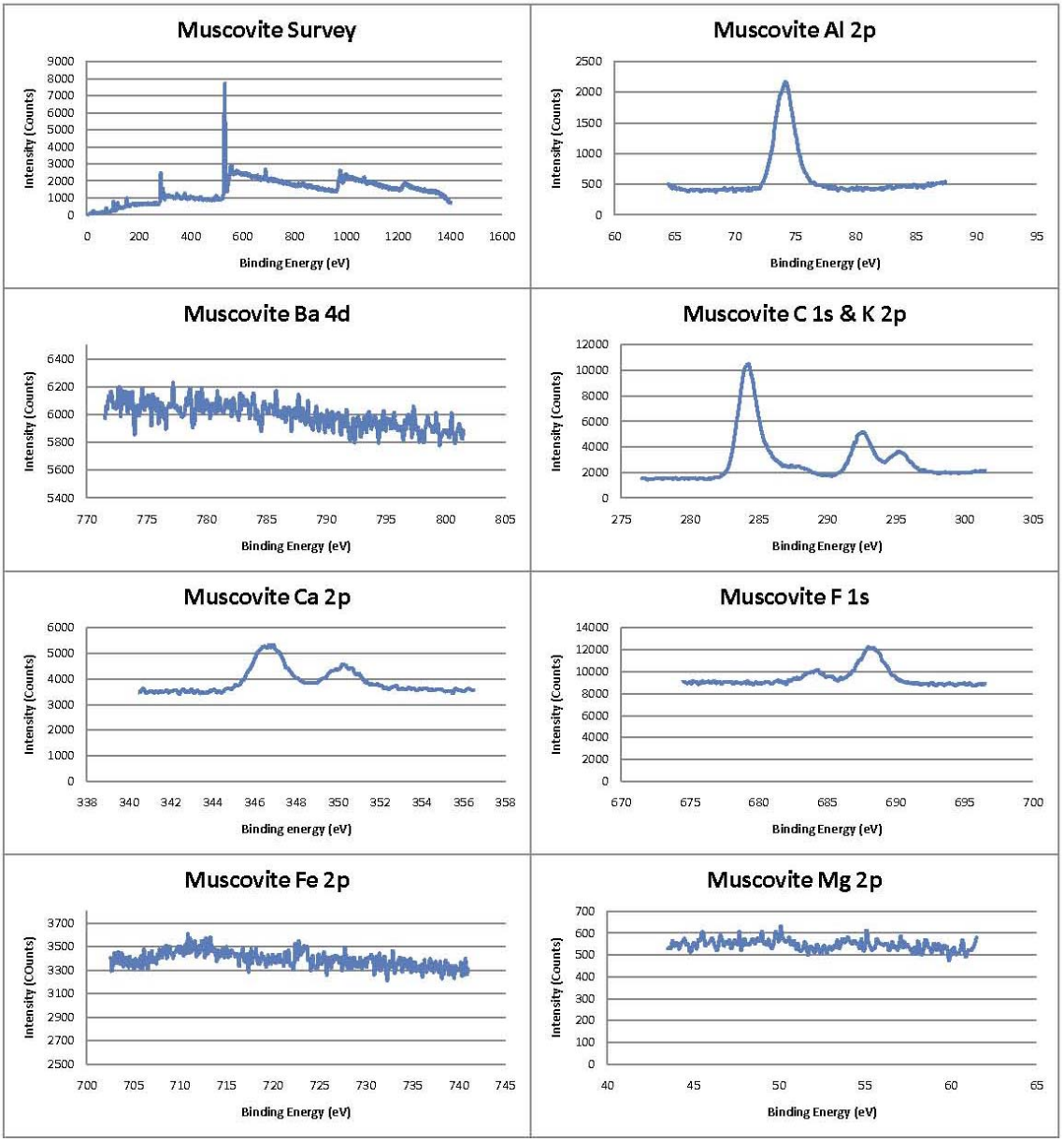

Muscovite XPS Peaks Continued

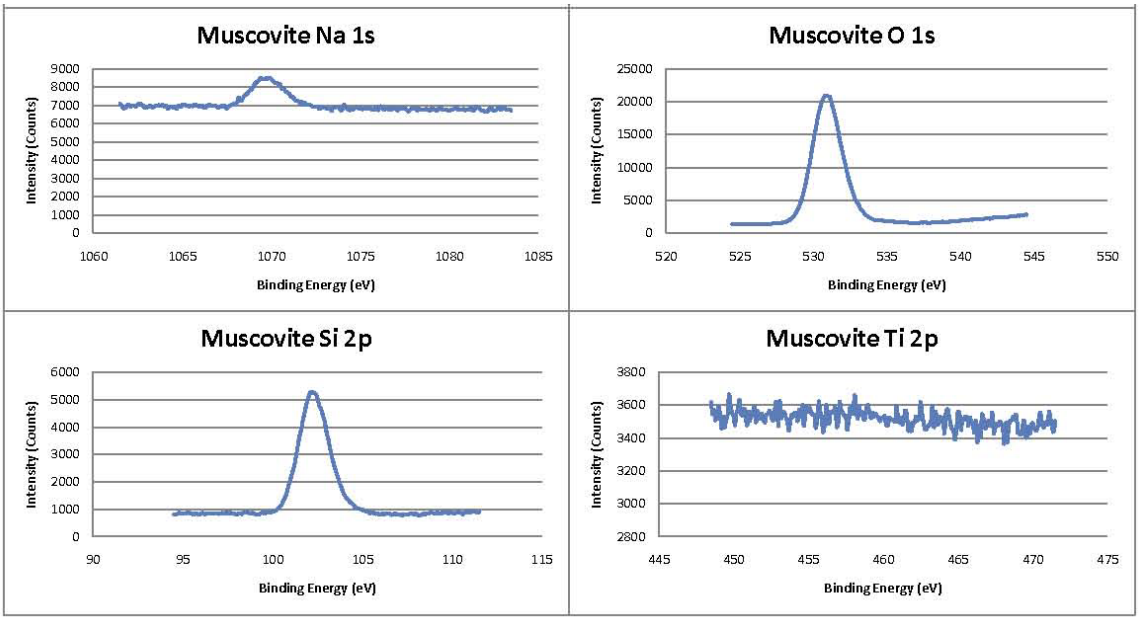

Olivine XPS Peak Results

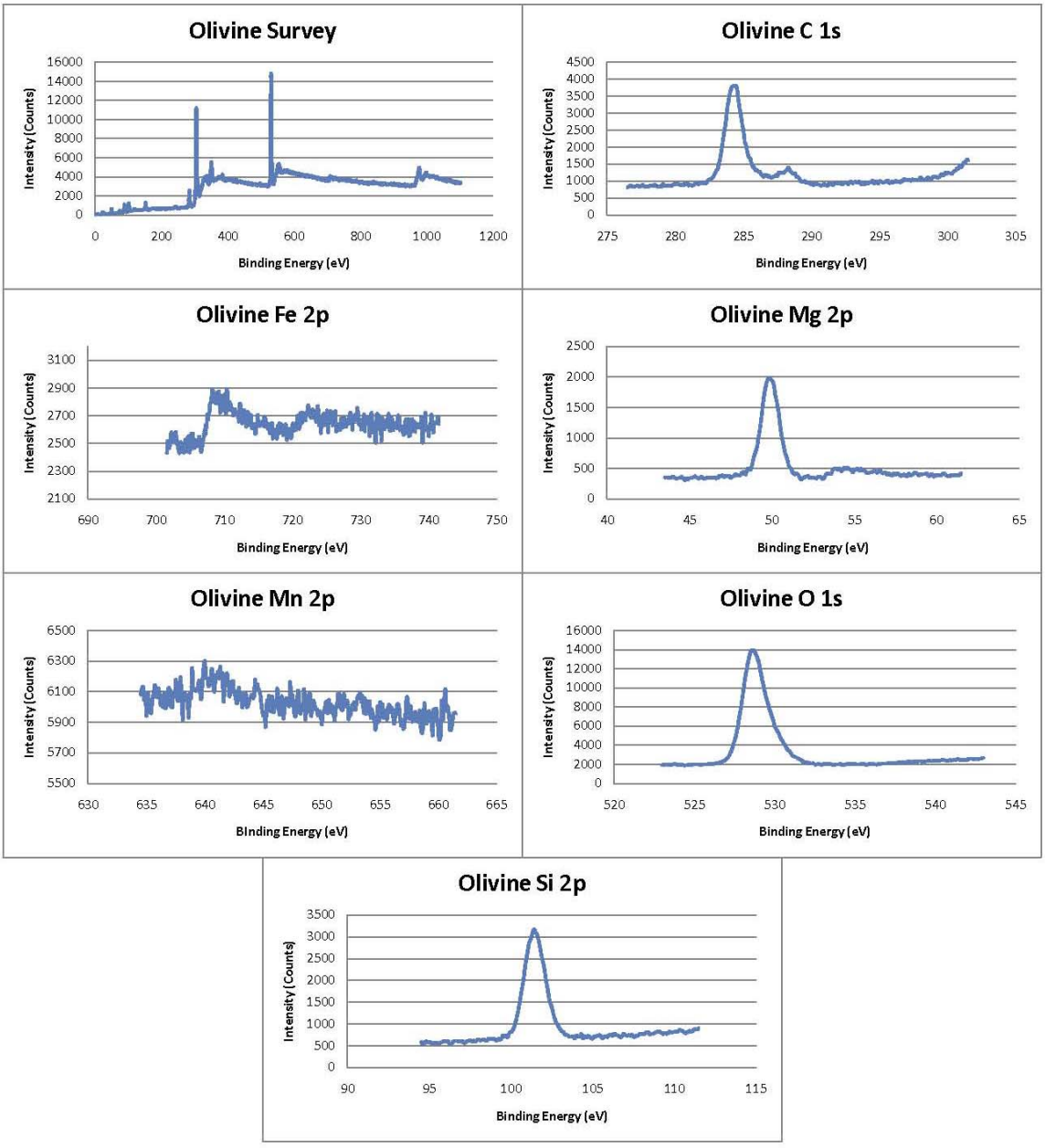

Quartz XPS Peak Results

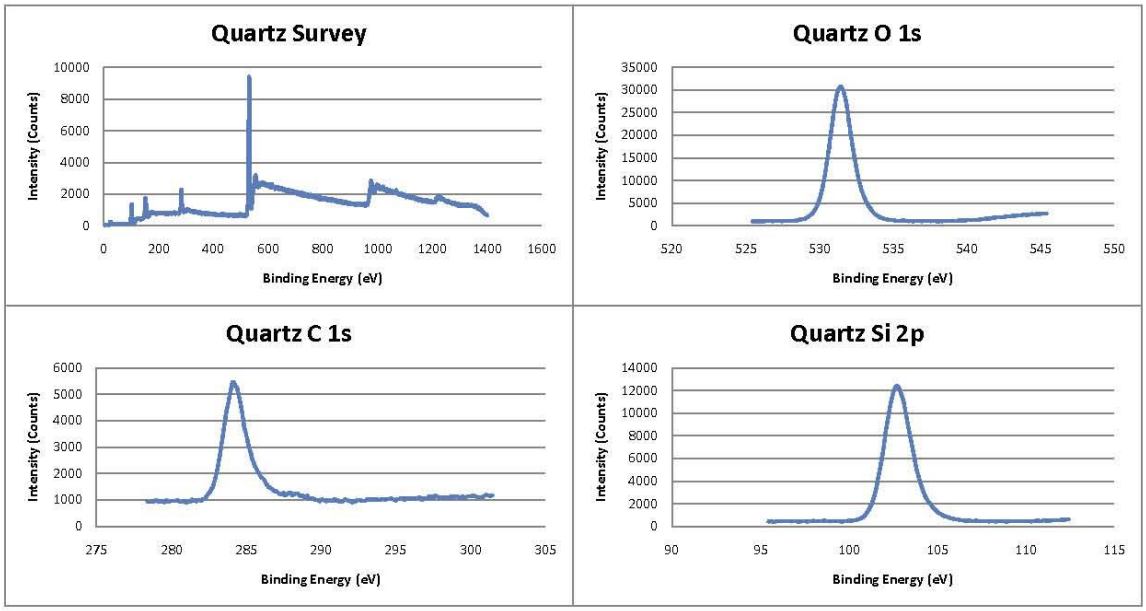

Rhodochrosite XPS Peak Results

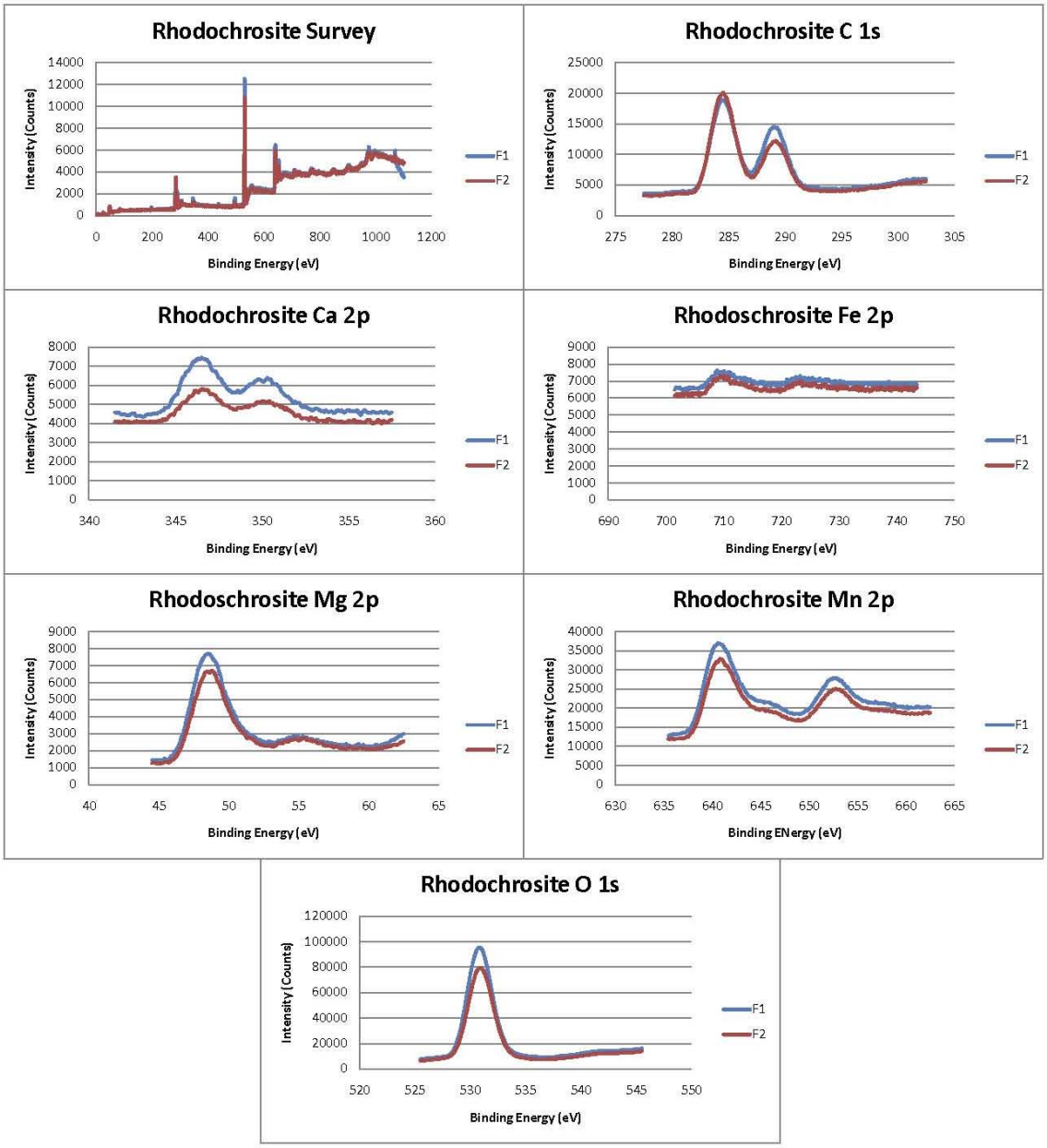

Siderite XPS Peak Results

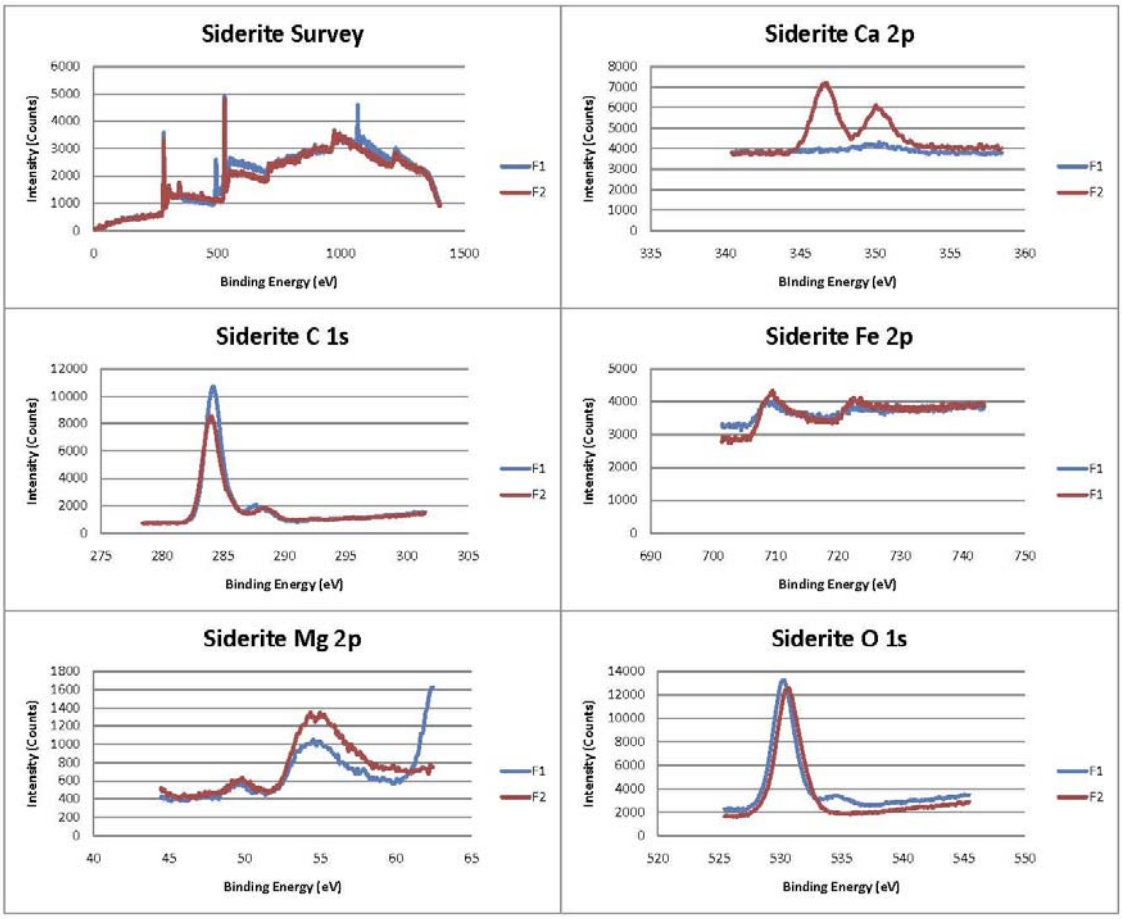

VITA

Name: Clint Matthew Miller

Address: 108 Halbouty Bldg., Texas A&M University,
College Station, TX 77843-3115

Email Address: boggie33ad@yahoo.com

Education: B.S. Geology, Texas A&M University, 2004
M.S. Geology, Texas A&M University, 2010